
Theses and Dissertations

Fall 2009

Assessment of source-receptor relationships of aerosols: an integrated forward and backward modeling approach

Sarika Kulkarni
University of Iowa

Follow this and additional works at: <https://ir.uiowa.edu/etd>

 Part of the [Chemical Engineering Commons](#)


Copyright © 2009 Sarika Kulkarni

This dissertation is available at Iowa Research Online: <https://ir.uiowa.edu/etd/392>

Recommended Citation

Kulkarni, Sarika. "Assessment of source-receptor relationships of aerosols: an integrated forward and backward modeling approach." PhD (Doctor of Philosophy) thesis, University of Iowa, 2009.
<https://doi.org/10.17077/etd.bxnc1m5k>

Follow this and additional works at: <https://ir.uiowa.edu/etd>

 Part of the [Chemical Engineering Commons](#)

ASSESSMENT OF SOURCE – RECEPTOR RELATIONSHIPS OF AEROSOLS: AN
INTEGRATED FORWARD AND BACKWARD MODELING APPROACH

by
Sarika Kulkarni

An Abstract

Of a thesis submitted in partial fulfillment
of the requirements for the Doctor of
Philosophy degree in Chemical and Biochemical Engineering
in the Graduate College of
The University of Iowa

December 2009

Thesis Supervisor: Professor Gregory R Carmichael

ABSTRACT

This dissertation presents a scientific framework that facilitates enhanced understanding of aerosol source – receptor (S/R) relationships and their impact on the local, regional and global air quality by employing a complementary suite of modeling methods. The receptor – oriented Positive Matrix Factorization (PMF) technique is combined with Potential Source Contribution Function (PSCF), a trajectory ensemble model, to characterize sources influencing the aerosols measured at Gosan, Korea during spring 2001. It is found that the episodic dust events originating from desert regions in East Asia (EA) that mix with pollution along the transit path, have a significant and pervasive impact on the air quality of Gosan. The intercontinental and hemispheric transport of aerosols is analyzed by a series of emission perturbation simulations with the Sulfur Transport and dEposition Model (STEM), a regional scale Chemical Transport Model (CTM), evaluated with observations from the 2008 NASA ARCTAS field campaign. This modeling study shows that pollution transport from regions outside North America (NA) contributed ~ 30 and 20% to NA sulfate and BC surface concentration. This study also identifies aerosols transported from Europe, NA and EA regions as significant contributors to springtime Arctic sulfate and BC. Trajectory ensemble models are combined with source region tagged tracer model output to identify the source regions and possible instances of quasi-lagrangian sampled air masses during the 2006 NASA INTEX-B field campaign. The impact of specific emission sectors from Asia during the INTEX-B period is studied with the STEM model, identifying residential sector as potential target for emission reduction to combat global warming. The output from the STEM model constrained with satellite derived aerosol optical depth and ground based measurements of single scattering albedo via an optimal interpolation assimilation scheme is combined with the PMF technique to characterize the seasonality and regional distribution of aerosols in Asia. This innovative analysis framework that combines the

output from source – oriented chemical transport models with receptor models is shown to reduce the uncertainty in aerosol distributions, which in turn leads to better estimates of source – receptor relationships and impact assessments of aerosol radiative forcing and health effects due to air pollution.

Abstract Approved: _____
Thesis Supervisor

Title and Department

Date

ASSESSMENT OF SOURCE – RECEPTOR RELATIONSHIPS OF AEROSOLS: AN
INTEGRATED FORWARD AND BACKWARD MODELING APPROACH

by
Sarika Kulkarni

A thesis submitted in partial fulfillment
of the requirements for the Doctor of
Philosophy degree in Chemical and Biochemical Engineering
in the Graduate College of
The University of Iowa

December 2009

Thesis Supervisor: Professor Gregory R Carmichael

Copyright by
SARIKA KULKARNI
2009
All Rights Reserved

Graduate College
The University of Iowa
Iowa City, Iowa

CERTIFICATE OF APPROVAL

PH.D. THESIS

This is to certify that the Ph.D. thesis of

Sarika Kulkarni

has been approved by the Examining Committee
for the thesis requirement for the Doctor of Philosophy
degree in Chemical and Biochemical Engineering at the December 2009
graduation.

Thesis Committee: _____
Gregory R Carmichael, Thesis Supervisor

Charles O Stanier

Julie L P Jessop

Patrick O'Shaughnessy

Kenneth A Rahn

To My Family

ACKNOWLEDGMENTS

I am happy to take this opportunity to acknowledge and thank all those people who have helped me to reach this stage of my career. I would like to first thank my advisor Prof. Gregory R Carmichael for allowing me to pursue this research. He has taught what it takes to be a good researcher and how to stay motivated and enjoy the work on a daily basis. I would like to extend my sincere thanks to my committee members: Prof. Charles O Stanier, Prof. Julie L P Jessop, Prof. Patrick O'Shaughnessy and Prof. Kenneth A Rahn for their support and interest in my research.

I consider myself extremely fortunate to work with several past and present research scientists and graduate students at the Center for Global and Regional Environmental Research (CGRER). This dissertation work would not have been possible without the support of Dr. Bhupesh Adhikary, Chao Wei, Dr. Alessio D'Allura, Dr. Youhua Tang, Dr. Tianfeng Chai, Dr. Scott Spak, Dr. Li Pan, and Dr. Gakuji Kurata. I would also like to thank the Department of Chemical and Biochemical Engineering, University of Iowa for giving me this opportunity to be a part of their graduate program. I am grateful to Linda Wheatley, Jane Frank and Jeremie Moen for their constant support. I would like to thank the University of Iowa, NSF and NASA for the financial support.

I am extremely grateful for the unconditional love and support received from my mother Shobha, my brother Sachin, my uncle Govind Rao, my parents-in-law: Sai Kumari and Bhaskara Sarma, my friends Abhinaya and Sridevi. I would like to thank Dr. Srinivas Achanta for being a great friend since 1997.

I would like to thank my husband, Nanda Chintalapati. If not for him, I would have never come to Iowa. His constant love, support, and encouragement were mainly responsible for the success of this research work. Last but not the least; I would like to thank my son Rohan, who came into my life in 2007. He has taught me how to stay focused in career while balancing the family life.

ABSTRACT

This dissertation presents a scientific framework that facilitates enhanced understanding of aerosol source – receptor (S/R) relationships and their impact on the local, regional and global air quality by employing a complementary suite of modeling methods. The receptor – oriented Positive Matrix Factorization (PMF) technique is combined with Potential Source Contribution Function (PSCF), a trajectory ensemble model, to characterize sources influencing the aerosols measured at Gosan, Korea during spring 2001. It is found that the episodic dust events originating from desert regions in East Asia (EA) that mix with pollution along the transit path, have a significant and pervasive impact on the air quality of Gosan. The intercontinental and hemispheric transport of aerosols is analyzed by a series of emission perturbation simulations with the Sulfur Transport and dEposition Model (STEM), a regional scale Chemical Transport Model (CTM), evaluated with observations from the 2008 NASA ARCTAS field campaign. This modeling study shows that pollution transport from regions outside North America (NA) contributed ~ 30 and 20% to NA sulfate and BC surface concentration. This study also identifies aerosols transported from Europe, NA and EA regions as significant contributors to springtime Arctic sulfate and BC. Trajectory ensemble models are combined with source region tagged tracer model output to identify the source regions and possible instances of quasi-lagrangian sampled air masses during the 2006 NASA INTEX-B field campaign. The impact of specific emission sectors from Asia during the INTEX-B period is studied with the STEM model, identifying residential sector as potential target for emission reduction to combat global warming. The output from the STEM model constrained with satellite derived aerosol optical depth and ground based measurements of single scattering albedo via an optimal interpolation assimilation scheme is combined with the PMF technique to characterize the seasonality and regional distribution of aerosols in Asia. This innovative analysis framework that combines the

output from source – oriented chemical transport models with receptor models is shown to reduce the uncertainty in aerosol distributions, which in turn leads to better estimates of source – receptor relationships and impact assessments of aerosol radiative forcing and health effects due to air pollution.

TABLE OF CONTENTS

| | |
|--|------|
| LIST OF TABLES | viii |
| LIST OF FIGURES | ix |
| CHAPTER 1 INTRODUCTION | 1 |
| 1.1 Background and Significance | 1 |
| 1.2 Research Objectives | 14 |
| 1.3 Specific Aims | 16 |
| 1.4 Outline | 17 |
| CHAPTER 2 RECEPTOR MODELING OF SURFACE AEROSOLS AT GOSAN, KOREA DURING THE 2001 ASIAN PACIFIC REGIONAL AEROSOL CHARACTERIZATION EXPERIMENT (ACE- ASIA) | 21 |
| 2.1 Introduction | 21 |
| 2.2 Background – ACE ASIA, Perfect Dust Storm and Gosan Data Set | 24 |
| 2.2.1 ACE – Asia Field Campaign | 24 |
| 2.2.2 Perfect Dust Storm | 24 |
| 2.2.3 Measurement Sample Collection and Analysis | 25 |
| 2.3 Methodology | 27 |
| 2.3.1 Qualitative Source Apportionment Studies using FA and PMF | 27 |
| 2.3.1.1 Factor Analysis (FA) | 27 |
| 2.3.1.2 Positive Matrix Factorization (PMF) | 29 |
| 2.3.1.3 Potential Source Contribution Function | 31 |
| 2.4 Results and Discussion | 33 |
| 2.4.1 FA Analysis Results | 33 |
| 2.4.2 PMF Source Identification | 34 |
| 2.4.3 FA and PMF Comparison | 37 |
| 2.4.4 Influence of Asian Dust Storms on Pollution Source Identification | 38 |
| 2.4.5 Impact of Particle Size on Source Identification | 39 |
| 2.4.6 Identification of Potential Source Regions by PSCF | 40 |
| 2.5 Summary | 43 |
| CHAPTER 3 UNDERSTANDING THE INTER-CONTINENTAL TRANSPORT OF AEROSOLS DURING SPRING 2008: A REGIONAL SCALE MODELING STUDY | 57 |
| 3.1 Introduction | 57 |
| 3.2. STEM Model Description | 60 |
| 3.3 Results and Discussion | 62 |
| 3.3.1 Evaluation of WRF Meteorology | 62 |
| 3.3.2 Comparison with ARCTAS DC8 Aircraft Observations | 63 |
| 3.3.3 Comparison with Surface Observations | 64 |
| 3.3.4 Regional Distribution of Aerosols | 65 |
| 3.3.5 Influence of Emission Perturbation in Major Source Regions on the Regional Distribution of Aerosols | 68 |

| | |
|---|-----|
| 3.3.6 Changes in Source Region Concentration due to Emission Perturbations..... | 69 |
| 3.3.7 Impact of Emission Perturbations on the Arctic Region..... | 71 |
| 3.4. Summary..... | 72 |
| CHAPTER 4 INFLUENCE OF ASIAN AEROSOLS AND TRACE GASES ON THE PACIFIC AND NORTH AMERICA DURING THE INTEX-B FIELD CAMPAIGN..... | 91 |
| 4.1 Introduction..... | 91 |
| 4.2. Model Description and Emissions Inventory | 94 |
| 4.3 Results and Discussion | 96 |
| 4.3.1 Comparison of Model Predictions with Aircraft Observations..... | 100 |
| 4.3.2. Comparison with Surface Observations | 106 |
| 4.3.3 Quasi-lagrangian Sampling | 111 |
| 4.3.4 Emission Sensitivity Runs..... | 114 |
| 4.4 Summary..... | 116 |
| CHAPTER 5 UNDERSTANDING THE SEASONALITY AND REGIONAL DISTRIBUTION OF ASIAN AEROSOLS: A MULTIYEAR REGIONAL SCALE MODELING STUDY WITH AOD ASSIMILATION USING OPTIMAL INTERPOLATION | 152 |
| 5.1 Introduction..... | 152 |
| 5.2 Methodology..... | 155 |
| 5.2.1 STEM Model Description | 155 |
| 5.2.2 Observed Data Description..... | 156 |
| 5.2.3 Data Assimilation Technique | 157 |
| 5.2.4 Calculation of Assimilated Aerosol Distributions..... | 158 |
| 5.2.5 PMF Receptor Model Description..... | 160 |
| 5.3 Results and Discussion | 162 |
| 5.3.1 Model Evaluation | 162 |
| 5.3.2 Regional Distribution | 163 |
| 5.3.3. PM2.5 Composition of India, China and Southeast Asia..... | 164 |
| 5.3.4 Seasonality..... | 166 |
| 5.3.5 Implications to Human Health..... | 173 |
| 5.4 Summary..... | 174 |
| CHAPTER 6 SUMMARY AND FUTURE DIRECTION..... | 194 |
| 6.1 Summary..... | 194 |
| 6.2 Future Direction..... | 196 |
| REFERENCES | 198 |

LIST OF TABLES

| | |
|--|-----|
| Table 3.1 Sulfate import sensitivity of source regions for spring 2008: Monthly mean average of sulfate at surface ($\mu\text{g}/\text{m}^3$) –domestic values are shown in bold | 75 |
| Table 3.2 Sulfate import sensitivity of source regions for spring 2008: Monthly mean response of sulfate ($\mu\text{g}/\text{m}^3$) – Percent change when compared to base is shown in parentheses | 75 |
| Table 3.3 BC import sensitivity of source regions for spring 2008: Monthly mean average of BC ($\mu\text{g}/\text{m}^3$) at surface –domestic values are shown in bold. | 76 |
| Table 3.4 BC import sensitivity of source regions for spring 2008: Monthly mean response of BC ($\mu\text{g}/\text{m}^3$) – Percent change when compared to base is shown in parentheses | 76 |
| Table 4.1 Model calculated lagrangian sampling between C-130 and DC-8 flights | 119 |
| Table 4.2 Model calculated lagrangian sampling between DC-8 and Mt. Bachelor | 121 |
| Table 4.3 Model calculated lagrangian sampling between C-130 and Mt. Bachelor. | 122 |
| Table 4.4 Model calculated lagrangian sampling of air mass between DC-8 and Trinidad Head. | 124 |
| Table 4.5 Model calculated lagrangian sampling of air mass between C-130 and THD. | 125 |

LIST OF FIGURES

| | |
|--|----|
| Figure 1.1 Source- receptor modeling framework showing the inter-dependence of emissions, source models, backward models and observational data..... | 18 |
| Figure 1.2 Source and receptor models (a) Source model (b) Receptor model..... | 19 |
| Figure 1.3 Schematic diagram of the STEM model | 20 |
| Figure 2.1 Geographic location of Gosan site (a) Gosan and the adjacent areas (b) Only Gosan..... | 45 |
| Figure 2.2 Coarse mode Factor Analysis (FA) results (a) Source profiles (Factor Loadings) (b) Source contributions (Factor Scores) | 46 |
| Figure 2.3 Fine mode Factor Analysis (FA) results (a) Source profiles (Factor Loadings) (b) Source contributions (Factor Scores) | 47 |
| Figure 2.4 Coarse mode Positive Matrix Factorization (PMF) results (a) Source profiles (b) Source contributions | 48 |
| Figure 2.5 Fine mode Positive Matrix Factorization (PMF) results (a) Source profiles (b) Source contributions | 49 |
| Figure 2.6 Comparison of PMF source profiles (a) Entire measurement period (b) NDS period | 50 |
| Figure 2.7 Comparison of PMF source profiles (a) PM ₁ fine classification (b) PM _{2.5} fine classification | 51 |
| Figure 2.8 Geographic location of the source regions used in the PSCF domain | 52 |
| Figure 2.9 PSCF maps of source areas representing the mixture source of sea salt and anthropogenic pollution source in fine mode (a) Source areas for contribution value > 1 (b) Source areas for contribution value < 1 | 53 |
| Figure 2.10 PSCF maps of source areas representing the industry source with Pb as leading tracer in fine mode (a) Source areas for contribution value > 1 (b) Source areas for contribution value < 1 | 54 |
| Figure 2.11 PSCF maps of source areas representing the natural dust emission source with Al as leading tracer in fine mode (a) Source areas for contribution value > 1 (b) Source areas for contribution value < 1 | 55 |
| Figure 2.12 PSCF maps of source areas representing the oil combustion source with V as leading tracer in fine mode (a) Source areas for contribution value > 1 (b) Source areas for contribution value < 1 | 56 |
| Figure 3.1 Regional distribution of SO ₂ , CO, BC and OC emissions during spring 2008 | 77 |
| Figure 3.2 Monthly mean biomass burning CO emissions for April 2008..... | 78 |

| | |
|---|-----|
| Figure 3.3 STEM model domain for ARCTAS with DC8 flight tracks for spring and summer overlaid along with the Lidar Station Teplokluchenka, Kyrgyz republic. | 79 |
| Figure 3.4 Comparison of WRF meteorological variables with ARCTAS DC8 aircraft observations..... | 80 |
| Figure 3.5 Comparison of STEM model aerosols with ARCTAS DC8 aircraft observations | 81 |
| Figure 3.6 Comparison of observed and modeled PM aerosol composition at Lidar Site Teplokluchenka, Kyrgyz republic | 82 |
| Figure 3.7 Monthly mean distribution of BC and sulfate at the surface for April 2008 | 83 |
| Figure 3.8 Transport pathways across the modeling domain illustrated by air mass back trajectories colored by altitude | 84 |
| Figure 3.9 Monthly mean latitude - altitude cross sections of sulfate at 130E, 125W, 70W and 10W during spring 2008..... | 85 |
| Figure 3.10 Monthly mean latitude - altitude cross sections of BC at 130E, 125W, 70W and 10W during spring 2008..... | 86 |
| Figure 3.11 Percent change in sulfate due to the emission perturbations in source regions..... | 87 |
| Figure 3.12 Percent change in BC due to the emission perturbations in source regions..... | 88 |
| Figure 3.13 Monthly mean area average concentrations of major source regions for April 2008..... | 89 |
| Figure 3.14 Impact of source region perturbation on the Arctic region (> 66.5 N)..... | 90 |
| Figure 4.1 NASA DC-8 and NCAR/NSF C-130 flight tracks along with the location of ground based observation sites including Kathmandu (KTM), Trinidad Head (THD) and Mt. Bachelor (MBO) during the INTEX-B (Phase 2) experiment. The numbers denote the research flight numbers for the DC-8 and C-130 aircraft. | 127 |
| Figure 4.2 Monthly mean CO at 3 kilometer AGL layer, DC-8 and C-130 observed and modeled CO vertical profiles and average CO latitudinal and longitudinal distributions during INTEX-B study period..... | 128 |
| Figure 4.3 Back trajectories of wind vectors and tagged CO tracers illustrating the source region of air masses sampled by the selected DC-8 and C-130 flights. | 129 |
| Figure 4.4 Comparison of meteorological variables from the WRF model with DC-8 (Top row a,b,c,d) and C-130 (bottom row e, f, g,h) observations. | 130 |

| | |
|--|-----|
| Figure 4.5 Comparison of STEM model predictions versus observed aerosols from the DC-8 and C-130 (a) Sulfate (DC-8) (b) NO ₃ (DC-8) (c) Sulfate (C-130) and (d) NO ₃ (C-130)..... | 131 |
| Figure 4.6 Mission wide average distribution of aerosols at the 3-kilometer AGL layer (a) Sulfate, (b) Nitrate, (c) OC and (d) Dust during INTEX-B | 132 |
| Figure 4.7 Mission wide average cross-sections of (a) sulfate (b) sulfate to potential sulfate ratio (c) VOC age (hours) and (d) OC/SO ₄ ratio at 45N during INTEX-B. | 133 |
| Figure 4.8 Observed AMS and modeled SO ₄ , and OC vertical profiles for INTEX-B C130 flights using criteria similar to Dunlea et al., 2008 (i.e. Observed AMS SO ₄ > 1 µg/m ³ and sampled west of 125W degrees longitude)..... | 134 |
| Figure 4.9 Observed AMS and modeled SO ₄ , and OC vertical profiles for INTEX-B C130 flights using criteria similar to Peltier et al., 2008 (i.e. Modeled CO > 100 ppb and predicted China anthropogenic CO > 50% of the predicted total anthropogenic CO)..... | 135 |
| Figure 4.10 Average vertical profiles of OC/SO ₄ ratio for INTEX-B campaign. The observed OC/SO ₄ ratio is calculated using the OC (OM/1.9) and SO ₄ measurements from AMS aboard the C-130 aircraft. The Dunlea et al., 2008 screening criteria are Observed AMS SO ₄ > 1 µg..... | 136 |
| Figure 4.11 Comparison of observed PM _{2.5} , sulfate and OC at Trinidad Head (THD), US (middle row) and Kathmandu, Nepal (bottom) during the INTEX-B campaign Top row curtain plots at THD. The white oval denotes the location of the lagrangian sampled air mass sampled by C130 flight 21 (05/05/06) that arrived at THD on 05/08/06..... | 137 |
| Figure 4.12 Comparison of observed and modeled trace gases at Mt. Bachelor (MBO), OR during INTEX-B campaign (a) Ozone (b) PAN (c) CO (d) NO..... | 138 |
| Figure 4.13 Curtain plots of modeled trace gases at Mt. Bachelor (MBO), OR during INTEX-B campaign (a) Ozone (b), PAN, (c) Dust along with (d) time series of these species at the surface level. The white oval shape denotes the lagrangian air mass sampled by C130 flight 21 (05/05/06) that arrived at MBO on 05/08/06..... | 139 |
| Figure 4.14 Horizontal distribution of modeled ozone, PAN, and dust at 18z, 3kilometer AGL layer along with redistributed concentration along back trajectories on April 22 (a,b), May 3 (c,d) and May 11 (e,f) during INTEX-B. | 140 |
| Figure 4.15 Time series of source region tagged CO tracers at 5.3kilometer AGL layer (a) and surface (b) along with the vertical profile of CO (c) at Mt. Bachelor (MBO). The white oval denotes the location of the lagrangian sampled air mass sampled by C130 flight 21 (05/05/06) that arrived at MBO on 05/08/06..... | 141 |

| | |
|--|-----|
| Figure 4.16 Comparison of observed and modeled trace gases and aerosols (surface) at Nepal Climate Observatory at Pyramid (NCO-P), Nepal during INTEX-B campaign | 142 |
| Figure 4.17 Comparison of observed and modeled trace gases and aerosols (625 m AGL) of Nepal Climate Observatory at Pyramid (NCO-P), Nepal during INTEX-B campaign | 143 |
| Figure 4.18 Quasi lagrangian sampling of air masses between DC-8 flight 15 (05/04/06), C-130 flight 21(05/05/06), and the two surface sites Mt. Bachelor (MBO) (05/08/06) and Trinidad Head (THD) (05/08/06) during INTEX-B..... | 144 |
| Figure 4.19 Comparison of observed and modeled CO, ozone and Ethane/CO ratio of DC-8 flight 15 and C-130 flight 21 airborne measurements. The square box denotes the time period where the model calculations suggested that quasi lagrangian sampling occurred..... | 145 |
| Figure 4.20 Modeled trace gases and aerosols extracted along the pseudo lagrangian back trajectory from MTB and THD that crossed C-130 flight 21 and DC-8 flight 15. The square boxes denote the time period where the lagrangian air mass was sampled by DC-8, C-130 air..... | 146 |
| Figure 4.21 Modeled meteorological parameters and trace gas species extracted along the trajectory pathway of the descending lagrangian air mass sampled on C-130 flight 15 that arrived at MTB on (04/26/06)..... | 147 |
| Figure 4.22 Regional distribution of anthropogenic BC emissions along with the percent contribution of residential, transportation, power and industrial sectors | 148 |
| Figure 4.23 Regional distribution of anthropogenic SO ₂ emissions along with the percent contribution of residential, transportation, power and industrial sectors | 149 |
| Figure 4.24 Regional distribution of BC concentration along with the percent contribution of residential, transportation, power, industrial sectors and biomass burning..... | 150 |
| Figure 4.25 Regional distribution of sulfate concentration along with the percent contribution of residential, transportation, power, industrial sectors and biomass burning..... | 151 |
| Figure 5.1 Four year average distributions of AERONET SSA, AERONET AOD, MODIS-AERONET AOD and MODIS fine mode AOD over land for 2001-2004..... | 176 |
| Figure 5.2 Comparison of modeled SSA with AERONET SSA observations at Kanpur | 177 |
| Figure 5.3 Regional distributions of SSA, BC AOD and dust AOD before and after SSA bias correction | 178 |

| | |
|---|-----|
| Figure 5.4 Comparison of observed and modeled PM ₁₀ (µg/m ³) at selected EANET locations..... | 179 |
| Figure 5.5 Four year averaged distributions of MODIS-AERONET AOD, Modeled AOD, PM ₁₀ mass, BC emissions, Sulfate and BC mass..... | 180 |
| Figure 5.6 Composition of four year averaged PM _{2.5} aerosols for the regions India, China, East China and Southeast Asia..... | 181 |
| Figure 5.7 Composition of four year averaged AOD and PM ₁₀ mass at selected megacities and regional observation sites. The PM ₁₀ is plotted on log scale to highlight the pollution related aerosols..... | 182 |
| Figure 5.8 Average seasonal distribution of India BC concentration (µg/m ³) during 2001 - 2004..... | 183 |
| Figure 5.9 Average seasonal distribution of China BC concentration (µg/m ³) during 2001 -2004..... | 184 |
| Figure 5.10 Average seasonal distribution of Southeast Asia BC concentration (µg/m ³) during 2001 – 2004..... | 185 |
| Figure 5.11 Seasonal cycle of PM _{2.5} aerosols at regional observation sites..... | 186 |
| Figure 5.12 Source profiles and contributions of PMF modeled AOD at Hanimadhoo..... | 187 |
| Figure 5.13 Source profiles and contributions of PMF modeled AOD at Gosan, Korea..... | 188 |
| Figure 5.14 Source profiles and contributions of PMF modeled AOD at selected megacities and regional observation sites. See figure 4 for the location of the sites..... | 189 |
| Figure 5.15 Contribution of PMF factors to total AOD at selected locations for the month of April representing the regional dust outflow..... | 190 |
| Figure 5.16 Contribution of PMF factors to total AOD at selected locations for the month of July representing the monsoon flow..... | 191 |
| Figure 5.17 Contribution of PMF factors to total AOD at selected locations for the month of October representing the local pollution influence..... | 192 |
| Figure 5.18 Population weighted exposure to PM _{2.5} levels greater than WHO guideline of 10 µg/m ³ | 193 |

CHAPTER 1

INTRODUCTION

1.1 Background and Significance

Deteriorating air quality is one of the major global problems faced by people all over the world, with vast reaching effects on the environment. Aerosols, defined as suspensions of solid/liquid particles in a gaseous medium, play a vital role in several air pollution problems. For particles in the atmosphere, the medium is air. They are emitted directly into the atmosphere (primary aerosols) or formed in the atmosphere by gas-to-particle conversion (secondary aerosols). These particles vary greatly in size, source, chemical composition, amount and distribution in space and time (Willeke *et al.*, 1993). Aerosols absorb and scatter sunlight, thereby altering the earth's radiative balance and subsequently leading to increased temperature, decreased rainfall, and a weaker hydrological cycle (Ramanathan *et al.*, 2001). The scattering of sunlight by aerosols is the leading cause of visibility reduction. Aerosols can also act as sites for chemical reaction to take place. They are involved in various reactions, including those that lead to the destruction of stratospheric ozone and perturb the photochemical oxidant cycle of the atmosphere (Seinfeld *et al.*, 1998). Unmitigated emissions of aerosols influence the atmosphere and the climate patterns on local, regional, and hemispheric scales (Guttikunda 2002). The last few decades have witnessed a tremendous increase in the amount of aerosols in the atmosphere due to the rapid industrialization and economic development worldwide (Streets *et al.*, 2003a; Streets *et al.*, 2003b). The human exposure to aerosols is associated with detrimental health impacts and increased mortality rates (Chow *et al.*, 2006). There is a great need to formulate emission reduction strategies for effective air quality management.

The characterization of the complex properties of aerosols is extremely important in devising aerosol abatement policies. Two major questions need to be addressed

whenever such strategies are formulated. Firstly what are the different sources contributing to the emission of aerosols? And where are these sources coming from? (Xie *et al.*, 2006). In other words, it is important to determine if the sources influencing the receptor sites are local, regional or intercontinental in nature. The characterization of sources at critical receptor locations and identifying the physical location of their origin is critical for policy making decisions. However, coming up with reasonable answers to the above two questions requires a variety of analysis tools encompassing ambient measurements of pollutant concentration and meteorological variables, building emission inventories for source categorization, and detailed models as illustrated in figure 1.1 (Brook *et al.*, 2004). This process involves identifying the sources of aerosols emitted into the atmosphere, estimating the emission rates of specific pollutants, understanding the transport pathways of pollutants from the source regions to downwind receptors, and assessing the dynamic behavior of aerosols resulting from the physical and chemical transformation processes that occur during the transport (Hopke 2003). There is great degree of spatial and temporal variability in the relative importance of these processes across the globe.

Simulating the complexity of aerosols with modeling methods is an arduous task. In order to understand the complex behavior of aerosols, there are two major types of models applied in atmospheric studies called the source and receptor models. The source models, also known as the forward “Chemical Transport Models” (CTMs), use the amount of emissions and simulate the different atmospheric processes to predict the ambient concentrations at a receptor. In contrast, the receptor models, also known as “backward models”, start with the ambient measurements and come up with the source contributions affecting a receptor (figure 1.2). Receptor models are widely used for air quality studies focused on source apportionment of airborne particulate matter (PM), which is defined as the process of estimating the relative contributions of different source types to ambient air pollutant concentrations (Watson *et al.*, 2002). Source and receptor

models are complementary to each other and applying them together can lead to better understanding of the complex “source – receptor” (S/R) relationships of aerosols, the variability in concentration of a species at a receptor location due to changes in emissions from a source region (Watson *et al.*, 2002). It is important to combine the information obtained from receptor models along with CTMs, in order to assess the source – receptor relationships of aerosols (Watson *et al.*, 2002; Brook *et al.*, 2004). Laupsa *et al.*, (2009) improved the PM_{2.5} predictions at Oslo, Norway by incorporating the feedback from receptor model calculations to improve the underlying emissions inventory that serves as input to the Air Quality Management system AirQUIS model. In addition the application of data assimilation methods, which integrate the observed data into the CTMs to obtain optimal estimates of environmental parameters, can further enhance our understanding of aerosol properties (Carmichael *et al.*, 2008). The next few sections present a brief overview of various receptor modeling methods, followed by CTMs and data assimilation methods used to date in air quality studies.

Receptor modeling is broadly classified into two different categories; namely multivariate receptor models and trajectory ensemble models (Hopke 2003). While multivariate receptor models are widely used for qualitative and quantitative source apportionment in air quality studies, the trajectory ensemble models, which incorporate back trajectories, are utilized for identification of the physical location of pollutant sources. Receptor modeling is primarily based on the principle of mass conservation. The individual source contributions to airborne particulate matter can be identified and apportioned by mass balance analysis (Hopke 2003). The multivariate receptor model is a broad term used for a variety of methods including the Factor Analysis (FA), Cluster Analysis (CA), Principal Component Analysis (PCA), Positive Matrix Factorization (PMF), UNMIX, Chemical Mass Balance (CMB), which are applied to chemical composition data and yield valuable information on pollution source type identification (Hopke 2003).

FA, CA, and PCA are purely statistical methods that are applied as data-reduction techniques to unravel the hidden source information and are apt for qualitative source apportionment studies. Further details on the concept and application of these methods to air quality studies have been described by Kulkarni 2004. Woo *et al.*, (2003) applied cluster analysis to classify the emission distributions of the Transport and Chemical Evolution over the Pacific (TRACE-P) field experiment into different chemical and regional groups. Dillner *et al.*, (2005) grouped the size distributions of elements with similar shapes of elements measured at two sites in Houston, Texas and attributed the different groups to pollution sources using cluster analysis. Lee *et al.*, (2002) used the cluster analysis on air mass back trajectories to link the pollution sources of Brigantine, NJ to their potential source regions.

Zhang *et al.*, (2003) applied factor analysis (FA) on the elemental composition data from Zhenbeitai, a surface site of the Asian Pacific Regional Aerosol Characterization Experiment (ACE) – Asia in China and concluded that the majority of the times (~90%) this site was impacted by dust transport from far-off location and only 10% of the times by local dust events during the sampling period. Senaratne *et al.*, (2004) performed source apportionment using Absolute Principal Component Analysis (APCA) on the elemental composition of 14 selected species obtained from Auckland, New Zealand and found that diesel emissions were the major contributors to brown haze in Auckland. Millet *et al.*, (2006) applied factor analysis on the gas and aerosol composition data obtained from the Chebogue Point, a surface measurement site for the International Consortium for Atmospheric Research on Transport and Transformation (ICARTT), 2004 field experiment and developed the chemical fingerprints of sources influencing the site. Mena-Carrasco *et al.*, (2007) applied FA to the observations, modeled data and bias (between observation and model) from DC8 flights during ICARTT 2004 to identify the underlying relationships between ozone and its precursor species. Several other studies

involving factor analysis in atmospheric studies can be found in the comprehensive review by Watson *et al.*, (2002).

All the above statistical based methods are suitable only for qualitative source apportionment studies as they can sometimes produce negative source composition and contribution, which violates the mass conservation of aerosols. To overcome this deficiency, Positive Matrix Factorization (PMF), UNMIX, and Chemical Mass Balance (CMB) methods were specifically designed for application to atmospheric data and are capable of producing both the qualitative and quantitative source apportionment results (Hopke 2003). These three models essentially solve the following mass balance equation.

$$X = GF + E \quad (1.1)$$

where X is an n by m matrix consisting of n number of observations for m chemical species. It is assumed that there are p sources influencing this data matrix. The aim of multivariate receptor models is to obtain two matrices G and F which explain the variation in the data set, where G is an n by p matrix of source contributions describing the temporal variation of the sources, F is a p by m matrix of source profiles, which is the chemical composition of the emissions, with each chemical species expressed as a mass fraction of the total, and E represents the unexplained data variance by the model.

The application of CMB, PMF and UNMIX is usually determined by the extent of information available for source apportionment. If the nature of the pollution sources influencing the measurements is known (i.e. p and F) then the only unknown is G and can be solved by CMB using an effective variance least squares approach. Further details on this methodology can be found in a review by Chow *et al.*, (2002) and the software is available from the US Environmental Protection Agency (EPA) at http://www.epa.gov/scram001/receptor_cmb.htm.

In reality, the source profiles information is not always readily available especially in the developing countries. In such a scenario, UNMIX and PMF are usually applied as they do not require “*a priori*” source information. However, there are differences in the mathematical formation of these two models. The EPA UNMIX model “unmixes” measured species concentration to infer the source contributions at the receptor site. This model uses the transformation method based on self-modeling curve resolution (SMCR) techniques to resolve the sources of pollution using eigen value analysis, which is based on Single Value Decomposition (SVD) technique. This method estimates the source profiles and contribution using an implicit least-squares analysis. Further details and related software can be obtained from EPA web at <http://www.epa.gov/heads/products/unmix/unmix.htm>. One of the limitations with the UNMIX model is that it scales the data matrix (X) in equation 1.1 either by row or column, which tend to distort the analysis results. To overcome this scaling issue, Paatero et al., 1994 showed that scaling each data point individually will result in higher influence of precise data than the ones which are prone to higher uncertainty. Traditional receptor methods based on Single Value Decomposition (SVD) technique cannot produce this result. Paatero et al., 1994 developed the PMF with a very different approach that uses the explicit weighted least-squares approach to obtain the source profiles and contributions. The PMF stand-alone software is also available from EPA at <http://www.epa.gov/heads/products/pmf/pmf.htm>.

In recent times, PMF has been extensively used in a variety of source apportionment studies and for assessing source-receptor relationships. Chueinta *et al.*, (2000) used PMF on aerosol composition data from Bangkok, Thailand and identified six sources as the major contributors to the Particulate Matter (PM) pollution in Bangkok. (Zhou *et al.*, 2005) identified five major pollution sources influencing Pittsburg by applying the (PMF) method to particle size-distribution data acquired from the Pittsburg

Air Quality Study (PAQS). Lapina *et al.*, (2004) employed PMF on the 1999 PM_{2.5} data of the 369 EPA monitoring sites and obtained 6 regional factors as the major contributors to PM for the entire monitoring network. This work in particular emphasizes the role of PMF in assessing the regional influence of the large scale – atmospheric processes. Wang *et al.*, (2003) applied the PMF technique to altitude stratified observations from C-130 aircraft during the 2000 Tropospheric Ozone Production about the Spring Equinox (TOPSE) to understand the various factors influencing the variability of tropospheric ozone and its seasonal characteristics at the middle and high latitudes. In yet another study focused on aircraft observation, Shim *et al.*, (2007) analyzed observations from the 1999 Pacific Exploratory Mission (PEM) Tropics – B, 2001 Transport and Chemical Evolution over the Pacific (TRACE-P), and 2004 Intercontinental Chemical Transport Experiment – North America (INTEX-NA) experiments using the PMF method and identified major sources contributing to the variability in observed oxygenated volatile organic compounds (OVOCs) and cyanides as terrestrial biosphere, biomass burning, industry/urban regions and oceans. References to other studies demonstrating the successful application of PMF in source apportionment studies are reviewed in Paatero (2000).

Once the pollution sources influencing the receptor are identified from measurements, it is essential to locate the origin of these sources. Application of trajectory ensemble models greatly assists in identifying the probable source regions that impact the receptor sites. Trajectories are lagrangian models that describe the path taken by air mass by sampling them backward in time for various starting times during the measurement study period. The direct calculations of trajectories are obtained from wind observations. However in practice trajectory calculations are based on the gridded output of numerical models (Stohl 1998). Several trajectory based approaches are used in source apportionment studies to infer probable location of emission sources by combining the trajectories with measured concentration. These ensemble methods treat the trajectories as a

sequence of segments that each represents a fixed amount of time (Stohl 1996; Stohl *et al.*, 2002). The trajectories arriving at a receptor site are defined by segment endpoints, which have two coordinates (latitude and longitude) that represent the air mass location at a particular time (Hopke 2003). The segment end points serve as input to the ensemble methods and produce spatial distribution of regions that influence the concentrations at the receptor site. Examples of the trajectory ensemble methods are Residence Time Analysis (RTA), Quantitative Transport Bias Analysis (QTBA), and Potential Source Contribution Function (PSCF), Concentration Weighted Trajectory fields (CWT), Residence Time Weighted Concentration (RTWC) and Area of Influence analysis (AIA) (Stohl 1996; Hsu *et al.*, 2003; Zhou *et al.*, 2004).

Polissar *et al.*, (2001) used the Potential Source Contribution Function (PSCF) method on the air mass back trajectories calculated from CAPITA Monte Carlo trajectory model to identify the likely source regions of the Underhill, Vermont fine particle sources. A review of other air quality studies using the concept of the trajectory clustering can be found in Hopke (2003). Diaz *et al.*, (2006) classified the air mass back-trajectories at the Izaña Global Atmospheric Watch (GAW) Observatory located on the mountain ridge that crosses the island from the centre to the Northeast part of Tenerife Island, using the K – means clustering method to identify the sources of air mass.

Receptor models are necessary but not sufficient to identify the sources and quantify their contributions to Particulate Matter (PM). It can be inferred from the above discussion that the receptor modeling studies require comprehensive measurements of concentration (Watson *et al.*, 2002). However, this availability is limited due to the prohibitive cost of operating the sampling instruments and the subsequent analysis of the data collected by them. In addition the experimental studies alone cannot explain the spatial and temporal variability of aerosols. The forward CTMs are of great help in such a scenario as they can provide model predictions of concentration which are spread over a large spatial domain and provide a continuous representation with time.

“Chemical Transport Models” are powerful tools that can diagnose the chemical and transport processes that influence the distribution of air pollutants in the atmosphere. They provide a means to link the emission sources with measured concentration and help in policy making decisions to improve the deleterious air quality. The CTMs are classified into different types based on their dimensionality. The simple box model (zero-dimensional) treats the concentration as same everywhere and varies with time: i.e. concentration $c_i(t)$ is only a function of time. The next one-dimensional (1-d) model treats concentration as a function of time and altitude while assuming the horizontally homogenous layers: i.e. $c_i(z,t)$. The two-dimensional models assume that concentration is a function of time and any two dimensions, while it is uniform along the remaining dimension e.g. $c_i(x,z,t)$. Finally, three-dimensional (3-d) models simulate concentration in all dimensions i.e. $c_i(x,y,z,t)$. As the dimensionality increases, both accuracy and complexity of the model also increase (Seinfeld *et al.*, 1998).

The CTMs are broadly classified into two categories – lagrangian and eulerian. The lagrangian model simulates the concentration of air pollutants as they move through space and time using the metrological field for advection and dispersion, thus providing time and space varying concentration. This model set up does not allow mass exchange between the air parcel and its surroundings, which prevents the inclusion of non-linear chemistry. Some of the examples are URBAT model, and CAPITA Monte Carlo (CMC) model (Calori *et al.*, 1999; Schichtel *et al.*, 2005). Lagrangian CTMs are computationally efficient and are ideal for predicting the transport of species from a given point source location. However, one essential drawback of lagrangian CTM is that it can't characterize the interaction of different sources due to the absence of non-linear chemical reactions. The eulerian CTM treats points fixed in space and allows the exchange of mass between grid cells and computes concentration of species as a function of time at different locations. The eulerian CTMs have the capability to handle non-linear chemical reactions. Even though including the non-linear chemical reactions in eulerian CTMs

demands high computational resources, the recent advances in computing technologies have made them more viable for use in air quality studies.

CTMs are also characterized based on their computational domain i.e. the area simulated. Global models simulate concentration of species on a global scale with spatial grid resolution of ~100 km or higher and fail to represent some of the underlying physical processes due to their coarse grid resolution. Regional and continental scale models with spatial grid resolution of ~ 80km and lower, overcome the limitation of global models but their performance is governed by the quality of lateral boundary conditions. The micro scale and urban scale models, which have a spatial grid resolution that extends from meters to a few kilometers, are used to simulate finer features exhibited by urban regions (Seinfeld *et al.*, 1998).

Atmospheric 3-D models provide a necessary framework for integration of the understanding of the individual atmospheric processes and the study of their interactions. (Seinfeld *et al.*, 1998). The CTM simulations are used to interpret the observations, thereby assessing our understanding of the underlying processes mentioned above. CTMs also provide S/R relationships that assist in understanding the influence of emission source regions on downwind receptor sites and assess the impact of long-range transport of air pollutants. The main processes that affect the concentration of chemicals in the atmosphere include transport, chemistry, emissions and deposition (Jacob 1999). The CTMs start with emissions, meteorology and a set of chemical initial and boundary conditions as input, and simulate the concentration of pollutants in the selected domain. Regional scale CTMs are necessary to study the impact of aerosols on a country, regional and continental scale (Adhikary 2008). One such regional scale model that has been used extensively in this study is STEM model.

The Sulfur Transport and dEposition Model (STEM), a regional scale model, has been developed at the University of Iowa in the 1980's (Carmichael *et al.*, 1984; Carmichael *et al.*, 1984; Carmichael *et al.*, 1986). This model has been used to

investigate the aerosols and trace gases throughout Asia. It takes a eulerian approach to solve the convective-diffusion equation shown below to simulate the concentration of a species.

$$\frac{\partial c_i}{\partial t} + \nabla \cdot (vc_i) = \nabla \cdot K \cdot \nabla c_i + R_i + S_i + G_i \quad (1.2)$$

where c_i denotes the gas phase concentration of species I, v denotes the wind velocity vector, K is the eddy diffusivity tensor, R_i is the chemical reaction term, S_i is the source term and G_i denotes the mass transfer between the gas and condensed phases. The eulerian approach divides the domain into a grid of discrete cells, applies operator splitting and several numerical methods to solve this equation. The data flow and schematic diagram of the STEM model is shown in figure 1.3.

Meteorological data are required to simulate the transport of species in the model set-up. STEM model can handle data from various meteorological models in different projections as it does not require uniform horizontal grid. MM5 (Anthes *et al.*, 1978), RAMS (Pielke *et al.*, 1992), and WRF (Skamarock *et al.*, 2005) are some of the meteorological models that have been incorporated into STEM in recent modeling studies. It is important to note that the STEM model has the same projection and grid resolution as the input meteorological model. The dust and sea salt emissions are calculated based on the meteorological parameters by the preprocessor. The dust emissions calculation methodology is described in Adhikary (2008) and the sea salt emissions are calculated using the methodology of Gong (2003).

The natural emissions including volcanic, biogenic, and anthropogenic and biomass burning emissions are not calculated inside the STEM model but are input as pre-calculated total emissions. The biogenic emissions are calculated using different models. The US EPA BEIS (Vukovich *et al.*, 2002) model is used to calculate the biogenic emissions over North America while global biogenic emissions calculated from

similar models are also available. The anthropogenic emissions are representative of population, economic activities, and different processes that emit species. It is an arduous task to manage these data and is simplified by using various assumptions, which lead to high uncertainty in the final emission estimates. The emission inventory of gaseous and primary aerosols including SO₂, NO_x, CO₂, CO, CH₄, BC, OC, NH₃ and Non Methane Volatile Organic Compounds (NMVOC) for the year 2000 was calculated by Streets *et al.*, 2003. The estimates of Asian NO_x emissions for the year 1990-2020 can be found in van Aardenne *et al.*, (1999). Global estimates of anthropogenic emissions can be obtained from EDGAR emissions data base (Olivier *et al.*, 1999). Bond *et al.*, (2004) created the global emissions of primary carbonaceous aerosols. The biomass burning emissions represent the emissions from natural forest fires, burning of agricultural wastes and deforestation for agriculture purposes. The global biomass burning emissions estimates can be obtained from various sources (van der Werf *et al.*, 2006; Al-Saadi *et al.*, 2008). The emissions from different sources are mapped to the STEM domain by the emissions preprocessor module.

It is necessary to specify the initial and boundary conditions for all the species in the model calculations. In STEM model, both fixed (time and space) boundary conditions and time varying boundary conditions from a global scale model have been used successfully in several modeling studies. Tang *et al.*, (2007) compared the model simulations with fixed and time varying boundary conditions from a global model for the continental US domain in 2004 and found that using global model boundary conditions enhanced the model prediction skills.

Photolysis is the one of the most important drivers of tropospheric ozone chemistry. In STEM model, the photolysis is calculated using the NCAR TUV radiation model (Madronich 2002), which includes calculation of 30 explicit photolysis rates. The TUV model requires total ozone column data, which is input from satellites including Ozone Mapping Spectrometer (OMI) and Total Ozone Mapping Spectrometer (TOMS).

The aerosol optical properties are calculated using OPAC (Hess *et al.*, 1998) algorithm in TUV model. The dry and wet depositions are important pathways by which aerosols are removed from the atmosphere (Seinfeld *et al.*, 1998). In STEM, dry deposition is modeled using the “resistance in series” method (Wesely *et al.*, 2000), while wet deposition is modeled as a first-order loss rate with precipitation.

The gas to particle conversion and water content of aerosol is simulated using SCAPE (Simulating Composition of Atmospheric Particles at Equilibrium) module (Kim *et al.*, 1995) in the STEM model. The SCAPE module treats inorganic aerosols only and bins them into four size bins including 0.1–0.3 μm , 0.3–1.0 μm , 1.0–2.5 μm , 2.5– 10 μm . STEM model uses SAPRC-99 (Carter 2000) chemical mechanism to incorporate 93 species and 255 gas phase chemical reactions. The ‘lumped mechanism’, which involves lumping together species with similar reaction rates and mechanisms, is used for modeling the complex Volatile Organic Compounds (VOCs). SAPRC-09 (Carter 2009) is the latest updated version of this reaction mechanism.

The aerosol distributions estimated by CTMs are prone to great uncertainty due to uncertainties evolving from the various modeling components and assumptions made to simulate them (Bates *et al.*, 2006). One of the several ways to reduce the uncertainty in CTM estimates is the data assimilation technique, a method that integrates the observations into the CTM model (Carmichael *et al.*, 2008). Recent air quality studies have applied the data assimilation techniques extensively to estimate optimal model parameters including, emission fields, concentrations, initial and boundary conditions in several air quality studies (Elbern *et al.*, 1997; Elbern *et al.*, 1999; Elbern *et al.*, 2000; Elbern *et al.*, 2001; Chai *et al.*, 2006) There are different types of data assimilation methods that are applied in air quality studies including statistical methods (nudging, Optimal Interpolation (OI), variational methods (3D-var, 4D-var) and sequential methods (Kalman Filter) (Bouttier *et al.*, 1999). Collins *et al.*, (2001) improved the predictions of MATCH model by assimilating the satellite-derived AOD values via OI

method. Tombette *et al.*, (2009) improved the one-day forecasts of aerosols from Polair 3D model with observed PM₁₀ over Europe using OI method. Chai *et al.*, (2006) assimilated the aircraft measurements from the TRACE-P field experiment into STEM 2k1 model by applying the 4D-Var technique and produced improved model predictions. Hakami *et al.*, (2005) used the STEM-2k1 model for assimilating the East Asia BC concentrations and recovery of its emissions, initial conditions and boundary conditions by applying the 4D-Var variational approach. Schichtel *et al.*, (2006) developed a hybrid source apportionment model to produce scaling coefficients for adjusting emissions and in the process refine the sulfate source contribution estimates of the BRAVO study by adapting a Bayesian least squares regression approach. Pan *et al.*, (2007) performed a top-down estimate of Asian Hg emissions using 4D-var technique to obtain optimal estimates of emission scaling factors which improved the STEM model results for the ACE-Asia campaign.

1.2 Research Objectives

The different receptor modeling methods and the forward CTMs described above have so far been applied for atmospheric studies relatively independent of each other. A US EPA (2001) report recommends that adapting a corroborative approach, which examines the results from a diverse set of analyses including modeling and observational methods, can provide a strong scientific basis for devising strategies to improve the deleterious air quality. There is a great need to use the measurements, receptor and forward modeling methods together for source apportionment studies in order to enhance our current understanding of the aerosol processes and be able to characterize the complex S/R relationships. This is the principal motivation for the present PhD research.

One of the objectives of this study is to understand the S/R relationships of aerosols during episodic pollution events and their impact on the surface air quality of downwind receptor sites. This can be achieved by analyzing the observed aerosol data

using multivariate receptor models and combining the output with trajectory ensemble models to obtain estimates of source profiles and contributions along with the identification of transport pathways and potential source regions influencing the receptor.

Another objective of this research is to understand the long range transport S/R relationships of aerosols on intercontinental and hemispheric scales. This requires the application of source – oriented approach with regional scale forward modeling. To accomplish this, the emissions from a particular source region of interest are perturbed. The emission perturbations are then propagated forward throughout the modeling domain and yield quantitative estimates of the influence of long – range and inter-continental transport of aerosols on surface and column distribution of aerosols.

Long range transport of pollution has implications on local, regional and global climate change. Another objective of this research is to study the influence of pollutants outflow from Asia to the Pacific and North America using a regional chemical transport model in conjunction with receptor models. This includes understanding the impact of emissions from anthropogenic sectors in Asia on the air quality over the Pacific and North America.

The forward CTM models provide model predictions of concentration with continuous spatial and temporal representation, which can't be achieved by observations. However, the CTMs are subject to great uncertainty due to uncertainty associated with the various modeling components including emissions, boundary conditions and wet removal processes. Observations need be incorporated into the model via data assimilation methods in order to reduce this uncertainty. Another research objective is to enhance the understanding of the S/R relationships of Asian aerosols by combining the information obtained from the observations, CTM and receptor models. The CTM model performance will be also be evaluated to assess its capability in representing the seasonal characteristics of Asian aerosols. The specific aims of this research study are listed next.

1.3 Specific Aims

1. Estimate the source profiles and the corresponding source contributions of elemental aerosol measurements at Gosan during Asian Pacific Regional Aerosol Characterization Experiment (ACE) – Asia field campaign by implementing the Positive Matrix Factorization (PMF) technique. This study will seek to understand the difference in the source characterization of coarse and fine mode aerosols. The transport pathways of pollution and potential geographic location of the sources contributing to the aerosols at Gosan will be identified by Potential Source Contribution Function (PSCF) technique.
2. Study the inter-continental transport of aerosols by perturbing emissions from major source regions including South Asia (SA), East Asia (EA), North America (NA) and Europe (EU) using the regional scale STEM model evaluated with observations from the Arctic Research of the Composition of the Troposphere from Aircraft and Satellites (ARCTAS) field campaign. This work will study the impact of domestic emissions when compared to the foreign emissions on the regional air quality of the major source regions.
3. Characterize the outflow of Asian aerosols to North America via the Pacific using the STEM model validated with NASA INTEX-B field campaign measurements. This work will also identify the possible cases of quasi-lagrangian air mass sampling of pollution plumes as it gets transported from Asia over the Pacific towards North America. In addition, the impact of individual emission sectors of Asia in the year 2006 on the aerosol mass loadings over the Pacific and North America will be studied.
4. Understand the regional distribution of Asian aerosols with STEM model assimilated with satellite-based AOD data via Optimal Interpolation (OI) technique. In addition, this study will also apply the ground based Single Scattering Albedo (SSA) in the

assimilation algorithm. This study will evaluate the STEM model performance in representing the seasonality of Asian aerosols using the PMF technique.

1.4 Outline

Chapter 1 of this thesis presented a brief literature overview of the various types of models used in air quality studies and stresses the need for a corroborative modeling approach that takes into account feedback from different models to understand the S/R relationships of aerosols. Chapter 2 of this thesis addresses the specific aim 1 mentioned above and demonstrates the application of receptor models to infer aerosol pollution sources influencing the observed concentrations. Chapter 3 of this thesis focuses on understanding the influence of perturbing source region emissions on the inter-continental and hemispheric scale transport of aerosols. This chapter demonstrates the application of forward modeling approach to characterize the S/R relationships and addresses the specific aim 2. Chapter 4 of this thesis studies the Asian pollutant outflow reaching the North America via Pacific. The impact of Asian emission sectors on the aerosol concentration over the Pacific is studied, which is listed as specific aim 3. Chapter 5 addresses the specific aim 4 and discusses the results of multi year aerosol distributions over Asia constrained with satellite AOD and ground based SSA. This chapter also demonstrates how the observations from satellites, forward model and receptor models can be combined to enhance the current understanding of aerosol S/R relationships. Chapter 6 provides a summary of this research and provides the possible future directions for this work.

Source-Receptor modeling framework

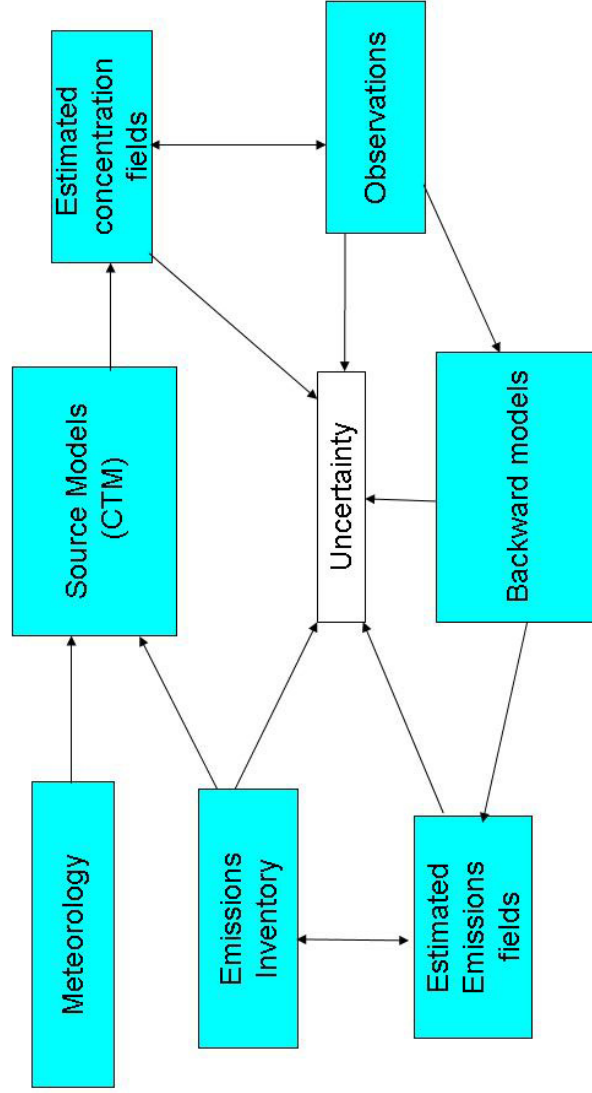


Figure 1.1 Source-receptor modeling framework showing the inter-dependence of emissions, source models, backward models and observational data

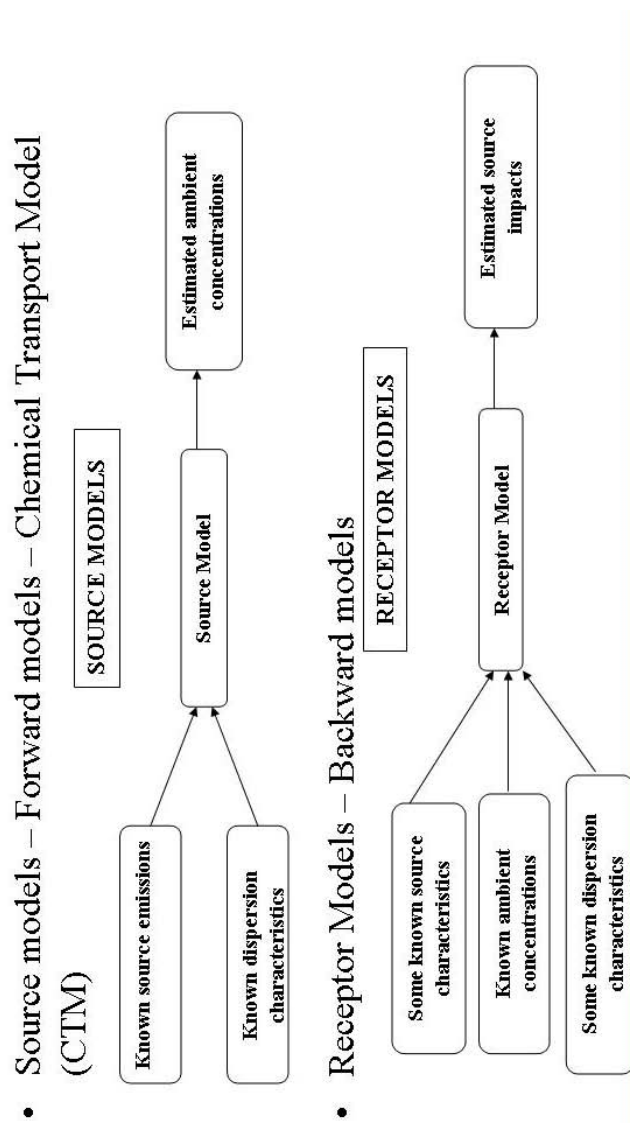


Figure 1.2 Source and receptor models (a) Source model (b) Receptor model.

Source: Source Apportionment Tutorial, Asian Aerosol Conference (AAC) Mumbai, December 2005

Data Flow Chart of U. of Iowa Regional Chemical Transport model, STEM (Sulfur Transport and dEposition Model)

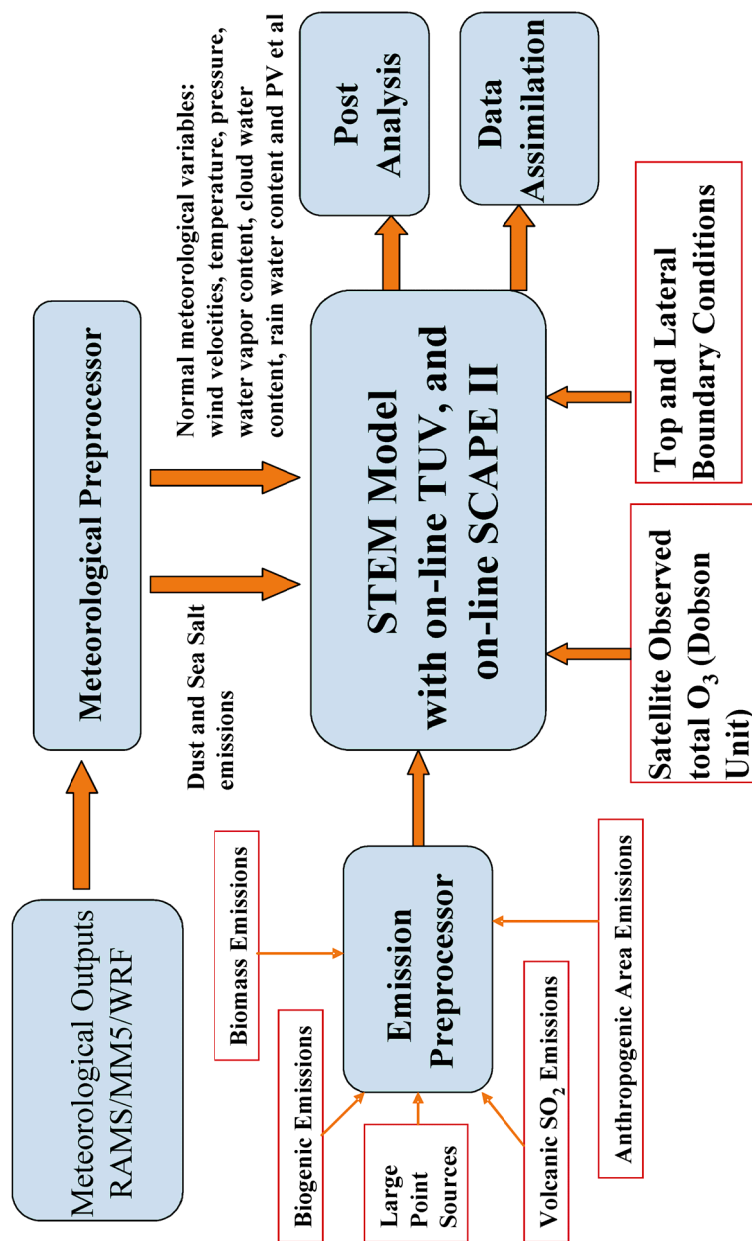


Figure 1.3 Schematic diagram of the STEM model

CHAPTER 2
RECEPTOR MODELING OF SURFACE AEROSOLS AT
GOSAN, KOREA DURING THE 2001 ASIAN PACIFIC
REGIONAL AEROSOL CHARACTERIZATION
EXPERIMENT (ACE- ASIA)

2.1 Introduction

The fact that aerosols are linked to various adverse effects including increased health risks, visibility reduction, altering earth's radiation budget, and changing the cloud properties by acting as cloud condensation nuclei (CCN), is a major cause of concern for the management of atmospheric air quality (Seinfeld *et al.*, 1998). The last few decades have witnessed a tremendous increase in the amount of aerosols released into the atmosphere due to the rapid industrialization and economic development worldwide particularly in the regions of East and South East Asia (Streets *et al.*, 2003a; Streets *et al.*, 2003b). These regions have diverse natural and anthropogenic aerosol sources and the rapidly increasing emissions have affected the atmosphere and the climate patterns on local, regional, and hemispheric scales (Guttikunda 2002). The characterization of complex properties of the Asian aerosol is extremely important in order to formulate emission reduction strategies for effective air quality management throughout the world. In particular, identification and apportionment of major pollution sources plays a critical role in air quality policy making decisions and requires extensive knowledge of the ambient aerosol chemical composition and the source contributions (Brook *et al.*, 2004). The multivariate receptor modeling methods including Chemical Mass Balance (CMB), Factor Analysis (FA) and Positive Matrix Factorization (PMF) are frequently used to identify the pollution sources and quantify their contributions (Hopke 2003). Numerous studies involving extensive observations and chemical transport modeling were conducted at Gosan, Korea during the 2001 Asian Pacific Regional Aerosol

Characterization Experiment (ACE- Asia) (Huebert *et al.*, 2003). Considerable number of source apportionment studies based on aerosol observations, were also undertaken. Kim *et al.*, (2005) investigated the impact of optical, physical and chemical properties of aerosols on the radiative forcing measured at Gosan during Asian dust and pollution episodes in 2001. While OC and EC concentrations were considerably higher during the pollution episode, the crustal marker species dominated the dust period. They found that the average diurnally averaged aerosol radiation forcing efficiencies during the episodes were similar reflecting the complex association of light absorbing aerosols with natural dust emissions. Ma *et al.*, (2004) analyzed the 17 trace metal aerosols collected by a 2-stage filter pack sampler from the end of March 2001 to the end of April 2001 by using Factor Analysis (FA) and classified the collected aerosol particles into sea salt rich, crustal rich, crustal/sea-salt/sulfur-rich and crustal/sea-salt rich particles. Han *et al.*, (2005) analyzed the trace elemental composition of aerosols measured at Gosan using the 8 – stage impactor during March – May 2002 period. In particular, this study applied Factor Analysis (FA), and Enrichment Factor (EF) calculation along with time series of specific source markers separately to individual stage data collected during the Non Dust Storm (NDS) period and identified soil, sea salt, coal combustion, metallurgical emissions, oil combustion and municipal incineration as the main sources impacting the air quality of Gosan. In yet another study, Han *et al.*, (2006) performed quantitative source apportionment studies using PMF to the same trace elemental aerosol composition along with total PM₁₂ mass obtained at Gosan and resolved 15 sources in eight size ranges (0.07 – 12 µm) and including continental soil, local soil, sea salt, biomass/biofuel burning, coal combustion, oil heating furnace, residual oil fired boiler, municipal incineration, nonferrous metal source, ferrous metal source, gasoline vehicle, diesel vehicle, copper smelter and volcanic emission. In addition, they concluded that the apportioned sources together contributed to 53% of the total PM mass.

In this study, the size-resolved and speciated trace elemental aerosol composition measurements at Gosan super site during the 2001 ACE- Asia field have been utilized to obtain estimates of pollution sources using a suite of receptor modeling methods including FA, PMF and Potential Source Contribution Function (PSCF). This analysis is limited to qualitative source apportionment studies due to lack of total PM mass measurements.

The principal goals of this work are to address the following issues

- To identify the major sources of pollution influencing the regional air quality of Gosan
- To compare the performance of FA and PMF techniques for qualitative source apportionment studies
- To study the impact of long range transport of aerosols during the Asian Dust Storm (ADS) at Gosan using PMF
- To investigate the importance of aerosol particle size on the source resolution process
- Identify the potential source regions contributing to the elemental concentration at Gosan using potential source contribution function (PSCF).

The structure of this chapter is as follows: section 2.2 on background studies gives an overview of the ACE – Asia field experiment, Gosan super site location, and the properties of the ambient aerosol composition measurements utilized in this study. Section 2.3 on methods briefly describes the different analyses techniques employed in this study. Section 2.4 on results and discussion presents addresses the above issues and the consequent implications followed by summary of the paper in the last section.

2.2 Background – ACE ASIA, Perfect Dust Storm and Gosan Data Set

2.2.1 ACE – Asia Field Campaign

East Asia has a large number of natural dust emission sources in the form of the Gobi and Taklimakan deserts. The rapid economic development of East Asia in the past two decades has resulted in a significant increase in the fossil fuel and biomass burning emissions (Woo *et al.*, 2003; Kulkarni 2004). It is well documented that a significant portion of the Asian aerosols traverse long distances over Pacific and can reach all the way to North American continent affecting the global atmosphere and climate (Husar *et al.*, 2001). The International Global Atmospheric Chemistry Program (IGAC) organized the ACE – Asia field experiment in spring of 2001 to better characterize the complex properties of Asian aerosols (Huebert *et al.*, 2003). This experiment deployed a variety of instruments involving several aircraft, ship, Lidar and a network of surface stations to provide detailed and comprehensive measurements of aerosol emissions and transport. The duration of the field experiment witnessed several natural dust events, which is a common spring time phenomena in the Asian continent. The prominent dust event, which generated a lot of interest among the research community, was the so called “Perfect dust storm” described below.

2.2.2 Perfect Dust Storm

During spring 2001 from April 4-14, a series of dust events occurred in the Asian mainland. The intensity of this dust storm was so large that it was named the “Perfect Dust Storm” by some researchers as it occurred at the time when the ACE – Asia field study was in progress. The dust storm was initialized on April 5 2001 in northwestern China due to a cold – air outbreak and strong surface winds. The dust emitted during this event was transported to the East and reached Mongolian-northeastern China on 7 April. The dust storm intensified due to the continuous emission of dust and by April 9, it

arrived over the Japan Sea. The dust storm continued to move eastwards and finally reached North America approximately 4 days later. Around April 8 another massive dust outbreak occurred in Mongolia due to strong frontal winds and moved eastwards along the similar route. Approximately 50 Tg of dust is estimated to have been emitted from the arid and semiarid regions of western China, northern China and Mongolia and the Loess plateau. During this transit period, the natural dust emissions interacted with the local pollution events and formed a complex mixture of aerosols (Seinfeld *et al.*, 2004; Uno *et al.*, 2004).

The majority of the measurement instruments deployed in the ACE-Asia field study were able to capture the features and movements of this dust event. The Gosan super site surface measurements were also in progress at the time of this dust storm occurrence. Gosan (126.16E, 33.29N, 78 MSL) (figure 2.1), located on the Western edge of the Cheju Island, South Korea, is a relatively clean area with no major industrial sources. In spring, the air masses flowing through Gosan are influenced by the anthropogenic activities and Asian dust storms. Thus Gosan serves as an ideal location to study the transport and transformation of ambient trace species in Northeast Asia and to study the impact of continental outflow (Carmichael *et al.*, 1997). This work has utilized the size and composition resolved aerosols measured at the Gosan super site in Korea during spring of 2001 from March 23 to April 29.

2.2.3 Measurement Sample Collection and Analysis

Size-resolved aerosol measurement samples were collected at Gosan by the DELTA (Detection and Evaluation of Long range Transport of Aerosols) group headed Dr. Thomas Cahill of the University of California, Davis, using the 8-stage drum impactor, as part of ACE- Asia field campaign. The aerosols were separated into eight size classifications based on the aerodynamic diameter. The diameter ranges in μm in the

decreasing order of size are: 5.0 – ~12, 2.5 – 5.0, 1.15 – 2.5, 0.75 – 1.15, 0.56 – 0.75, 0.34 – 0.56, 0.26 – 0.34, and 0.09 – 0.26.

The Synchrotron X-ray Fluorescence (S-XRF) technique was applied to analyze the raw samples of the elemental composition. Once the analyses were completed, a data set containing 296 samples of size- resolved composition measurements of the following 19 elements Aluminum (Al), Calcium (Ca), Sulfur(S), Silicon (Si), Chlorine (Cl), Potassium(K), Vanadium (V), Chromium (Cr), Manganese (Mn), Iron (Fe), Nickel(Ni), Copper (Cu), Zinc (Zn), Arsenic (As), Selenium (Se), Bromine(Br), Rubidium (Rb), and Lead (Pb) with 3-hour time resolution was developed. All the composition measurements along with corresponding uncertainties were reported in units of ng/m³. More information of the instrument and involved methodology can be elsewhere (Bench *et al.*, 2002; Shutthanandan *et al.*, 2002). For the rest of this paper, we will refer to these elements by their atomic symbols.

The species included in this dataset are markers representing the various sources influencing Gosan. It is well known that the majority of the anthropogenic pollution sources are primarily emitted as smaller sized particles (with aerodynamic particle size less than 2.5 µm) into the atmosphere. Therefore availability of higher size-segregated ambient aerosol samples can be of great assistance in identifying the diverse pollution sources. This dataset includes 5 size measurements of aerosol samples less than 1.15 µm facilitating improved source identification. In addition, the relatively shorter measurement sampling times like 3 hours used in these measurements, can greatly reduce the effect of the sample dilution and do a better job of preserving the source signatures. Thus this dataset provides an excellent opportunity to perform source apportionment studies. However, application of quantitative source apportionment is limited by the unavailability of measurements of total PM mass, ionic and the carbonaceous species. In addition, Na, an important tracer representing primarily the natural sea salt emissions, could not be detected by the S-XRF technique making it extremely difficult to

characterize the influence of marine sources, which tend to have a significant impact on the air masses arriving at Gosan. The dominant influence of natural dust emissions and their long range transport discussed earlier in section 2.2 further complicates the source resolution process. Nonetheless, the high size – and time – resolution of the ambient measurements, make it ideal for performing the semi-quantitative source apportionment studies and help in obtaining estimates of the source contributions. In the next section, the different methods used for analysis are described.

2.3 Methodology

In this section the various modeling methods employed for analyzing the elemental composition of aerosols measured at Gosan during spring 2001 are described.

2.3.1 Qualitative Source Apportionment Studies using FA and PMF

Receptor modeling techniques like FA and PMF are convenient to apply on aerosol measurements obtained from locations with little or no information on the pollution sources since they do not require “a priori” source profiles as input. (Hopke 2003). While FA is purely a statistical approach widely applied in various fields, the PMF is specifically designed to cater to the needs of atmospheric data. In this study, the FA and PMF techniques were used for qualitative source apportionment studies. In the next few sections, the FA and PMF methodology are discussed in detail.

2.3.1.1 Factor Analysis (FA)

Factor Analysis (FA), an advanced statistical technique, is extremely useful in identifying the relationships among variables that are driven by common processes such as sources, transport, and chemistry. Factor Analysis (FA) is particularly useful for source apportionment studies when there is no prior information available about the nature of the major aerosol sources affecting a particular receptor station. FA has been

widely used for analyzing atmospheric data and is well documented in the atmospheric literature (Huang *et al.*, 1999; Kulkarni 2004; Ma *et al.*, 2004). So without going into many details, we only give a brief overview of FA here.

Factor Analysis (FA) is essentially a variable reduction procedure that is applied to reduce a data set consisting of large number of inter-correlated variables into a small number of factors, which account for most of the variance in the original variables. FA assumes that the observed variables are linear combinations of the underlying factors, which describe the common variance in the dataset. It solves the following equation

$$X = AF \quad (2.1)$$

where X denotes the observation data, A denotes the factor loadings, which is a measure of association of sources with species and corresponds to the composition of sources and F is the factor score matrix, which is a linear combination of species, represents the temporal variation of source contribution.

FA accounts for the common variance of observed variables by analyzing an adjusted correlation matrix, a correlation matrix with squared multiple correlations on the diagonal using the eigen value – eigen vector analysis. The number of factors is determined based on the number of eigen values greater than 1 and the amount of variance explained. Typically in atmospheric studies, the FA solution is subject to varimax rotation, which tends to maximize the number of zeros and ones in the factor loading matrix in order to obtain physically realistic and easily interpretable sources. In general, the FA solution comes up with sources that have negative contributions. This violates the mass conservation assumption rendering it unfit for quantitative source apportionment studies. In addition, FA does not produce unique solution and is prone to rotational ambiguity. Despite the inherent drawbacks, FA is still a very valuable tool for obtaining initial estimates of the unknown sources influencing a receptor. In this study we

have used the FA with varimax rotation and eigen value one criterion along with 90% explained variance to obtain an initial estimate of the source contributions at Gosan.

2.3.1.2 Positive Matrix Factorization (PMF)

PMF, a form of factor analytic method, has been widely used in the atmospheric field for source apportionment studies involving ambient concentration measurements with unknown source profiles (Huang *et al.*, 1999; Lee *et al.*, 1999; Paterson 1999; Polissar *et al.*, 1999; Chueinta *et al.*, 2000; Kim *et al.*, 2005; Kim *et al.*, 2005). This model was first developed by Prof. Paatero at The University of Helsinki, Finland (Paatero *et al.*, 1993; Paatero *et al.*, 1994; Paatero *et al.*, 2002). Below is a brief description of the PMF methodology.

Suppose X is an n by m matrix consisting of n number of observations for m chemical species. It is assumed that there are p sources influencing this data matrix. The aim of PMF is to obtain two matrices G and F which explain the variation in the data set. Mathematically this can be represented by the following equation

$$X = GF + E \quad (2.2)$$

where G is an n by p matrix of source contributions describing the temporal variation of the sources, F is a p by m matrix of source profiles and E represents the unexplained data variance by the model.

The above equation can be represented in component form as

$$x_{ij} = \sum_{h=1}^p g_{ih} f_{hj} + e_{ij} \quad (2.3)$$

PMF solves the above equation using an explicitly weighted least square approach and minimizes the objective function $Q(X, \sigma, G, F)$ defined as

$$Q = \sum_{i=1}^n \sum_{j=1}^m \left(\frac{x_{ij} - \sum_{h=1}^p g_{ih} f_{hj}}{\sigma_{ij}} \right)^2 \quad (2.4)$$

where σ is the known matrix of error estimates.

The error estimates (σ) of individual data points are used to determine the weights of the least square fit on the data matrix. The G (source contributions) and F (source profiles) are determined so that the value of Q is minimized. In addition, the solution is always positively constrained. That is each of the elements G and F is always positive. The solution to the above equation is found by using a unique iterative algorithm PMF2 developed by Prof. Paatero and is described in detail elsewhere. It is highly recommended to use the robust mode in the PMF analysis in order to reduce the distortion of the results caused by large values in the dataset. The computational details of the robust mode calculation can be found in Paatero (2000).

The PMF output also results in a parameter called explained variation (EV) which signifies the contribution of each chemical species in each source. EV values are normalized so that their value lies between 0 and 1 and are considered to be a scaled version of the source profile matrix (F). They are very useful for qualitative source identification especially in cases where mass closure requirement is not met by the data matrix. The details of the EV calculation can be found in Juntto *et al.*, (1994), Lee *et al.*, (1999) and Paatero (2000).

The quality of the PMF fit to the data is largely dependent on the data matrix and the corresponding error estimates. There is no easy way to obtain the error estimates of the measurements. The analytic uncertainty is only part of the unknown total random error. So the error estimates should be chosen judiciously in PMF analysis. The PMF solution does not produce a unique solution. It is found by trial and error. The quality of the PMF fit is judged by the analysis of the Q values and by looking at the factors to see

if they are meaningful and realistic. The rotational freedom of the solution is greatly reduced due to the positive constraint imposed on it. Still there exists some rotational ambiguity which is controlled by the parameter FPEAK in the PMF analysis. Details of the FPEAK parameter can be found in Junnto *et al.*, (1994), Lee *et al.*, (1999), and Paatero (2000).

The occurrence of below-detection limit (BDL) values and missing values is quite common in the concentration measurements of the atmosphere. The PMF method is capable of handling the BDL and missing data values which the traditional factor analytic methods fail to do. Polissar *et al.*, (1998) has made the following recommendations to deal with the concentration and error estimates of the BDL and missing values encountered in the data set:

For missing values: concentration $x_{ij} = \tilde{u}_{ij}$

Error estimates $\sigma_{ij} = 4 \tilde{u}_{ij}$

For BDL values: concentration $x_{ij} = \frac{1}{2} d_{ij}$

Error estimates $\sigma_{ij} = \frac{1}{2} \hat{d}_{ij} + d_{ij}/3$

where x_{ij} , σ_{ij} , d_{ij} , \tilde{u}_{ij} , \hat{d}_{ij} denote the concentration, error estimate, the method detection limit, the geometric mean of the measured concentration and the arithmetic mean of the detection limit value of the species j respectively. In this study we have applied the PMF to the coarse and fine mode data measured at Gosan to obtain estimates of the source abundances.

2.3.1.3 Potential Source Contribution Function

The (PSCF) technique, developed by Ashbaugh *et al.*, (1985), combines the chemical measurement data with the air mass back trajectories to obtain information about pollution sources influencing a receptor site. The primary aim of PSCF method is to connect the observed concentrations of selected species and the most probable source of their air mass origin. This method has been applied in several air quality studies

(Cheng *et al.*, 1993; Sirois *et al.*, 1995; Polissar *et al.*, 2001; Wang *et al.*, 2004) and is briefly described below.

Air mass back trajectories arriving at a receptor site are calculated with the aid of a trajectory model. The location of an air parcel at a particular time is represented by the trajectory segment endpoints as latitude and longitude (Hopke 2003). In order to calculate PSCF, the entire geographic region covered by the trajectories is divided into an array of grid cells. The calculated PSCF will then be a function of the cell indices i,j .

Let N denote the total number of trajectory segment endpoints during the sampling period T . If n denotes the segment endpoints falling into an i,j^{th} cell, then the probability of randomly selected air parcel endpoint to reside in the i,j^{th} cell is given by

$$P(A_{ij}) = \frac{n_{ij}}{N} \quad (2.5)$$

In the same i,j^{th} cell, suppose m_{ij} is the number of segment endpoint denotes the trajectories arriving at the receptor for the time when concentrations exceed a pre-selected criterion value measured at the sampling location. The probability of such an event is given by

$$P[B_{ij}] = \frac{m_{ij}}{N} \quad (2.6)$$

The PSCF is defined by

$$P_{ij} = \frac{P(A_{ij})}{P(B_{ij})} = \frac{m_{ij}}{n_{ij}} \quad (2.7)$$

P_{ij} denotes the conditional probability that an air parcel passing through the i,j^{th} cell had the concentrations exceeding the set-criterion upon arrival at the receptor (Hopke 2006). The PSCF technique can be of great help in identifying the potential source regions contributing to the pollutant emissions at the receptor site.

2.4 Results and Discussion

The size- resolved speciated measurement dataset obtained from Gosan, Korea during spring of 2001 from March 23 to April 29 in 8 stages was reclassified into two size classes as coarse ($>1.15 \mu\text{m}$), and fine ($<1.15 \mu\text{m}$) to understand the characteristic difference in aerosol particle behavior in two size modes. Note that the summation of stages 1, 2 and 3 comprised the coarse mode concentration and the remaining 5 stages together accounted for the fine mode aerosol concentration.

The Asian Dust Storm (ADS) influence was very pronounced for 2 distinct time periods – April 10 – 14, 2001 and April 25-26, 2001 during this measurement campaign. In order to ascertain the dominant influence of the Asian dust events, the sampling days corresponding to the above time periods were excluded and this dataset was named as Non Dust Storm (NDS) period data. The possibility of Asian Dust influence to persist much longer not just on the intense dust event days will be explored further in the later parts of this section.

2.4.1 FA Analysis Results

The FA was applied to the coarse and fine mode trace elemental composition data obtained at Gosan. The eigen value one criterion along with the 90% explained variance was used to decide the number of factors. The retained factors were subject to varimax rotation to enhance the interpretability of the sources. Only species that displayed loadings greater than 0.5, were considered significant in the process of source identification. The temporal variation of the species that exhibited the highest loading was compared with standardized source contribution of that source for improving the source attribution. The results of the FA analysis in coarse and fine modes are shown in the figures 2.2 and 2.3. The FA analysis produced 3 – factor and 4 – factor solutions as the most likely sources in the coarse and fine mode respectively.

The coarse mode factor 1 had strong association of major dust marker species including Al, Si, K, Ti, Mn, and Fe along with V, Ni and Cr. The temporal variation of this factor followed closely the variation in Al. So this factor was identified as the long range transported natural dust emissions. Factor 2 was very well correlated with various industrial marker species including Cl, Zn, Mn, and Br and the temporal variation of this factor matched that of Zn. So this factor was classified as a miscellaneous industry source. Factor 3 was attributed to local pollution mixed with long range transported dust due to the close association of S, Ca, As, Se along with traces of Al, Si, K and strong similarity in the factor contribution and S time series.

Following similar procedural steps as applied in coarse mode source identification above, the most likely sources that impact the fine mode aerosol composition were identified as natural dust emission with Al as leading tracer, local pollution displaying close relation with S, a distinct oil combustion source with high loadings of Ni and Cr and a general industry source with Pb as the dominant species. The identified source contributions displayed similar temporal pattern as that of the species with highest loading on the particular factor. The major sources identified in the coarse and fine mode were similar with varying contributions of individual species except that a distinct oil combustion source was identified in the fine mode. This is expected behavior as majority of the anthropogenic source emissions including oil combustion, occur predominantly in fine mode.

2.4.2 PMF Source Identification

PMF, described in the section 2.3, was also used for source apportionment to the coarse and fine mode aerosol concentration of Gosan. Only qualitative source apportionment studies were performed due to lack of PM mass measurements. The uncertainty estimates were readily available along with measurements and used without any modifications. The missing values were substituted by the geometric mean calculated

from the available data and the corresponding uncertainty was set to 4 times the geometric means based on the recommendations of Polissar *et al.*, (2001). The robust mode of PMF was used in the analysis to reduce the impact of episodic dust events. The final PMF solution was obtained by trial and error after experimenting with the number of sources and following the general guidelines for obtaining optimal PMF solution including Q value and FPEAK parameter evaluation along with the interpretability of the resolved factors. The solution was not dependent on the FPEAK parameter. So FPEAK value of zero was used throughout the analysis. The normalization option of mean $G = 1$ was used in all the analyses. So the source contributions are in arbitrary units. The scaled source profile matrix (EV) was helpful in identifying the sources along with source profile matrix F. The lack of reliable information about the Gosan pollution sources and the impact of episodic dust events greatly complicated the source resolution process. In addition, since this analysis is limited only to qualitative source apportionment analysis, it was found that correlating the species with the resolved factors along with studying the variation in source contributions simplified the source identification process. Even though the source profile matrix F and scaled source profile matrix EV were calculated, only the source profiles in the form of species – factor correlation and comparison of the temporal variation of normalized sources with the corresponding highest correlated species are discussed here. Only correlations above 0.5 were treated as significant in source identification process. The PMF solution in the coarse and fine modes is discussed below.

After careful examination of the source profiles and the variation in the normalized source contributions, 4 distinct source signatures were identified by PMF analysis in coarse mode and the results are depicted in figure 2.4. Factor 1 was well correlated with all the species except Cl and Cu. The fact that the natural dust tracers including Al, Si, Fe, Ti, and Mn were highly correlated with factor and the well – matched temporal variation of the factor with Al, qualify this factor as the natural dust

emission source. Factor 2 displayed strong association of Zn, Cl and Br as evident by their correlation values (> 0.5). As the normalized contribution matched closely with that Zn, an industrial tracer, this factor was attributed to industry source. Factor 3 was closely associated with S and Ca along with Al, Si. Since heterogeneous surface reactions on dust provide a pathway for additional aerosol sulfate production (Tang *et al.*, 2004), this factor was identified as local pollution source mixed with long range transported dust which was significantly altered by the mechanism of dust heterogeneous chemistry. Factor 4 had only Cu as the major species. This could possibly be a distinct Cu smelting source.

The fine mode PMF solution including the source profiles and the corresponding source contributions is shown in figure 2.5. The source 1 shows close association of the Al, Si Ca, Ti, Mn Fe and Rb which are all tracers of natural dust emission tracers. So this source has been attributed to natural dust emissions. The source 2 had close association of Br, S along with Se. While Br and S together can represent the sea salt signature, S and Se together could also indicate the coal combustion source. Due to the absence of Na, a clear sea salt tracer, in the measurements, this source could not be conclusively attributed to a particular source. So source 2 was identified as the mixed pollution and marine source. The source 3 was identified as oil combustion source signature based on the high correlation and similar temporal pattern as V. Finally, the source 4 had high loadings of the following industrial source markers – Pb, Zn, K, and Mn. The source contribution closely matched the temporal variation of Pb. As this factor had markers from various industrial pollution sources, this source was attributed to the general industry source. Overall 4 distinct source signatures were identified in fine mode, which differed significantly in their composition from the source signatures identified in coarse mode.

2.4.3 FA and PMF Comparison

While FA is purely a statistical approach used for qualitative source identification, PMF is a variant of factor analytic approach designed specifically for atmospheric data analysis and well – suited for quantitative source apportionment studies. The inherent data limitations caused by missing significant portions of PM constituents including ionic and carbonaceous species and lack of PM mass availability, have forced the PMF analysis to be limited only to qualitative source apportionment studies. As described above, FA and PMF were used for identifying the sources that impact the air masses arriving at Gosan. So this provided us an opportunity to compare the FA and PMF qualitative source apportionment results discussed in the previous section.

The source profiles in FA are a measure of correlation of species with sources. As the PMF source profiles discussed here are shown in the form of species – source correlations, the FA and PMF source profiles for fine mode aerosol composition shown in figures 3a and 5a can be directly compared. Both FA and PMF identified natural dust emissions, mixed pollution and marine source, miscellaneous industry and oil combustion as the significant sources in fine mode but with slightly varying composition. For instance, FA identified the oil combustion source based on high Ni loading, while PMF identified the same source with V as the leading tracer. Since V and Ni are both major tracers for oil combustion source, it can be concluded that the identified source is essentially the same. Likewise, FA and PMF identified the similar set of sources including natural dust emissions, local pollution and industry for the coarse mode elemental composition (figures 2.3a and 2.5a) except for an additional Cu source identified by PMF. It was quite remarkable to see closely matching qualitative source apportionment results obtained by FA and PMF considering the vast difference in their calculation and implementation methodology. Based on this analysis, it can be safe to conclude that the performance of FA and PMF is identical for qualitative source

apportionment studies. However, PMF is superior to FA for quantitative source apportionment studies, as it produces positively constrained solution.

2.4.4 Influence of Asian Dust Storms on Pollution Source

Identification

It is well documented that the present ambient concentration data set was subject to dominant influence of the natural dust emissions as discussed in section 2.2. To ascertain the extent to which the natural dust emissions influenced the air masses arriving at Gosan receptor site, PMF was run on the coarse and fine modes for another distinct time period - the Non Dust Storm (NDS) period along with the entire concentration data discussed above. Note that the measurements corresponding to the following time periods – April 10 – 14 2001 and April 25 – 26 2001, which were heavily influenced by dust emissions, were excluded from the sampled measurements and constituted the NDS period concentration. The results of PMF analysis on fine mode aerosol composition during the NDS period are shown in figure 2.6. For ease of comparison, the source profiles obtained previously and that for NDS period are shown here. The sources look identical with slightly varying compositions for both entire measurement and NDS periods except for an additional Cu source resolved for the NDS period. It was quite surprising to see the similarity in the identified sources for the two data sets. Identical source profiles (not shown here) were identified by PMF for the entire measurement and NDS period data using the coarse mode elemental composition. Based on the above discussion, it can be concluded the impact of Asian dust events on the air masses arriving at Gosan was ubiquitous and not just restricted to particular dust event periods during the sampling period. Similar measurements over a longer time period capturing the annual seasonal variability can assist further in enhanced understanding of the impact of the dust events on regional air quality of Gosan.

2.4.5 Impact of Particle Size on Source Identification

The aerodynamic particle diameter is a critical parameter in aerosol characterization and source identification. This size parameter is of great importance in source characterization as the pollution particles are emitted into atmosphere in different size modes by the diverse sources. In general PM₁ (particles with aerodynamic diameter < 1 μm) and PM_{2.5} (particles with aerodynamic diameter < 2.5 μm) definitions are typically used for defining the fine mode aerosols in atmospheric literature. Since the anthropogenic pollution aerosols are predominantly emitted as fine mode particles, the higher the size resolution, the better the yield of source apportionment results. So far, in this discussion the particles with size < 1.15 μm has been used as fine mode definition. As the present trace elemental composition had high size resolution, a different fine mode classification (particle size < 2.5 μm) has been used to study the impact of the size distribution on source resolution process by applying PMF. The 8 – stage impactor data was reclassified so that the first 2 stages (particle size > 2.5 μm) were added together to obtain the coarse mode aerosol composition and the remaining 6 stages (particle size < 2.5 μm) comprised the fine mode. This new fine mode size classification was utilized in PMF analysis and the results were compared with the previous PMF analysis described earlier. Even though all the procedural steps including careful observation of source profiles and temporal variation of source contributions were followed, the PMF results discussion is limited to comparing the source profiles in the form of factor – species correlation as shown in figure 2.7. The general source signatures identified are more or less the same but some of the source compositions show a vast difference. In addition, the PM_{2.5} fine size mode classification identifies an additional Cu source category. Pb and Zn were identified as the leading tracers for the industry source and the oil combustion source was identified by V in both the cases. The natural dust source signature looked identical with the only major difference being that V is well – correlated with dust emissions in PM_{2.5} fine classification, which is not the case with the PM₁ fine mode

classification. The source category that exhibited the vast difference was the local pollution significantly altered by interaction with long range transport of dust. This source was easily distinguished from the dust emission source in the PM_{10} fine mode. However, identifying the local pollution source was difficult in the $PM_{2.5}$ mode as the major dust tracers were significant in more than one source. The scaled F source profile matrix (EV) along with the relatively lower correlation of dust tracers and association of Zn, As, and Se helped in identifying the local pollution source for the $PM_{2.5}$ fine classification. Based on this analysis, it can be concluded that the aerosol particle size greatly influences the identification of pollution sources. The apportionment of pollution sources at any given receptor requires long term, speciated aerosol composition with high size resolution. In addition, this analysis highlights the need for higher size resolution of aerosol composition measurements in order to enhance the identification of diverse pollution sources, which have dramatically varying emissions in different size modes.

2.4.6 Identification of Potential Source Regions by PSCF

The PMF solution identified the potential sources affecting Gosan. It would be more intuitive if PMF solution can be combined with trajectory ensemble models to identify the physical location of their origin. The probable source locations were obtained by the application of Potential Source Contribution Function (PSCF) using the meteorological data from STEM model.

The STEM-2k1 3 – d Chemical Transport Model was used extensively in flight planning during the ACE – Asia field experiment in spring 2001 (Kurata *et al.*, 2004; Tang *et al.*, 2004). The STEM model was run on a 80 km domain and used the meteorological fields provided through the RAMS (Regional Atmospheric Modeling System) model (Uno *et al.*, 2003) driven by ECMWF $1^\circ \times 1^\circ$ reanalysis data. The meteorological fields were output with an 80 km horizontal resolution, 18 vertical layers up to 15 km with a 3 hour time interval. Kurata *et al.*, (2004) evaluated the STEM – 2k1

model performance by comparing the segregated air –mass trajectories using the observed and model predicted concentrations from the aircraft mission of the TRACE-P field experiment. In this work the backward trajectories were calculated utilizing the meteorological data from the Regional Atmospheric Modeling System (RAMS) model with 3 hour time resolution, 5 – days backward in time below 3000 km in altitude for the entire measurement time period at Gosan. The trajectories ended when they touch the ground, or went out of the model domain or exceeded the 5-day calculations period. To reduce the high degree of uncertainty of PSCF values associates with the edge of the trajectory domain, any grid cell with the trajectory end points less than 5 (i.e. $n_{ij} < 5$) were excluded from the PSCF analysis. This has facilitated the coupling of the PMF results with the PSCF and provided valuable information about the sources influencing Gosan.

The coarse mode PMF results were predominantly influenced by natural dust emissions. In contrast, the PMF analysis results for the fine mode better resolved local pollution sources along with the natural dust emission source. Hence the PSCF analysis was primarily focused on the fine mode PMF results. Overall PMF analysis identified sea salt mixed with anthropogenic pollution source, industry source with Pb as the leading tracer, natural dust emission source and an oil combustion source. The PMF source contributions are in arbitrary units and normalized to unit mean. The PSCF criterion for classifying the air-mass trajectories below 3000m in altitude were based on the PMF source contributions. Since all the PMF resolved sources were influenced by local source emissions and emissions from long range transport, the source contribution values above and below the unit mean value will be ideal to distinguish the diverse sources and will be of great help in obtaining estimates of potential source areas overlaid on a map using PSCF. The main source regions present in this domain are shown in figure 2.8. In general PSCF values are overlaid on the grid cells of the model domain map to represent the potential source regions. The highest probable source areas are denoted by the dark red

values on the map. A value of 0.8 on the PSCF plots (For e.g. figure 2.9) indicates that 80% of the trajectories for the data points meeting the selection criterion pass over that grid cell. The following format has been used for showing the PSCF output. The top and bottom panel plots show the probable source regions for the source contribution values greater than the average value and less than average value respectively. The left panel plots shows the PSCF output by grid cells, while the right panel plots show the PSCF values arranged by administrative regions.

Figure 2.9 represents the potential source areas of the source representing the mixture of sea salt and anthropogenic pollution with criteria values based on its normalized source contribution time series. The most probable source regions for the high values (source contribution > 1) of this source (figure 2.9a) are found to originate in the vicinity of Gosan and coming from the Japanese island areas on the east and some provinces in Central China region on the northwest as seen both in the grid cells with bright yellow values (PSCF > 0.6). The below average source contribution values of this source originated from Northern and Central China regions located in the northwest direction and from Korean region (figure 2.9b). The northwest direction was the trail followed by the perfect dust storm and represents the contribution of long range transported aerosols to the source.

PSCF plots similar to those shown above were also constructed for the other 3 sources identified by PMF. Figure 2.10 shows the PSCF plots for the Industry source with Pb as the leading tracer. The above average source contribution values were coming from Central and Northern China regions located in the north-west direction of Gosan, which was the path flowed by the intense dust storm as displayed in figure 10a. This would represent the contribution from the long-range transport of aerosols. The below average contribution values for this source originated from the nearby regions of Japan and Korea located in the northeast direction which denote the local pollution component figure 2.10b.

Likewise, the potential source regions for the natural dust emission source are represented in the figure 2.11. The higher source contribution values originate from the northwest direction, where the Taklimakan desert is situated (figure 2.11a). The lower values for this source were coming from the northeast and east directions in the vicinity of Gosan indicating local pollution (figure 2.11b).

The potential source regions for the oil combustion source are shown in figure 2.12. The origin of high source contribution values of this particular source is located in the east direction indicating local sources and the nearby megacities like Beijing (figure 2.12a). The low values of this source are associated with regions in the northwest direction representing the long range transport component (figure 2.12b). Based on this analysis, it can be concluded that the sources identified from the PMF analysis had contributions from two components – local pollution and long range transport of aerosols. The intense dust storm that originated from the desert areas was the dominant source region influencing all the sources. However, the local pollution sources were also significant as illustrated in the PSCF analysis figures.

2.5 Summary

An extensive suite of chemically and temporally resolved aerosol trace elemental composition data measured using 8- stage impactor at the Gosan super site during the 2001 ACE- Asia campaign were analyzed by applying a variety of receptor modeling methods. The major pollution sources influencing the air masses arriving at Gosan were determined using Factor Analysis (FA) and Positive Matrix Factorization (PMF). The natural dust emissions, industry, and local pollution source signatures were identified as the major sources in both the coarse and fine mode aerosols. In addition, a distinct oil combustion source category was identified only in the fine mode aerosols. The quantitative source contribution estimates could not be obtained due to lack of PM mass measurements. The dominance of natural dust emissions, which interacted with the

pollution aerosols, during the sampling period, further complicated the source resolution process. The results of the qualitative source apportionment studies using FA and PMF have been compared. It was found that FA and PMF produced identical solutions for this particular dataset. The Non Dust Storm (NDS) PMF case study, performed by removing the aerosol samples corresponding to intense dust event days, identified similar sources as that of the PMF analysis including the entire measurement period data. The NDS case study results suggested that the Asian dust influence was ubiquitous and not just restricted to the episodic dust events for this sampling period. Finally the importance of aerosol particle size on the source identification was studied by using PM_{10} and $PM_{2.5}$ fine mode data classifications. PSCF was applied to obtain the geographic location of the most probable origins of the major pollution sources identified by PMF. PSCF analysis found that the PMF sources were influenced both by the anthropogenic sources in the vicinity and long range transport from the dust source regions. The source-receptor relationships obtained through the receptor modeling analysis in this study are valid only the given measurement period. These relationships do not hold good for other time periods. Despite the inherent data limitations, this analysis helped in characterization of the major pollution sources and identified their geographic origin influencing the regional air quality of Gosan during the episodic transport of dust from the desert regions of East Asia.

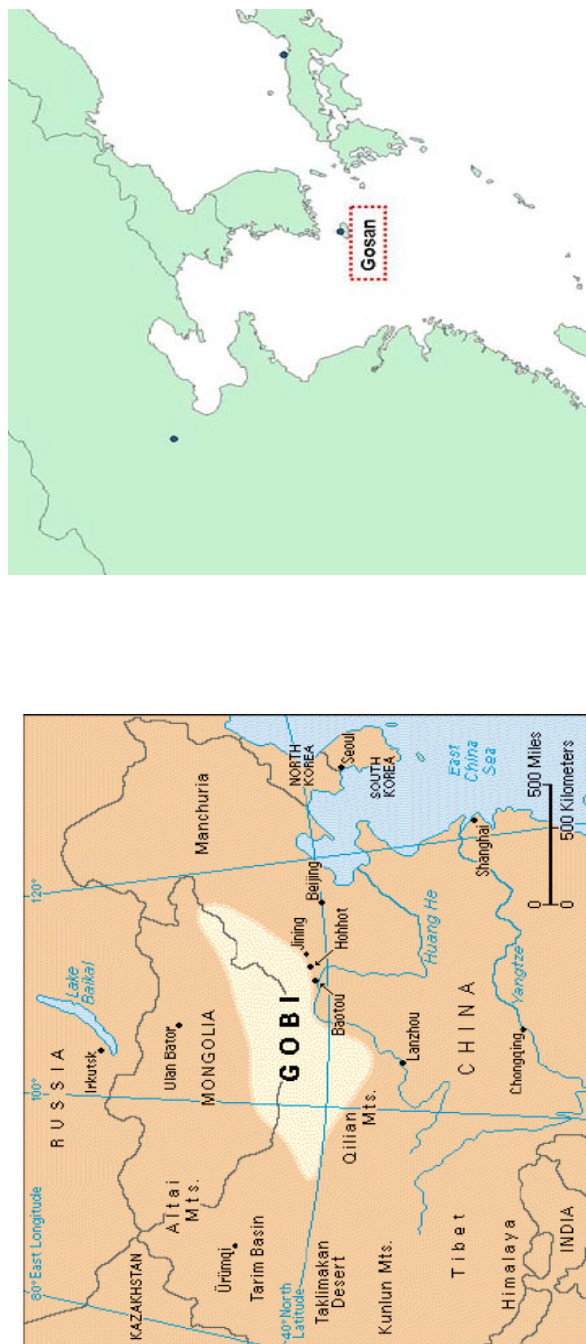


Figure 2.1 Geographic location of Gosan site (a) Gosan and the adjacent areas (b) Only Gosan

Source: (a): [http:// www. Lakepowell.net/asiandust.htm](http://www.Lakepowell.net/asiandust.htm)

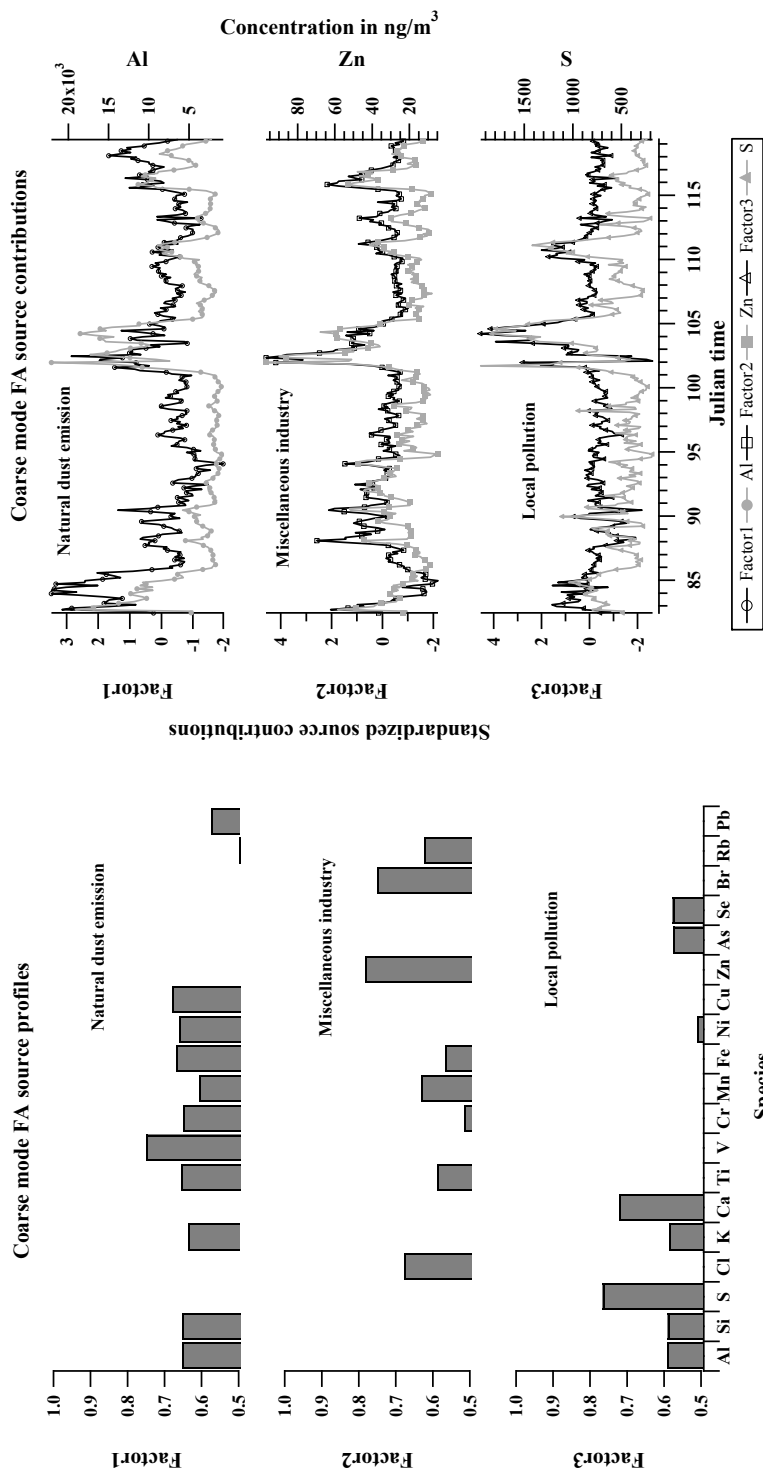


Figure 2.2 Coarse mode Factor Analysis (FA) results (a) Source profiles (Factor Loadings) (b) Source contributions (Factor Scores)

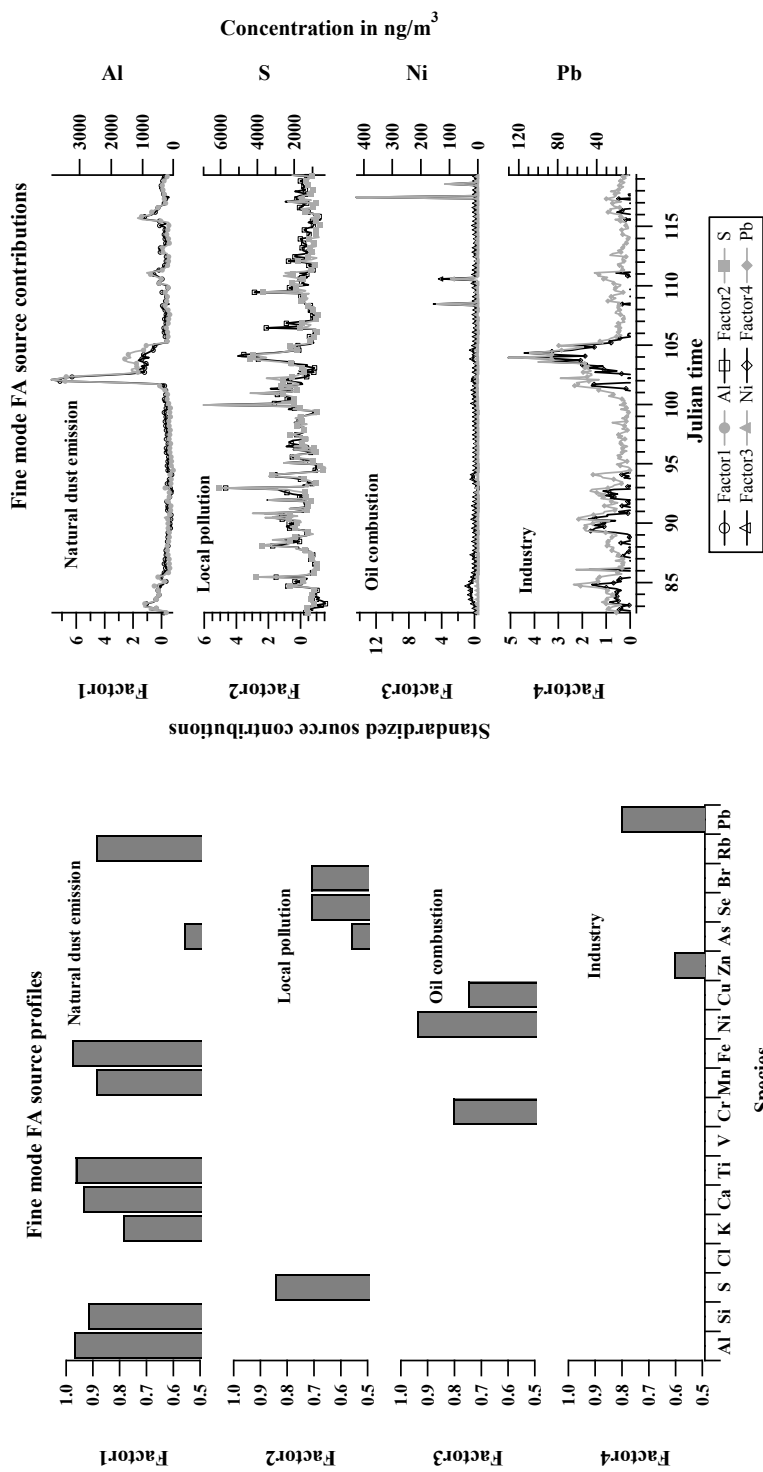


Figure 2.3 Fine mode Factor Analysis (FA) results (a) Source profiles (Factor Loadings) (b) Source contributions (Factor Scores)

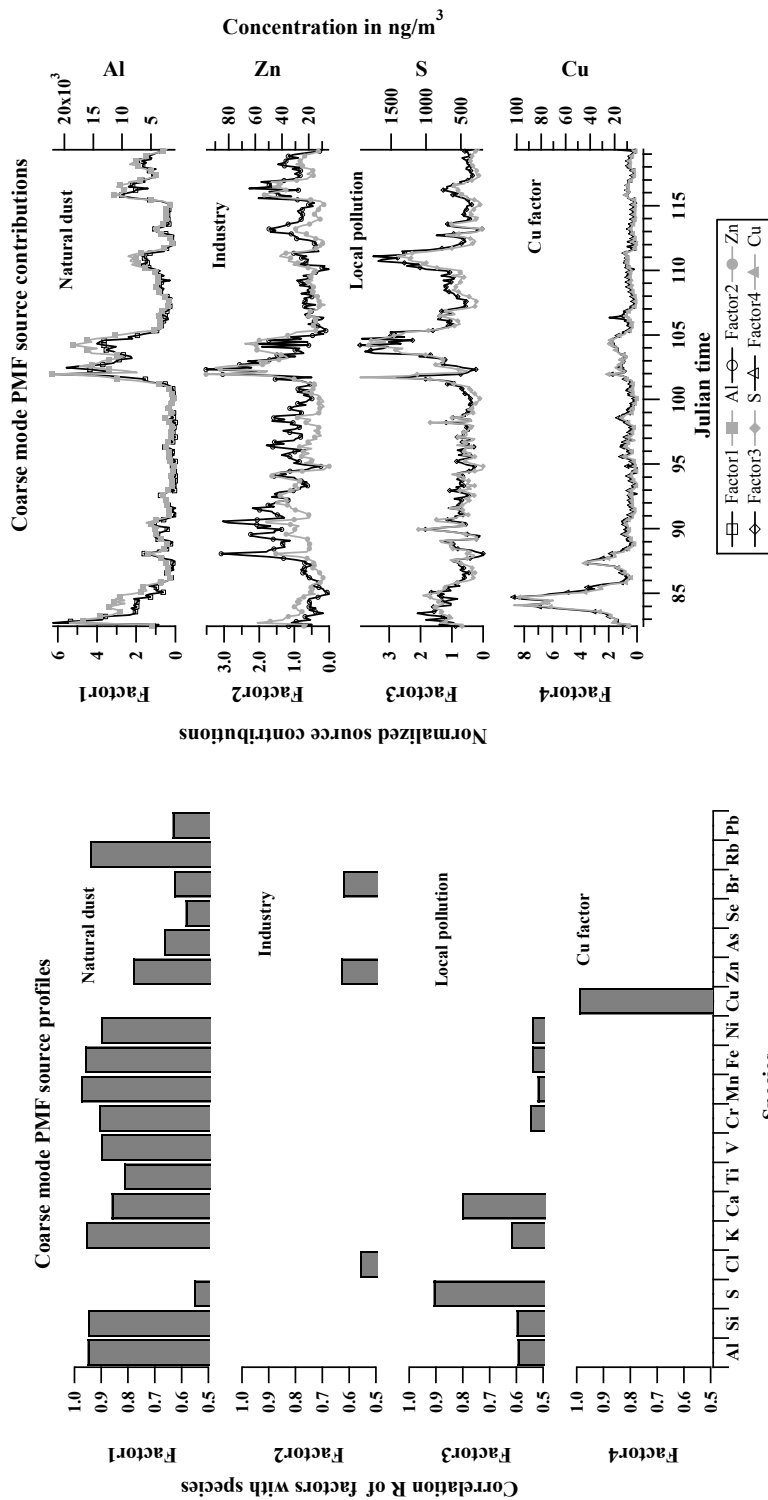


Figure 2.4 Coarse mode Positive Matrix Factorization (PMF) results (a) Source profiles (b) Source contributions

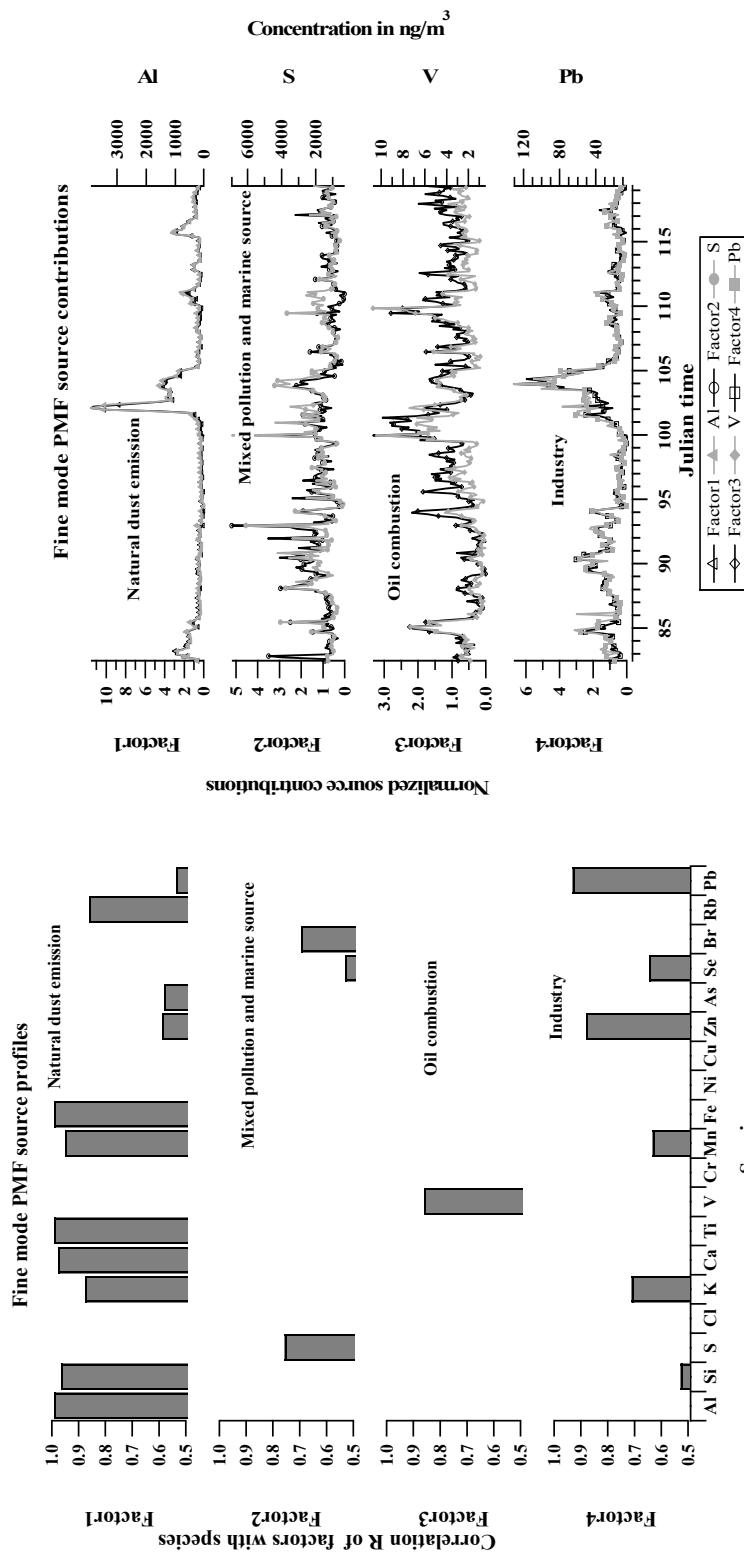


Figure 2.5 Fine mode Positive Matrix Factorization (PMF) results (a) Source profiles (b) Source contributions

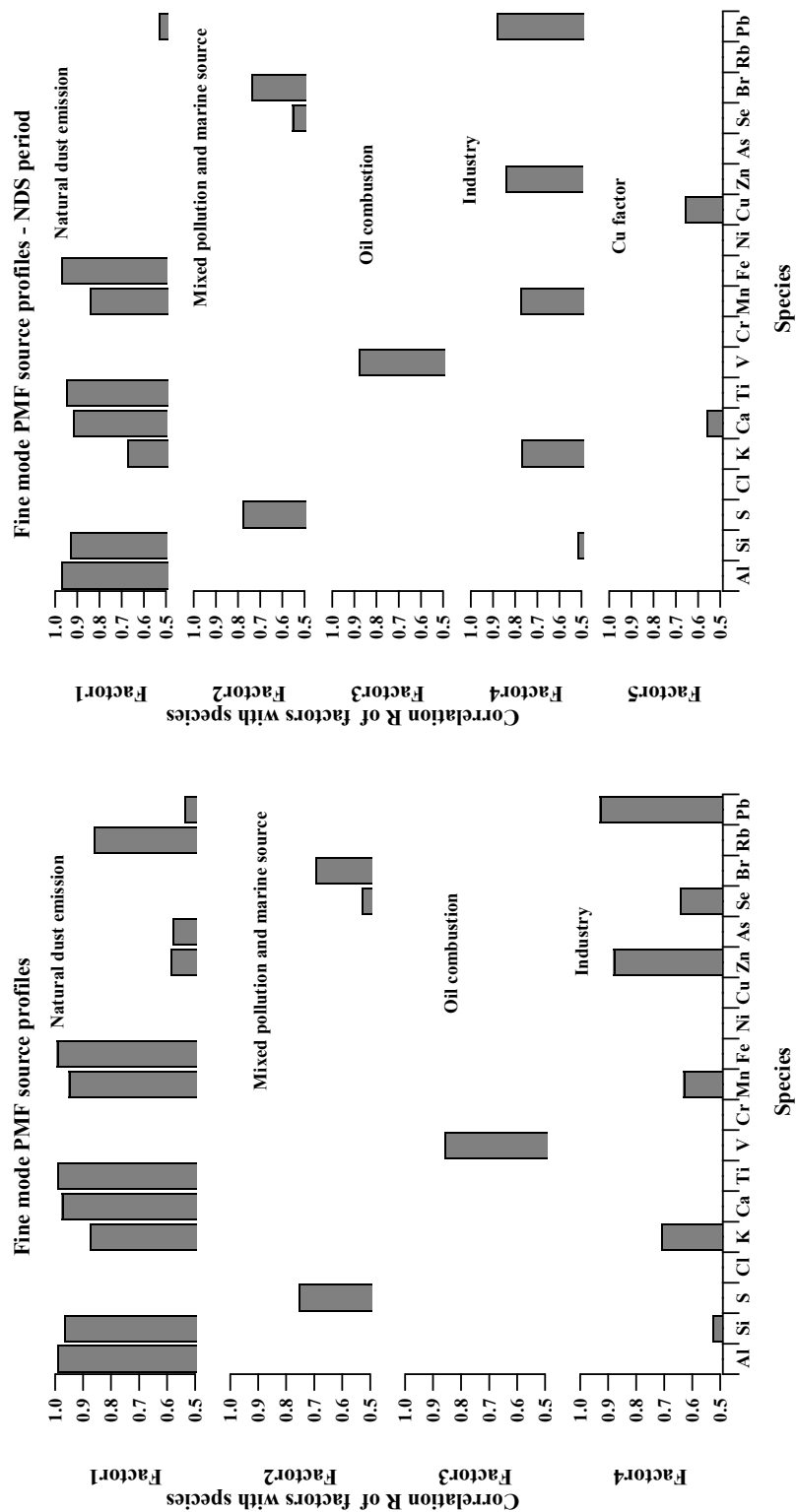


Figure 2.6 Comparison of PMF source profiles (a) Entire measurement period (b) NDS period

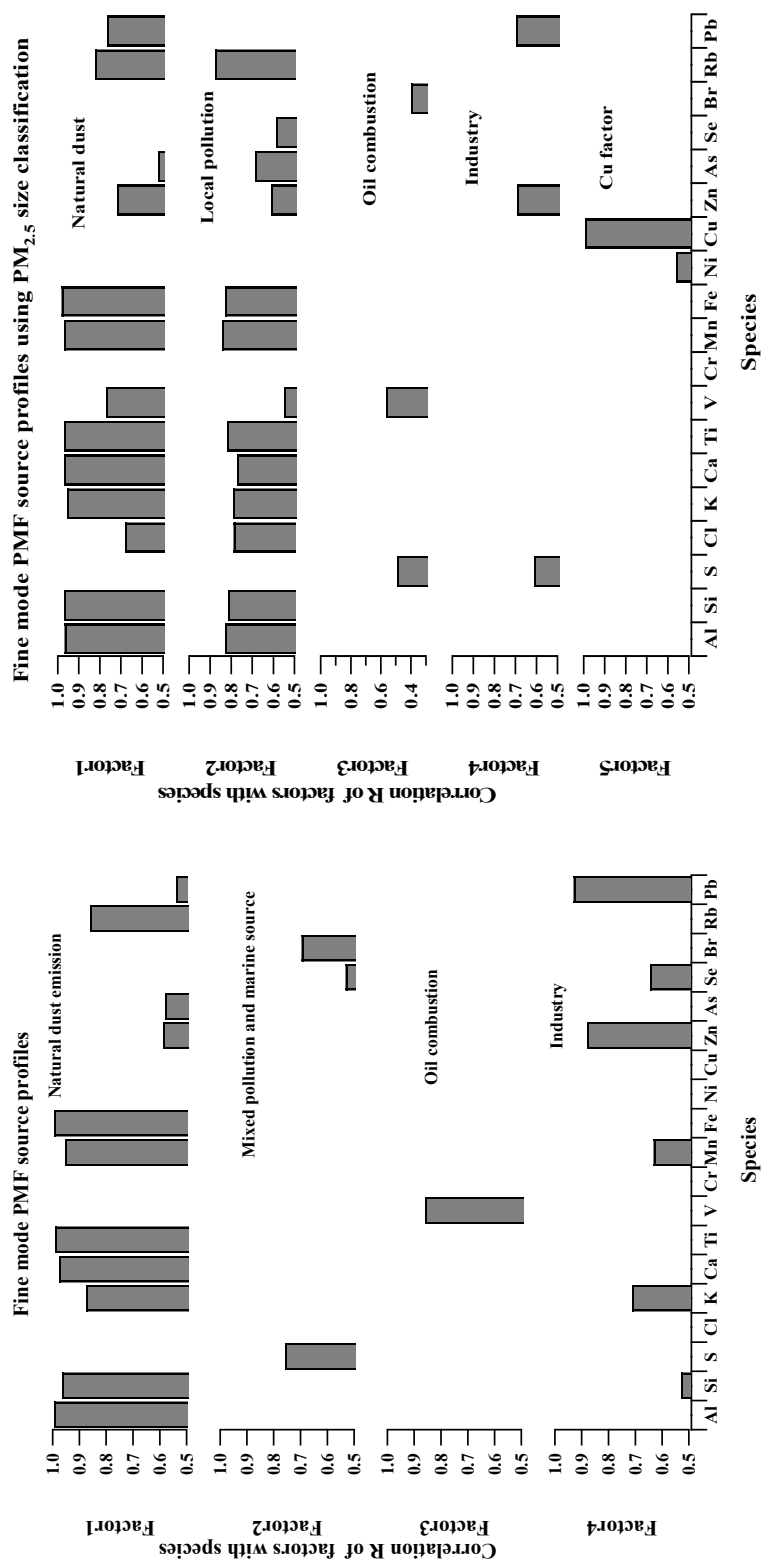


Figure 2.7 Comparison of PMF source profiles (a) PM₁ fine classification (b) PM_{2.5} fine classification

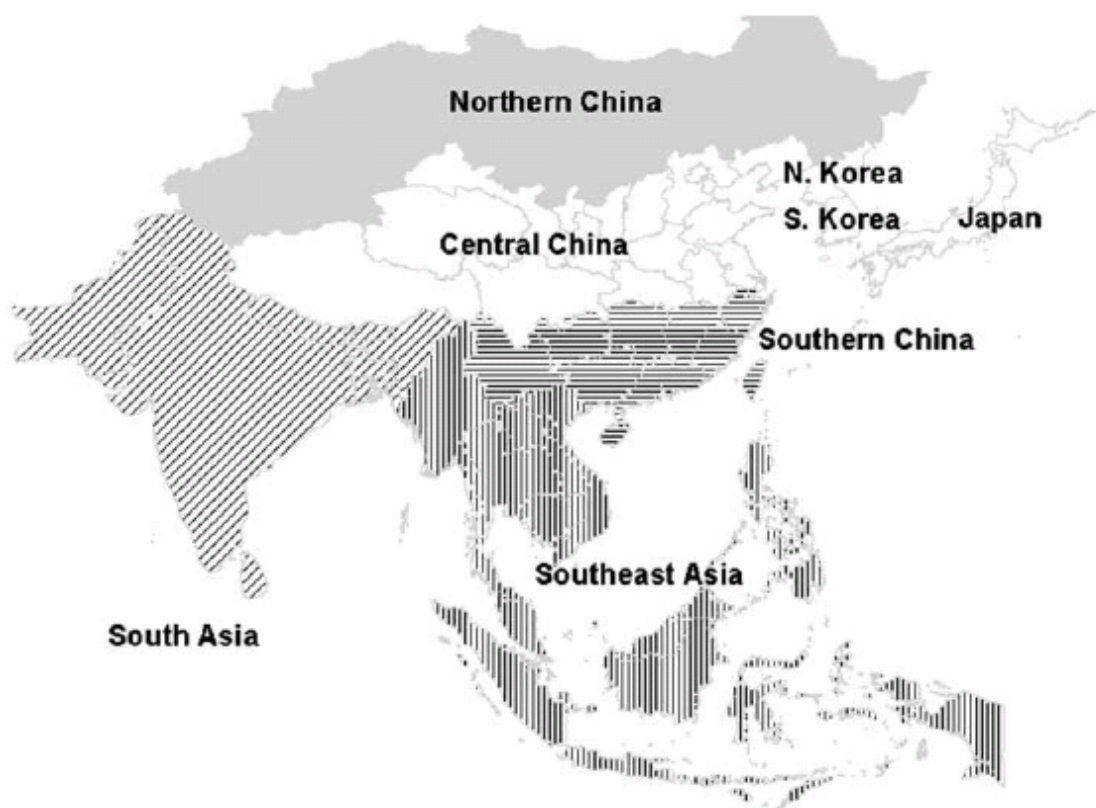


Figure 2.8 Geographic location of the source regions used in the PSCF domain

Source: Streets, D. G., K. F. Yarber, J. H. Woo and G. R. Carmichael (2003). "Biomass burning in Asia: Annual and seasonal estimates and atmospheric emissions." *Global Biogeochemical Cycles* 17(4).

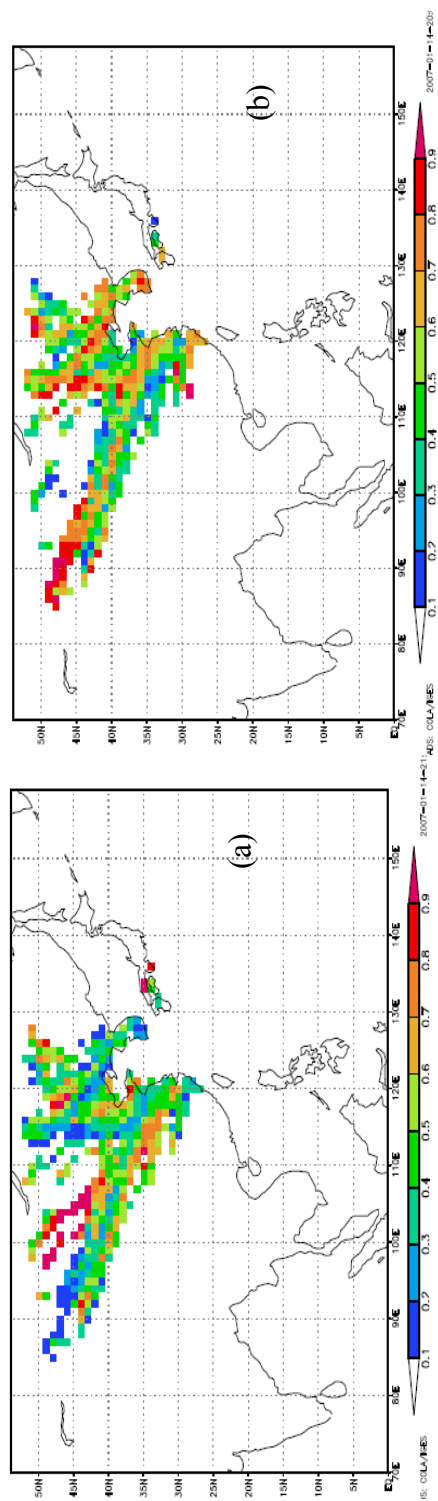


Figure 2.9 PSCF maps of source areas representing the mixture source of sea salt and anthropogenic pollution source in fine mode (a) Source areas for contribution value > 1 (b) Source areas for contribution value < 1

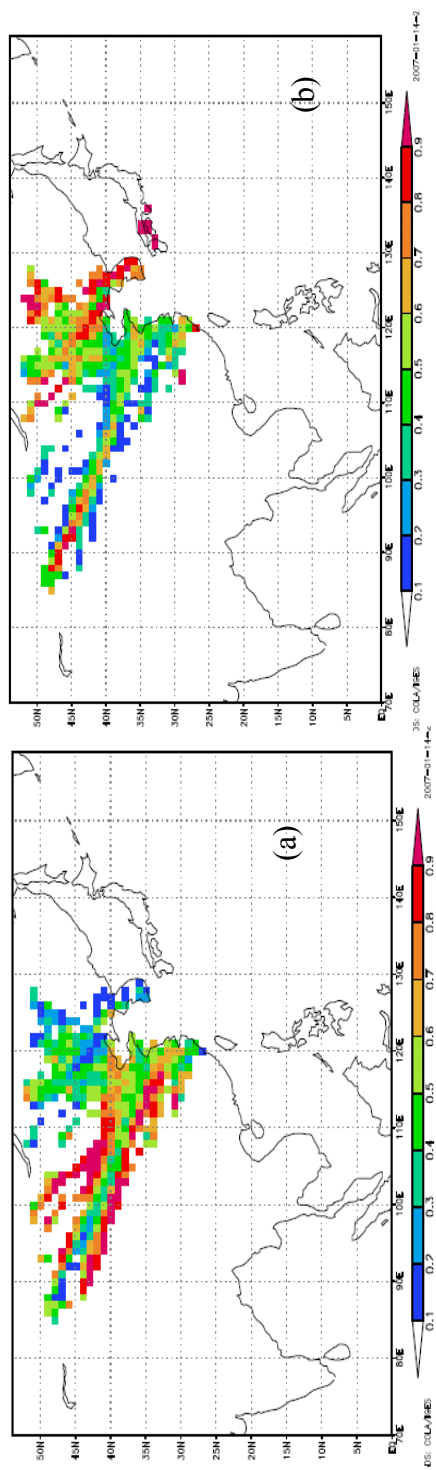


Figure 2.10 PSCF maps of source areas representing the industry source with Pb as leading tracer in fine mode (a) Source areas for contribution value > 1 (b) Source areas for contribution value < 1

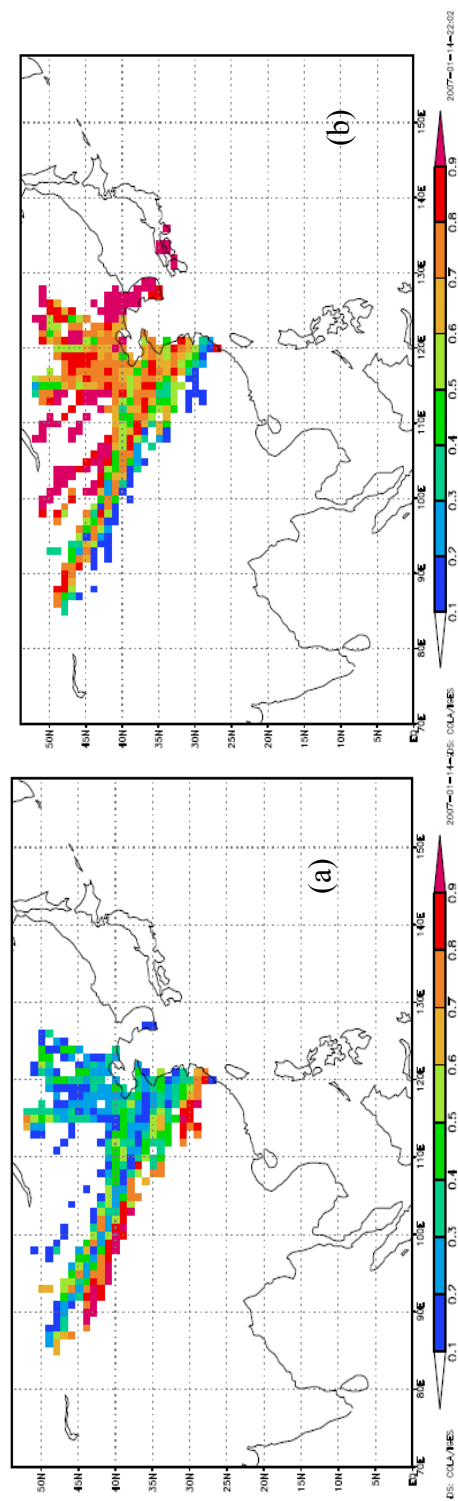


Figure 2.11 PSCF maps of source areas representing the natural dust emission source with Al as leading tracer in fine mode (a) Source areas for contribution value > 1 (b) Source areas for contribution value < 1

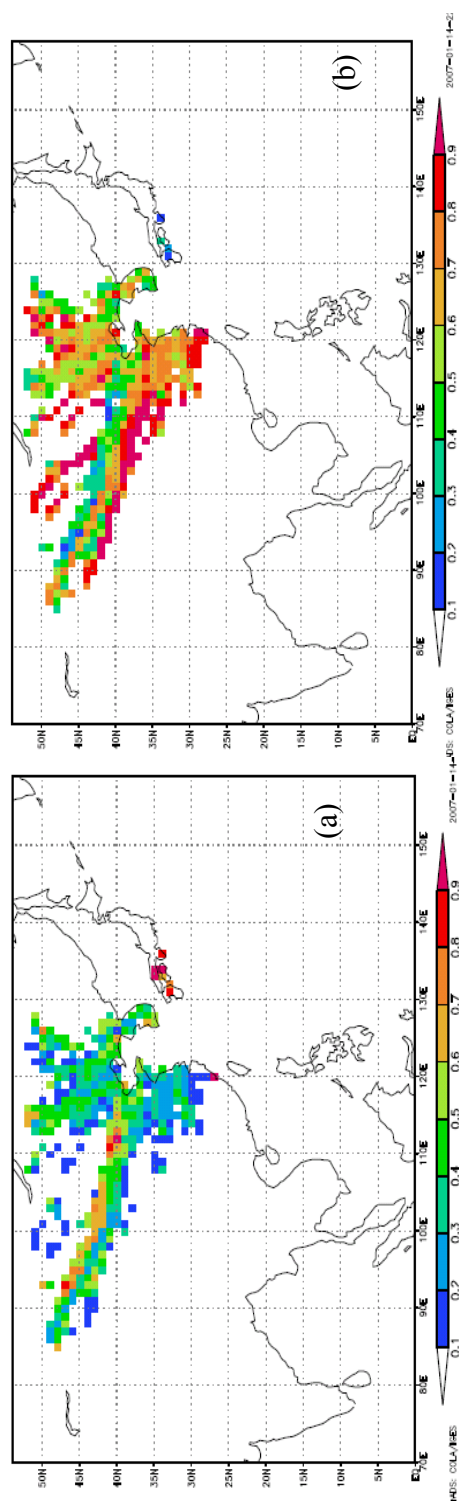


Figure 2.12 PSCF maps of source areas representing the oil combustion source with V as leading tracer in fine mode (a) Source areas for contribution value > 1 (b) Source areas for contribution value < 1

CHAPTER 3
UNDERSTANDING THE INTER-CONTINENTAL
TRANSPORT OF AEROSOLS DURING SPRING 2008: A
REGIONAL SCALE MODELING STUDY

3.1 Introduction

Aerosols are ubiquitous components of the atmosphere that are linked to various adverse impacts including visibility degradation, alteration of cloud properties and affecting the radiative balance of the atmosphere (Seinfeld *et al.*, 1998). Although aerosols impact the atmosphere in several different ways, the magnitude of the impacts remains uncertain (Koch *et al.*, 2007). Numerous modeling and observational studies have shown that the concentration of aerosols at a particular location is influenced by natural, anthropogenic and long-range transport emissions (TF-HTAP 2007; Liu *et al.*, 2009). The present global emissions are capable of creating pollution levels that exceed the air quality standards through out the Northern Hemisphere (TF-HTAP 2007; NRC 2009). The rapidly increasing global emissions when coupled with suitable meteorological conditions may offset the domestic mitigation strategies to reduce aerosol emissions (Liu *et al.*, 2009).

Recent studies have focused on the intercontinental transport (ICT) of aerosols, which is defined as transport of air pollutants from a source continental (e.g. Asia) to receptor continent (e.g. North America) (Yienger *et al.*, 2000; Liang *et al.*, 2004; Park *et al.*, 2004; Liu *et al.*, 2005; Chin *et al.*, 2007; Liu *et al.*, 2008). The ICT of aerosols leads to increase in concentration during large scale episodic pollution events or by contributing to enhancement of background concentration. (Background concentration is defined as the concentration that exists in absence of anthropogenic emissions at a location). The background concentration of a species is determined by long transport times and mixing of air masses from various source regions. In essence, the background

concentration of a species represents the spatial influence of several episodic transport events on a large time scale. Park *et al.*, (2004) found that over 30% of the background concentration of sulfate in North America has Asian origin. Chin *et al.*, (2007) have shown the pollution from Africa and Europe travel eastward and merge with the Asian pollution before reaching North America. The spatial extent of the influence of ICT of aerosols depends on various factors including wind speed, precipitation, frontal activity and global distribution of emissions (Holloway *et al.*, 2003). The impact of ICT of aerosols on the atmospheric column aerosol loadings is relatively higher when compared to the surface concentrations (TF-HTAP 2007).

The emission regions of Asia and North America are located at the origins of the North Pacific and North Atlantic mid –latitude cyclone tracks that are capable of lofting the pollutants into the free troposphere facilitating efficient and rapid transport of air pollutants to the downwind continents (TF-HTAP 2007). Aerosols transported into the free troposphere travel faster and longer distances than the pollutants in the boundary layer due to higher wind speeds and relatively lower particle loss mechanisms. The ICT of aerosols from East Asia is at its peak during springtime when prevailing cold fronts vent the pollutants from the boundary layer to lower free troposphere which is followed by the rapid westerly flow that transports the pollutants across the Pacific before influencing North America (TF-HTAP 2007; NRC 2009). This transport mechanism was confirmed by recent field campaigns including TRACE-P (Jacob *et al.*, 2003) and INTEX-B (Singh *et al.*, 2009).

The transoceanic transport of biomass burning aerosols from Southeast Asia is considered to be one of the major sources leading to enhanced CO and ozone over the North and Central Pacific (Pochanart *et al.*, 2004). Koch *et al.*, (2005) found that Black Carbon (BC) from Southeast Asia contributes largely to Arctic BC and is one of the major causes of Arctic Haze. In addition, the seasonal variability of the pollution transport mechanism in Asia is governed by Monsoon system (Pochanart *et al.*, 2004).

Similar to Asian pollution transport to US, the warm conveyor belts transport pollution from the US boundary layer to Europe in the upper troposphere (NRC 2009). A minor portion of the US pollution is also advected across the boundary layer to Europe via trans-Atlantic pathway and significantly impacts the concentration of aerosols over Europe (Holloway *et al.*, 2003). Studies have shown that the trans-Eurasian transport of pollution from Europe occurs at high latitudes and low altitudes, and contributes to aerosol enhancements over Eurasia and East Asia (Pochanart *et al.*, 2004).

There is a great need for understanding the influence of the inter-continental transport of aerosols on regional/local air quality, which requires establishing the ICT source receptor (S/R) relationships. The Task Force on Hemispheric Transport of Air Pollution (TF-HTAP) was established in 2004 by United Nations Economic Commission for Europe, New York and Geneva (UNECE) to obtain best estimates of inter-continental S/R relationships of aerosols to enhance the current understanding of the hemispheric transport of air pollutants. The TF-HTAP coordinated modeling intercomparison experiments by analyzing the global model results of perturbing the emissions by 20% in four major source regions including Europe (EU), South Asia (SA), East Asia (EA) and North America (NA) on an annual basis. The expected regional emissions changes in the next decade are in the order of 20%. In addition, the 20% perturbation magnitude responds in a more linear fashion (TF-HTAP 2007).

The goal of this study is to understand the hemispheric and inter-continental transport of aerosols from a regional modeling perspective using the tracer version of the STEM model. We discuss the results of perturbing the emissions by 20% in the major source regions used in the TR-HTAP analysis and their influence on receptor continents during spring 2008, which had coincident measurements from the Arctic Research of the Composition of the Troposphere from Aircraft and Satellites (ARCTAS) field campaign (Jacob *et al.*, 2009). This chapter is organized as follows. The STEM model is described briefly, followed by model performance evaluation using ARCTAS DC8 aircraft

observations and surface measurements at Lidar Station Teplokluchenka, Kyrgyz republic in Central Asia. The emission perturbation experiments results are discussed with emphasis on Black Carbon (BC) and sulfate aerosols and their influence on surface concentrations. We also discuss how the remote locations like the Arctic are influenced by the emission perturbations in these major source regions.

3.2. STEM Model Description

The STEM model is a regional scale chemical transport model, and was used in flight planning during the ARCTAS field campaign. In the past, the STEM model has been used in several other field campaigns including TRACE-P/ACE-Asia (Carmichael *et al.*, 2003; Tang *et al.*, 2004), ICARTT (Mena-Carrasco *et al.*, 2007; Tang *et al.*, 2007), INTEX-B (Adhikary *et al.*, 2009), ITCT (Tang *et al.*, 2004) and PACDEX (Stith *et al.*, 2009). The STEM model was developed at the University of Iowa in early 1980's (Carmichael *et al.*, 1986). The STEM model is flexible and can be mapped to any projection based on the input meteorological model. For this study the STEM computation domain has been to 60x60km horizontal resolution with 249x249 grid cells with 31 vertical layers up to 10 hPa. The domain is centered over Arctic region and includes the major emission regions of North America, Europe, East Asia and part of South Asia. The Weather Research Forecasting (WRF-ARW) meteorological model provided the meteorological input every 6 hours with meteorological input from National Center for Environmental Prediction (NCEP) Global Forecasting System (GFS) with 1°x1° resolution provided the initial and boundary conditions along with ice sheet coverage (D'Allura 2009). The NCEP SST (Sea Surface Temperature) analysis was incorporated according to Hines *et al.*, (2008), who developed the polar-optimized version of WRF. The WRF single moment 5-class microphysics, the Kain-Fritsch subgrid-scale cumulus scheme, the Noah Land Surface Model, and MYJ boundary layer

parameterization were some of the specific settings used for this Arctic centered domain based on the recommendations of Hines *et al.*, (2008).

We used the 2008 ARCTAS pre-mission emission inventory developed by David Streets, in support of the ARCTAS field campaign. This inventory is a composite data set of global emissions and includes the emissions of the BC, CH₄, CO, CO₂, Hg, NH₃, NO_x, OC, SO₂, and VOC by three categories including anthropogenic, biomass and international shipping. Further details on this emission inventory can be found at the <http://www.cgrer.uiowa.edu/arctas/emission.html>. The emission distributions of anthropogenic SO₂, CO, BC and OC interpolated to the STEM modeling domain from Streets emissions inventory, are shown in figure 3.1. East Asia has the highest emission densities for all anthropogenic emissions as seen in the figure. The South Asia region has high carbonaceous aerosol emissions consistent with the regional pattern of widespread biofuel usage. BC and OC follow a similar emission distribution. The daily emission forecasts from biomass burning available from RAQMS modeling group during the ARCTAS campaign were used in this study. Figure 3.2 shows the monthly mean biomass CO distribution for April 2008. The biomass burning activity was witnessed in the regions of North America, North Asia (> 40N) and South Asia (< 40N) during this period.

Dust and sea salt emissions were calculated online in STEM based on the parameterization described by Tang *et al.*, (2003) and Gong (2003), respectively. The dry deposition of aerosols was modeled using the ‘Resistance in Series Parameterization’ (Wesley *et al.*, 2000). The dry deposition of sulfate was calculated and all other aerosols were scaled to sulfate. Similarly the wet deposition was calculated for sulfate based on precipitation rate and other species were scaled to it. The hydrophobic and hydrophilic BC and OC are initialized and converted to hydrophilic tracers using a fixed aging rate of $7.1E-6 \text{ sec}^{-1}$ (Adhikary 2008). Sulfate is calculated using SO₂ conversion parameterization with rates between 1 and 10% per hour as used in the ACE- Asia

analysis (Uno *et al.*, 2003). We have used fixed top and lateral boundary conditions similar to previous STEM model studies (Carmichael *et al.*, 2003).

The base case model was run with the settings mentioned above. The emission source regions for the perturbation experiments were defined as East Asia (EA, 96-155E, 14-48N), North America (NA, 124-60W, 12-50N), Europe (EU, 8W -50E, 26-65N) and South Asia (SA, 52 – 94E, 7-33N). The gridded ARCTAS emissions of BC, OC, SO₂ and CO were increased by 20% for each region defined above individually keeping the rest of the inventory constant. The perturbed emissions were then gridded to the STEM domain and series of modeling runs were conducted to assess their impact. The STEM model was run separately for each source region perturbed emissions to study its impact on the other three source regions and on the entire domain. The next section discusses the base case model results evaluated against the observations from ARCTAS campaign and surface measurements from the Lidar surface site in Central Asia.

3.3 Results and Discussion

3.3.1 Evaluation of WRF Meteorology

Figure 3.3 shows the modeling domain of the WRF-STEM model with ARCTAS DC-8 flight tracks from spring and summer portions of the campaigns overlaid on it. The figure also shows the location of the Lidar Station Teplokluhenka (Kyrgyz Republic) surface measurement site, which is discussed later in the paper. The WRF meteorological model performance is evaluated by comparing with DC-8 aircraft observations from the ARCTAS campaign. The comparison of key meteorological parameters which influence the chemical transport including the temperature, Relative Humidity (RH), wind speed and wind direction, with DC-8 observations is shown in figure 3.4. The observed and modeled values are binned by flight altitudes every 1000 m in figure 3.4. The variability seen in the observed temperature altitude profile is captured well by the model except at altitudes below 1km where the model shows a positive bias as seen in top left panel. The

RH comparison is not a robust evaluation of WRF prediction skills since RH is calculated using a parameterized equation in the STEM meteorological preprocessor. Nevertheless, we show the RH comparison, as it is important for chemical transport. The model does reasonably well in capturing the RH vertical distribution in the lower troposphere but displays a large negative bias at altitudes above ~ 4 km. This behavior is due to the complex ice and cloud formation properties at high altitudes in the polar region during spring time. The WRF model deviates from the observed RH when the temperature is below ~ 250 K. The model captures the observed wind speed well with a small negative bias. The comparison of observed and modeled wind direction shows that the model exhibits a slight negative bias across all the altitudes. Similar behavior is seen in the comparison of data from summer campaign as seen the figure 3.4 except that the negative bias in RH is seen at altitudes above ~ 6 km due to higher temperatures in summer when compared to spring. Overall the WRF model shows appreciable skill in capturing the variability seen in the observations, suggesting that the large scale transport patterns are well represented in the WRF simulations.

3.3.2 Comparison with ARCTAS DC8 Aircraft

Observations

The long range transport of aerosols across the Pacific occurs in relatively discrete plumes across the Pacific during spring time (Adhikary *et al.*, 2009). While the observations show that the transport often occurs in more discrete layers, the CTMs tend to spread them in vertical layers of the atmosphere and substantially alter the average vertical profile of modeled aerosols. This leads to considerable differences between the observed and modeled aerosol vertical profiles. Figure 3.5 shows the comparison of observed and modeled values of BC, SO₄ and SO₂. The top three panels show the comparison for the spring portion of the ARCTAS campaign. The model is able to capture the magnitude of BC observation with a low positive bias at altitudes below

~5km, but substantially overpredicts at higher altitudes as seen in figure 3.5. The top second panel shows the comparison of observed and modeled SO₄. The model does well in capturing the observed magnitude and variability with a low negative bias at altitudes below ~6km. At higher altitudes, the model shows relatively larger positive bias. The low negative bias can be explained by the systematic underprediction of modeled SO₂ when compared to observations. The SO₂ underprediction in part could be attributed to low values of SO₂ emissions in the current emissions inventory. The overprediction of aerosols at higher altitudes could be related to the underprediction of RH at those altitudes leading to an underestimation of in-cloud scavenging. The model captures the trend but tends to overpredict BC, SO₄ and SO₂ for the summer portion of the ARCTAS campaign as seen in the bottom panels. Since summer is intense biomass burning season, it is possible that the model is over estimating the contribution from RAQMS daily biomass burning emissions to BC concentration. Additional model runs will be performed without the daily biomass burning emissions to assess their impact in the near future. In addition, our prior experience with INTEX-B observations, we found that there was a huge difference between the preliminary and final versions of aircraft observations. The observed and modeled data discrepancy for the summer portion can be partly attributed to the fact that ARCTAS observations used in this analysis are still preliminary data. The model will be further evaluated when the final version of ARCTAS observations become available.

3.3.3 Comparison with Surface Observations

Aerosol PM mass observations were available at the ground based measurements sites of Lidar Station Teplokluchenka (LST) in the Kyrgyz republic through the EPA PM Measurement and speciation study. Figure 3.6 shows the comparison of observed and modeled PM₁₀, PM_{2.5}, BC and temperature at Lidar site in Central Asia during spring and summer of 2008. (April 1 to September 30 2008). The observed PM_{2.5} and temperature

were available during spring, while the PM_{10} and BC were only available for summer. The modeled $PM_{2.5}$ and temperature are underpredicted but are able to capture the temporal variability well seen in observations. The modeled PM_{10} closely matches the observations as seen in the third panel of the figure. Since summer season is associated with profound biomass burning activity, the modeled biomass CO and MODIS AOD is also overlaid on the PM_{10} and BC plots. The modeled values capture the base line observed BC fairly well. The model shows enhancement in BC at times that corresponds to the peaks in biomass CO around August 28 2008, suggesting influence of biomass burning emissions. However, this enhancement was not seen in observed values. But the MODIS AOD shows an increase in AOD value to 0.6. It is possible that this biomass burning was seen only at altitudes above the surface. Due to model displacement errors, this peak is seen at the surface in the modeled biomass CO. The peak at September 16 is associated with biomass burning as seen from both the observations and model. More detailed analysis of the origin of the air masses associated with the different peaks will be conducted using backward trajectories in combination with regional source tagged tracers. Overall, the model performs adequately in simulating the aerosols as seen in the comparison of modeled aerosols with aircraft and surface observations described above. The regional distribution of aerosols in the modeling domain will be discussed next.

3.3.4 Regional Distribution of Aerosols

Sulfate and BC, the major contributors to $PM_{2.5}$ aerosols, can be transported across continents and have varied emission sources. Sulfate is produced by the oxidation of SO_2 , which is associated largely with fossil fuel combustion emissions. BC has additional emission sources including biofuel and biomass burning. Sulfate and BC are important to study the health impacts of $PM_{2.5}$ aerosols. In addition, both are important climate forcing agents as BC absorbs the solar radiation, while sulfate scatters solar radiation, which have implications to atmospheric aerosol radiative forcing. So the results

of the emission perturbation runs are focused on BC and SO₄. The regional distribution of monthly mean sulfate and BC at the surface for April 2008 is shown in figure 3.7. The surface concentration of sulfate over East Asia is two times higher than that seen over eastern US and Europe. This is caused by higher SO₂ emissions in the region and relatively faster SO₂ oxidation rates. The magnitude of sulfate outflow from East Asia over the Pacific is comparable to the values seen in Eastern US and Europe. The Indo Gangetic plain in South Asia also shows high sulfate concentrations at the surface. The regional distribution also identifies East and South Asia as the pollution hotspots. The BC concentration over East Asia is almost 2-3 times higher than that seen over the surface at continental US. This study shows an enhancement in BC for regions between 40 and 60N (which was not seen in sulfate distribution), suggesting the strong impact of the biomass burning on the aerosol loadings at higher latitudes during the spring season.

The different pathways that transport aerosols across the Northern Hemisphere during spring are illustrated in figure 3.8 using sample trajectories colored by altitude during April 2008. Ten day forward trajectories at 40N from three different longitudes including 130E (East Asia), 100W (North America) and 30E (Europe) are shown in left panel of figure 3.8. It is evident from the figure that the pollution from East Asia can reach North America via the Pacific route, the US pollution is transported to Europe by passing over the Atlantic and the European pollution can significantly impact the Central and East Asia between 40 and 60N latitudes under favorable meteorological conditions. Figure 3.8 also shows the ten day back trajectories from the same longitudes as used previously but at 80N, suggesting that transport of pollution major source regions to the Arctic during spring which will be discussed in more detail later in later sections. The transport pattern of pollution to the Arctic can also be seen in the right panel of figure 3.8, which displays the five day back trajectories from the ARCTAS DC8 flight 10 on 17 April 2008 that sampled over the North Pole.

To further understand the relative magnitudes of sulfate and BC across the domain, the altitude- latitude cross sections are shown at 130E (exit boundary of East Asia), 125W (entrance boundary of North America), 70W (exit boundary of North America) and 10W (entrance boundary for Europe) for sulfate and BC in figures 3.9 and 3.10. Sulfate enhancements can be seen from surface up to ~5km between 30-50N at 130 E consistent with the high SO₂ emissions in East Asia. The surface concentration of sulfate for the same latitudes at 125 W is 3-4 times less than the values seen at 130E. However, the concentrations aloft between 6 – 8 kms are much closer. The concentration gradient across different altitudes suggests that the majority of the SO₂ emissions occur in the boundary layer, resulting in efficient sulfate deposition across the Pacific. However the emissions that are lofted out of the boundary layer get transported across the Pacific at higher altitudes and their influence is seen in the outflow regions at higher altitudes. It can be inferred from this discussion that pollution transport impacts at the receptors above the surface are higher than that at the surface. The North American outflow at its exit boundary 70W shows enhancements up to ~5 km. The sulfate values at the incoming boundary of the European outflow are lower at the surface as seen in bottom right panel. However, the concentration gradients seen here are much lower than that seen at 130E - 125W and tend to occur at lower altitudes within and slightly above the boundary layer. This is again consistent with the discussion in the introduction about the alternate transatlantic transport pathway of pollution that occurs by advection across the boundary layer. The vertical latitude cross sections of BC follow the similar pattern. However the concentration gradients of BC between 130E and 125W are higher compared to sulfate. It is important to point out that for the Arctic region (70N and above), the concentrations of sulfate and BC are ~ 1-2 and 0.05-0.2 µg/m³ respectively at all altitudes in the cross sections described above. This suggests the significant impact of the major source regions on the Arctic region during the spring season.

3.3.5 Influence of Emission Perturbation in Major Source

Regions on the Regional Distribution of Aerosols

The impact of ICT of aerosols on air quality of the downwind receptor continents was further analyzed by this modeling study. Figures 3.11 and 3.12 show the percent change in sulfate and BC concentrations at surface due to emission perturbation in the source regions. The percent change is calculated using the following expression $(\text{perturbed} - \text{base case}) \times 100 / \text{base case}$. The top left panel in figure 3.11 shows the percent change in sulfate due to 20% emissions increase in EA. It is important to remember that the percent change in concentrations will be determined by which other source regions contribute to sulfate. It can be seen that this increase in East Asian emissions leads to 7-15% increase in the pollutant outflow over the Pacific, 5-10 % increase over the US west and 1-5 % increase over the rest of the US and Atlantic. This suggests that the enhancement in emissions of East Asia will be transported to US and have the potential to offset domestic emission controls for mitigating air quality in the western US regions. The percent change in sulfate due to a 20% increase in North American emissions is shown in top right panel of figure 3.11. The North American outflow concentration changes by 5-15% and the concentration over Europe changes by 1-5 %. It is interesting to note that the percent change in concentration due to North American outflow is much lower when compared to East Asian outflow to North America despite the shorter transport distance. This is due to the difference in the prevailing meteorology and transport mechanism in the two outflow regions mentioned earlier. The bottom left panel shows the percent change due to the perturbation of emissions in Europe. It is evident that the transport of pollution from Europe occurs at high latitudes and has a significant impact on the downwind Central and East Asian regions. The European outflow moves eastward and then takes the northwest direction influencing the outflow over Pacific. This behavior is consistent with the findings of Chin *et al.*, (2007) discussed earlier. The European outflow has high SO₂ emissions when compared to the East Asian outflow due to the

transport mechanism of pollutants primarily occurring in the boundary layer. Consequently, the impact of European SO₂ emissions on the downwind locations is much longer and broader in spatial extent due to slower rates of SO₂ to sulfate conversion because of the prevailing colder temperatures (Chin *et al.*, 2007).

The influence of the South Asian emissions could not be studied extensively due to its proximity to model domain boundaries. It can be seen from the bottom right panel of figure 3.11 that the South Asian emissions are exported towards the East Asia during spring time. However, this transport feature is valid only for the spring season as seasonality plays an important role in the transport of pollution from South Asia which will be discussed further in Chapter 5.

The percent change in BC contributions due to the emission perturbations in the source regions are shown in a similar way as sulfate in figure 3.12. BC tends to follow the similar transport pathway as sulfate but the spatial extent and the magnitude of percent change in BC is lower when compared to Sulfate. For instance the outflow of BC from Europe to the Pacific is much lower than sulfate largely due to the significant role of open burning emissions on BC.

3.3.6 Changes in Source Region Concentration due to Emission Perturbations

The influence of perturbed emissions on the concentrations were studied further by calculating the area average of sulfate and BC concentration for each source region. We have the same domain definitions that were used for perturbing the source emissions described in section 3.2. The monthly mean area averages of sulfate for the source regions from the base and various perturbation runs are summarized in Table 3.1. Figure 3.13 shows that area average monthly mean concentrations from the base case run. It can be inferred from the figure that EA has the highest area average BC and sulfate concentration followed by EU, SA and NA. The area averages of BC and sulfate for EA

region are ~ 2 times higher than NA. This difference in concentrations plays a significant role in determining the influence of long range transport of aerosols from EA during springtime on NA surface concentrations. From a policy perspective, it would be insightful if the impacts of emission perturbations within the region can be compared to the same from outside the region. To obtain a quantitative estimate of ICT S/R relationships, we have implemented the same metrics used in the TF-HTAP results (TF-HTAP 2007) which are briefly described here.

1. The response is defined as the absolute difference in concentration due to changes in the foreign and domestic source regions (Domestic denotes the impact of region on itself and foreign refers to the outside regions).
2. The relative importance of domestic and foreign emissions is discussed using the term “import sensitivity”, which is defined as the sum of the responses from perturbing the emissions in foreign regions divided by the response due to the domestic emission perturbation.

The area average, response and the import sensitivities were calculated for the different emission perturbation runs and are summarized in tables 3.1 and 3.2 for sulfate and BC. Table 3.1 reports the monthly mean area average sulfate concentration and the corresponding response of the perturbed runs. The anthropogenic emissions have the largest impact in the source region itself as seen from the table (values in bold). The monthly mean import sensitivities range from 13 to 31 percent. The NA region import sensitivity is 31% suggesting that one-third of the NA sulfate is contributed by sources coming from outside the region. This value is close to study of Park *et al.*, (2004) who reported that 30% of the background sulfate concentration has Asian origin. There is great uncertainty associated with calculations pertaining to the SA region as only half of the area is covered and is in the vicinity of the model boundaries in this model set up. The area average, response and import sensitivity values for BC are summarized in table 3.2 in a similar manner as sulfate. The magnitude of percent change values of BC are lower

than sulfate all along consistent with the regional concentration distribution described earlier. The import sensitivities vary from 1 to 21 % with a region maximum as high as 42% for NA. This modeling study shows that one-fifth (~21%) of the surface BC concentration for NA region comes from outside the region during spring time.

3.3.7 Impact of Emission Perturbations on the Arctic Region

Arctic haze phenomenon, defined as the blob of pollution engulfing the arctic region during spring time, has garnered a lot of attention in the past few years due to its role in melting the ice areas and potential implications to climate change and radiative forcing (Koch *et al.*, 2005; Generoso *et al.*, 2007a; Generoso *et al.*, 2007a; Quinn *et al.*, 2008; Jacob *et al.*, 2009). Due to the prevailing cold temperatures over the polar region during spring, a massive buildup of long range transported pollutants from the mid-latitudes occurs in the arctic region (Generoso *et al.*, 2007b). One of the main objectives of the ARCTAS field campaign was to understand and analyze the pollution transport pathways into the arctic region (Jacob *et al.*, 2009). Warneke *et al.*, (2009) analyzed the ARCPAC (Aerosol, Radiation and Cloud Processes affecting the Arctic Climate) observations from NOAA WP-3 aircraft in April 2008 and found that the forest fire emissions from Siberia-Lake Baikal area along with the agricultural burning emissions in Kazakhstan- Southern Russia region were transported into the Arctic region. Our modeling study period gave us an opportunity to study the impact of the perturbed emissions on the arctic region during spring.

In this study the arctic region was defined as the region above 66.5 N and all longitudes. The area average of the arctic region from the base case and the corresponding response and percent change in concentrations of sulfate and BC due to emission perturbations in source regions are shown in figure 3.14. It is clearly evident that there is a continued buildup of sulfate and BC concentration, with concentrations

approximately 2 and 3 times their starting values for sulfate and BC. EU region is the largest contributor to Sulfate and BC values to the Arctic region followed by NA and EA regions. Koch et al., 2005 found that that BC from Southeast Asia was the largest contributor to Arctic BC. This study could not ascertain the influence of SA region on the arctic due to the domain definition of SA region and its vicinity to the model boundaries. The temporal variability in the arctic contribution and percent change from emission perturbation is governed by the prevailing meteorology. The top right panel shows the percent change in sulfate due to the emission perturbation in source regions. On average, a 20% emission perturbation in the EU, NA and EA regions causes ~ 5, 2.3 and 1.6 percent change in Arctic sulfate. The same perturbations cause 2.3%, 0.6% and 0.5% change in BC concentrations. This implies that one-fourth of the change in EU region SO₂ emissions gets transported to the arctic region. The findings of this study are significant from a policy perspective and can greatly assist in devising emission mitigation strategies to reduce the transboundary pollution transport to the Arctic.

3.4. Summary

There are rising concerns on the role of ICT of air pollution influence on the surface air quality over the world. Studies have shown the ICT of pollutants is large during the spring season. The ICT S/R relationships are usually obtained from global model studies. The main objective of this work is to study the ICT of aerosols from a regional modeling perspective. In this study, we have the used the STEM regional tracer model to understand the ICT of aerosols on surface air quality during spring 2008. The WRF meteorology evaluated with ARCTAS DC8 aircraft observations was used to drive the transport in STEM model. The STEM model predictions were evaluated using the chemistry measurements from ARCTAS DC8 aircraft and ground based measurements from Lidar site in Central Asia. The STEM model performance was satisfactory in simulating the observations.

The regional distribution of sulfate and BC was analyzed across the domain and identified East Asia as the major hotspot of SO₂ and BC emissions. The BC distribution closely followed the RAQMS biomass BC emissions distribution. The latitude vertical cross sections at the 130E, 125W, 70W and 10W showed that the transpacific transport of pollution from EA to NA occurs at altitudes above the boundary layer, while transatlantic transport of pollution from NA to EU occurred within the boundary layer during spring. The relative impact of ICT of aerosols from the source regions to the downwind receptor regions were studied by conducting model runs using emissions enhanced by 20% in major source regions including EA, NA, EU and SA. This modeling analysis showed that the emission perturbation in EA have significant impacts on the aerosol concentrations over the Pacific and NA. Despite the shorter transport distance, the impact of transatlantic transport of pollution from NA to EU region is lower than the transpacific transport of pollution from EA to NA due to the difference in the transport mechanisms. This modeling study showed that the European pollution travels eastwards and merges with Asian outflow over the Pacific corroborating the findings of Chin et al., 2007. The pollution transport from regions outside NA contributed ~30 and 20% to its sulfate and BC concentration at surface. The STEM model showed a buildup of sulfate and BC over the Arctic throughout the modeling period. The influence of emission perturbations in the source regions on the Arctic was also analyzed and found that EU, NA and EA were the major contributors to Arctic sulfate and BC.

It is important to point out that all the results in this study represent only the spring season. Similar emission perturbation runs for summer (July-September) 2008 have been complete and the analysis is currently underway, which will help us provide insights into the influence of seasonality on the ICT of aerosols. In this study, the modeling analysis was limited to surface concentration distribution. However, the ICT of aerosols influence on the column loadings is much higher than that at surface. Aerosol Optical Depth (AOD) is an important metric to study the impact of ICT of aerosols on the

atmospheric column. Our future work will focus on understanding the influence of ICT on the AOD and columns loadings of species. In summary, this modeling study has provided insights into the ICT of aerosols during spring season at a regional scale.

Table 3.1 Sulfate import sensitivity of source regions for spring 2008: Monthly mean average of sulfate at surface ($\mu\text{g}/\text{m}^3$) –domestic values are shown in bold

| | Receptor region | EA | NA | EU | SA |
|---|-----------------|--------------------|-------------------|------------------|-----------------|
| Base case | | 6.21 | 2.45 | 3.27 | 3.01 |
| Source Regions (whose emissions are perturbed) | EA | 7.12 ± 1.48 | 2.52 ± 0.81 | 3.29 ± 0.45 | 3.02± 0.44 |
| | NA | 6.21±1.25 | 2.76± 0.88 | 3.32±0.44 | 3.02±0.44 |
| | EU | 6.28±1.26 | 2.48±0.79 | 3.79±0.52 | 3.12±0.45 |
| | SA | 6.27±1.25 | 2.45±0.78 | 3.27 ± 0.45 | 3.43±0.5 |

Table 3.2 Sulfate import sensitivity of source regions for spring 2008: Monthly mean response of sulfate ($\mu\text{g}/\text{m}^3$) – Percent change when compared to base is shown in parentheses

| | Receptor regions | EA | NA | EU | SA |
|---|------------------|--------------------|---------------------|----------------------|------------------------|
| Source Regions (whose emissions are perturbed) | EA | 0.9 (14.3%) | 0.07 (2.6%) | 0.01 (.4%) | 0.01 (.14%) |
| | NA | 0 (0) | 0.31 (12.8%) | 0.05 (1.5%) | 0.01 (.27 %) |
| | EU | 0.06 (1%) | 0.03 (1%) | 0.51 (15.6 %) | 0.11 (3.6%) |
| | SA | 0.05 (0.8 %) | 0 (0) | 0 (0) | 0.41 (13.7%) |
| Total import Sensitivity (maximum) | | 13% (18.8 %) | 31% (62.8 %) | 13% (26.5 %) | 31% (54.6%) |

Table 3.3 BC import sensitivity of source regions for spring 2008: Monthly mean average of BC ($\mu\text{g}/\text{m}^3$) at surface –domestic values are shown in bold.

| | Receptor region | EA | NA | EU | SA |
|---|-----------------|------------------|------------------|------------------|-------------------|
| Base case | | 1.82 | 0.28 | 0.42 | 0.63 |
| Source Regions (whose emissions are perturbed) | EA | 1.95±0.51 | 0.29 ±0.08 | 0.42 ±0.09 | 0.63±0.21 |
| | NA | 1.82±0.5 | 0.31±0.09 | 0.42±0.09 | 0.63±0.21 |
| | EU | 1.82 ±0.5 | 0.28 ±0.08 | 0.47 ±0.1 | 0.64 ±0.21 |
| | SA | 1.82 ±0.5 | 0.28 ±0.08 | 0.42±0.09 | 0.68± 0.22 |

Table 3.4 BC import sensitivity of source regions for spring 2008: Monthly mean response of BC ($\mu\text{g}/\text{m}^3$) – Percent change when compared to base is shown in parentheses

| | Receptor regions | EA | NA | EU | SA |
|---|------------------|------------------|---------------------|---------------------|---------------------|
| Source Regions (whose emissions are perturbed) | EA | 0.13 (8%) | 0.004 (1.4%) | 0.0009 (0.2%) | 0 (0) |
| | NA | 0 (0) | 0.027 (10 %) | 0.002 (0.5%) | 0 (0) |
| | EU | 0 (0) | 0.001 (0.4 %) | 0.05 (12.5%) | 0.004 (0.7%) |
| | SA | 0 (0) | 0 (0) | 0 (0) | 0.05 (8.5%) |
| Total import Sensitivity (maximum) | | 0.7% (5%) | 21.3% (42.6%) | 7.6% (18.3%) | 8.9% (19.7%) |

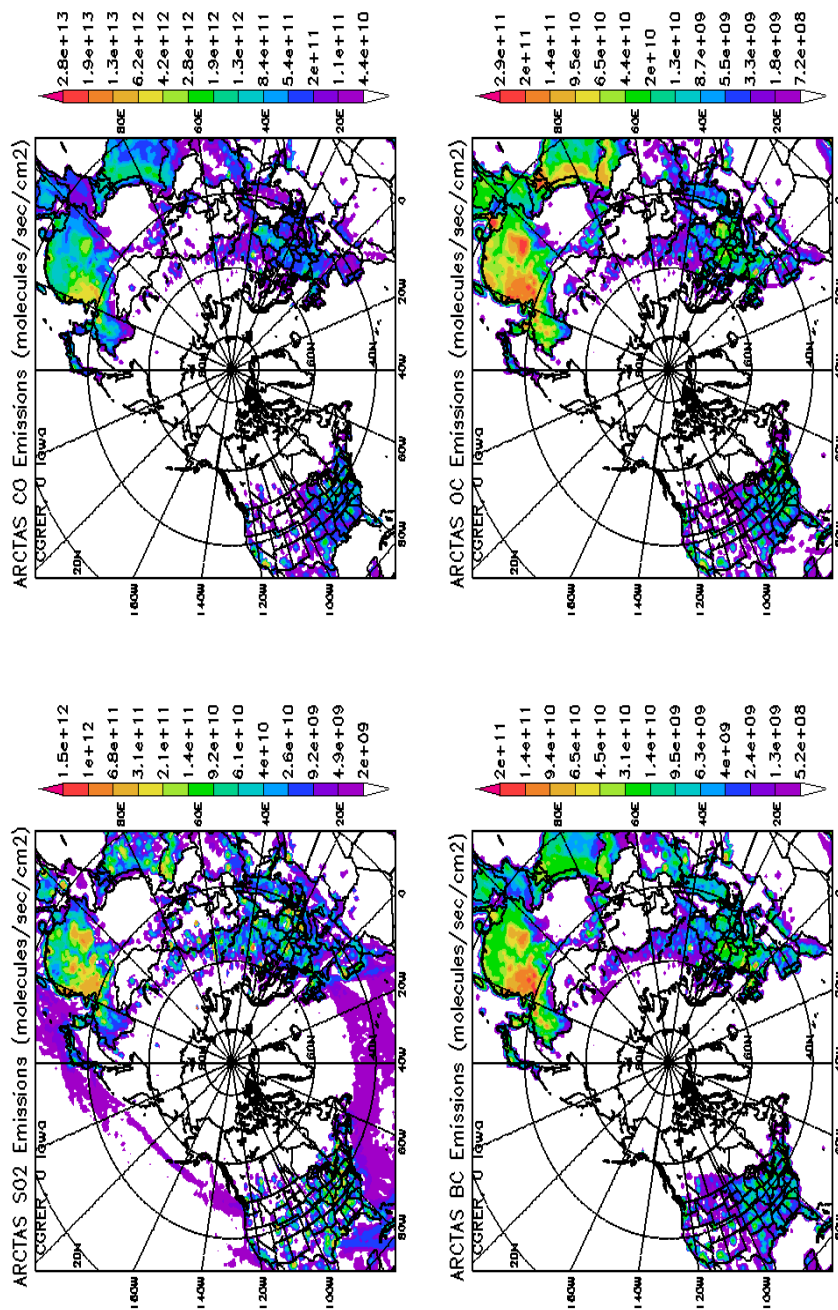


Figure 3.1 Regional distribution of SO₂, CO, BC and OC emissions during spring 2008

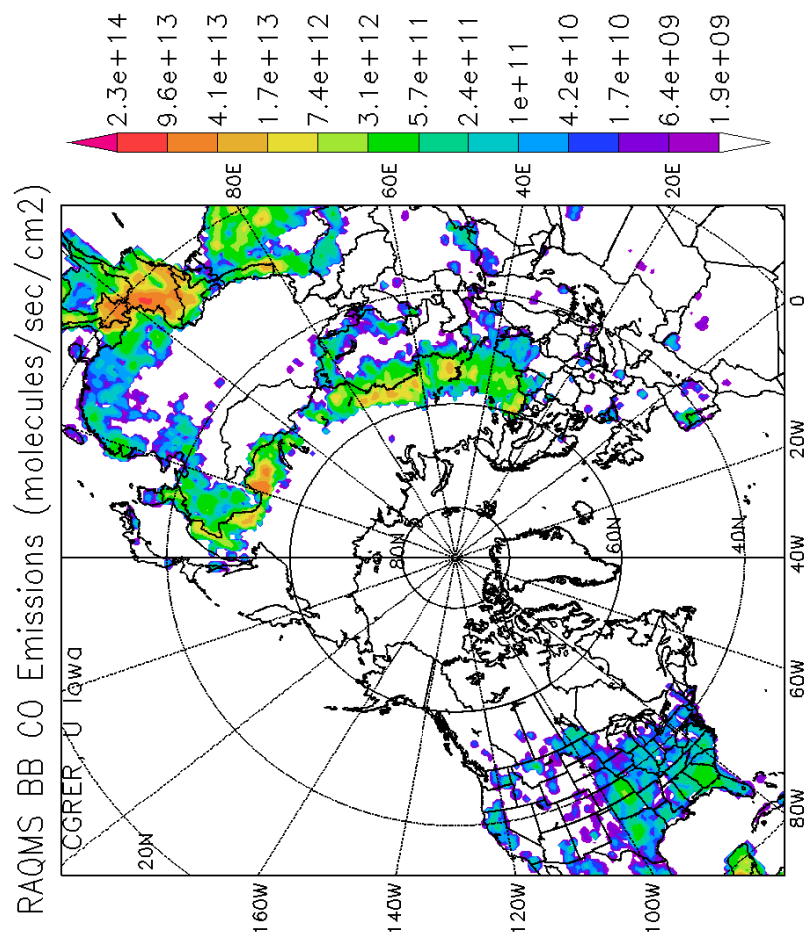


Figure 3.2 Monthly mean biomass burning CO emissions for April 2008

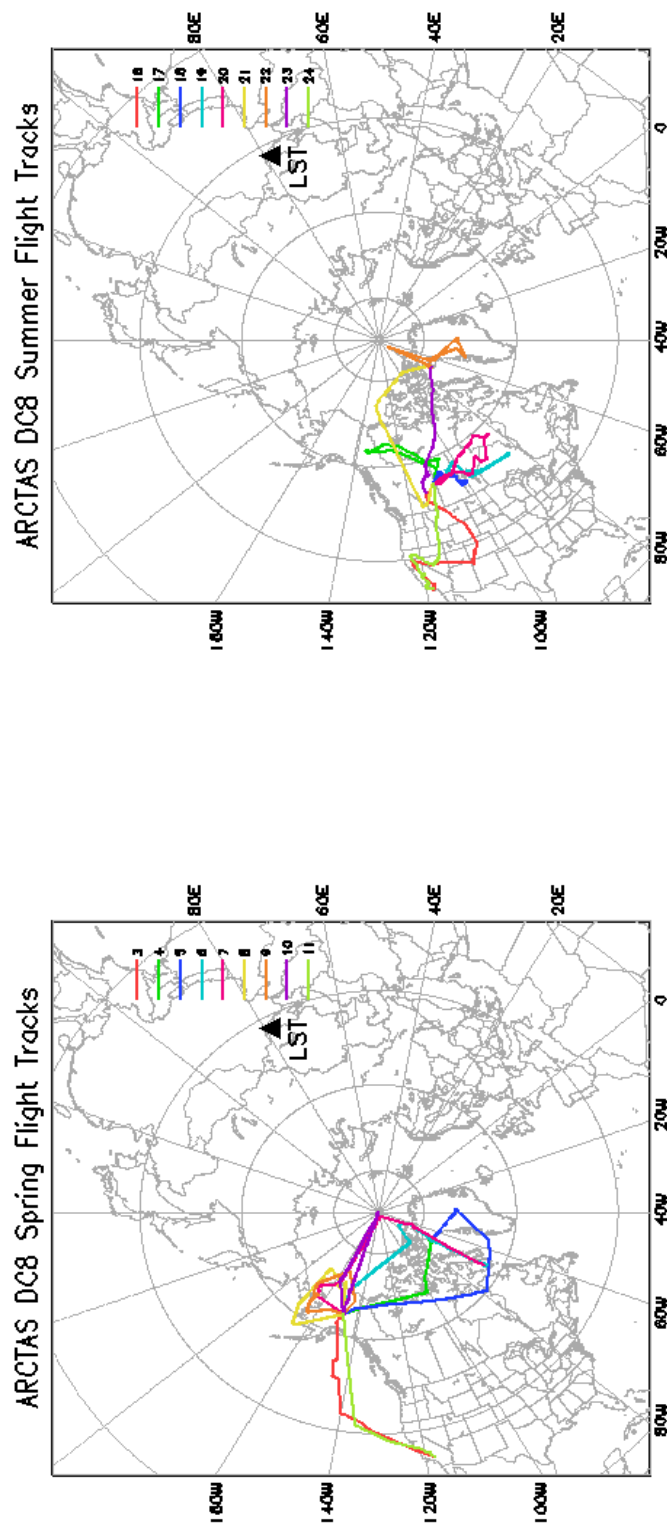


Figure 3.3 STEM model domain for ARCTAS with DC8 flight tracks for spring and summer overlaid along with the Lidar Station Teplokluchenka, Kyrgyz republic.

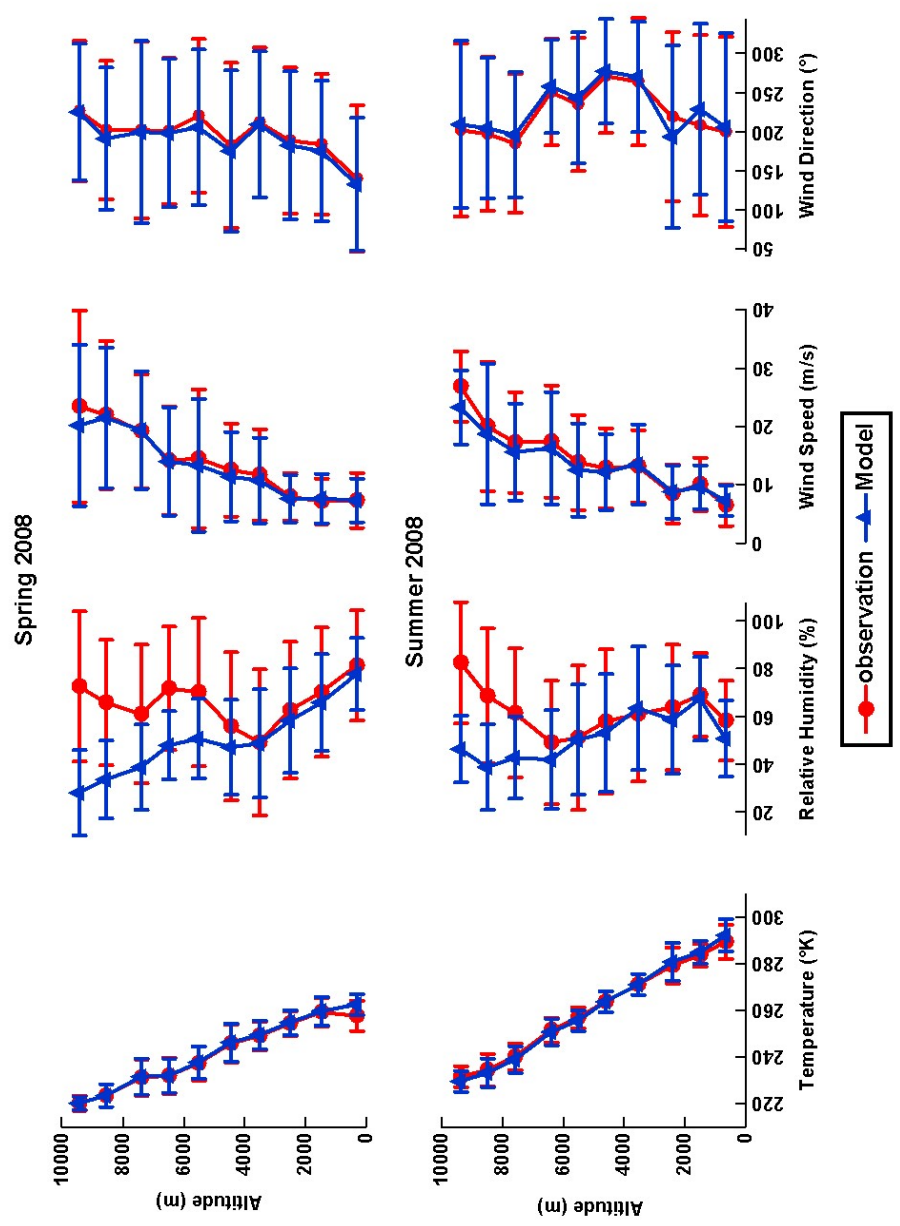


Figure 3.4 Comparison of WRF meteorological variables with ARCTAS DC8 aircraft observations

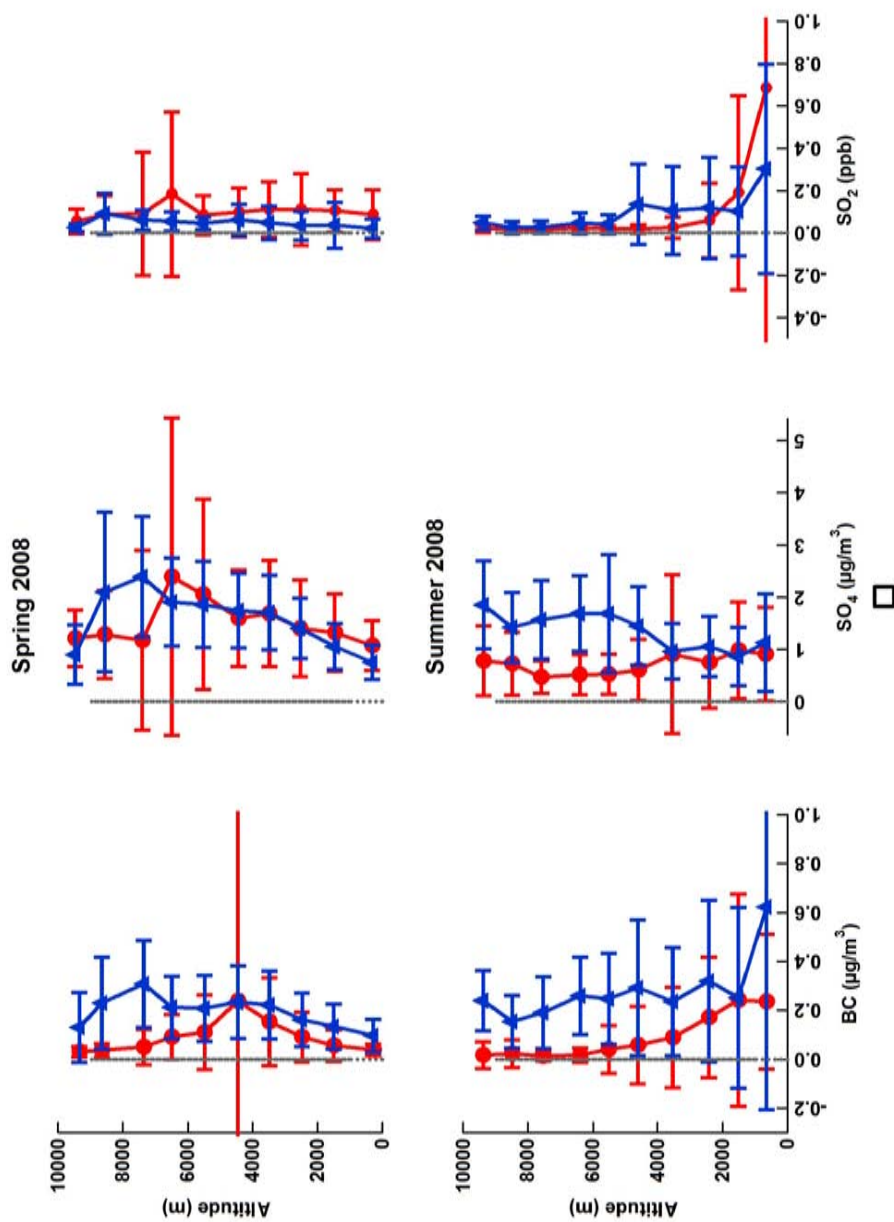


Figure 3.5 Comparison of STEM model aerosols with ARCTAS DC8 aircraft observations

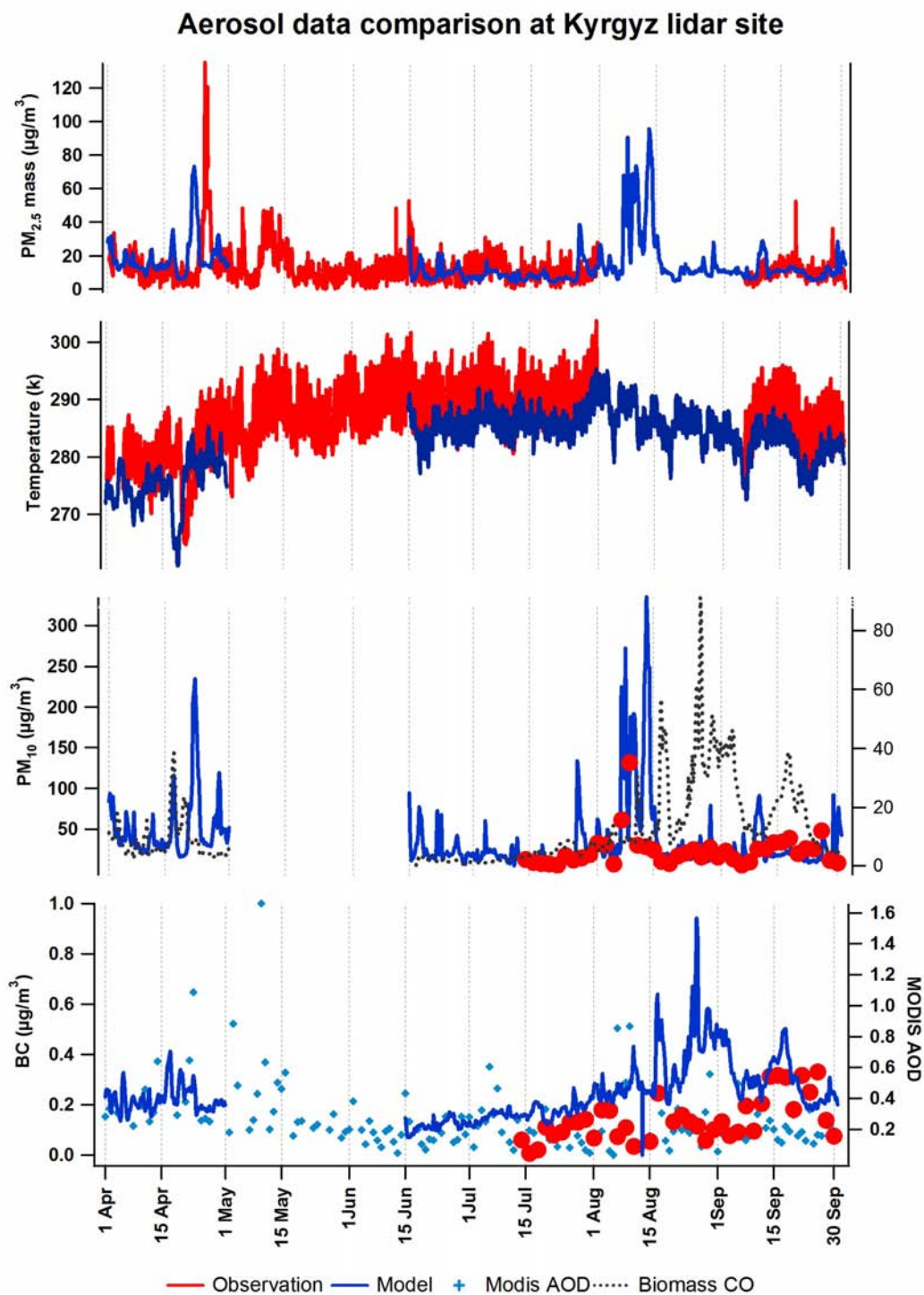


Figure 3.6 Comparison of observed and modeled PM aerosol composition at Lidar Site Teplokluchenska, Kyrgyz republic

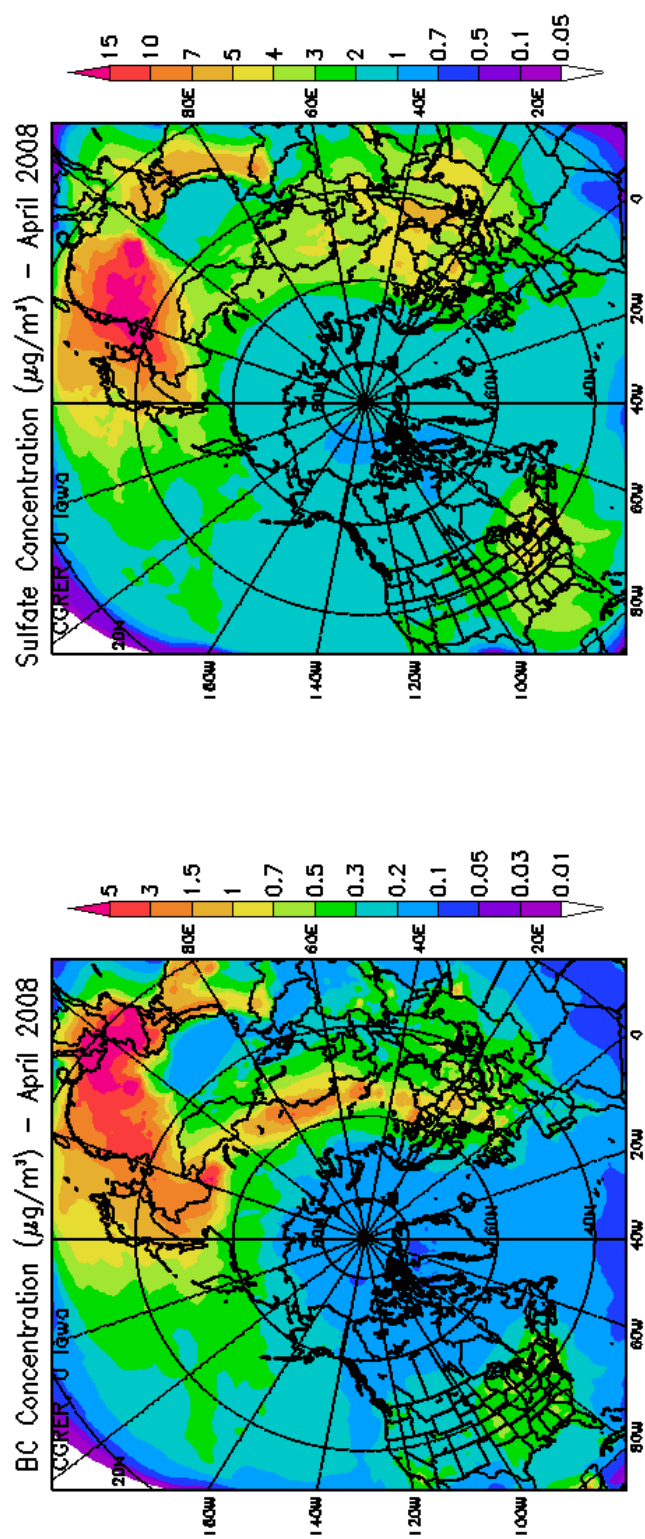


Figure 3.7 Monthly mean distribution of BC and sulfate at the surface for April 2008

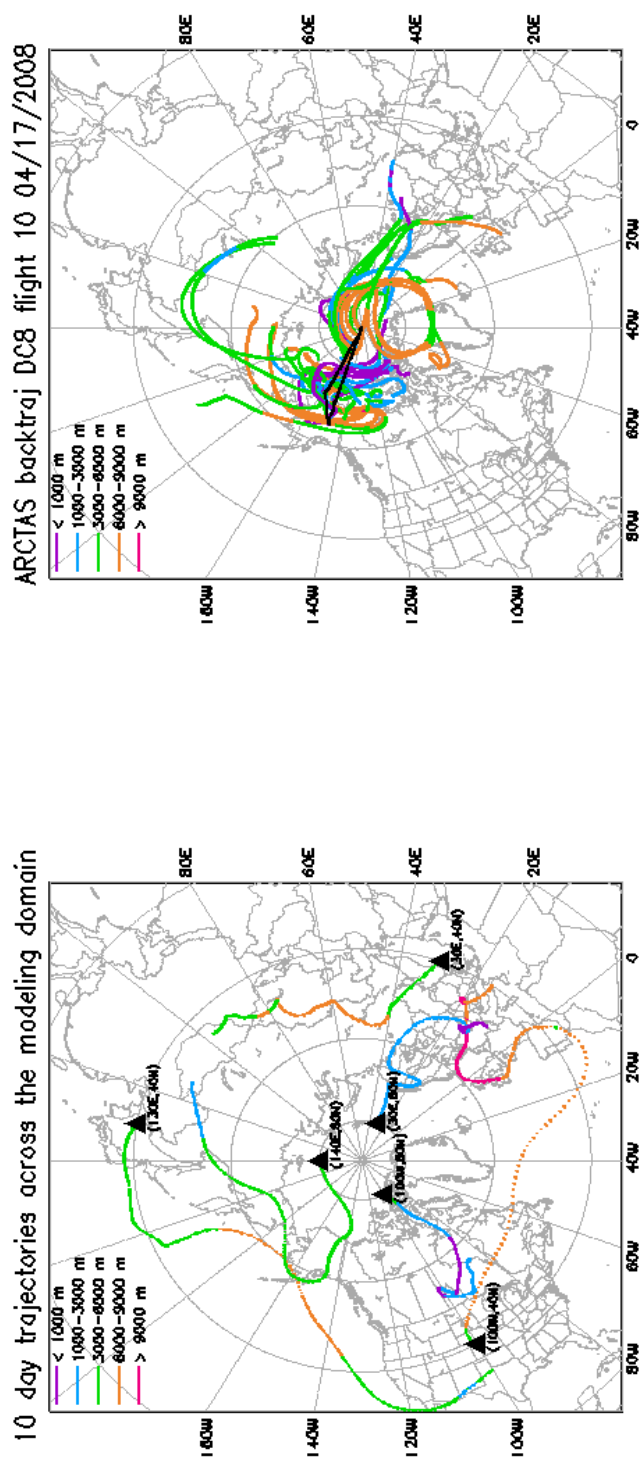


Figure 3.8 Transport pathways across the modeling domain illustrated by air mass back trajectories colored by altitude

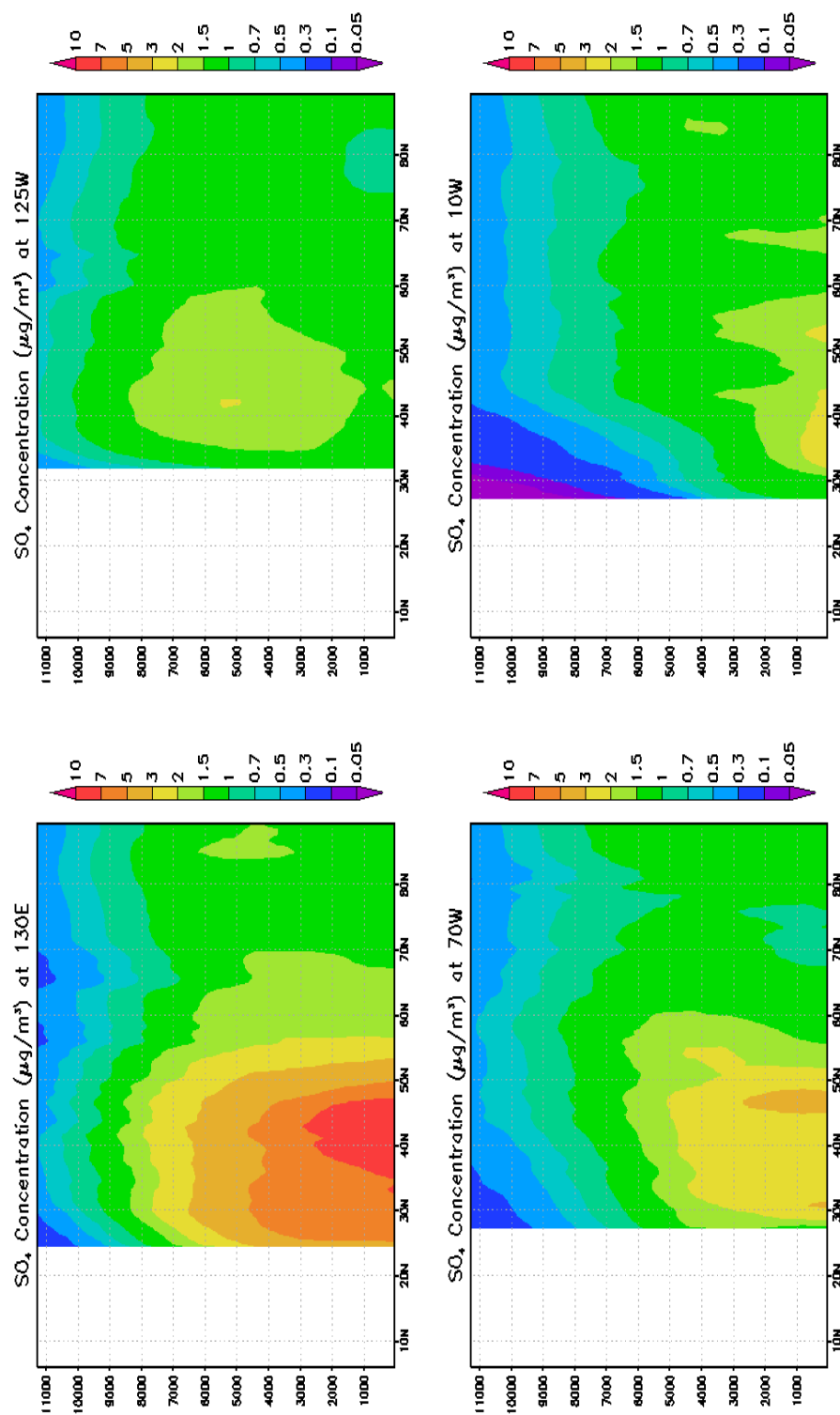


Figure 3.9 Monthly mean latitude - altitude cross sections of sulfate at 130E, 125W, 70W and 10W during spring 2008

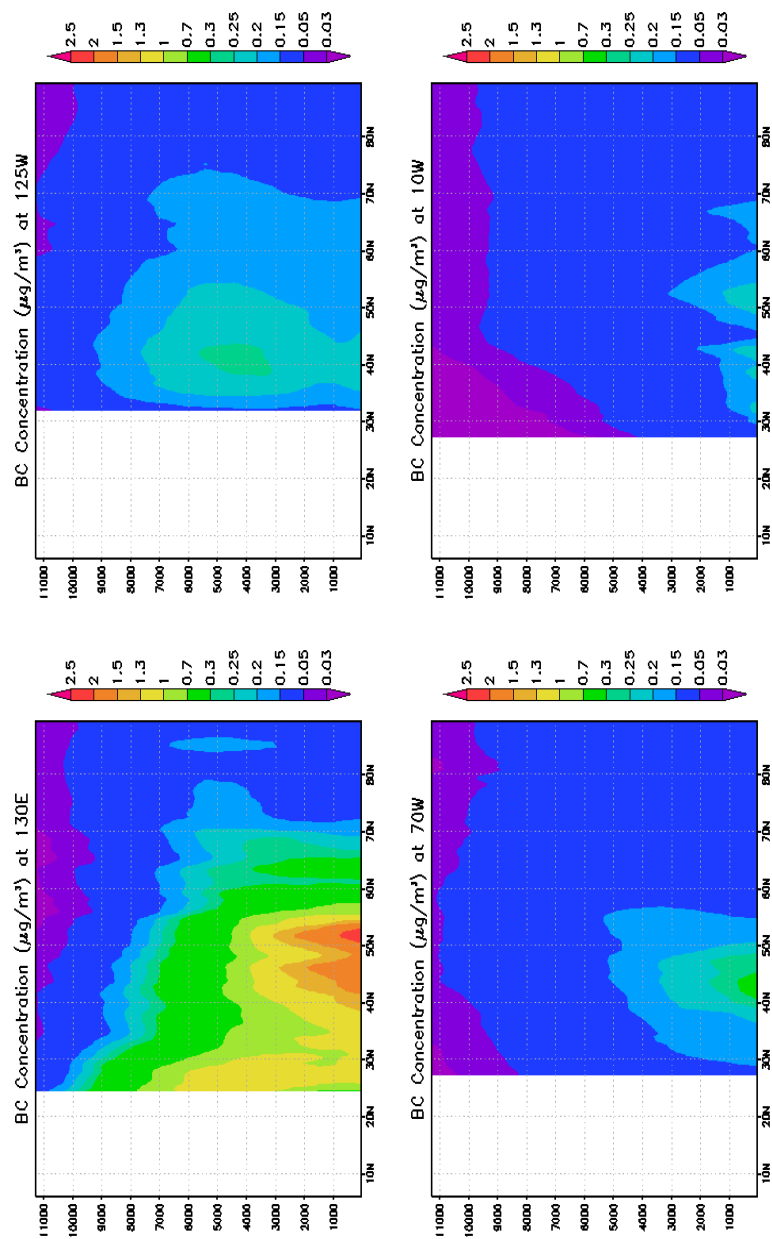


Figure 3.10 Monthly mean latitude - altitude cross sections of BC at 130E, 125W, 70W and 10W during spring 2008

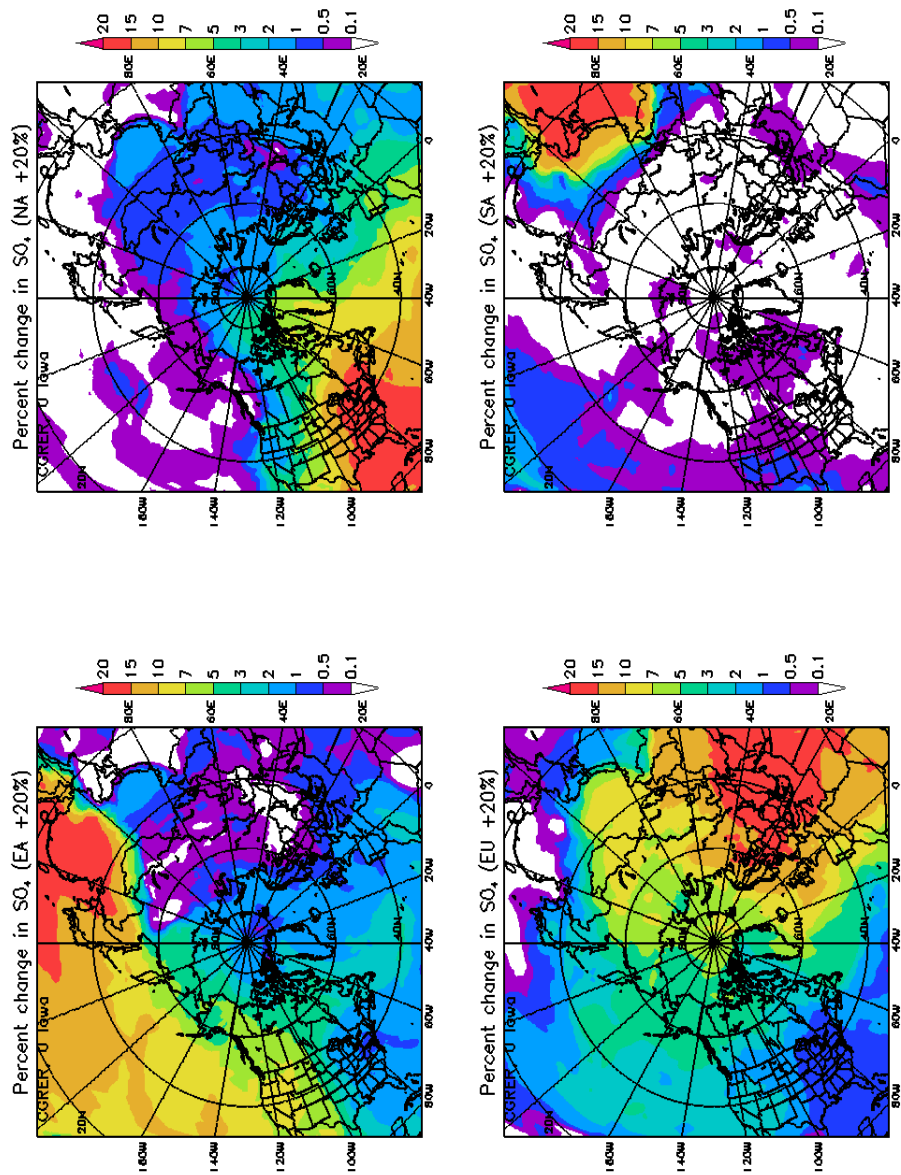


Figure 3.11 Percent change in sulfate due to the emission perturbations in source regions

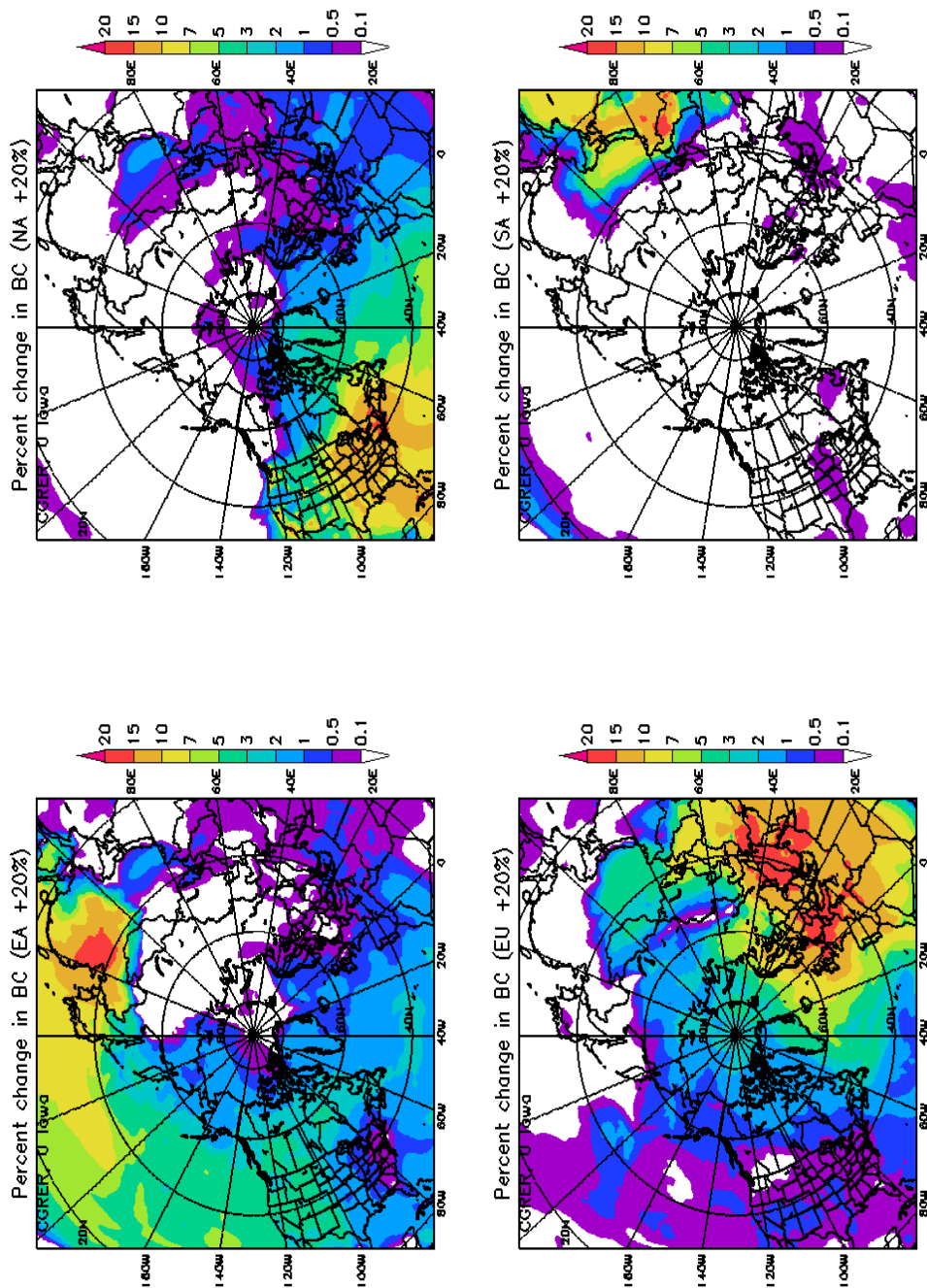


Figure 3.12 Percent change in BC due to the emission perturbations in source regions

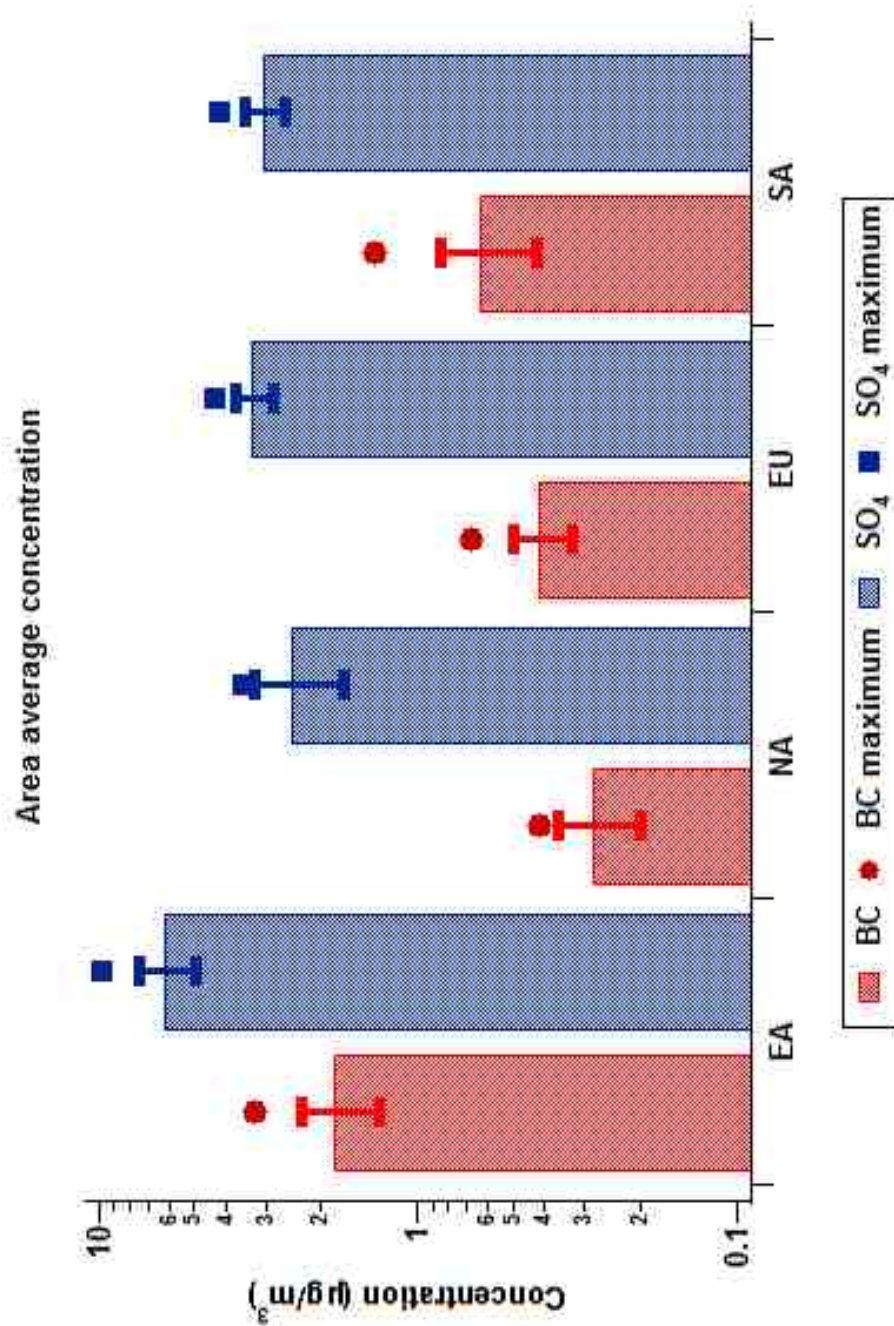


Figure 3.13 Monthly mean area average concentrations of major source regions for April 2008

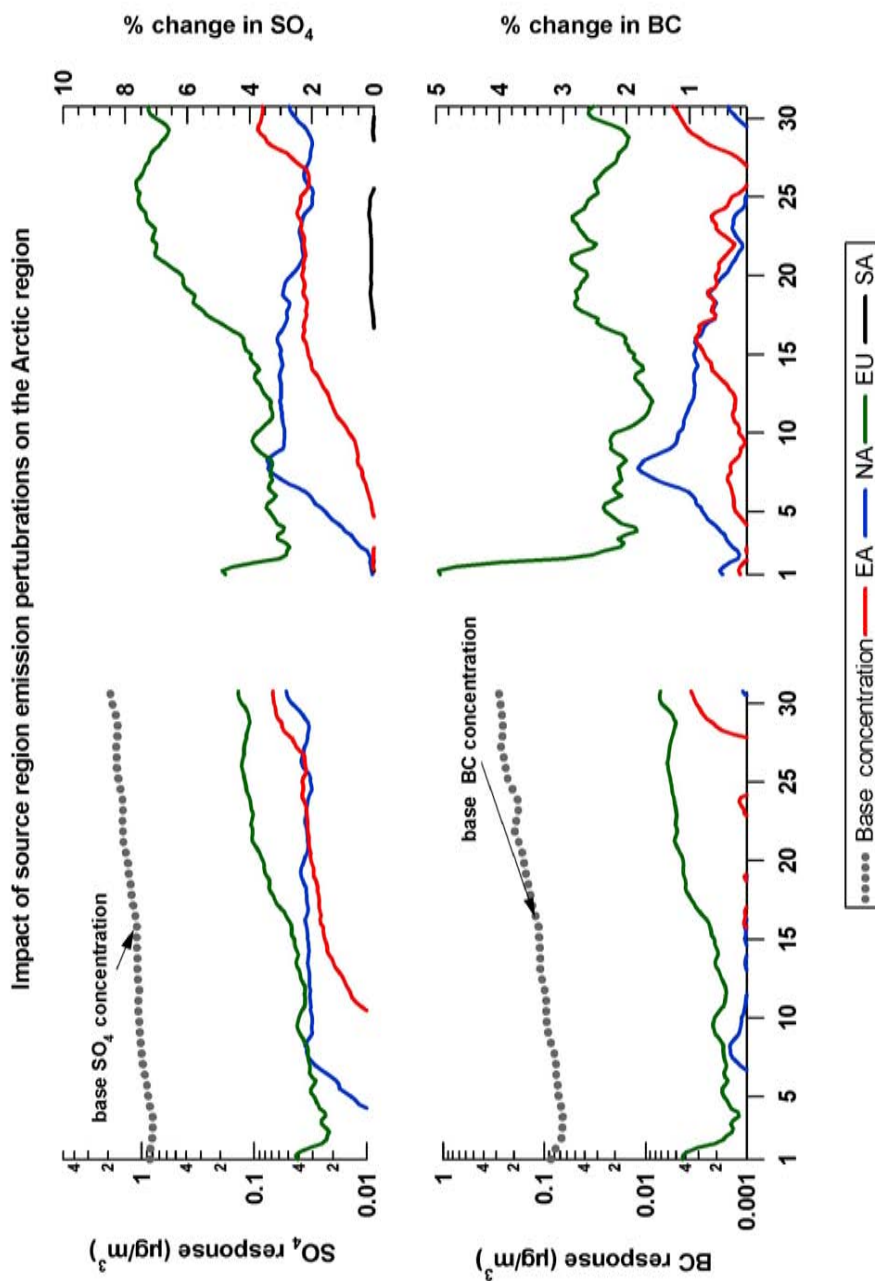


Figure 3.14 Impact of source region perturbation on the Arctic region (> 66.5 N)

CHAPTER 4
INFLUENCE OF ASIAN AEROSOLS AND TRACE GASES
ON THE PACIFIC AND NORTH AMERICA DURING THE
INTEX-B FIELD CAMPAIGN

4.1 Introduction

Economic development in the last few decades throughout much of Asia has led to rapid increase in anthropogenic emissions of aerosols and trace gases (Streets *et al.*, 2003a). Studies have shown that some of these aerosols and trace gases emitted from Asia reach North America and significantly enhance ozone and aerosol concentration over background levels (Jaffe *et al.*, 1999; VanCuren 2003; Liang *et al.*, 2004; Hadley *et al.*, 2007; Zhang *et al.*, 2008). The transport of pollutants from the Asian mid-latitudes to North America is particularly strong during the spring season (Yienger *et al.*, 2000; Bey *et al.*, 2003; Liang *et al.*, 2004). Long range transport of aerosols and gaseous pollutants could partially offset domestic emission controls over North America (Liu *et al.*, 2008). In addition, rising Asian aerosol emissions may have a climatic impact on North America (Levy *et al.*, 2008).

In the recent past, several airborne field campaigns have been conducted to study the rising impact of Asian pollution over the Pacific and North America. The TRACE-P and ACE-Asia field campaigns studied the outflow of Asian emissions to the western Pacific during the spring of 2001 (Jacob *et al.*, 2003; Seinfeld *et al.*, 2004). PHOBEA-II and ITCT-2K2 field campaigns were undertaken to characterize the atmospheric environment of the eastern Pacific during the spring of 2001 and 2002 respectively (Bertschi *et al.*, 2004). The Intercontinental Chemical Transport Experiment, Phase B (INTEX-B) campaign was conducted during the spring of 2006 by the National Aeronautics and Space Administration (NASA) (Singh *et al.*, 2009).

One of the scientific objectives of the INTEX-B field campaign was to understand the transport and evolution of Asian pollution with implications for North American air quality and climate. Multiple airborne measurements from the NASA DC-8 and the NSF/NCAR C-130 aircraft were made to characterize the atmospheric environment of the Pacific and western North America (Dunlea *et al.*, 2008; McNaughton *et al.*, 2009; Singh *et al.*, 2009). The INTEX-B campaign, with the NASA DC-8 aircraft stationed over Hawaii and Anchorage and the NSF/NCAR C-130 stationed over Seattle, provided a much better geographical coverage of the inflow of Asian emissions to the east central Pacific and western North America. In addition to the airborne measurements, observations from different remote sensing instruments on board the NASA satellites and various ground based surface stations were also made (e.g. Wolfe *et al.*, 2007; Dunlea *et al.*, 2008; McNaughton *et al.*, 2009; Reidmiller *et al.*, 2009; Singh *et al.*, 2009).

Global and regional chemical transport models were used to assist the flight planning of the airborne observation missions during INTEX-B. Chemical transport models (CTMs) are often used to interpret the formation/destruction of chemical species as they are transported away from source regions. One of the major advantages of a modeling study is its ability to provide continuous three dimensional distributions of pollutants across a wide geographical space so that effective mitigation strategies can be designed. Despite the uncertainties associated with various modeling components of CTMs including emissions, deposition, chemical reactivity and boundary conditions, they provide valuable means to link observed pollutant concentrations with their emission sources. The Sulfur Transport and dEposition Model (STEM), regional chemical transport model, has been previously used to assist in flight planning activities and to interpret the measurements from multiple platforms in several other field campaigns including the ACE-Asia, TRACE-P, ITCT-2k2 and ICARTT (Carmichael *et al.*, 2003; Tang *et al.*, 2004b; Tang *et al.*, 2004a; Tang *et al.*, 2007).

During the INTEX-B field campaign, the STEM model was deployed in the flight planning and was also used to interpret observations made from the airborne platforms. This is the first application of the regional scale STEM model to simulate the aerosols and trace gases at a horizontal resolution of 50 kms covering a large geographic area extending from the source regions of Asia, to the Pacific and all the way to US coast as seen in Figure 1 later. This spatial coverage is generally obtained through global scale models at a lower horizontal resolution. The large spatial extent of the STEM model domain has provided a great opportunity to study the inflow of Asian aerosols into the Pacific and North America.

The main objective of this study is to understand the influence of the Asian aerosols and trace gases on the Pacific and North America at a regional scale using the STEM model. The results discussion includes an analysis of the simulated aerosols with DC-8/C-130 observations and ground based measurements from Mt. Bachelor (MBO) and Trinidad Head (TDH) in western US along with Kathmandu and Nepal Climate Observatory at Pyramid (NCO-P) in Nepal. The influence of long-range transport of aerosols on the US is studied by combining the model predictions of aircraft and surface observations with region tagged CO tracers and air mass back trajectories. Several cases of possible quasi lagrangian sampling that occurred between the DC-8/C-130 aircrafts and North American ground based measurement sites are identified using modeled air mass back trajectories. The impact of emissions from specific sectors in Asia including residential, industrial, power and transportation is studied by a series of model sensitivity runs.

This chapter is organized as follows: the STEM regional model description and the emissions inventory used in this study are described in section 4.2. The results of the model intercomparison with aircraft and surface observations and regional aerosol distributions are presented in detail in section 4.3. The analysis of the quasi lagrangian

sampling instances identified by the model is described in section 4.3. The sectoral emission sensitivity runs results are presented in section 4.3 followed by the summary.

4.2. Model Description and Emissions Inventory

The STEM model was developed at the University of Iowa in the early 1980s (Carmichael *et al.*, 1986) and has continuously undergone development since then to its current version which is the STEM-2K3 version (Tang *et al.*, 2007). The STEM model is a regional chemical transport model which features the SAPRC-99 chemical mechanism (Carter 2000). Online photolysis rate calculations in the STEM model are performed using the TUV (Tropospheric Ultra-Violet Radiation) model (Madronich 2002). The TUV model needs total ozone column to calculate the absorption of UV radiation by ozone molecules. Since the STEM model is a regional model simulating the troposphere, column ozone data from satellite is used. For this study, we have used the column ozone data from the Ozone Mapping Spectrometer (OMI) (including STEM calculation for the troposphere) instrument on board the NASA Aura spacecraft. Thirty different photolysis rates are calculated using the STEM-TUV model. The STEM model uses the SCAPE II (Simulating Composition of Atmospheric Particles in Equilibrium Aerosol Solver) aerosol module to simulate inorganic gas to particle conversion and aerosol particle growth (Kim *et al.*, 1995). The inorganic aerosols in the STEM-SCAPE model are binned into four size bins of 0.1-0.3 μm , 0.3-1.0 μm , 1.0-2.5 μm and 2.5 – 10.0 μm . The model was run for the entire INTEX-B field campaign with 1 week for model spin up.

STEM does not require a uniform horizontal grid and can be mapped to any map projection based on the meteorological model. STEM preprocessor extracts all of the topography and other land use variables that were used in the meteorological model along with the meteorological parameters necessary for simulating chemical transport and removal processes. Thus, STEM has the same map projection and grid resolution as the meteorological model. For this study, the WRF-ARW (Weather Research Forecasting)

Version 2.1.2 meteorological model developed at NCAR was used (Skamarock *et al.*, 2005). The WRF model horizontal resolution was 50x50 kilometer with 314x200 grid cells. The model has 21 vertical levels with the model top at 50 hPa. Vertical spacing was defined to have the highest density in the first kilometer. The STEM model is parameterized to simulate the pollutant transport and chemistry in the troposphere. Therefore the chemistry model was simulated with only the first 18 layers reaching up to 10.5 kilometer above ground layer (AGL) height. Significant stratospheric air-mass intrusion within the model domain at higher latitudes (without any stratospheric chemistry/parameterization in the STEM model) limited the chemistry model's ability to simulate higher altitudes. GFS 1°x1° model forecast at 18 UTC from the National Center for Environmental Prediction (NCEP) was used to initialize the WRF model and as a boundary condition at a 6 hour interval. The physics options used in the WRF model are as follows: WSM-3 class simple ice scheme for microphysics, RRTM scheme for longwave/shortwave radiation, Monin-Obukhov scheme for surface layer, Noah land-surface model, YSU scheme for the boundary layer option and Grell-Devenyi ensemble scheme for the cumulus parameterization. The WRF model prediction skills are evaluated with INTEX-B observations later in the section 3.

Gridded anthropogenic emissions for Asia were obtained from the emissions inventory developed for the INTEX-B mission (Zhang *et al.*, 2009). The horizontal resolution of the gridded emissions inventory was 0.5°x0.5° ranging from 8-50° N and 80-150° E. Emissions of Volatile Organic Compounds (VOCs) were available based on the SAPRC-99 speciation. The National Emissions Estimate (NEI-2001v3) obtained from Jeff Vukovich, who updated the NEI 1999 emissions, at the US Environmental Protection Agency (EPA) were used an input for the region of North America. This emissions inventory has been previously used as input in STEM model, to study the regional air quality over North America during the ICARTT mission (Mena-Carrasco *et al.*, 2007;

Tang *et al.*, 2007). The global emissions inventory from the EDGAR database was used for regions outside the INTEX-B Asia and North America domains (Olivier *et al.*, 2001).

Daily emissions forecasts from biomass burning were available from the Regional Air Quality Modeling System (RAQMS) modeling group during the INTEX-B field campaign (Al-Saadi *et al.*, 2008). The same biomass burning emissions was utilized in this post field mission study. Biogenic emissions of terpene and isoprene were taken from a 12 year averaged data from the ORCHIDEE model (Lathiere *et al.*, 2006). It has been shown that using the top and lateral boundary conditions from a global model enhances STEM model prediction skill (Tang *et al.*, 2007). In this study, the Model for Ozone and Related Chemical Tracers (MOZART-4) global model was used to provide top and lateral boundary conditions (Pfister *et al.*, 2008). Dust emissions are calculated online using a parameterization based on previous studies using the STEM model (Tang *et al.*, 2004; Uno *et al.*, 2004). Emissions of sea salt within the STEM model are based on the work by S. L. Gong (Gong 2003). The tracer version of the STEM model has been utilized for emissions sensitivity runs. This version of the model employs simple decaying rates for most primary species without chemical reactions and includes wet scavenging and dry deposition to produce tracer model predictions.

4.3 Results and Discussion

Figure 4.1a shows the horizontal modeling domain of the WRF-STEM model. Figures 1a and 1b also show the flight tracks of the DC-8 and the C-130 during the INTEX-B field campaign. As shown in figure 4.1, there is substantial amount of geographic space covered by the DC-8 flights over the central Pacific while the C-130 airborne observations cover a good portion of the eastern Pacific during the 2006 spring season. Figure 4.1 also shows the location of ground based measurement stations including Mt. Bachelor (MBO) Oregon, Trinidad Head (THD) California, Kathmandu

(KTM) and Nepal Climate Observatory at Pyramid (NCO-P) Nepal discussed later in this paper.

The modeled monthly mean CO distribution is shown in figure 4.2a. CO hotspots over much of eastern China and India are seen at the 3 kilometer AGL layer and the regions with enhanced CO extend north of ~ 10 N. A substantial amount of CO is seen entering the domain from Europe as shown along the northern boundary. Figure 4.2 also presents the mission wide averaged latitudinal and longitudinal CO distributions within the STEM modeling domain. Since STEM model was run on a Lambert Conformal projection, there are some latitudes and longitudes outside the model domain which are blank in the figure 4.2 subplots. The CO distribution along 45N shows strong zonal transport with CO transported into the domain from Europe to Asia largely within the boundary layer as seen in the distribution in the western portion of the domain (i.e., < 100 E longitude). CO from emissions in East Asia is transported out over the Pacific via frontal systems resulting in lifting of the CO above the boundary layer and into the free troposphere. The bulk of the CO transported is at altitudes of 4-5 kilometer as shown in the cross section along 145E longitude. As the polluted air masses reach the eastern Pacific, the frontal systems tend to move pole ward, and aged air masses subside and mix with CO emitted from North America leading to enhanced CO levels within the boundary layer as shown in the 125W cross section.

STEM model comparisons with observations from the DC-8 and C-130 flights are also shown in figure 4.2. The predicted and DC-8 observation values for all flights are binned into every 1000 meters flight altitude and then plotted. The horizontal error bars are the standard deviations of both model predictions and observations. The C-130 airborne observations and STEM model predictions are binned and averaged every 500 meters in altitude. The CO predictions capture the main features in the observation, and predict values within 5-15% of observations, but with lower variability. The results show that the model underestimates observed CO for both the DC-8 and C-130 airborne

observations. The model underpredicts CO at altitudes below ~ 5 kilometer, to a greater extent for the DC-8 (~ 20 ppb, 15%) than for the C-130 flights (~ 7 ppb bias, 6%). At higher altitudes, the model shows a slight positive bias with respect to the DC-8 observations. The underestimation of CO could be attributed to several factors such as uncertainties in the anthropogenic and biomass emissions and chemical loss mechanisms some of which are discussed later in the paper.

Figure 4.3 shows both the back trajectories and tagged CO tracer contributions to air mass sampled by the DC-8 and C-130 during INTEX-B. Three flights each from Hawaii (RF 11, 12, 13) and Alaska portions (RF 15, 16, 17) of the DC-8 mission were selected and 5-day back trajectories were calculated using the WRF meteorology for way points (latitude, longitude) along the flight tracks. Similarly, five C-130 (RF 15, 17, 18, 21, 24) flights that had substantial sampling over the eastern Pacific were chosen to calculate back trajectories. The trajectories were initiated at the actual latitude, longitude, altitude and time of the airplane research flights. The trajectories were calculated along every minute of the flight path; however, to reduce the clutter in the figure 4.3, trajectories are plotted only every thirty minutes.

The back trajectory analyses show different transport patterns for the Hawaii and Alaska portions of the mission. The Hawaii portion is dominated by air masses passing over east central China reaching as far back as South Asia. In figure 4.3, air mass trajectories are colored by the altitude along the trajectory, and as expected the higher altitude air travels further reflecting the increase in wind speed with altitude. The back-trajectories for the C-130 show that the air-masses spent a substantial time over the Gulf of Alaska.

The lifetime of CO in the atmosphere is about 1-2 months (Liang et al., 2004). Thus for 3D modeling studies, it is useful to tag CO emissions from different source regions to help identify the potential areas that influence a particular air mass. In the tagged CO analysis, only primary CO (enhancements above background) is tracked. To

estimate total ambient CO levels, these enhancements would be added to a background concentration which is typically on the order of 90 ppb and accounts for the contribution to total CO from initial, top and lateral boundary conditions, biomass burning and net secondary production from chemical reactions. The tagged CO analysis shows that emissions from China contribute ~ 70% to the CO enhancements from anthropogenic emissions above background in these regions. The influence from South and Southeast Asia is highest in the mid/upper troposphere and its contribution is ~ 15%. At the higher latitudes associated with the DC-8 Alaska flights, there is a small contribution from South and Southeast Asia emissions. The contributions from USA and Canada sources range from 20 – 40% with the largest contribution at lower levels, reflecting the impact of offshore transport from North America during this season.

To evaluate the robustness of the model – calculated trajectories, the results of the meteorological variables simulated by the WRF model are described next. The WRF model skill is evaluated for four key meteorological parameters including temperature, Relative Humidity (RH), wind speed and wind direction, that are essential for chemical transport with observations onboard the DC-8 and C-130 in figure 4.4. The predicted and DC-8 observation values for all flights are binned into every 1000 meters flight altitude and then plotted. The horizontal error bars are the standard deviations of both model predictions and observations. The C-130 airborne observations and STEM model predictions are binned and averaged every 500 meters in altitude. Figure 4.3a shows that the model is able to capture the vertical temperature profile quite well across all DC-8 flights. The standard deviation of the model and observed variables are also similar. The STEM meteorological pre-processor calculates relative humidity (RH) based on parameterized equations involving temperature pressure and water vapor mixing ratio. The WRF model captures the observed air pressure very well across all altitude bins (figure not shown). The comparison of RH is strictly not a robust evaluation of WRF model skill since it is based on the governing RH parameterized equation. However,

since RH is an important parameter for chemical transport models, we present the comparison. The results presented in figure 4.4b show that the model does fairly well in capturing the vertical distribution of the RH. The model shows a small positive bias in the lower troposphere and a larger negative bias in the upper troposphere. As shown in figure 4.4c, the WRF model captures the observed wind speed measured by the DC-8 flights up to 6 kilometer after which the model has a negative bias. For wind direction, the model shows low positive and negative bias across all flight altitudes (figure 4.4d). Similar results are found for the comparisons with the C-130 (figure 4.4e-h).

4.3.1 Comparison of Model Predictions with Aircraft Observations

The comparison of observations to modeled aerosols along the flight tracks is challenging as the aerosols are transported in relatively discrete plumes across the Pacific. Dunlea *et al.*, (2008) reported that for some of the flights during INTEX-B, the models missed transport of large polluted air masses that were so intense that missing these concentrations could easily modify the average vertical profiles of aerosols. Figure 4.5 presents the comparison of model predicted and observed aerosols from the DC-8 and C-130. For the C-130 observations, only the AMS data is used for comparison but Dunlea *et al.*, (2008) showed that the AMS and PILS instrument measured similar concentration of nitrate and sulfate during the INTEX-B study. The predicted sulfate values are generally well captured for the DC-8 flights in terms of both mean values and variability (e.g., both the model and observations show the largest variability in 1 to 4 kilometer altitude range). However, the model fails to capture the elevated sulfate levels above 2 kilometer that were observed by the C-130. In addition the predicted variability is also much lower than the observations. The evaluation of modeled SO₂ with both DC-8 and C-130 observations (not shown here) showed that SO₂ is systematically underpredicted by the model. Thus, it is possible that the current emission inventory might be low on

SO₂ emissions. However, the predicted results below 2 kilometer for both the DC-8 and C-130 are well captured for both sulfate and SO₂. The large underpredictions in the mid troposphere for the C-130 may reflect other issues related to transport and removal of sulfur compounds in the model. The nature of the pollutant transport in discrete plumes across the Pacific could also contribute significantly to the underprediction of modeled SO₂ and sulfate.

The comparison of nitrate aerosols from the DC-8 shows that the model overpredicts the nitrate concentration at lower altitudes while it underpredicts nitrate aerosols at higher altitudes. However, the modeled HNO₃ gas phase values are underpredicted, but total nitrate (gas + particulate nitrate) is well captured (not shown here). This suggests that the partitioning in the model to particulate phase on dust, sea salt and potassium maybe too strong. The HNO₃ partitioning between gas phase and particulate phase needs to be analyzed further using a box model study constrained with observations. Model comparison of nitrate aerosols with the C-130 measurement shows that the model overpredicts the observation at all altitudes although the overprediction is smaller at higher altitudes.

While the AMS instrument onboard the C-130 measures organic aerosols, the STEM model calculates concentration of primary organic carbon only. Thus, comparison of modeled OC with AMS organic matter (OM) is complex. However, if one were to convert AMS OM to OC with the OM/OC ratio of 1.9 reported for this study (Dunlea et al., 2008) and which is consistent with values for rural and remote aerosols reported elsewhere (Turpin and Lim, 2001; Aiken et al., 2008) the STEM model underpredicts the observations, consistent with missing SOA formation and the importance of SOA to global OA highlighted by previous studies (Volkamer *et al.*, 2006; Zhang *et al.*, 2007). If the difference between the observed and predicted OC is assumed to be due to secondary organic aerosol (SOA), then SOA accounts for about 40% of the OC.

Monthly averaged horizontal distributions of aerosols show strong zonal patterns with the bulk of the aerosol confined between 10 to 50N as shown in figure. 4.6. The dust distribution shows maximum values in the western part of the domain reflecting the strong source regions during this time period (i.e., Central Asia and China). The sulfate distribution shows a strong west to east gradient, with the peak values in the west reflecting the heavily populated and industrial regions of India and China. OC shows a similar pattern, but with elevated levels also over Southeast Asia, reflecting the importance of biomass burning. Particulate nitrate shows a different pattern, with elevated levels over South Asia and a large region extending across the Pacific. These patterns generally reflect regions with high NO_x and NH_3 emissions.

Modeling studies allow analysis of pollutant evolution as air masses are transported away from the source regions. Figure 4.7 shows the mission wide averages of calculated sulfate, potential sulfate ($\text{SO}_2 + \text{sulfate}$) and VOC age (Tang et al., 2004). The VOC age is a relative clock and gives qualitative information on the age of air masses, and can be made more quantitative by calibration with other air mass age indicators (e.g., trajectory analysis). The VOC age calculations are done with the modeling domain without boundary conditions so that the VOC inferred age at the western boundary is young. We present the results at 45N latitude because most of the C-130 Pacific flights occurred between 40-50N latitude as seen in figure 4.1. Our results show that as we move east there is a distinct sulfate plume extending from about 3 to 7 kilometer. In addition there is a second sulfate peak at similar altitudes associated with the North America plume located around 130W. Also plotted is the calculated sulfate to potential sulfate ratio (i.e., the sum of sulfate plus SO_2 expressed as sulfate) ratio, which shows that the portion of available sulfur in the form of sulfate increases across the Pacific, consistent with SO_2 transformation to sulfate as it advects eastward to North America. Modeled results show that as air masses approach the North American continent, the ratio of sulfate to potential sulfate decreases at the lower altitudes signifying the influence of

North American SO₂ emissions on the air mass. However we also see regions within the boundary layer extending from 130W to 150E with ratios greater than 0.8, reflecting the fact that air masses reaching near the surface can have very long residence times. This is more clearly seen in the plot of VOC air mass age. The aging of the air masses as they are transported to the east is clearly seen, with air in the upper troposphere taking on average 6 to 8 days to reach North America, which is similar to transport times found in previous studies (Jaffe *et al.*, 1999; Reidmiller *et al.*, 2009). Furthermore air masses near the surface over the Pacific can have ages exceeding 10 days. A clear delineation between North America outflow and long range transport for Asia is seen at 130W. The VOC age has a similar distribution as the sulfate to potential sulfate ratio (as expected as this is another chemical clock). Note that the distributions of VOC age and the ratio of sulfate to potential sulfate distribution are similar east of 100E. West of 100E the sulfate to potential sulfate ratio is large reflecting the fact that the inflow boundary conditions bring in aged air masses from the western boundary. STEM model results based on monthly mean OC and sulfate mixing ratios agree with Peltier *et al.*, (2008) C-130 observations in that up to an altitude of ~3 kilometer the ratio of OC/sulfate is about 1 or higher. As we follow the Asian air mass (from VOC age or from the sulfate/potential sulfate ratios) we found that the ratio declines as we move up in altitude to values ~0.4, which is also consistent with the observations.

It is interesting to point out that the mean sulfate distribution does show an enhancement in sulfate in the region where the C-130 operated. While the model extraction at the time and locations of the actual flights show only a slight enhancement in sulfate in the 2-7 kilometer altitude range (figure. 4.5a), a displacement of the predicted feature slightly to the west would be consistent with the observations. As discussed earlier with respect to the predicted meteorology, the negative bias in the wind speed above ~5 kilometers could have resulted in a slight displacement in longitude and latitude of the mean distributions.

Using these results the modeled OC to sulfate ratios was also examined as this has been discussed previously by Dunlea *et al.*, (2008) and Peltier *et al.*, (2008) for the same INTEX-B campaign. The OC to sulfate ratio reflects the differences in emissions, wet removal, and formation processes. Dunlea *et al.*, (2008) compared organic carbon (converted from OM measurements) ratio with AMS sulfate, while Peltier *et al.*, (2008) examined the water soluble organic carbon (WSOC) with sulfate aerosols using their PILS instrument. Both studies compared the aerosol ratios of organic carbon to sulfate with their own separate definitions of Asian air mass origin to elucidate the transport and transformation of aerosols across the Pacific. Dunlea *et al.*, (2008) identified air masses of Asian origin using observed AMS sulfate $> 1 \mu\text{g}/\text{m}^3$ and included only those data sampled by the C-130 west of 125W degrees longitude. Peltier *et al.*, (2008) screened data for Asian CO greater than 75% of the total anthropogenic FLEXPART CO as air masses originating from Asia. The STEM modeled values were examined using the data screening criteria defined by Dunlea *et al.*, (2008). We also classified the STEM model data similar to Peltier *et al.*, 2008 study using predicted CO greater than 100 ppb and tagged China anthropogenic CO greater than 50% of the predicted total anthropogenic CO as screening criteria. Dunlea *et al.*, (2008) showed that AMS and PILS instrument both showed similar results for sulfate concentration. We used AMS sulfate and AMS OC (calculated from OM) data for comparison as it was readily available for both Peltier *et al.*, (2008) and Dunlea *et al.*, (2008) screening techniques mentioned above.

The sulfate, OC and the OC to sulfate ratios screened in these ways are shown in Figures 4.8, 4.9 and 4.10. Also shown are the OC to sulfate ratios for all the data points for the C-130 flights (no screening). Using all the data the OC to sulfate ratio is approximately 1 in the lowest 3 km, and drops to a value of ~ 0.3 between 3 and 6 km altitude range. The Peltier screening method shows a similar altitude dependency of the OC to sulfate ratio, with lower values (~ 0.6) in the lower altitudes. This is the result of their screening method that removes some of the freshest air masses from North America

(which occur in the lowest 3 km and which have higher OC to sulfate ratios). The Dunlea screening method looks only at air masses that have large enhancements of Asian pollution. It removes the North American air masses as well as Asian air masses that have low pollution contributions. Their results show a different vertical profile with the lowest values (< 0.2) occurring near the surface and increasing to ~ 0.3 at 3 km. Above 3 km the value remains at ~ 0.3 . At altitudes above 4 km all the profiles show that the ratio is of order 0.3-0.4.

The STEM predicted OC to sulfate ratio profiles for the various screening methods are also shown in figure 4.8. The magnitude of the OC/SO₄ ratio from the STEM model is larger than the corresponding observed AMS ratio. This may be due to the substantial underprediction of sulfate aerosol, although OC is also underpredicted as discussed above. While the absolute ratios are biased high, the predicted profiles capture the important features of the observation based ratios. For example the impacts of the various screening methods on the profiles are clearly shown. The Peltier method results in a reduction of the ratios at all altitudes, with the greatest differences in the lower 2 km. The Dunlea screening results in a greater reduction in the ratios. These results can be understood in the context of the information presented in figure 4.7 and its discussion. Both screening techniques remove contributions of OC and sulfate of North American origin. The criterion used by Dunlea *et al.*, (2008) removes a substantially larger fraction of the North America contribution. The low values near the surface in the Dunlea screening is due to the fact that these observation points are very aged as reflected in the monthly mean air mass age distributions shown in figure 4.7c. These results support the idea that the OC to sulfate ratio is lower in more aged air masses. However, these results should be interpreted cautiously. Peltier *et al.*, (2008) compared WSOC/sulfate ratios while we compared OC/sulfate ratios. Our results show that Asian air mass classified according to observed Asian tracers show different altitude profile than modeled monthly mean ratios. Results based on observation sampling strategy, which is biased towards

sampling polluted plumes, could also influence the results of aerosol transport and transformation compared to monthly/seasonal mean values.

4.3.2. Comparison with Surface Observations

Observations of trace gases and aerosols were available from surface sites at Mt. Bachelor (MBO) and Trinidad Head (THD) during the INTEX-B sampling period. Aerosol mass measurements were also available from the Atmospheric Brown Cloud (ABC) sites at Trinidad Head (THD) and Kathmandu, Nepal (KTM) during the INTEX-B field campaign. We present the model comparison of aerosol mass at THD with observations, modeled aerosol curtain plots over THD and comparison of modeled and observed aerosol mass at KTM in figure 4.11. Aerosols were sampled every day in KTM while sampling was done every other day in THD. The results show that the model is able to capture the magnitude of the total $PM_{2.5}$ mass at THD with some underprediction during the first week. Modeled sulfate is also lower than observed at THD consistent with the comparison of predicted values with the airborne measurements from the DC-8 and C-130. The general trends are captured except for the episode around May 1, which was missed by the model. The model does predict elevated sulfate over THD during this time period, but only for altitudes above 4 kilometers. The OC concentrations are within the magnitude of the observations at THD, unlike the airborne comparison where the STEM model significantly underpredicted observed OC inferred from AMS OM measurements. At KTM, modeled $PM_{2.5}$ mass concentration and variability are well captured. Modeled sulfate levels are also similar to the observations while the modeled OC is underpredicted. The underprediction of OC is likely attributable to local emission sources which are not captured by the regional emissions inventory used in this study. The OC underprediction could also have resulted from the lack of secondary organic formation mechanism in the STEM model.

The comparison of predicted CO, Ozone, NO and PAN with measurements from Mt. Bachelor during the INTEX-B is shown in figure 4.12. Apart from the first few days of the comparison, the model is able to capture the magnitude and variation of measured CO at Mt. Bachelor. The model is also able to capture both the magnitude as well as the temporal trend of ozone and PAN. Modeled NO is within the range of observed values but shows less variability. It is important to note that modeled PAN is much closer in agreement to the measurements at Mt. Bachelor than when compared to the airborne DC-8 and C-130 measurements. The predictions also accurately capture the three synoptic events observed in this period. Figure 4.13 shows the curtain plots of ozone, PAN and dust over Mt. Bachelor illustrating the vertical distribution of these pollutants. The ozone curtain shows strong influence of stratospheric ozone throughout the INTEX-B period. PAN vertical structure shows influence of local sources as well as elevated plumes associated with long range transport. Dust shows a somewhat different vertical distribution over Mt. Bachelor, with three distinct events passing over Mt. Bachelor. The peak in the dust concentration is located 3-8 kilometer AGL. The superimposed figure of modeled surface level dust, ozone and PAN shown in figure 4.13, illustrates the different characteristics of these three pollution events. The first peak around 22nd of April has very high ozone concentration and relatively low PAN (with peak ozone being anti-correlated with PAN), and low dust values. The second peak around May 3rd has both high ozone and PAN but low dust concentration. Finally the peak around 11th May has high ozone, dust and PAN.

To help put these measurements in perspective modeled ozone, PAN and dust distribution at 3 kilometer AGL at 18Z for April 22, May 3 and May 11 are shown in figure 4.14. Wind barbs are also plotted in these figures to illustrate the transport patterns. On April 22, modeled ozone is high over MBO along the eastern side of the ridge bringing descending air of stratospheric origin from the North. The ridge clearly separates the ozone transported from Asia which is on the western side of the ridge. Thus

the air over MBO has high ozone and low dust as shown clearly in the vertical profiles in figure 4.14. On May 3rd, there is another weak ridge over the eastern Pacific which transports pollution from the North. This ridge is not as strong as on April 22. To the east of the ridge ozone and PAN are correlated, with maximum values at the surface, and moderate values aloft. Dust values at the surface remain low, reflecting the lack of local emissions and wet removal along its transport path. The third pollutant peak over MBO around May 11 shows zonal flow transporting dust, ozone, PAN and other pollutants from Asia to the west coast of the US.

To further understand the characteristics of these three pollutant events from source origin perspective, the observed data of selected chemical species were combined with the air mass back trajectories. For this analysis, we used 12 day backward trajectories calculated from the model to assess the impact of long range transport over MBO. The location of an air parcel at a particular time was represented by the trajectory segment endpoints as latitude and longitude. The entire geographic region covered by the trajectories was divided into an array of grid cells. It was assumed that the concentration did not change from the value observed at MBO for a particular time along the back trajectories. Let $m_{i,j}$ be the number of segment endpoints in i,j th grid cell that denote the trajectories arriving at MBO when the time corresponds to a particular pollution event described above. The average concentration of each grid cell $C_{i,j}$ was calculated by using the equation 4.1:

$$C_{i,j} = \frac{1}{m_{i,j}} \sum_{k=1}^{m_{i,j}} C_k \quad (4.1)$$

where C_k denotes the observed concentration at the time when the back trajectory was initialized. Thus the concentration of species was reconstructed along the path of back trajectories. Further details are explained in (Kurata *et al.*, 2004). The trajectories were colored by the mean observed pollutant concentration associated with them and these results are also shown in figure 4.14. The reconstructed concentration plot of ozone

along the trajectory path for the first event around April 22 clearly shows the path of the high ozone (grid cells colored in red) coming from the north with relatively lower values along the Asian transport path. Similar plots for PAN and dust (not shown here) show low values consistent with the above findings. Like wise, plot of PAN for the second peak event on May 3 shows that high values of PAN and ozone (not shown) with relatively lower dust (not shown) originate along the path coming from the north/northwest direction. Finally for the third peak of May 11, the dust plot clearly shows that the high values of dust, along with PAN and ozone (not shown) are transported along the zonal flow originating from Asia. These results corroborate the findings discussed above.

To further understand the emission source regions that influence the pollution levels at MBO, tagged tracer analysis was performed. Figure 4.15 shows the time series of source region tagged anthropogenic CO over MBO at the 5.3 kilometer AGL and at the surface. Connecting these two figures, we show the modeled CO curtain over MBO. China CO and continental US (CONUS) CO dominate the source regions during this period, with the importance of China sources increasing with altitude. The tagged CO tracer study also corroborates the earlier finding that the first two peak events were influenced by pollutants coming from the North (as shown by elevated Canada CO tracer) while the final pollution episode was impacted by zonal transport of pollutants from Asia.

A suite of measurements including meteorological parameters, aerosols, trace gases and AOD were also available from the NCO-P (27.9 N, 86.7 E), a remote monitoring station located at 5079 m asl on the southern Himalayan region at the confluence of the secondary valley of Lobuche and the main Khumbu Valley. The high altitude remote monitoring sites provide a great opportunity to study the atmospheric background conditions and to assess the impact of human activities on the remote environments. Further details about this site can be found elsewhere (Bonasoni *et al.*,

2008). It is important to note here that this site is located at very high altitude of 5079 m and the surrounding region has a very complex terrain and topography which is a difficult task to represent in regional scale models. The comparison of modeled meteorological variables including pressure, temperature, RH, wind speed and wind direction along with ozone and BC at surface (AGL) are shown in figure 4.16. The simulated values capture the general trend seen in the observed meteorological variables but show a systematic positive bias.

The modeled values of ozone seem to capture the peaks except for missing the two peaks in early May and show a high negative bias. Moore et al., 2009 analyzed the seasonality of ozone at NCO-P for 2006 and found that the NCO-P site shows a springtime maxima in ozone and attributed it to the stratospheric and tropospheric sources. The predicted bias seen in observation could be attributed to the impact of stratospheric ozone. In addition, the predicted bias could also be associated with the model topographical representation errors due to the complex terrain. The model seems to predict the observed BC values well as seen in the second panel of figure.

The impact of model topography on the predicted values at NCO-P was investigated further and found that model grid cell topography altitude for the location of NCO-P was approximately ~4150 m (which is approximately 1000 m lower than the site altitude). The surrounding model grid cells in the vicinity of the NCO-P location, showed a tremendous altitude variation (~ 1000-1500 m). The model data was extracted at various altitudes and it was found that the modeled and observed pressure and temperature were in close agreement at ~4775m. These results are shown in figure 4.17. However, this enhances the positive bias seen in wind speed and wind direction. This point towards the need for higher resolution regional scale modeling studies than the one used in this study to interpret the observations made at such high altitude sites.

4.3.3 Quasi-lagrangian Sampling

Quasi-Lagrangian sampling involves taking measurements of an air parcel at one location, and later sampling of what is believed to be the same, or a very similar parcel, at a different downwind location and time (Latto 2009). The identification of quasi-lagrangian sampling along flight paths requires elaborate iterative air mass trajectory calculations. The INTEX-B campaign with the DC-8 and C-130 aircrafts was designed to be executed such that pollutant ageing could be studied by conducting quasi-lagrangian sampling of air masses between the two aircrafts (Singh *et al.*, 2009) Backward and forward trajectories between the C-130 and DC-8 flights were calculated to determine times when such lagrangian sampling might have occurred between the two aircraft.

Due to the spatial and temporal resolution of the predicted meteorological fields used in this study, the following criteria were set to identify possible instances of lagrangian sampling: a) difference of the trajectory location and the flight path time step is within three hours; b) trajectory path and flight path are within 1 degree latitude/longitude of each other on top of the time constraint; and c) the altitudes of the trajectory and aircraft location are within 1000 meters. These assumptions are similar to the methodology used by Latto *et al.*, 2009 for the INTEX-B mission (Latto 2009). This analysis was further extended to include the surface sites.

Figure 4.18 illustrates the backward and forward trajectories from one of the C-130 flights with the DC-8 and the surface sites of Mt. Bachelor and Trinidad Head, meeting our criteria for lagrangian sampling. Tables 1-5 present the detailed times from the C-130 to DC-8, and from DC-8 and C-130 to the two surface sites, which met these lagrangian sampling criteria. We include only the results for air masses that arrived more than a day later at the surface sites to avoid counting the air masses where the C-130 flew directly over or near these surface sites.

Our results from lagrangian sampling between the DC-8 to C-130 are similar to those found by Fuelberg et al, 2008. Quasi - lagrangian sampling instances were identified between DC-8 flight 14, 15, 16 and 17 to C-130 Flights 21 and 24 by these two studies. The STEM model calculations did not find lagrangian sampling between DC-8 flights 14, 15 and 16 with C-130 flights 20, 22, and 23, which was found by Fuelberg et al., study. In addition, the STEM model results found lagrangian sampling between DC-8 flights 12 and 15 with C-130 flights 18 and 23, which was identified by Fuelberg et al. 2008. These variations are seen due to differences in the input meteorological model. Fuelberg et al., (2008) did not do a similar study with the surface sites hence the results in this study can not be directly compared.

To illustrate how this information can be used, one case of model calculated quasi-lagrangian sampling between the two airborne platforms which was later sampled at the two surface sites. Figure 4.18 illustrates the position of the DC-8 and C-130 (DC8-C130-case study) for the case we are analyzing and figure 4.19 presents the time series of both modeled and observed CO and ozone time series of DC-8 flight 15 and C-130 flight 21 (these flights occurred one day apart). The model is shown to capture many of the important observed features, but misses fine structures, reflecting the limitation of models to resolve the complex layering of trace gas species in the atmosphere. The square boxes capture an example where the calculation suggests that quasi lagrangian sampling occurred. The CO and ozone levels change between these times due to chemical conversion and mixing processes. Also plotted are the ratios of observed C_2H_6/CO . Since these species have a similar loss rate with respect to OH the ratios should be preserved (at least wrt to chemical processing). The ratio values within the windows both show a cluster of values around 0.009. The relationships between observed quantities between the two aircraft cannot be easily answered without carefully analyzing the reaction mechanism, transport path and removal processes.

To illustrate how the composition changes along the pseudo lagrangian paths, we extracted the model calculation of CO and ozone along the back trajectory path from MTB and the modeled aerosols from Trinidad Head that crossed the same C130-flight 21 and the DC-8 flight 15 track as shown in figure 4.20. For these particular trajectories the passing heights over the surface sites are between 3-4 kilometers as shown in the curtain plots for MBO and THD. The C-130 was ~ 1 day down wind of the DC-8 observations and MBO and THD were ~ 2 days downwind of the C-130. For the trajectories connecting the DC-8, C-130 at MBO, the observed CO concentrations were ~120 ppb while the O₃ values were ~50 ppb. However, for the trajectories connecting the DC-8, C-130 and THD, the sulfate aerosol increased from ~0.3 μg/m³ to ~0.6 μg/m³, to ~1.5 μg/m³ respectively. The extraction of species along the path of wind back trajectories shown in figure 4.20 illustrates that the pollutant concentration can vary significantly without them passing through a significant emission source region.

An important research area in the long range transport of pollutants is related to how do pollutants transported from one continent to the other influence the near surface concentrations. One important mechanism is that air masses descend to the surface where they mix with locally emitted pollutants. To demonstrate this, we analyzed a case where the back trajectories suggested that air sampled by the C-130 descended as the air masses moved on-shore. The case we are discussing is C-130 flight -15, the flight track and the path of the trajectory is shown in figure 4.21. Again we have extracted modeled values along this trajectory path. The air mass altitude according to model calculation sinks from about 7000 meters to 3200 meters. As the air mass sinks, the temperature and RH increase as shown in figure 4.21 (e.g., from April 21 to 24). During this period PAN decreases consistent with the thermal decomposition of PAN while NO_x increases. Ozone also increases along with the increases in NO_x. The air mass descends rapidly on April 25, and begins to mix with boundary pollution, as seen in the increases in CO, NO_x, and PAN while the ozone levels decrease.

It was difficult to derive any clear conclusions from the quasi lagrangian and sinking air mass case studies described above due to the large uncertainties associated with such calculations. The quasi lagrangian sampling calculations are subject to great uncertainty due to constraints set for identifying such sampling instances. Latto (2009) used a 6 hour time constraint for their quasi-lagrangian sampling calculations during the INTEX-B sampling period and found that the highest uncertainty was associated with this time constraint as the large scale meteorological features, routinely seen over the Pacific, can travel large distances in 6 hour time span. Latto (2009) also found that the other constraints of altitude, latitude and locations are also significant sources of uncertainty. The composition of the quasi-lagrangian sampled air masses is influenced by various processes including vertical mixing, dilution, surface deposition and chemical oxidation, which are difficult to characterize both by observations and models over the Pacific outflow region. The three-dimensional chemical transport model studies with a higher resolution than the 50 km resolution used in this study, coupled with detailed photochemical box model analysis will be helpful in analyzing the quasi lagrangian sampled air parcels. In addition, the quasi lagrangian sampling opportunities should be carefully planned by looking at the available meteorological forecasts.

4.3.4 Emission Sensitivity Runs

The alarming growth in Asian emissions due to the unprecedented economic and industrial growth is one of the major factors for deteriorating air quality across the globe. The growing Asian emissions also have climatic impacts and alter the Earth's radiative balance (Adhikary 2008). It becomes extremely important to understand the influence of source regions and specific emission sectors on global air quality and climate in order to devise effective emission reduction strategies. Koch *et al.*, (2007) applied the NASA Goddard Institute for Space Studies (GISS) Global Circulation Model (GCM) to study

the impact of major source regions and emission sectors on the aerosol radiative forcing calculations for the Northern hemisphere.

In this study, the influence of sectoral emission categories including transportation, residential, power and industry on the regional concentration distributions of Asia is investigated with a series of modeling runs using STEM tracer model during the INTEX-B sampling period. The results discussion is focused on BC and sulfate due to the regional difference in their emission sources. The base case BC emission distributions with all sectors included along with percent contribution of each sector across the Asian region is shown in figure 4.22. The major BC emission hotspots are East China and the Indo Gangetic plain (top panel). The residential sector is the major contributor to emissions throughout the region as seen in the middle left panel. The transportation sector accounts for most of the BC emission in Japan and Korea suggesting that the vehicular traffic emissions the major source of BC in this region. The contribution of power and industry sectors to BC emissions is much lower across the region except in parts of East China. The base SO₂, (a precursor) for sulfate, emissions distribution shown in figure 4.23, indicates that East China is the major source of SO₂ emissions along with some large point sources across the Indian region. The power sector is the dominant contributor to SO₂ emissions followed by the industry sector. In Southeast Asia, the residential sector is a significant contributor to SO₂ emissions suggesting the influence of coal burning for residential heating purposes.

The influence of major anthropogenic emission sectors on the regional BC and sulfate distribution is studied by conducting a series of model runs by eliminating the emissions of a particular sector each time. The standard base case model run includes emissions from all sectors. The contribution of each sector to the concentration and AOD is obtained by calculating the difference between the base case and run with the sector excluded. Since biomass burning contributes significantly to BC, a model run was

conducted by excluding the daily biomass burning emissions from RAQMS model during the INTEX-B sampling period.

The regional concentration distribution of BC and sulfate along with percent contribution of particular sectors are shown in figures 4.24 and 4.25 in a similar manner as the emission distribution plot. India, East China and Southeast Asia are the major BC hotspots consistent with the emissions pattern. The residential sector is the major contributor to BC over Asia and the outflow over the Pacific. The industry sector also contributes significantly to BC concentration. The BC industrial emissions come primarily from small industries in the rural regions. Figure 4.24 shows that the power and industry sectors account for the major portion of the sulfate concentration across the region again consistent with the SO₂ emissions pattern described above. Similar pattern was seen in the BC and AOD distribution plots not shown (here).

Studies have shown that targeting BC emissions is one of the ways to address the global warming problem (Koch *et al.*, 2007). The sector based emission modeling studies can provide insights which can help us target sectors with large BC components. This study indicates that the residential sector in Asia should be the potential target for mitigating the global warming problem. This study also points out that the BC from industrial and transportation sectors has significant impact on the Pacific outflow and should also be a potential target for emission reduction.

4.4 Summary

STEM, a regional chemical transport model was used to simulate the outflow of aerosols and trace gases from Asia to North America during the spring of 2006. The model performance was evaluated with observations from the NASA INTEX-B field campaign. The STEM chemical transport was driven by the recently developed Weather Research and Forecast (WRF) meteorological model. Results from the WRF model showed that it was able to capture the meteorological variables adequately to simulate

chemical transport. Tagged CO tracer studies along with back trajectory analysis were performed to identify the source regions of observed pollutants.

Comparison of modeled sulfate to airborne observations showed that the model underestimates the magnitude of sulfate concentration in the eastern Pacific. This appears to be due to an under estimation of sulfur emissions and a transport-related displacement of the predicted location of the mid-tropospheric peak in sulfate. The mission wide average modeled aerosol distributions were presented to put the airborne observations in perspective as most of the airborne sampling was designed to capture higher concentrated pollutant plumes.

STEM modeled pollutant concentration values were also compared with measurements made at two surface sites: Mt Bachelor, Oregon and Trinidad Head, California. The model is able to adequately capture the magnitude and synoptic variations of trace gases and aerosols at both these sites. The results from Kathmandu and NCO-P, Nepal suggest areas where model improvements are needed to represent South Asian outflow.

Modeling experiments were performed to evaluate the impact of sectoral Asian emissions over the Pacific for the year 2006. The results showed that power and industrial sector were the major contributors to sulfate concentration, while residential and biomass burning sectors accounted for a major portion of the BC concentration. This study also showed the industrial sector also contributes significantly to the BC over East China, unlike other regions.

These results show that regional scale chemical transport models provide an important tool for the analysis of comprehensive data sets such as that obtained in INTEX B. However there remain important limitations. For example, this study pointed out problems in the prediction of the gas-particle partitioning of nitric acid, and sulfate over the western USA. This study also discusses the model limitations in describing the concentration changes that occur during the quasi-lagrangian sampling events. Further

improvements in the models will require better estimates of emissions, a better understanding of aerosol-gas phase interactions, and a better understanding of the root causes of errors in the prediction of important aspects of the photochemical processes (model deficiencies or something else?).

Table 4.1 Model calculated lagrangian sampling between C-130 and DC-8 flights

| C130 | | | DC8 | | |
|-------------------|------------|----------|------------------|------------|----------|
| Flight .no (date) | Start time | End time | Flight no (date) | Start time | End time |
| 18 (4/28) | 23:42 | 23:42 | 12 (4/28) | 0:02 | 0:02 |
| 21 (5/5) | 21:26 | 21:26 | 14 (5/1) | 11:32 | 11:34 |
| 21 (5/5) | 23:43 | 23:43 | 14 (5/1) | 11:31 | 11:31 |
| 21 (5/5) | 21:39 | 21:50 | 15 (5/4) | 21:54 | 22:34 |
| 21 (5/5) | 22:07 | 22:33 | 15 (5/4) | 22:44 | 23:23 |
| 21 (5/5) | 23:01 | 23:05 | 15 (5/4) | 21:23 | 21:26 |
| 21 (5/5) | 23:17 | 23:23 | 15 (5/4) | 21:22 | 21:14 |
| 23 (5/9) | 21:03 | 0:00 | 15 (5/4) | 21:23 | 21:24 |
| 23 (5/9) | 23:34 | 23:35 | 15 (5/4) | 0:55 | 0:58 |
| 23 (5/9) | 23:30 | 23:30 | 15 (5/4) | 1:01 | 0:57 |
| 24 (5/11) | 16:43 | 16:43 | 16 (5/7) | 1:45 | 1:48 |
| 24 (5/11) | 17:24 | 17:25 | 16 (5/7) | 1:48 | 1:51 |
| 24 (5/11) | 17:36 | 17:37 | 16 (5/7) | 1:49 | 1:53 |
| 24 (5/11) | 18:18 | 18:19 | 16 (5/7) | 1:49 | 1:47 |
| 24 (5/11) | 18:37 | 18:39 | 16 (5/7) | 1:47 | 1:51 |
| 24 (5/11) | 19:18 | 19:18 | 16 (5/7) | 1:47 | 1:47 |
| 24 (5/11) | 20:26 | 20:32 | 16 (5/7) | 23:15 | 1:44 |
| 24 (5/11) | 20:47 | 20:49 | 16 (5/7) | 1:45 | 1:23 |
| 24 (5/11) | 21:29 | 21:33 | 16 (5/7) | 23:16 | 1:45 |
| 24 (5/11) | 21:43 | 21:43 | 16 (5/7) | 1:44 | 1:46 |
| 24 (5/11) | 21:45 | 21:46 | 16 (5/7) | 23:16 | 23:14 |
| 24 (5/11) | 22:05 | 22:14 | 16 (5/7) | 23:12 | 23:13 |
| 24 (5/11) | 22:17 | 22:17 | 16 (5/7) | 23:14 | 23:11 |
| 24 (5/11) | 22:24 | 22:25 | 16 (5/7) | 23:11 | 1:48 |
| 24 (5/11) | 22:37 | 22:40 | 16 (5/7) | 1:47 | 1:51 |
| 24 (5/11) | 23:14 | 23:33 | 16 (5/7) | 1:49 | 1:51 |

Table 4.1 continued

| C130 | | | DC8 | | |
|-------------------|------------|----------|------------------|------------|----------|
| Flight .no (date) | Start time | End time | Flight no (date) | Start time | End time |
| 24 (5/11) | 0:01 | 0:01 | 16 (5/7) | 1:48 | 1:50 |
| 24 (5/11) | 16:45 | 17:01 | 17 (5/9) | 0:02 | 1:57 |
| 24 (5/11) | 17:17 | 17:24 | 17 (5/9) | 23:58 | 0:01 |
| 24 (5/11) | 17:36 | 17:42 | 17 (5/9) | 0:10 | 0:10 |
| 24 (5/11) | 18:16 | 18:17 | 17 (5/9) | 0:02 | 0:05 |
| 24 (5/11) | 18:40 | 18:40 | 17 (5/9) | 0:03 | 0:04 |
| 24 (5/11) | 19:17 | 19:17 | 17 (5/9) | 0:03 | 0:04 |
| 24 (5/11) | 23:15 | 23:19 | 17 (5/9) | 0:03 | 0:05 |
| 24 (5/11) | 23:25 | 23:41 | 17 (5/9) | 0:03 | 0:59 |
| 24 (5/11) | 23:45 | 23:46 | 17 (5/9) | 23:58 | 0:59 |
| 24 (5/11) | 0:06 | 0:09 | 17 (5/9) | 23:59 | 0:10 |

Table 4.2 Model calculated lagrangian sampling between DC-8 and Mt. Bachelor

| DC8 | | | MTB | | |
|--------------|-------|-------|-----------|-------|-------|
| Fl.No (date) | Stime | Etime | Date | Stime | Etime |
| 14(5/1) | 12:40 | 12:47 | 5/5/2006 | 12:30 | 15:30 |
| 14(5/1) | 13:08 | 13:13 | 5/5/2006 | 0:00 | 5:00 |
| 15(5/4) | 21:16 | 21:17 | 5/7/2006 | 22:00 | 7:30 |
| 15(5/4) | 0:44 | 0:44 | 5/6/2006 | 9:30 | 13:00 |
| 16(5/7) | 1:48 | 1:48 | 5/11/2006 | 5:30 | 13:00 |
| 17(5/9) | 0:03 | 0:04 | 5/12/2006 | 10:00 | 9:30 |
| 17(5/9) | 0:15 | 0:19 | 5/14/2006 | 0:00 | 3:00 |
| 17(5/9) | 0:32 | 0:47 | 5/13/2006 | 15:00 | 4:30 |

Table 4.3 Model calculated lagrangian sampling between C-130 and Mt. Bachelor.

| C130 | | | MTB | | |
|--------------|-------|-------|-----------|-------|-------|
| Fl.No (Date) | Stime | Etime | Date | Stime | Etime |
| 15(4/21) | 21:36 | 21:36 | 4/26/2006 | 2:30 | 3:00 |
| 15(4/21) | 22:22 | 22:22 | 4/25/2006 | 13:00 | 23:30 |
| 15(4/21) | 0:00 | 0:13 | 4/25/2006 | 2:00 | 15:00 |
| 16(4/24) | 18:34 | 18:37 | 4/27/2006 | 16:30 | 7:30 |
| 16(4/24) | 18:40 | 19:42 | 4/26/2006 | 7:00 | 10:30 |
| 16(4/24) | 19:51 | 19:51 | 4/27/2006 | 1:20 | 10:00 |
| 16(4/24) | 19:55 | 19:55 | 4/27/2006 | 23:00 | 1:20 |
| 16(4/24) | 20:39 | 20:39 | 4/27/2006 | 0:00 | 0:00 |
| 16(4/24) | 20:43 | 20:58 | 4/28/2006 | 11:00 | 11:00 |
| 16(4/24) | 21:49 | 22:01 | 4/27/2006 | 16:30 | 18:30 |
| 16(4/24) | 22:09 | 22:09 | 4/26/2006 | 20:00 | 23:00 |
| 16(4/24) | 22:57 | 23:00 | 4/26/2006 | 14:00 | 22:30 |
| 17(4/26) | 19:15 | 19:18 | 4/29/2006 | 6:00 | 10:00 |
| 17(4/26) | 19:39 | 19:39 | 4/29/2006 | 6:00 | 13:00 |
| 17(4/26) | 20:01 | 22:07 | 5/1/2006 | 3:30 | 4:00 |
| 17(4/26) | 22:07 | 22:07 | 5/1/2006 | 23:00 | 4:00 |
| 17(4/26) | 22:11 | 22:12 | 5/1/2006 | 17:00 | 4:00 |
| 17(4/26) | 23:03 | 23:03 | 4/29/2006 | 23:30 | 1:30 |
| 18(4/28) | 17:17 | 17:17 | 5/2/2006 | 20:30 | 7:30 |
| 19(5/1) | 18:52 | 19:08 | 5/3/2006 | 8:00 | 22:00 |
| 19(5/1) | 0:41 | 1:14 | 5/4/2006 | 1:00 | 5:00 |
| 20(5/3) | 19:14 | 19:51 | 5/5/2006 | 9:30 | 15:30 |
| 20(5/3) | 23:24 | 23:32 | 5/7/2006 | 7:30 | 10:30 |
| 20(5/3) | 23:36 | 23:37 | 5/8/2006 | 5:00 | 0:30 |
| 20(5/3) | 0:18 | 0:59 | 5/5/2006 | 0:00 | 2:30 |
| 21(5/5) | 23:25 | 23:48 | 5/7/2006 | 8:00 | 2:30 |
| 21(5/5) | 0:52 | 0:52 | 5/7/2006 | 2:30 | 5:30 |

Table 4.3 continued

| C130 | | | MTB | | |
|--------------|-------|-------|-----------|-------|-------|
| Fl.No (Date) | Stime | Etime | Date | Stime | Etime |
| 22(5/8) | 16:51 | 17:54 | 5/10/2006 | 0:00 | 18:00 |
| 22(5/8) | 22:12 | 22:13 | 5/10/2006 | 9:30 | 17:30 |
| 22(5/8) | 22:30 | 22:32 | 5/10/2006 | 11:00 | 18:00 |
| 22(5/8) | 23:27 | 23:27 | 5/12/2006 | 19:10 | 0:30 |
| 22(5/8) | 0:09 | 0:09 | 5/11/2006 | 17:00 | 20:30 |
| 22(5/8) | 0:13 | 0:17 | 5/12/2006 | 7:00 | 0:00 |
| 23(5/9) | 17:33 | 17:34 | 5/12/2006 | 10:30 | 23:30 |
| 23(5/9) | 18:15 | 18:19 | 5/12/2006 | 11:00 | 19:30 |
| 23(5/9) | 19:59 | 20:02 | 5/11/2006 | 1:30 | 3:30 |
| 23(5/9) | 0:59 | 1:02 | 5/11/2006 | 4:30 | 23:00 |
| 24(5/11) | 17:28 | 17:34 | 5/12/2006 | 18:00 | 1:30 |

Table 4.4 Model calculated lagrangian sampling of air mass between DC-8 and Trinidad Head.

| DC8 | | | THD | | |
|-----------|------------|----------|-----------|------------|----------|
| Flight No | Start time | End time | Date | Start time | End time |
| 10(4/17) | 20:03 | 20:07 | 4/21/2006 | 17:30 | 14:00 |
| 10(4/17) | 20:08 | 20:36 | 4/18/2006 | 23:00 | 9:00 |
| 14(5/1) | 12:40 | 12:47 | 5/5/2006 | 15:00 | 8:30 |
| 14(5/1) | 13:01 | 13:06 | 5/4/2006 | 1:00 | 10:30 |
| 16(5/7) | 23:08 | 23:09 | 5/10/2006 | 3:00 | 12:30 |
| 16(5/7) | 1:47 | 1:47 | 5/11/2006 | 21:30 | 3:30 |
| 16(5/7) | 1:52 | 1:52 | 5/12/2006 | 0:00 | 2:30 |
| 17(5/9) | 0:05 | 0:05 | 5/11/2006 | 14:30 | 17:30 |
| 17(5/9) | 0:15 | 0:17 | 5/13/2006 | 20:00 | 2:30 |
| 17(5/9) | 0:32 | 0:35 | 5/12/2006 | 7:00 | 17:30 |

Table 4.5 Model calculated lagrangian sampling of air mass between C-130 and THD.

| C130 | | | THD | | |
|--------------|------------|----------|-----------|------------|----------|
| Fl.No (Date) | Start time | End time | Date | Start time | End time |
| 15(4/21) | 21:32 | 21:32 | 4/24/2006 | 15:30 | 18:00 |
| 15(4/21) | 22:12 | 22:12 | 4/23/2006 | 14:30 | 20:30 |
| 15(4/21) | 22:54 | 22:55 | 4/24/2006 | 0:30 | 8:30 |
| 15(4/21) | 23:54 | 0:10 | 4/23/2006 | 19:00 | 14:00 |
| 16(4/24) | 18:33 | 18:33 | 4/27/2006 | 2:00 | 4:30 |
| 16(4/24) | 18:38 | 18:43 | 4/27/2006 | 2:30 | 20:00 |
| 16(4/24) | 19:03 | 19:04 | 4/26/2006 | 10:30 | 23:30 |
| 16(4/24) | 19:22 | 19:25 | 4/26/2006 | 9:30 | 23:30 |
| 16(4/24) | 20:54 | 20:57 | 4/28/2006 | 13:00 | 18:30 |
| 17(4/26) | 19:10 | 19:13 | 4/29/2006 | 1:00 | 6:00 |
| 17(4/26) | 19:19 | 19:20 | 4/30/2006 | 22:30 | 15:00 |
| 17(4/26) | 19:33 | 19:34 | 4/30/2006 | 6:30 | 0:00 |
| 17(4/26) | 22:11 | 22:11 | 4/30/2006 | 16:00 | 19:00 |
| 17(4/26) | 23:08 | 23:08 | 4/30/2006 | 22:00 | 13:30 |
| 18(4/28) | 0:38 | 0:38 | 5/3/2006 | 20:30 | 0:00 |
| 20(5/3) | 18:48 | 18:48 | 5/6/2006 | 3:00 | 3:00 |
| 20(5/3) | 19:24 | 19:24 | 5/8/2006 | 21:30 | 23:30 |
| 20(5/3) | 19:49 | 20:39 | 5/6/2006 | 9:00 | 9:00 |
| 20(5/3) | 19:51 | 20:04 | 5/8/2006 | 6:00 | 13:30 |
| 20(5/3) | 21:24 | 21:27 | 5/7/2006 | 7:30 | 15:30 |
| 20(5/3) | 23:12 | 23:14 | 5/8/2006 | 1:00 | 6:30 |
| 20(5/3) | 23:27 | 23:31 | 5/6/2006 | 23:00 | 23:30 |
| 20(5/3) | 23:36 | 23:39 | 5/8/2006 | 19:30 | 0:30 |
| 20(5/3) | 23:42 | 23:42 | 5/5/2006 | 13:30 | 17:30 |
| 20(5/3) | 23:46 | 0:02 | 5/8/2006 | 18:00 | 6:00 |
| 20(5/3) | 23:51 | 0:06 | 5/6/2006 | 20:00 | 5:30 |
| 20(5/3) | 0:14 | 0:47 | 5/5/2006 | 14:30 | 23:30 |
| 20(5/3) | 0:53 | 1:03 | 5/6/2006 | 18:30 | 10:00 |
| 21(5/5) | 18:40 | 18:40 | 5/8/2006 | 1:00 | 9:30 |

Table 4.5 continued

| C130 | | | THD | | |
|--------------|------------|----------|-----------|------------|----------|
| Fl.No (Date) | Start time | End time | Date | Start time | End time |
| 21(5/5) | 19:20 | 19:45 | 5/5/2006 | 0:00 | 17:00 |
| 21(5/5) | 19:21 | 19:21 | 5/8/2006 | 4:00 | 13:30 |
| 21(5/5) | 23:23 | 23:24 | 5/7/2006 | 22:30 | 0:30 |
| 21(5/5) | 23:51 | 23:52 | 5/7/2006 | 19:30 | 3:30 |
| 21(5/5) | 0:05 | 0:07 | 5/7/2006 | 18:30 | 7:30 |
| 21(5/5) | 0:09 | 0:09 | 5/8/2006 | 17:30 | 18:00 |
| 21(5/5) | 0:44 | 0:44 | 5/8/2006 | 8:00 | 11:30 |
| 21(5/5) | 0:45 | 0:46 | 5/7/2006 | 0:30 | 6:00 |
| 21(5/5) | 0:50 | 0:51 | 5/7/2006 | 1:00 | 9:30 |
| 22(5/8) | 16:58 | 17:02 | 5/11/2006 | 20:00 | 7:30 |
| 22(5/8) | 17:18 | 17:18 | 5/10/2006 | 9:30 | 10:30 |
| 22(5/8) | 17:55 | 17:55 | 5/10/2006 | 7:30 | 18:00 |
| 22(5/8) | 22:09 | 22:12 | 5/10/2006 | 17:00 | 4:00 |
| 22(5/8) | 22:45 | 22:45 | 5/10/2006 | 7:30 | 10:00 |
| 22(5/8) | 23:20 | 23:26 | 5/11/2006 | 16:30 | 13:30 |
| 23(5/9) | 18:17 | 18:18 | 5/11/2006 | 16:30 | 22:00 |
| 24(5/11) | 17:31 | 17:31 | 5/12/2006 | 22:30 | 10:30 |

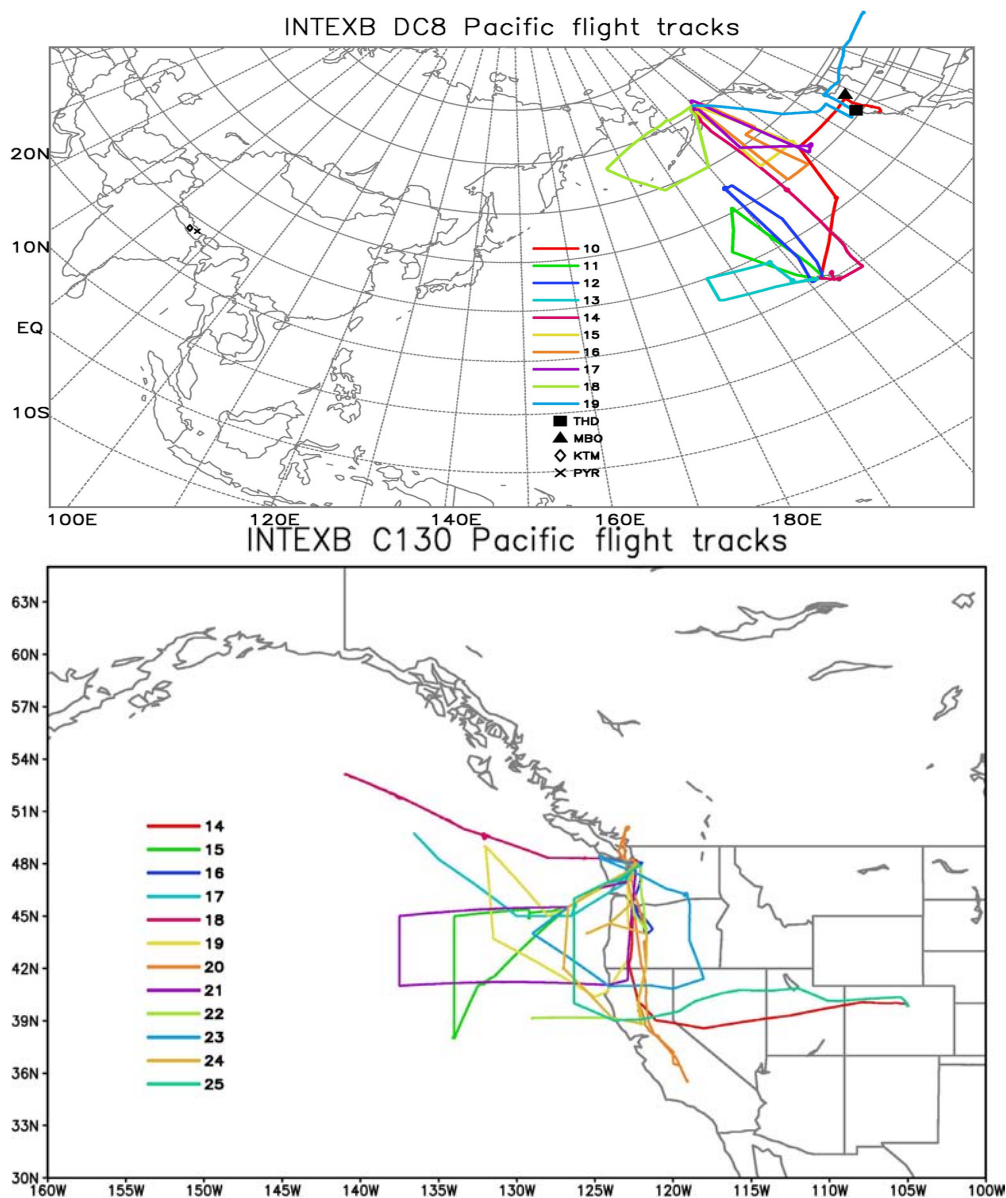


Figure 4.1 NASA DC-8 and NCAR/NSF C-130 flight tracks along with the location of ground based observation sites including Kathmandu (KTM), Trinidad Head (THD) and Mt. Bachelor (MBO) during the INTEX-B (Phase 2) experiment. The numbers denote the research flight numbers for the DC-8 and C-130 aircraft.

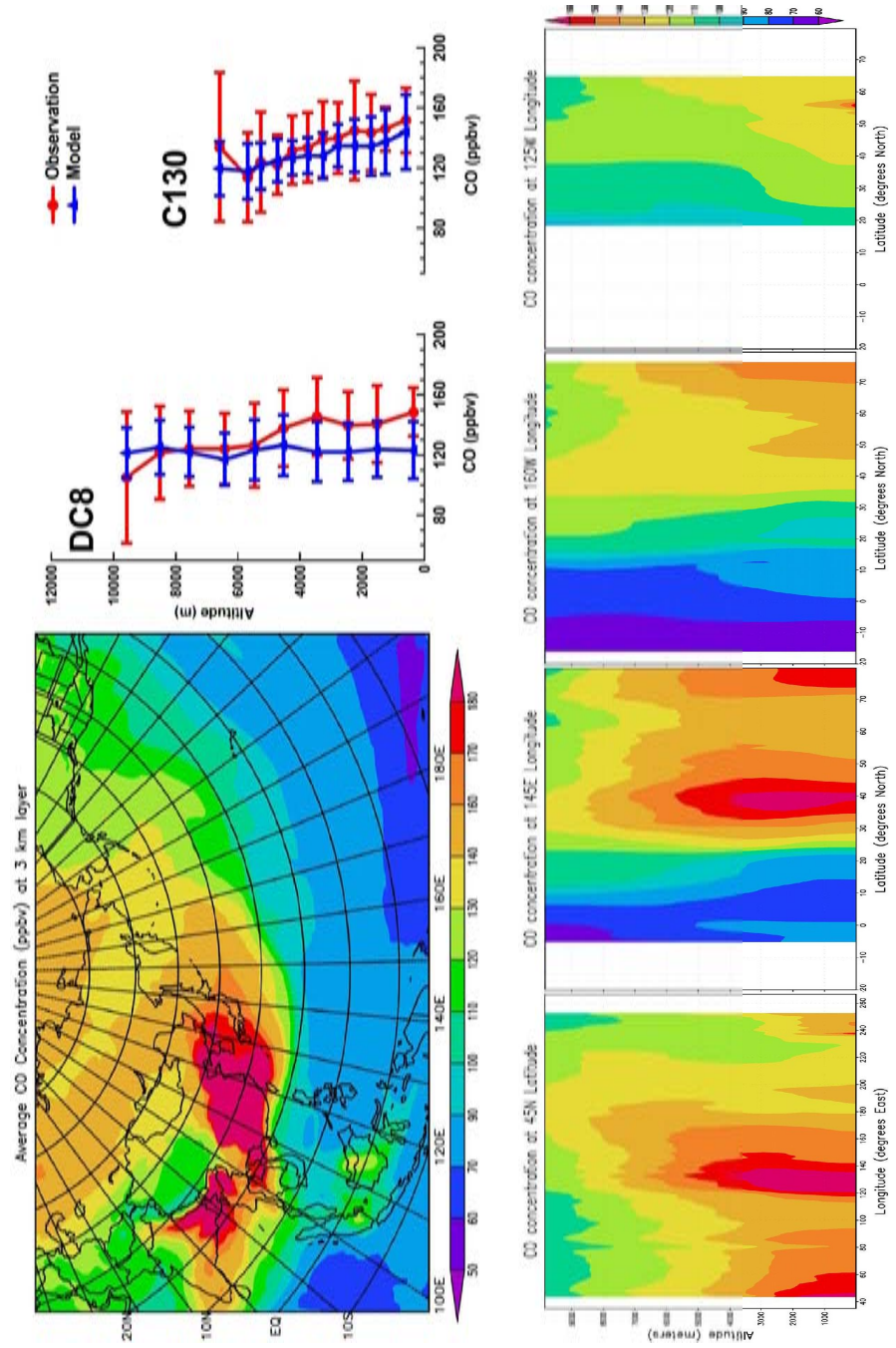


Figure 4.2 Monthly mean CO at 3 kilometer AGL layer, DC-8 and C-130 observed and modeled CO vertical profiles and average CO latitudinal and longitudinal distributions during INTEX-B study period.

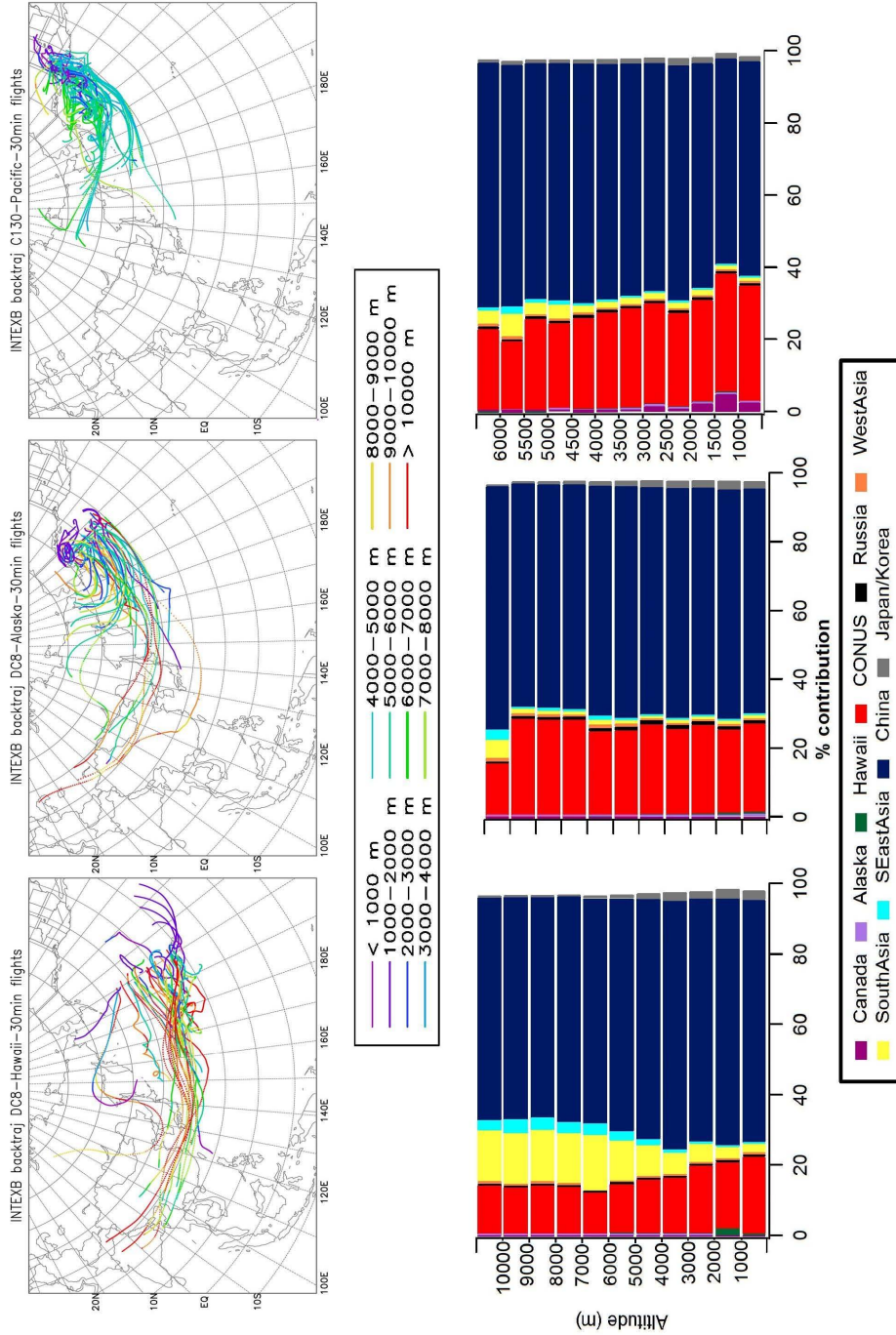


Figure 4.3 Back trajectories of wind vectors and tagged CO tracers illustrating the source region of air masses sampled by the selected DC-8 and C-130 flights.

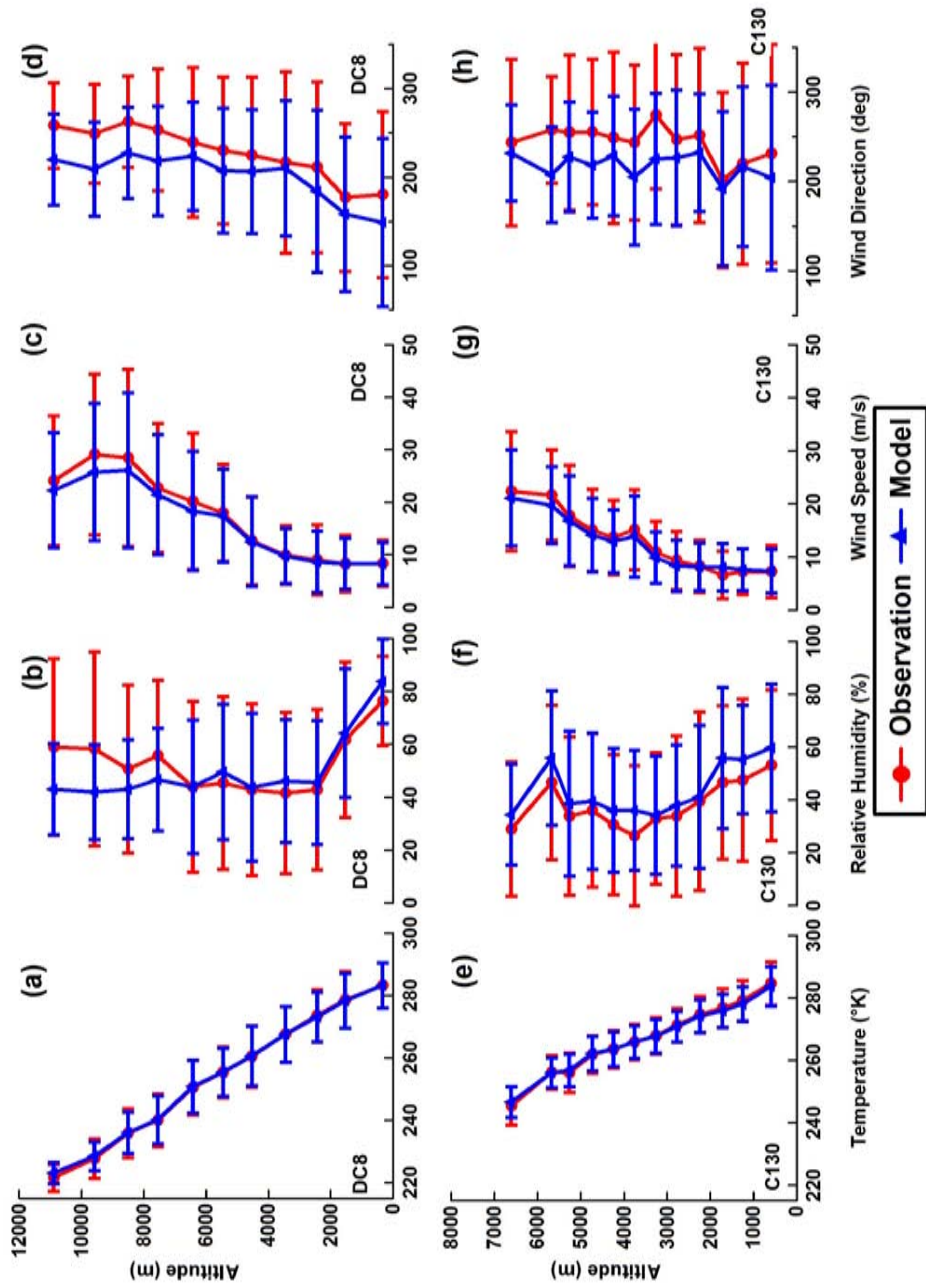


Figure 4.4 Comparison of meteorological variables from the WRF model with DC-8 (Top row a,b,c,d) and C-130 (bottom row e, f, g,h) observations.

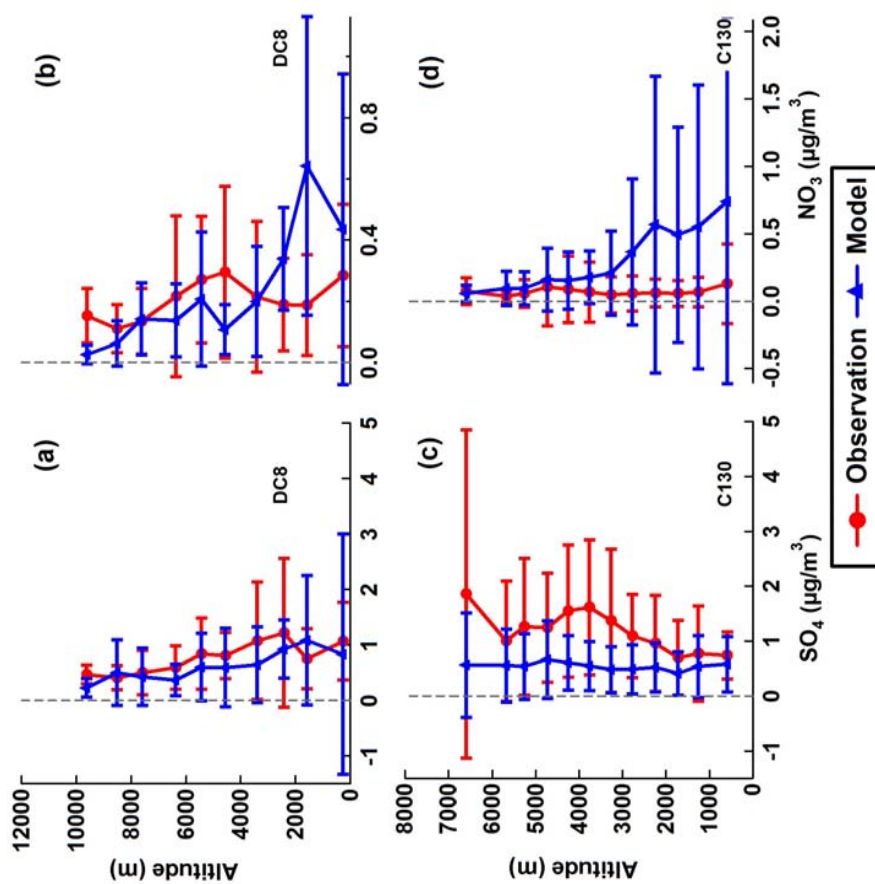


Figure 4.5 Comparison of STEM model predictions versus observed aerosols from the DC-8 and C-130 (a) Sulfate (DC-8) (b) NO₃ (DC-8) (c) Sulfate (C-130) and (d) NO₃ (C-130)

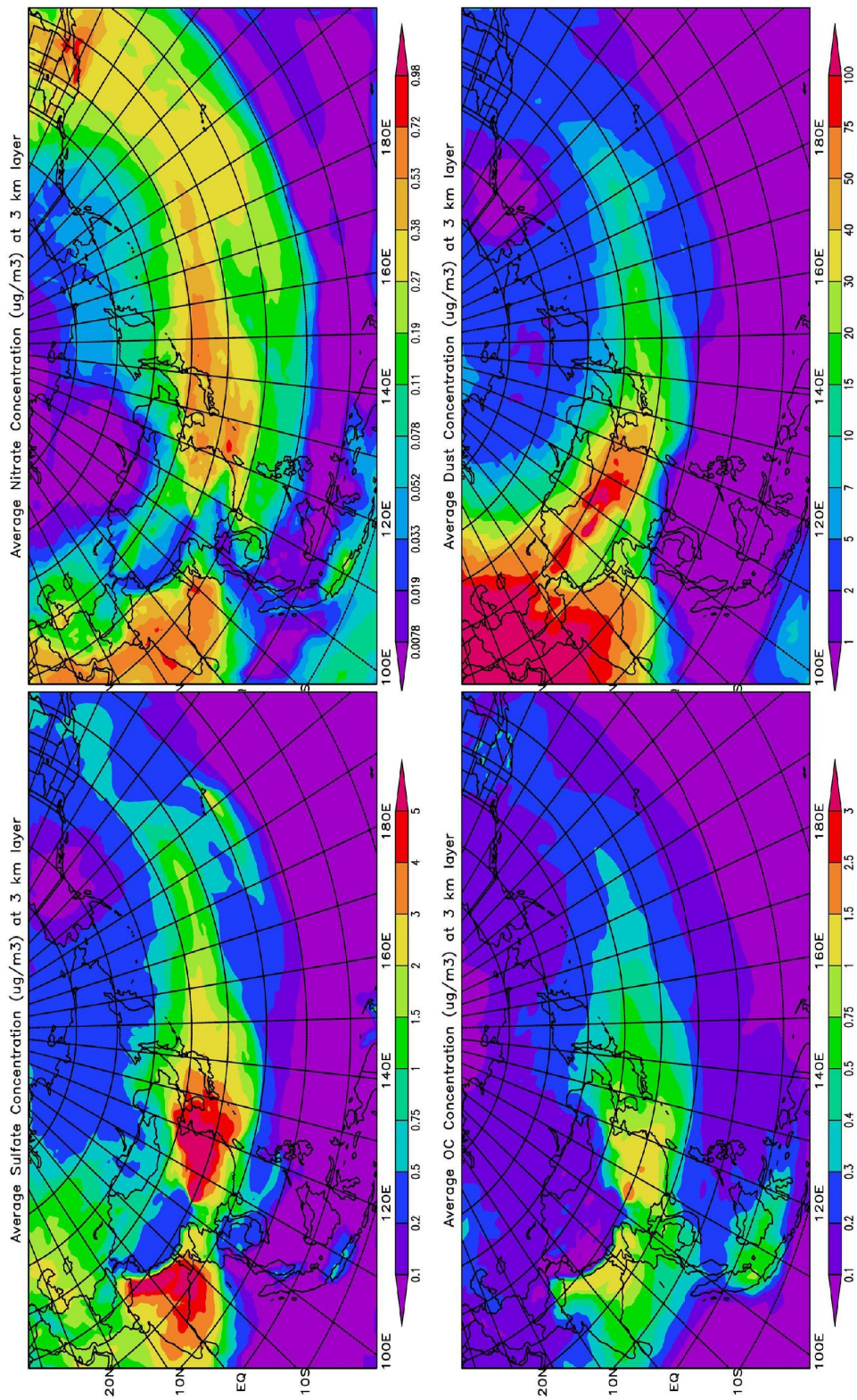


Figure 4.6 Mission wide average distribution of aerosols at the 3-kilometer AGL layer (a) Sulfate, (b) Nitrate, (c) OC and (d) Dust during INTEX-B

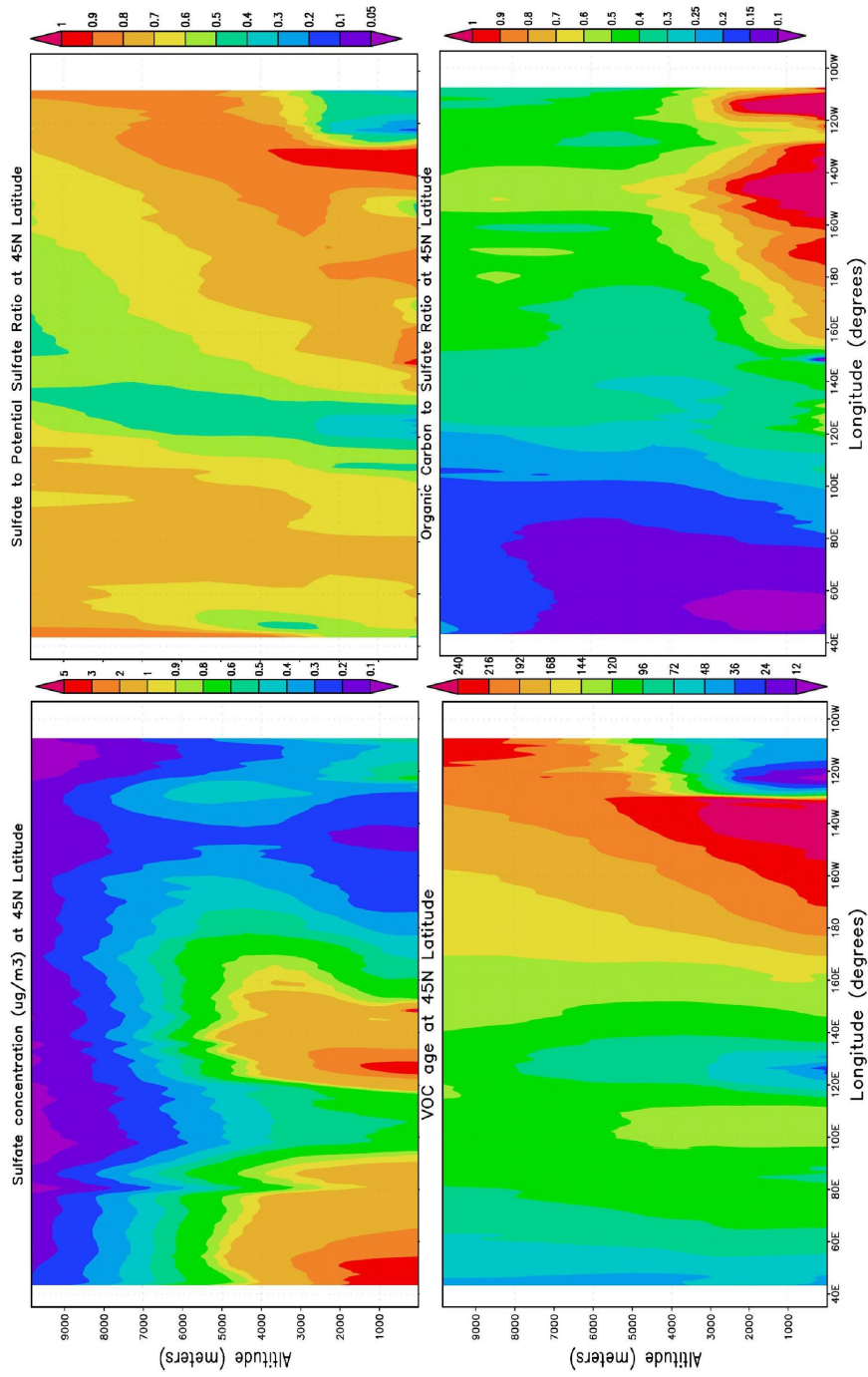


Figure 4.7 Mission wide average cross-sections of (a) sulfate (b) sulfate to potential sulfate ratio (c) VOC age (hours) and (d) OC/SO₄ ratio at 45N during INTEX-B.

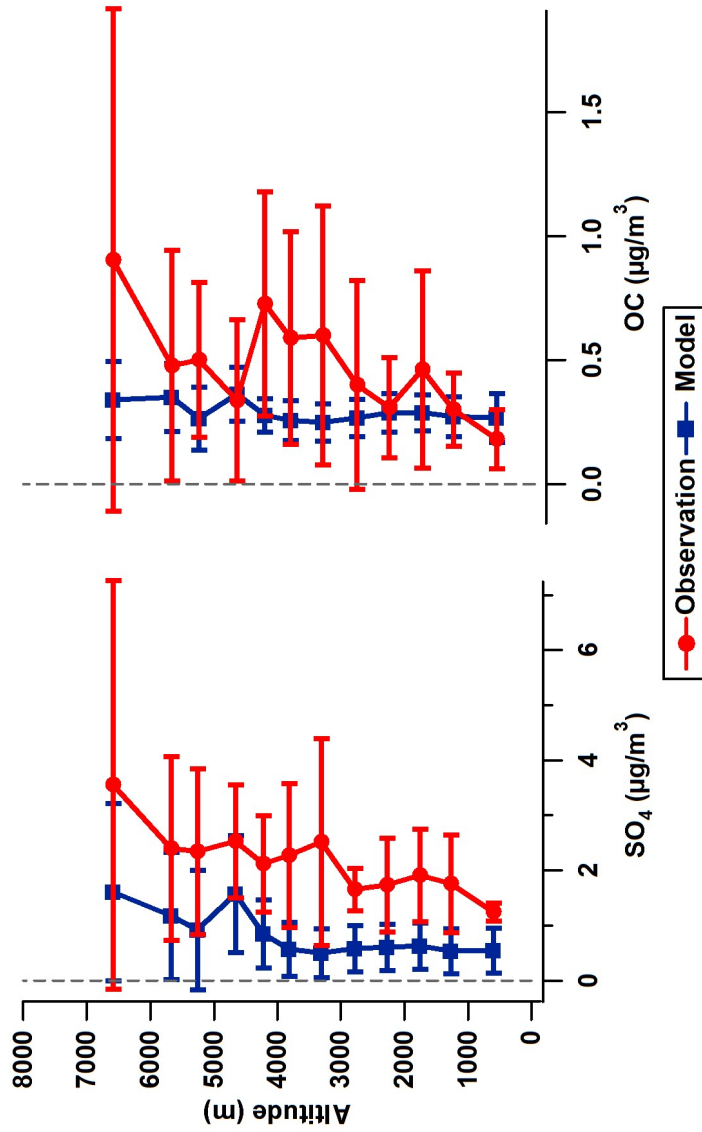


Figure 4.8 Observed AMS and modeled SO₄, and OC vertical profiles for INTEX-B C130 flights using criteria similar to Dunlea *et al.*, 2008 (i.e. Observed AMS SO₄ > 1 µg/m³ and sampled west of 125W degrees longitude)

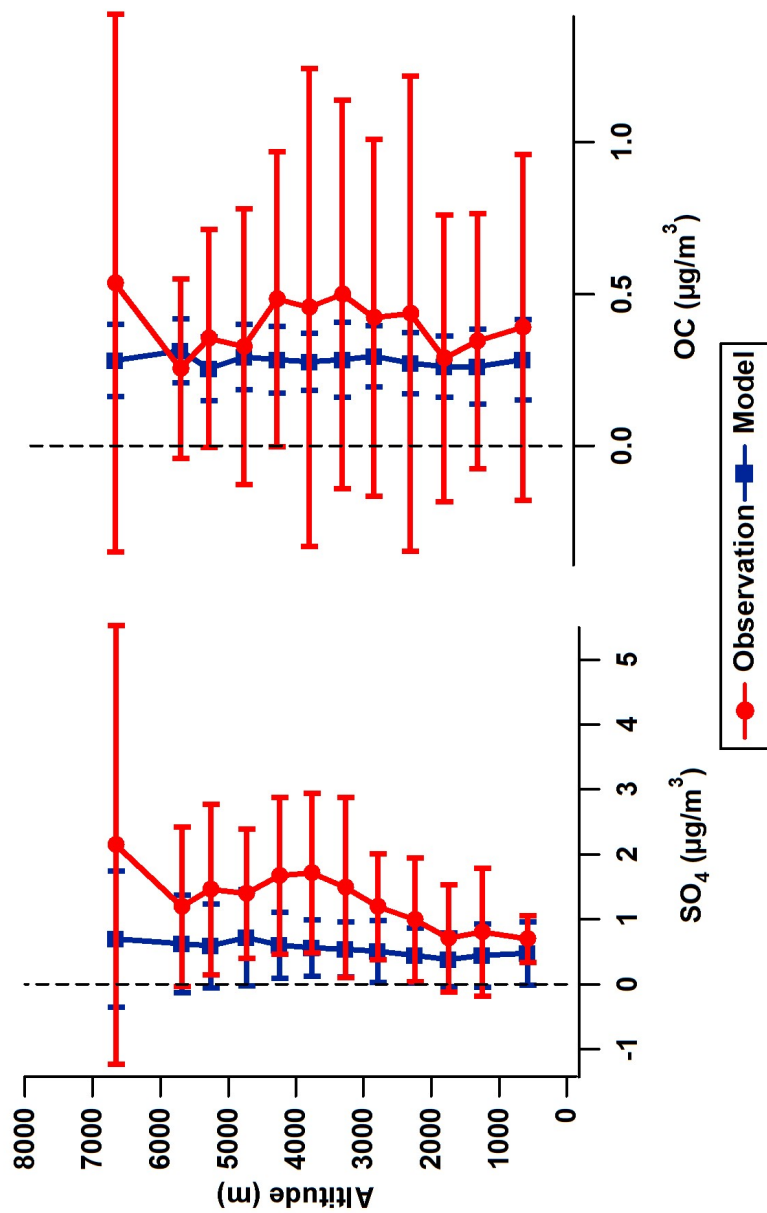


Figure 4.9 Observed AMS and modeled SO_4 and OC vertical profiles for INTEX-B C130 flights using criteria similar to Peltier *et al.*, 2008 (i.e. Modeled $\text{CO} > 100$ ppb and predicted China anthropogenic $\text{CO} > 50\%$ of the predicted total anthropogenic CO)

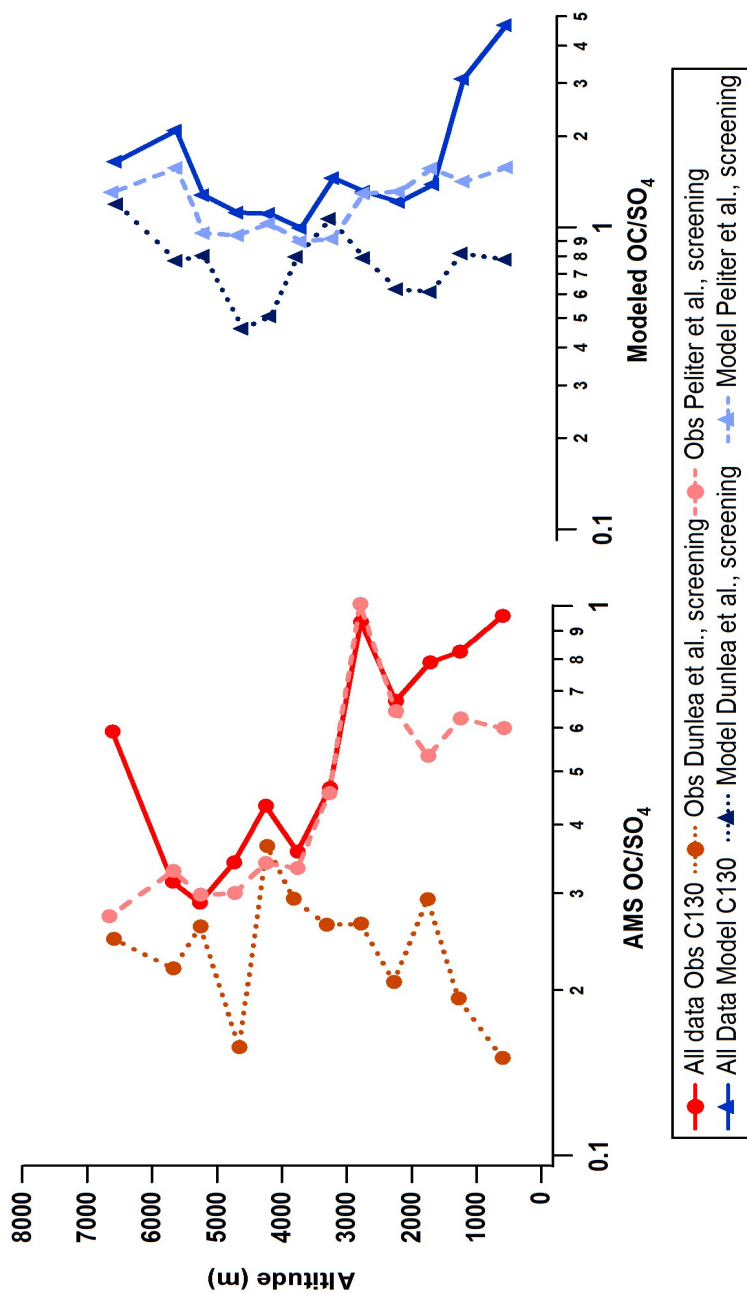


Figure 4.10 Average vertical profiles of OC/SO₄ ratio for INTEX-B campaign. The observed OC/SO₄ ratio is calculated using the OC (OM/1.9) and SO₄ measurements from AMS aboard the C-130 aircraft. The Dunlea et al., 2008 screening criteria are Observed AMS SO₄ > 1 μg

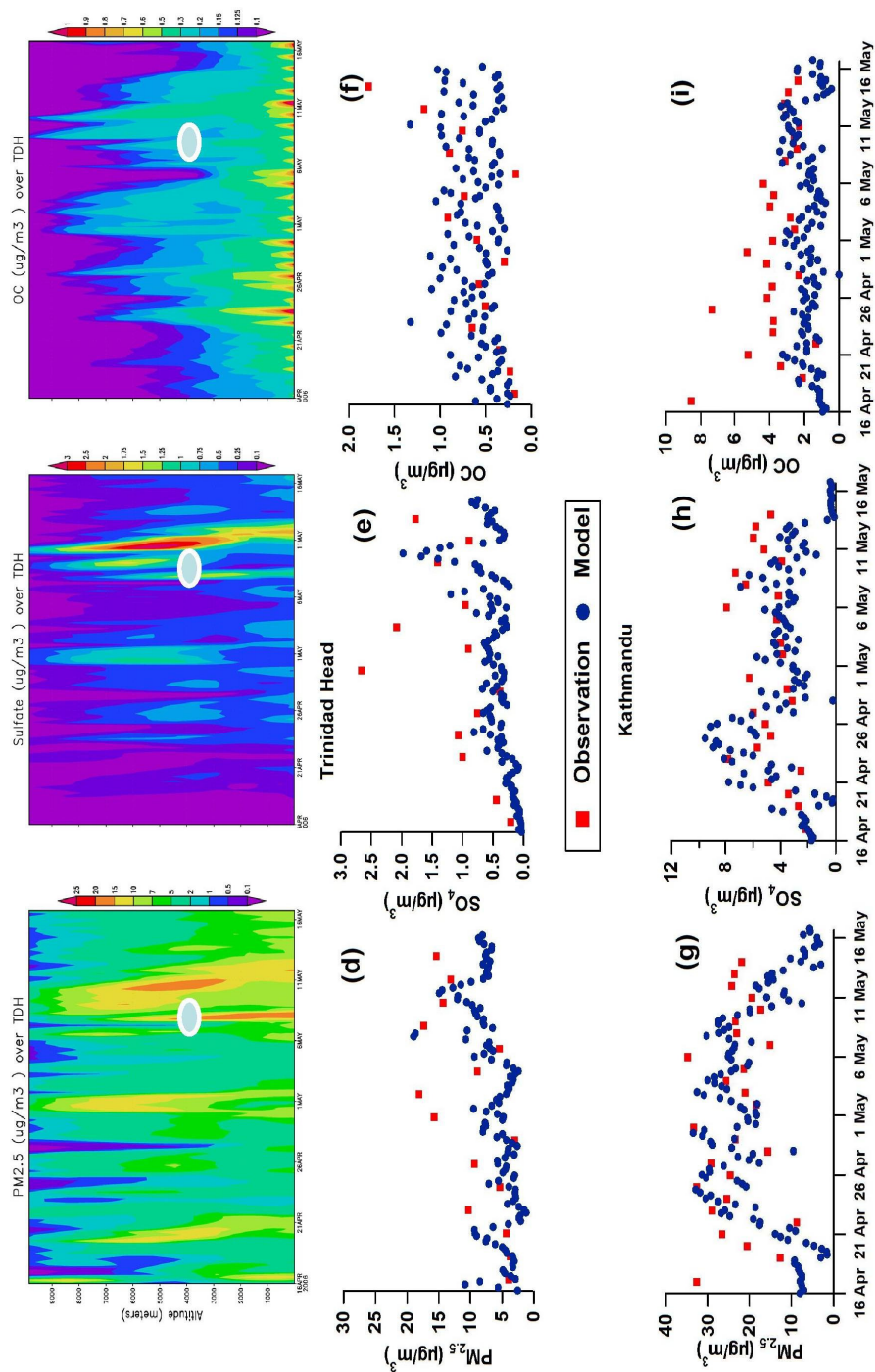


Figure 4.11 Comparison of observed PM_{2.5}, sulfate and OC at Trinidad Head (THD), US (middle row) and Kathmandu, Nepal (bottom) during the INTEX-B campaign. Top row curtain plots at THD. The white oval denotes the location of the lagrangian sampled air mass sampled by C130 flight 21 (05/05/06) that arrived at THD on 05/08/06

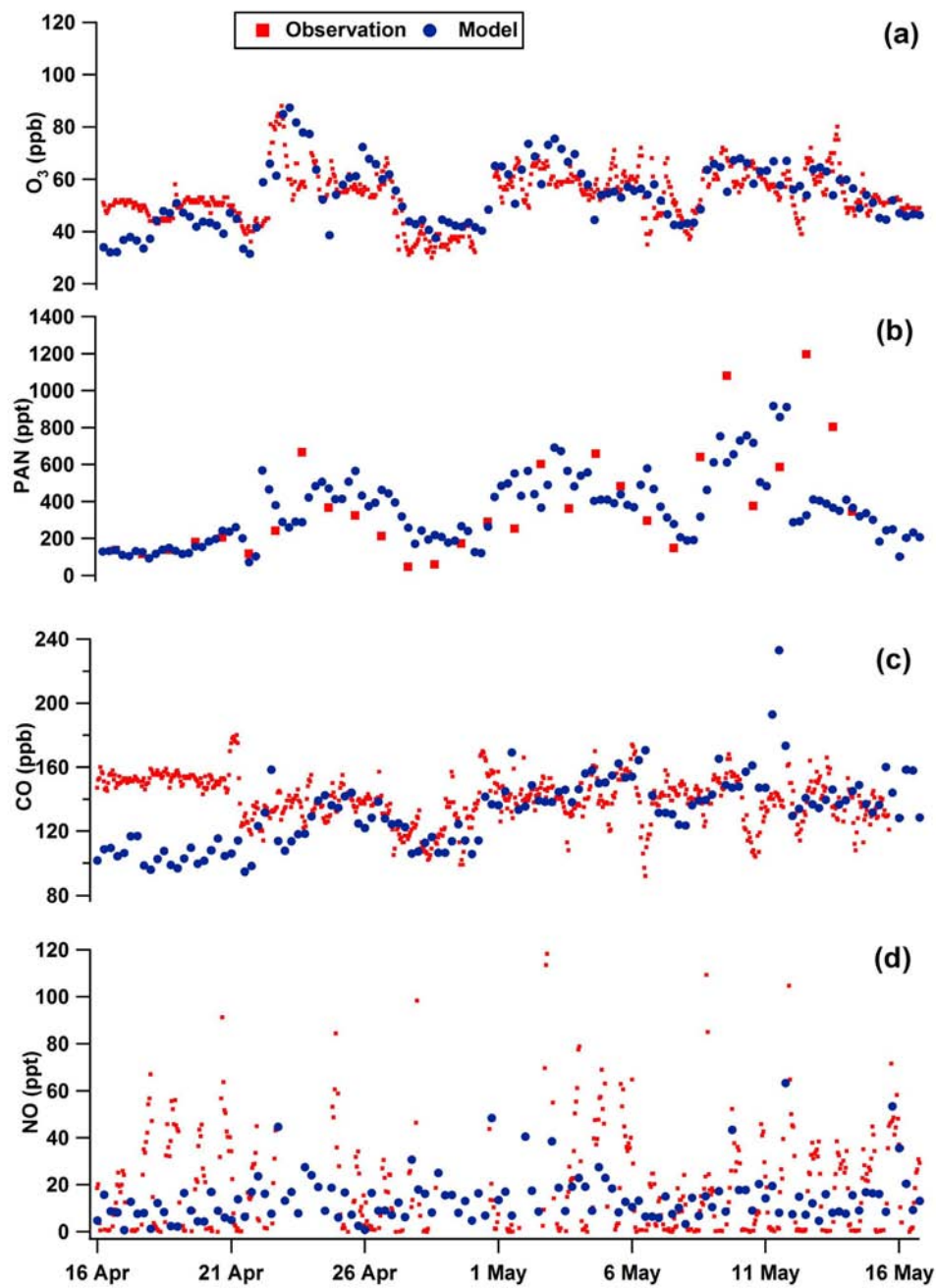


Figure 4.12 Comparison of observed and modeled trace gases at Mt. Bachelor (MBO), OR during INTEX-B campaign (a) Ozone (b) PAN (c) CO (d) NO.

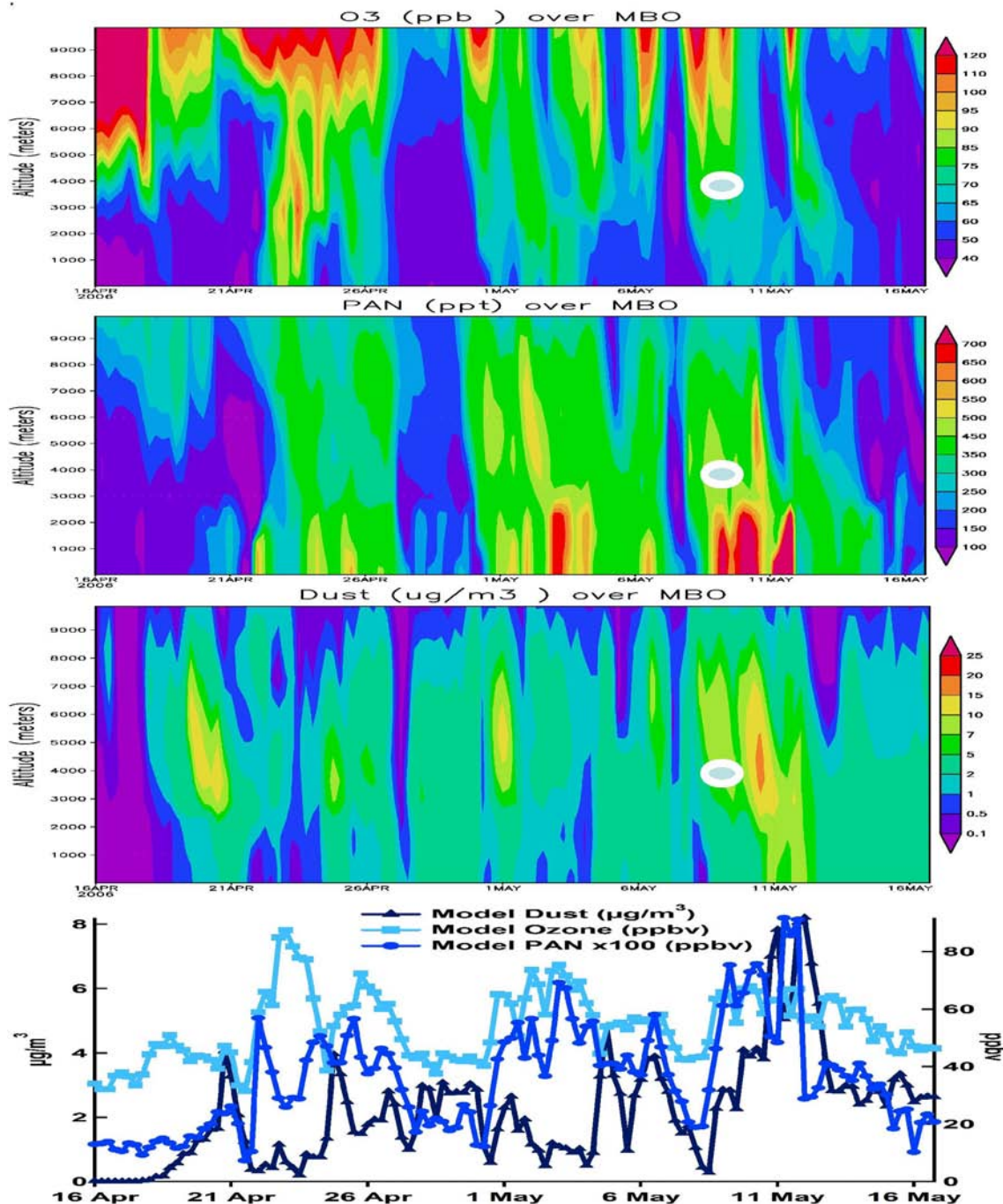


Figure 4.13 Curtain plots of modeled trace gases at Mt. Bachelor (MBO), OR during INTEX-B campaign (a) Ozone (b), PAN, (c) Dust along with (d) time series of these species at the surface level. The white oval shape denotes the lagrangian air mass sampled by C130 flight 21 (05/05/06) that arrived at MBO on 05/08/06

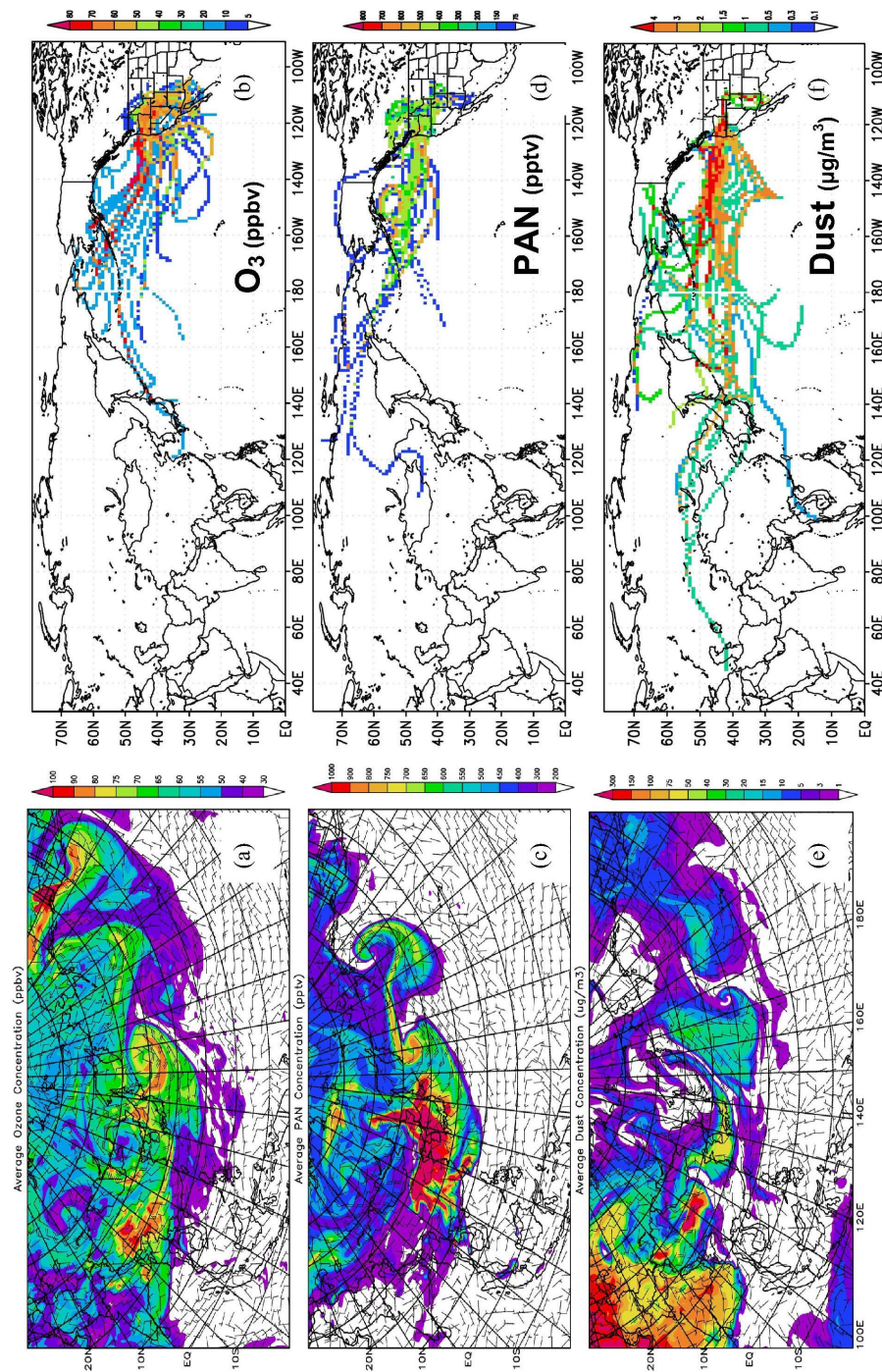


Figure 4.14 Horizontal distribution of modeled ozone, PAN, and dust at 18z, 3kilometer AGL layer along with redistributed concentration along back trajectories on April 22 (a,b), May 3 (c,d) and May 11 (e,f) during INTEX-B.

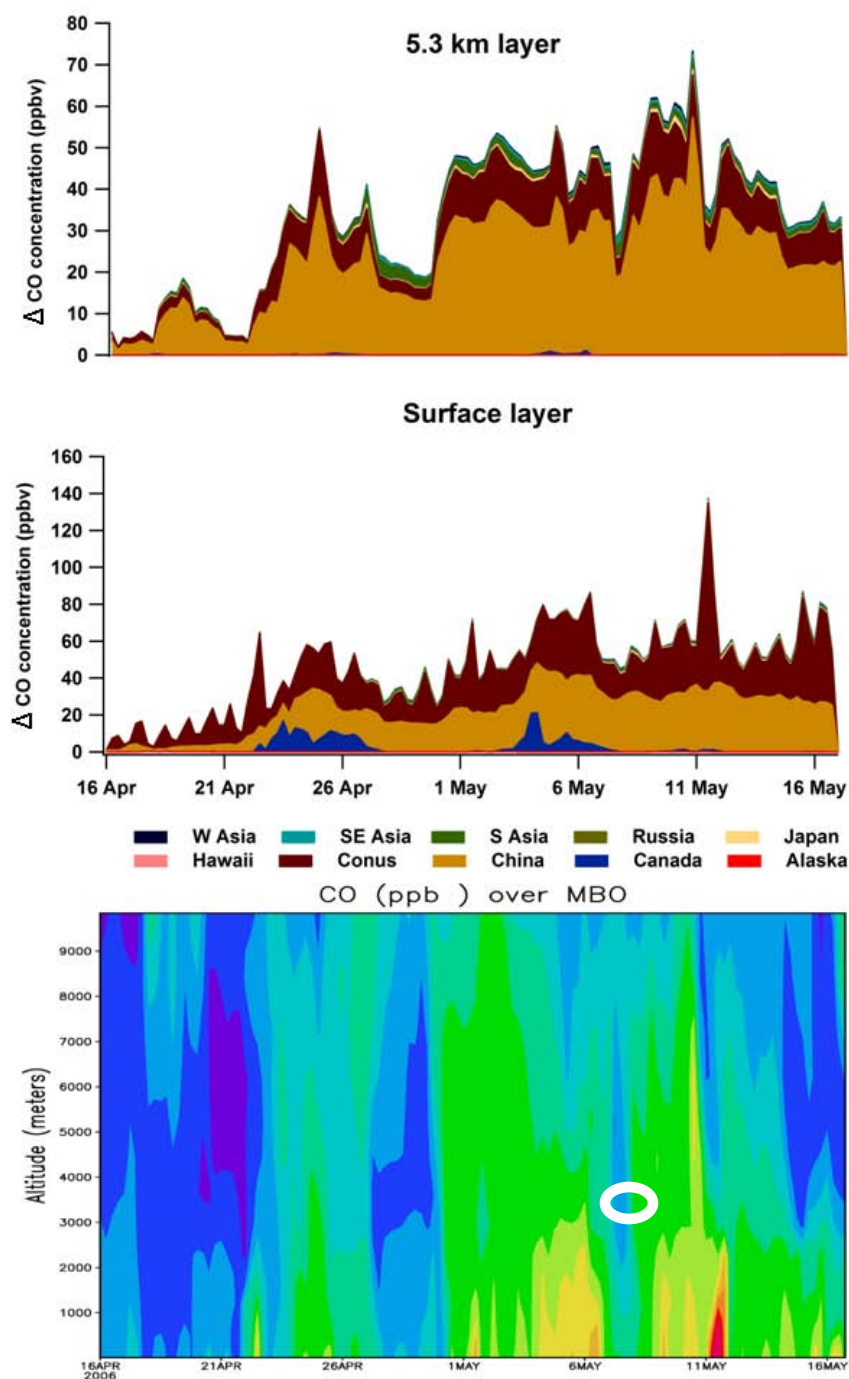


Figure 4.15 Time series of source region tagged CO tracers at 5.3kilometer AGL layer (a) and surface (b) along with the vertical profile of CO (c) at Mt. Bachelor (MBO). The white oval denotes the location of the lagrangian sampled air mass sampled by C130 flight 21 (05/05/06) that arrived at MBO on 05/08/06

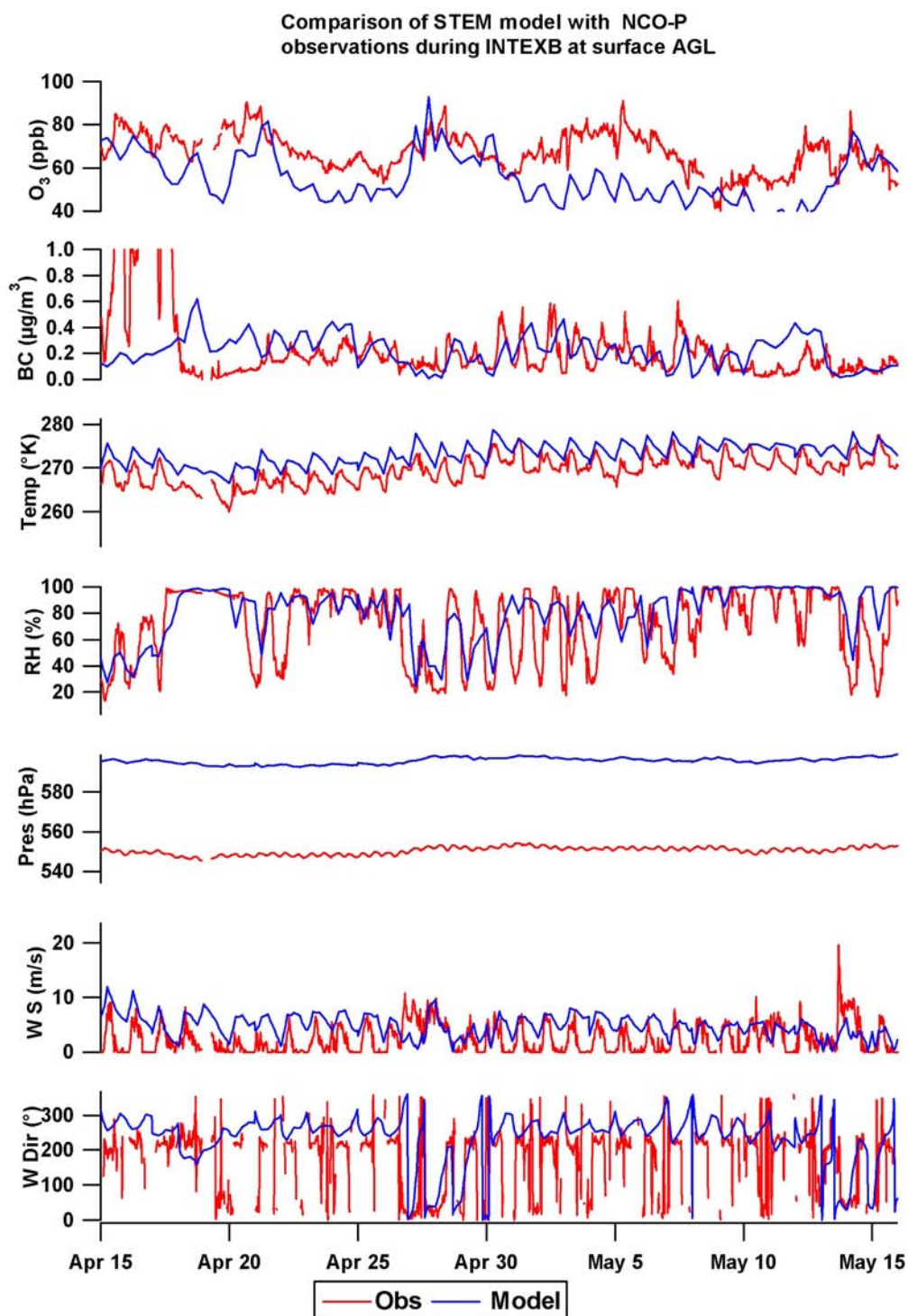


Figure 4.16 Comparison of observed and modeled trace gases and aerosols (surface) at Nepal Climate Observatory at Pyramid (NCO-P), Nepal during INTEX-B campaign

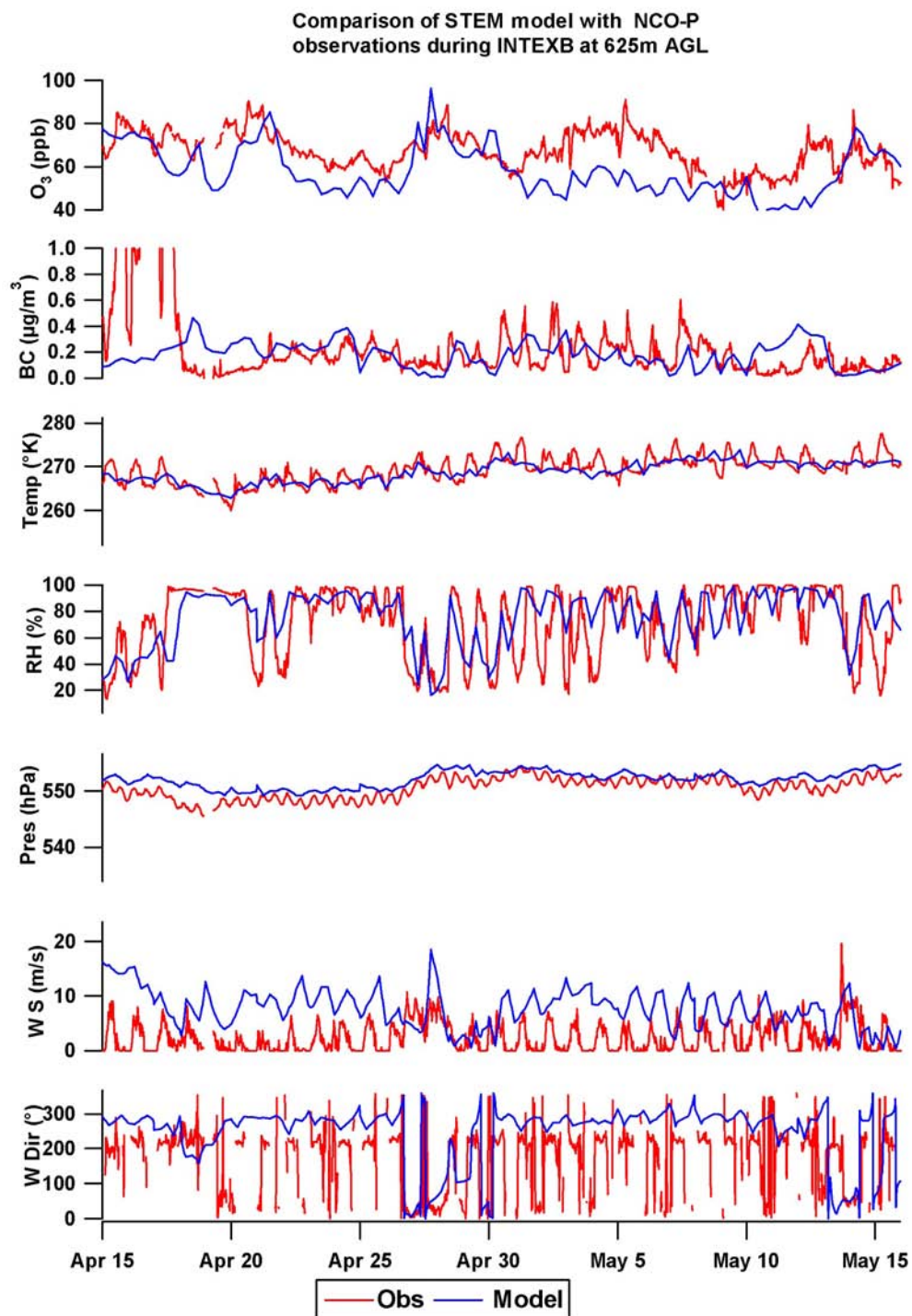


Figure 4.17 Comparison of observed and modeled trace gases and aerosols (625 m AGL) of Nepal Climate Observatory at Pyramid (NCO-P), Nepal during INTEX-B campaign

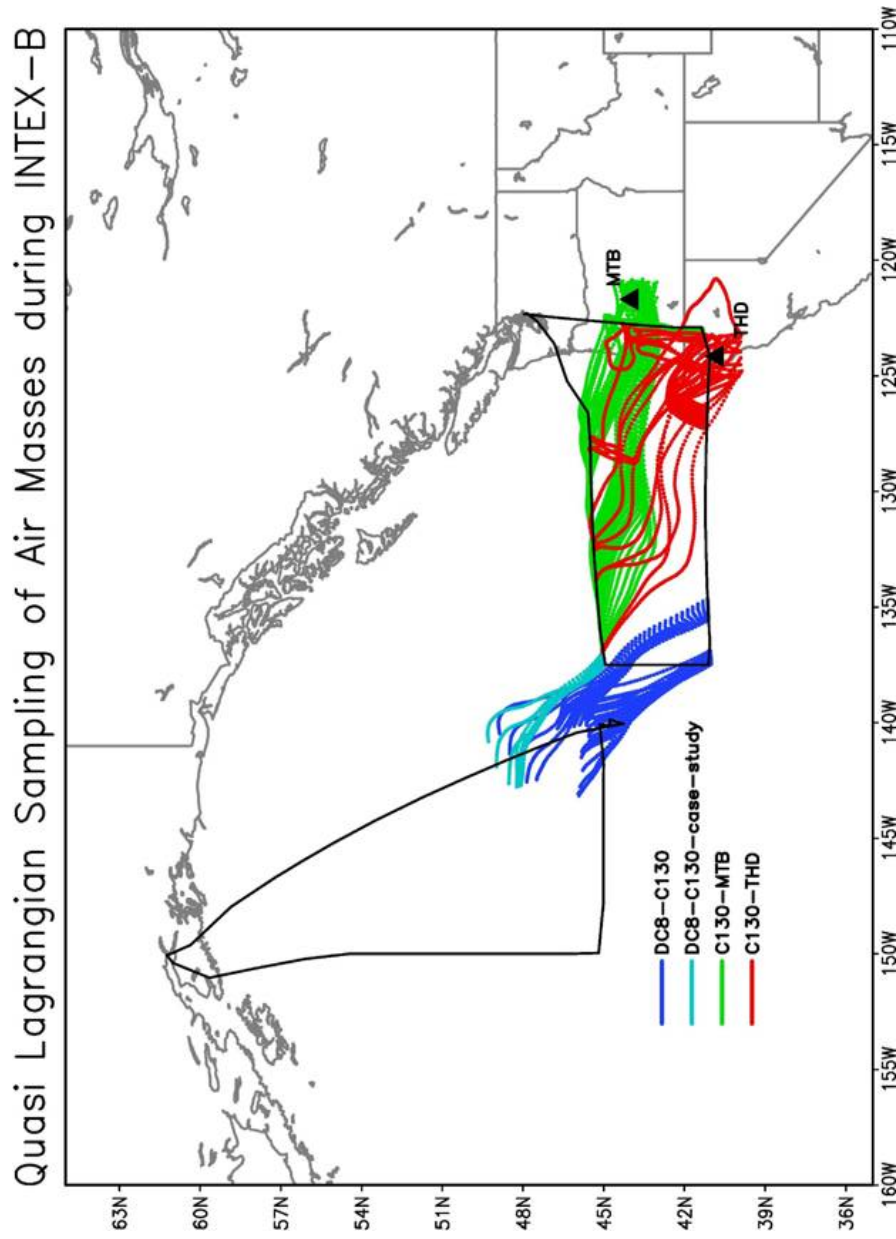


Figure 4.18 Quasi lagrangian sampling of air masses between DC-8 flight 15 (05/04/06), C-130 flight 21(05/05/06), and the two surface sites Mt. Bachelor (MBO) (05/08/06) and Trinidad Head (THD) (05/08/06) during INTEX-B.

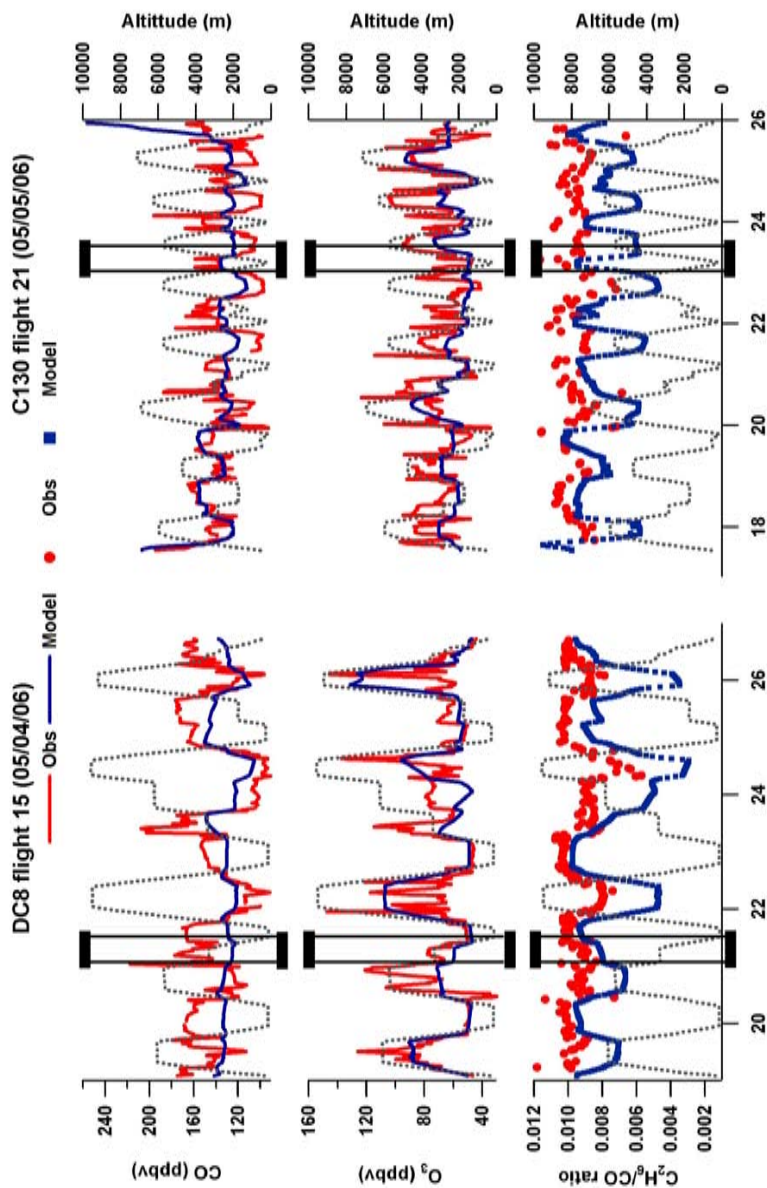


Figure 4.19 Comparison of observed and modeled CO, ozone and Ethane/CO ratio of DC-8 flight 15 and C-130 flight 21 airborne measurements. The square box denotes the time period where the model calculations suggested that quasi-lagrangian sampling occurred.

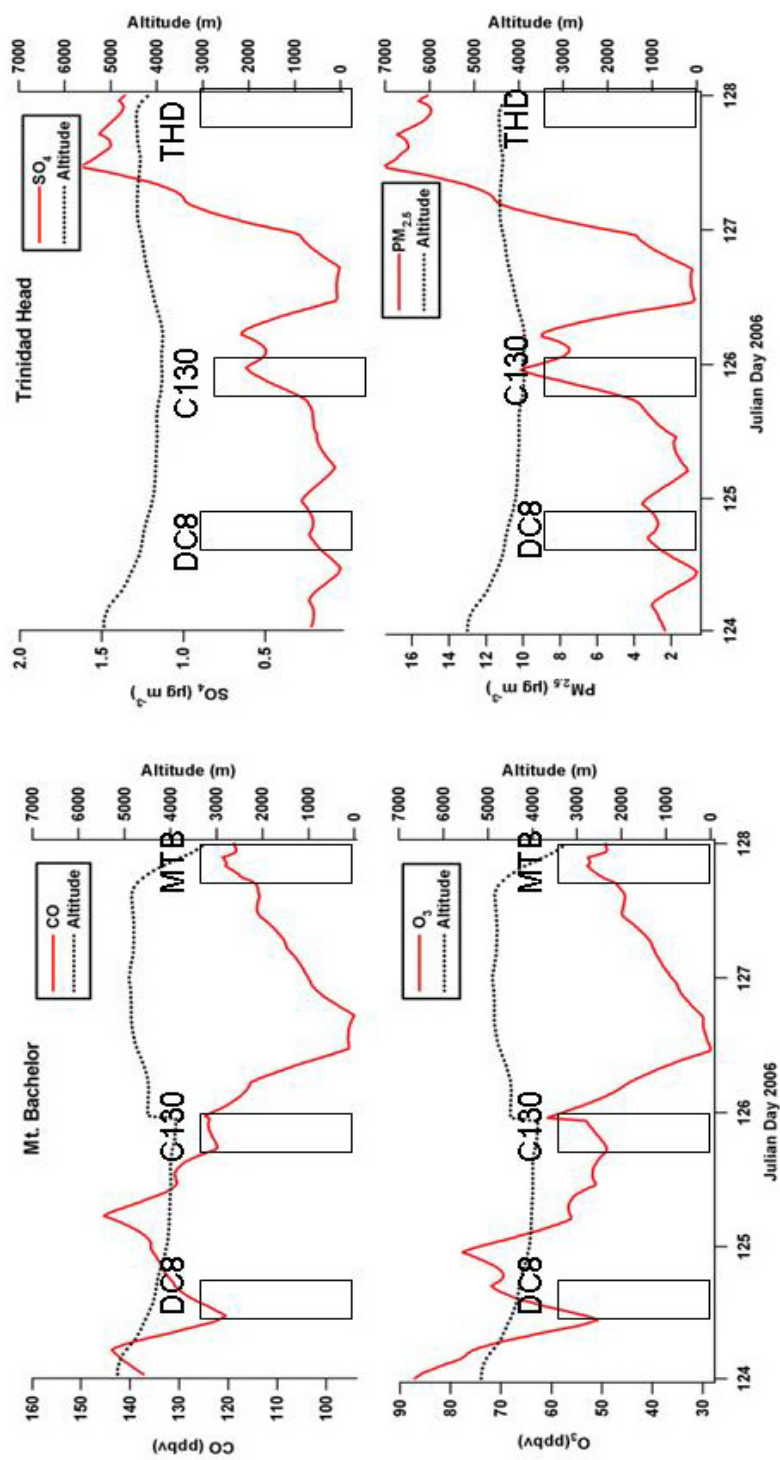


Figure 4.20 Modeled trace gases and aerosols extracted along the pseudo lagrangian back trajectory from MTB and THD that crossed C-130 flight 21 and DC-8 flight 15. The square boxes denote the time period where the lagrangian air mass was sampled by DC-8, C-130 air

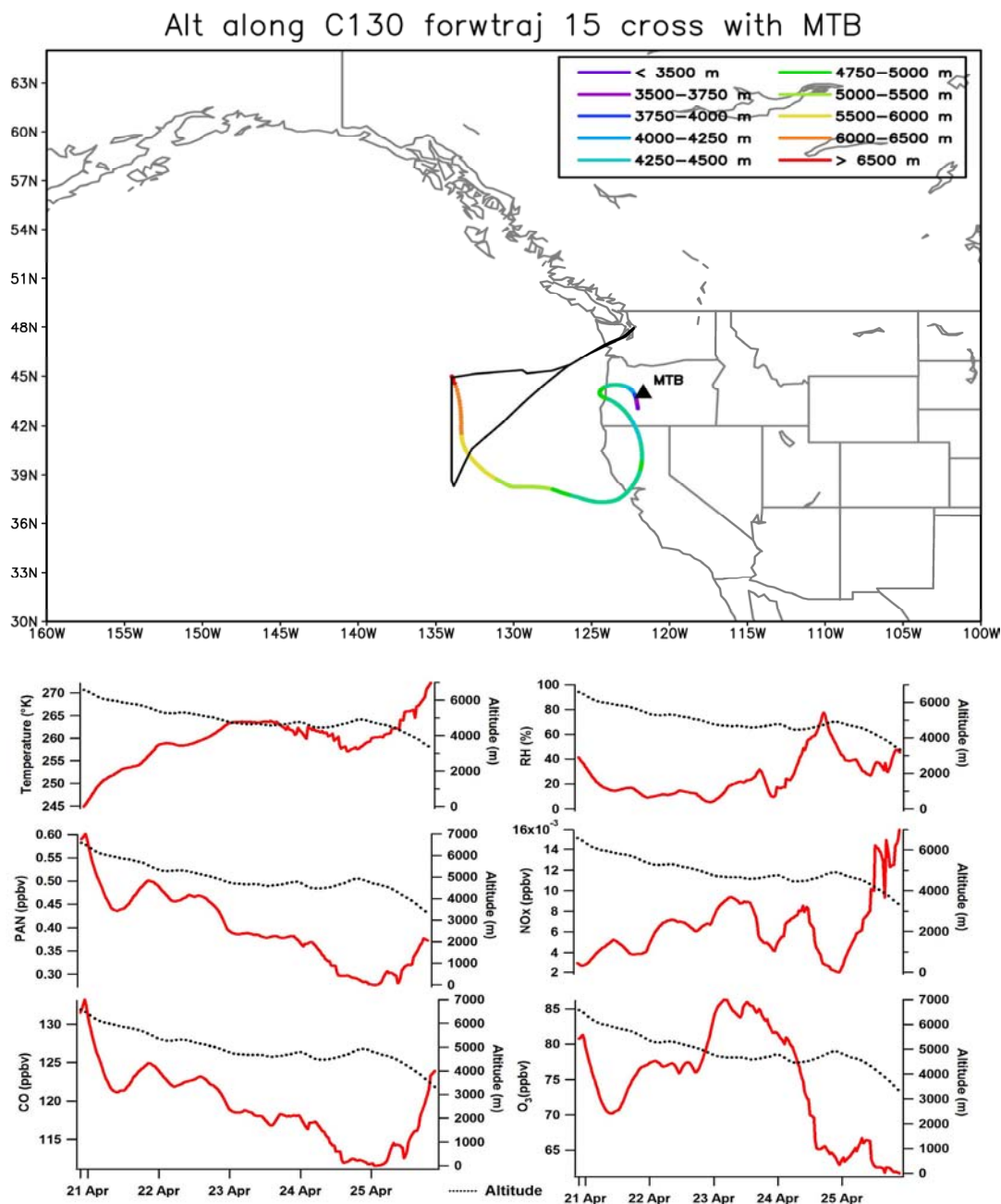


Figure 4.21 Modeled meteorological parameters and trace gas species extracted along the trajectory pathway of the descending lagrangian air mass sampled on C-130 flight 15 that arrived at MTB on (04/26/06).

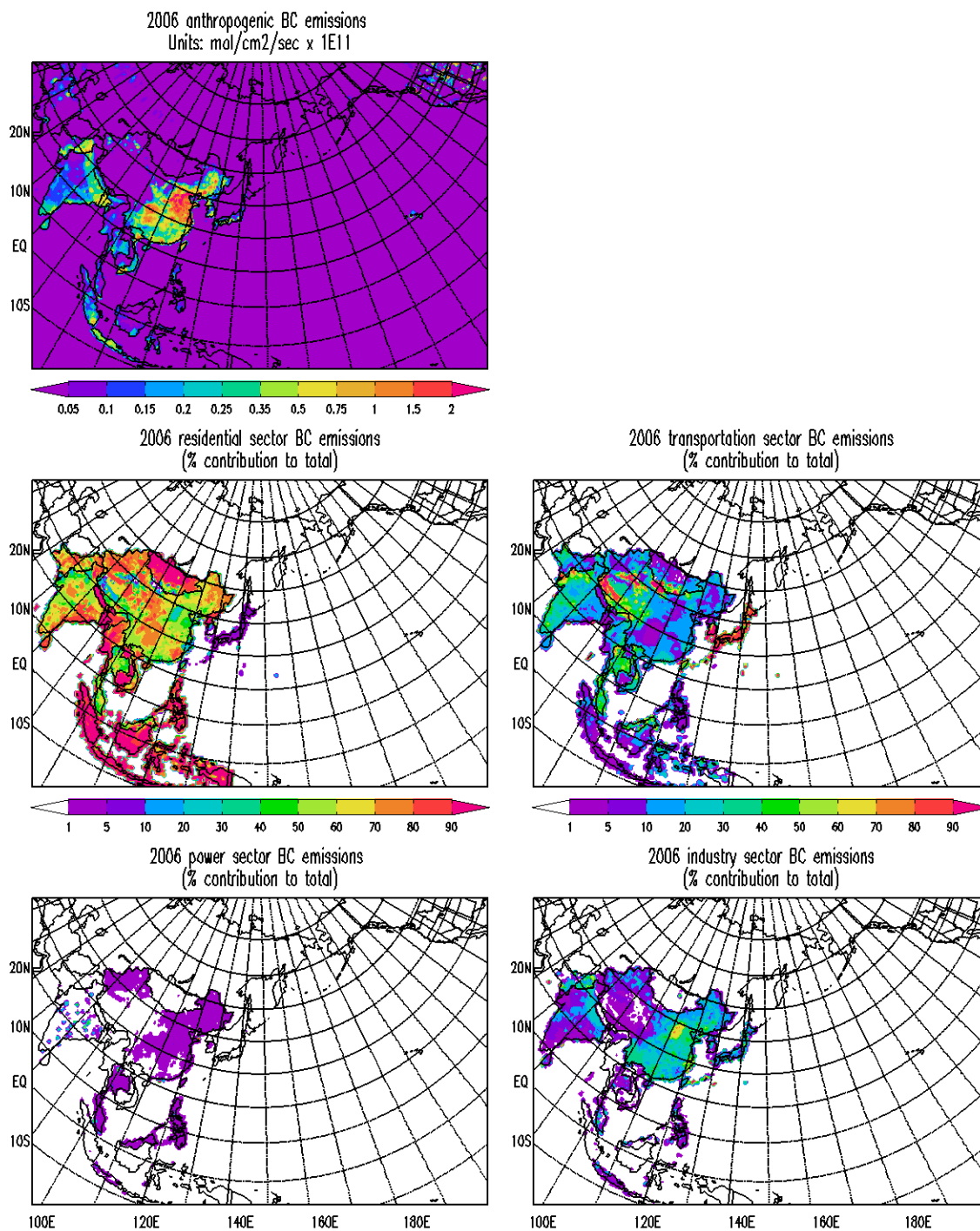


Figure 4.22 Regional distribution of anthropogenic BC emissions along with the percent contribution of residential, transportation, power and industrial sectors

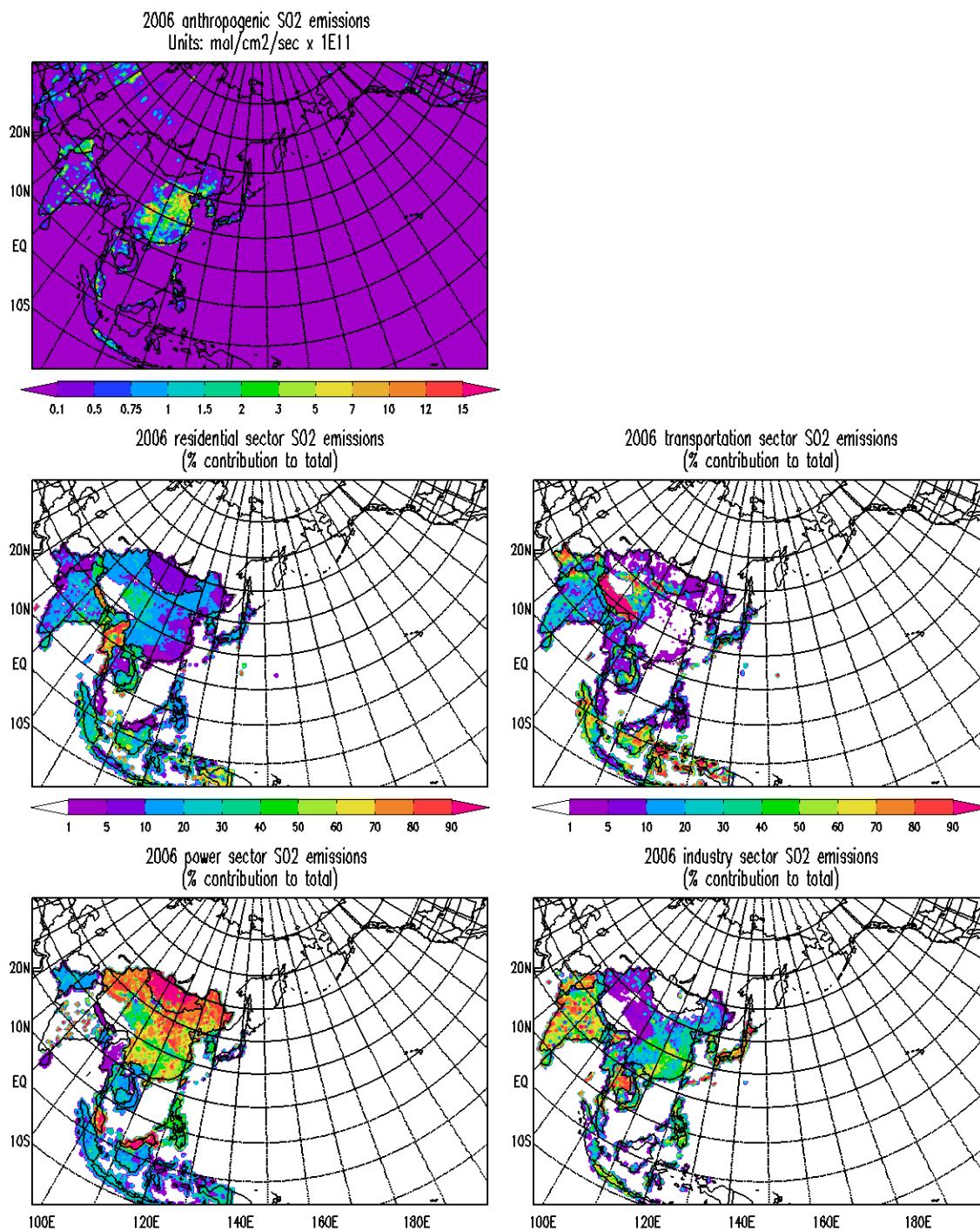


Figure 4.23 Regional distribution of anthropogenic SO₂ emissions along with the percent contribution of residential, transportation, power and industrial sectors

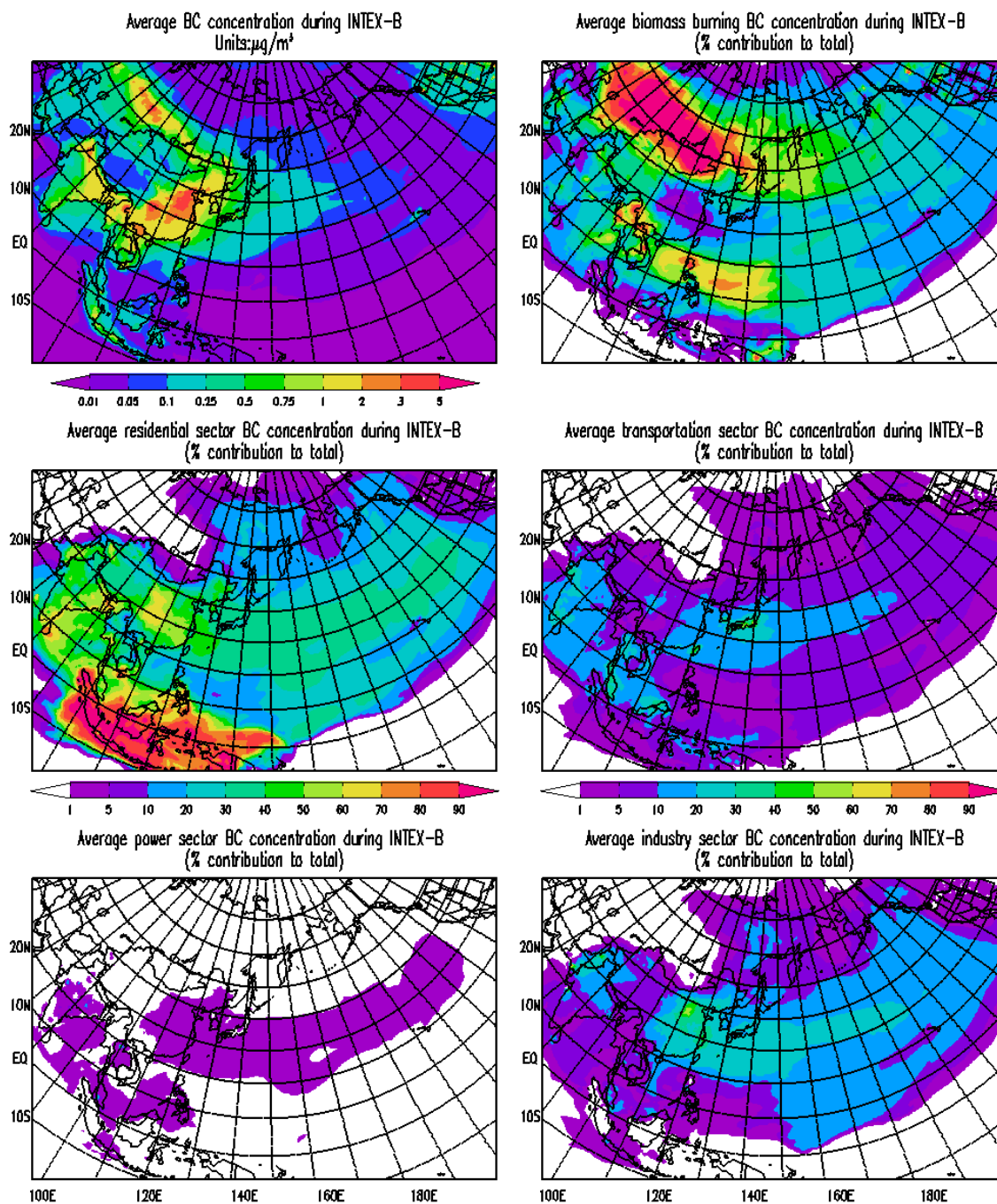


Figure 4.24 Regional distribution of BC concentration along with the percent contribution of residential, transportation, power, industrial sectors and biomass burning

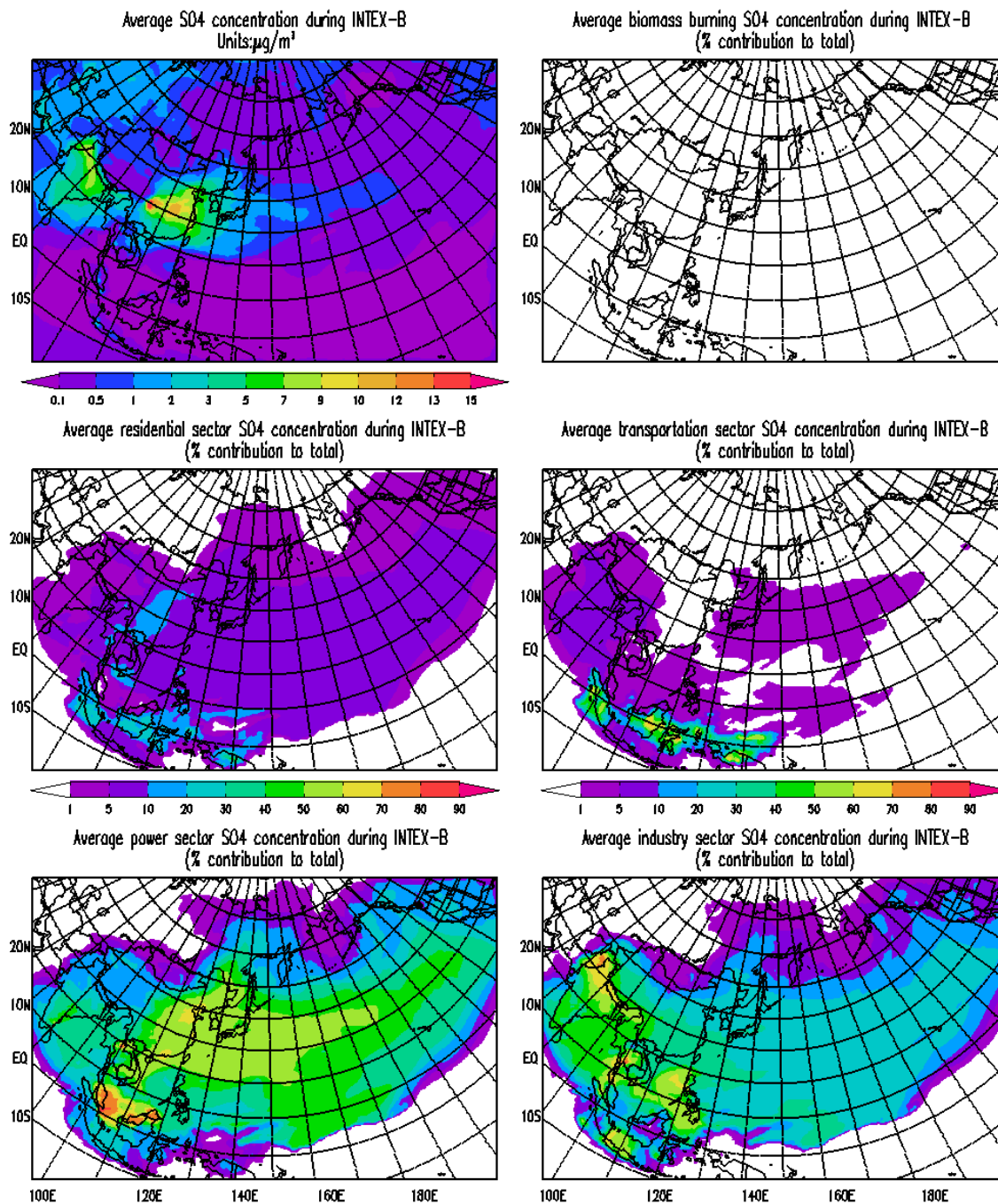


Figure 4.25 Regional distribution of sulfate concentration along with the percent contribution of residential, transportation, power, industrial sectors and biomass burning

CHAPTER 5
 UNDERSTANDING THE SEASONALITY AND REGIONAL
 DISTRIBUTION OF ASIAN AEROSOLS: A MULTIYEAR
 REGIONAL SCALE MODELING STUDY WITH AOD
 ASSIMILATION USING OPTIMAL INTERPOLATION

5.1 Introduction

The Asian continent has witnessed an unprecedented economic development in the past few decades due to rapid industrialization throughout the region (Zhang *et al.*, 2009). This has led to tremendous increase in the regional anthropogenic emissions of a wide variety of aerosols including soot, sulfates and organics. These increased emissions have implications to local, regional and hemispheric air quality, and can cause considerable damage to human health and ecosystems around the globe (Guttikunda 2002). This complex mixture of aerosols and their precursors has been characterized as Atmospheric Brown Clouds (ABCs) (Ramanathan *et al.*, 2007; Ramanathan *et al.*, 2008a). The combustion of fossil fuels associated with the industrial sector and transportation, widespread usage of biofuels for residential heating and cooking purposes, and open biomass burning lead to the formation of the ABCs (Ramanathan *et al.*, 2008a). These ABCs alter the radiative forcing over Asia reducing the amount of radiation reaching the surface and increase the heating in the atmosphere. These changes have several adverse impacts including decrease in the amount of rainfall from Indian summer monsoon, glaciers and snow packs in the Himalayan region. (Ramanathan *et al.*, 2008b)

There is great need to study the Asian aerosols to gain a better understanding of the aerosols emissions and their precursors due to their adverse impacts including visibility reduction, health impacts and altering the Earth's radiative balance discussed above. Several field campaigns including Indian Ocean Experiment (INDOEX) (Ramanathan *et al.*, 2001), ACE-Asia (Huebert *et al.*, 2003), and ABC (Ramanathan *et*

al., 2007) project have provided valuable information on Asian aerosol. Chemical Transport Models (CTMs) have been extensively used to interpret and obtain broader geographic scale perspectives from the field campaign observations. CTMs provide a means to link the emissions with observations and provide valuable information for policy-making decisions. In addition, the import and export of Asian pollutants is governed in large part by the seasonality of the monsoon system (Pochanart *et al.*, 2004). There is significant inter-annual variability associated with the seasonality of Asian aerosols (Adhikary *et al.*, 2008). Regional scale modeling studies greatly assist in understanding this complex seasonality of the Asian region (Adhikary 2008).

CTMs are prone to great uncertainty due to the underlying uncertainties associated with emissions, meteorology and various chemical processes (Bates *et al.*, 2006). One of the several ways to reduce this uncertainty is to integrate the observations into CTMs via data assimilation (Carmichael *et al.*, 2008). There are various kinds of data assimilation methods (Bouttier *et al.*, 1999). Optimal Interpolation (OI), a statistical data assimilation method, has been used in recent air quality studies to obtain improved CTM predictions (Generoso *et al.*, 2007; Tombette *et al.*, 2009). Aerosol Optical Depth (AOD), defined as the integrated extinction coefficient over a vertical column of unit cross section, is a measure of radiation extinction at the encounter of aerosol particles in the atmosphere. Another parameter of interest in the aerosol radiative forcing calculations is the Single Scattering Albedo (SSA), which is defined as the ratio of scattering extinction to total extinction. The use of satellite and ground based AOD assimilation to constrain modeled distribution, has greater significance in understanding the spatial and temporal distribution of Asian aerosols (Adhikary 2008). The modeled CTM distributions of absorbing and scattering aerosols can be constrained further using the observed SSA.

Collins *et al.*, (2001), first introduced the assimilation of satellite-derived AOD from Advanced Very High Resolution Radiometers (AVHRR) observation values into the Model for Atmospheric Transport and Chemistry (MATCH) model to produce

improved aerosol predictions for the 1999 INDOEX period. These results were subsequently used to provide improved regional aerosol distributions (Rasch *et al.*, 2001) and aerosol radiative forcing calculations (Collins *et al.*, 2002). Generoso *et al.*, (2007) assimilated Aerosol Optical Depth (AOD) obtained from Polarization and Directionality of the Earth Reflectances (POLDER) and improved global aerosol distributions simulated by the Laboratoire de Me'te'orologie Dynamique–Interaction with Chemistry and Aerosol (LMDz-INCA) model of aerosols.

In this study, we present the results of the Sulfur Transport and dEposition Model (STEM) tracer model simulations for a four year period (2001-2004) to describe the regional aerosol distributions and their seasonal cycle. The aerosol distributions with reduced uncertainty were produced by implementing the assimilation via the OI method for the simulated period. The observed SSA was used as an additional constraint to adjust the scattering and absorbing aerosols. Furthermore, the CTM output was combined with the receptor – oriented Positive Matrix Factorization (PMF) technique to study the seasonal cycle of aerosol distributions. The implication of Asian aerosols on human health and radiative forcing calculations are also discussed.

The idea of combining the assimilated CTM output with PMF technique was first explored in Adhikary *et al.*, (2008) to evaluate the performance of the assimilated model results in describing the regional features of aerosol seasonality and emission distributions. Carmichael *et al.*, (2009) presented the regional aerosol distributions from STEM model calculated over a four-year period and constrained by satellite derived AOD. This work is a continuation of the STEM model assimilation results presented in Adhikary *et al.*, (2008) and Carmichael *et al.*, (2009) and integrated observed SSA along with AOD to further improve the regional distribution of aerosols.

The chapter is organized as follows: the analysis methodology including the STEM model set up, assimilation procedure, AOD/SSA observations, and PMF method, is described in section 5.2. The regional distribution of assimilated aerosols, the PM and

AOD composition at selected locations across the modeling domain are described in section 5.3. The results of applying the PMF technique on selected locations, is used to describe the seasonal cycle of aerosols in section 5.3. Finally the human health and radiative forcing implications are also presented in section 5.3 followed by summary.

5.2 Methodology

5.2.1 STEM Model Description

The University of Iowa's STEM model was used to produce the three dimensional aerosol distributions for four years from 2001 to 2004. In the past, the STEM model has been applied in several other modeling studies focused on understanding the distribution of trace gases and aerosols in this region (Carmichael *et al.*, 2002; Carmichael *et al.*, 2003; Adhikary *et al.*, 2007; Adhikary *et al.*, 2008). In this study, STEM model has been used to obtain multiyear aerosol concentrations with high spatial and temporal resolution for the first time. The model computational domain covers the region from 20S to 50N in latitude and 40E to 140E in longitude and has been set up with a 50km horizontal resolution comprising 219x179 grid cells and 23 vertical layers extending up to 14 km in altitude. The land use dependant variables were modeled using the 25 different USGS defined land use types. The meteorological input required drive the transport was obtained from PNNL-MM5 model at a temporal resolution of three hours. The MM5 simulations were driven by lateral boundary conditions and SSTs from the NCEP/NCAR global reanalysis using a simple relaxation scheme that blends the global reanalysis and the model solution over a 15-grid point wide buffer zone in the lateral boundaries. The wind and precipitation variations at the diurnal, seasonal, and interannual time scales are well represented by the model. The STEM model used fixed boundary conditions for this multi-year period (Carmichael *et al.*, 2003). The boundary conditions varied spatially and vertically based on observations from previous aircraft field experiments. Further details on the PNNL-MM5 model are discussed in Adhikary *et al.*, 2008.

The TRACE-P emission inventory with a 0.5x0.5 degree resolution, developed by (Streets *et al.*, 2003) was used as input in this study. The global BC and OC emission estimate from (Bond *et al.*, 2004) and global EDGAR emissions (Olivier *et al.*, 1999) were used to fill the geographic areas that extended beyond the TRACE-P domain. The monthly mean biomass burning emissions of carbonaceous aerosols obtained at 1x1 degree resolution from van der Werf *et al.*, (2006), were interpolated to the STEM domain. Dust and sea salt emissions were calculated online as a function of meteorological variables based on the work by Tang *et al.*, (2004) and Gong (2003) respectively. The aerosols simulated for this study were sulfate, BC, OC, other PM_{2.5} (i.e., non carbonaceous aerosols such as fly ash, road dust, and cement, which were simulated as a single mass component), fine and coarse mode sea salt and fine and coarse mode dust. These constituents comprise the primary components of PM_{2.5} and PM₁₀. Sulfate is calculated using SO₂ conversion parameterization with rates between 1 and 10% per hour as used in the ACE- Asia (Uno *et al.*, 2003). The dry deposition of aerosols was based on resistance in series mechanism described by Wesely *et al.*, (2000), and wet deposition was modeled as a loss rate that varies with precipitation. The emissions of carbonaceous and sulfate aerosols were limited to the sub-micron range (diameter < 1 μm). Dust and sea salt transport were modeled as fine mode (less than 2.5 μm) and coarse mode (2.5 μm < diameter < 10 μm).

5.2.2 Observed Data Description

Satellites and ground based observation networks provide a variety of aerosol optical parameters including AOD, Single Scattering Albedo (SSA), Angstrom Exponent and Asymmetry Parameter that can be used to constrain the CTM predictions. This study has used the monthly mean Level 2 AOD measurements at 550 nm from the MODIS instrument onboard the TERRA satellite along with Level 2 AOD products from AERONET (Aerosol Robotic NETwork) ground-based observation network including

the AOD and SSA. The sparsely distributed AERONET AODs were integrated with the MODIS AODs as described by Chung *et al.*, (2005). The fine mode AOD fraction over ocean from the MODIS retrieved AODs was also utilized in the assimilation procedure.

Surface observations from ABC sites and from the EANET (Acid Deposition Monitoring Network in East Asia) network were also used. The EANET network, consisting of 51 sites, measures concentration of several gaseous and aerosol species to understand the state of acid deposition in East Asia. In this study we have used the available monthly mean PM₁₀ data from the selected EANET sites for the 2001-2004 period (EANET 2001; EANET 2002; EANET 2003; EANET 2004).

5.2.3 Data Assimilation Technique

We have applied the Optimal Interpolation (OI) data assimilation technique used by Collins *et al.*, (2001) to improve the MATCH model predictions for the INDOEX period. In the OI method, the available observations are used to produce (analysis), which is supposedly the better estimate of the true state and it replaces the current state of the model (background). In this study, the observations are AOD measurements.

Equation 1 shows mathematical relationship between the aerosol model prediction (background), the observation and the assimilated aerosol (analysis).

$$\tau'_m = \tau_m + K(\tau_o - H\tau_m) \quad (5.1)$$

where τ'_m is the analysis AOD, τ_o and τ_m are the observed and model predicted AOD respectively. K is the Kalman gain matrix and H is the interpolation function that maps the modeled space to the observation space. In this study, the observed AOD is interpolated to the STEM model grid transforming H to an identity matrix.

The Kalman gain matrix K is calculated by the following equation:

$$K = BH^T (HBH^T + O)^{-1} \quad (5.2)$$

B and O denote the error covariance matrices of the modeled and observation fields respectively. The equations used to calculate the B and O matrices are shown below.

$$O = (f_o \tau_o + \varepsilon_o)^2 I \quad (5.3)$$

where ε_o (equal to 0.04) is the minimum Root Mean Square (RMS) error of the observation and f_o (equal to 0.1) is the fractional error in observation AOD, and

$$B_{ij} = (f_m \tau_m + \varepsilon_m)^2 \exp\left[-\frac{d_x^2 + d_y^2}{2l_{xy}^2}\right] \quad (5.4)$$

with ε_m (equal to 0.1) is the minimum RMS uncertainty in the modeled AOD, and f_m is the fractional error in the model AOD is set to 0.5. Variables d_x and d_y are the horizontal distances between two model grid points i and j (equal to 1 grid cell i.e. 50 km), and l_{xy} is the horizontal correlation length scale for errors in the model fields (equal to 5 grid cells 250 km). Further details and the assumptions used in calculating the B and O matrices can be found elsewhere (Khattatov *et al.*, 2000; Collins *et al.*, 2001).

5.2.4 Calculation of Assimilated Aerosol Distributions

The assimilation method described above can be used in either dynamic or post – processing modes. The results presented here focus on providing long term monthly averaged aerosol distributions for use in follow-on analysis such as calculations of aerosol radiative forcing or health and ecosystem impact analysis. For this application, we have applied data assimilation in post processing mode.

The methodology used to generate the assimilated aerosols distribution is briefly described here. First the STEM model simulated the three dimensional aerosol concentration fields for all four years (2001- 2004) at three hour time step. Monthly mean aerosol distributions were generated by averaging this output. The AOD for each individual species was calculated from these distributions by using species specific

extinction coefficients data reported in Penner *et al.*, 2001. The two dimensional distribution of modeled AOD and the MODIS-AERONET integrated AOD were input as the background and observation to the OI algorithm described above to produce assimilated AOD (analysis).

The OI methodology differs from Collins *et al.*, (2001) in some aspects. We have assimilated the sea salt aerosols while Collins *et al.*, (2001) treated them as constant. In addition, our assimilation procedure utilizes the coarse and fine mode data obtained from MODIS. The fine mode AOD was used to adjust the anthropogenic aerosols including sulfate, BC and OC, while dust, sea salt, other PM species were adjusted by coarse mode AOD. Finally the assimilated three dimensional aerosol concentration distributions were generated by linear adjustment of the background model fields using the ratio of assimilated AOD to modeled AOD at monthly scales. If a model grid cell did not have the observed fine/coarse mode AOD, then the total observed AOD (if available) was used to adjust all the species. This procedure was used in the papers by Adhikary *et al.*, (2008) and Carmichael *et al.*, (2009).

If additional observational information is available, it can be included in the assimilation procedure. For example this study has also used the available AERONET SSA data to adjust the absorbing and scattering aerosols separately and the methodology is described below.

The assimilated total AOD was assumed to remain unchanged at each model grid cell. It was also assumed that the BC was the only absorbing species. In this study, the simulated SSA was calculated using the following equation

$$SSA_{model} = \frac{totalAOD - BCAOD}{totalAOD} \quad (5.5)$$

Since the highest uncertainty in the scattering calculations is due to dust, we only allowed dust and BC AODs to be modified in order to satisfy the SSA constraint. The

total AOD and other species except dust and BC remained constant; the sum of BC and dust AODs should remain the same before and after bias correction, i.e.

$$BCAOD_{model} + dustAOD_{model} = BCAOD_{SSA} + dustAOD_{SSA} \quad (5.6)$$

The BC AOD can be calculated based on the SSA equation above as

$$BCAOD = (1 - SSA) \times total\ AOD \quad (5.7)$$

which was utilized to adjust the BC and dust aerosols using the observed SSA.

5.2.5 PMF Receptor Model Description

PMF (Positive Matrix Factorization), a form of factor analytic method, has been widely used in the atmospheric field for source apportionment studies involving ambient concentration measurements with unknown source profiles (Lee *et al.*, 1999; Paterson *et al.*, 1999; Polissar *et al.*, 1999; Chueinta *et al.*, 2000; Kim *et al.*, 2005). The aim of PMF is to obtain two matrices **G** and **F**, which explain the variation in the data set **X**, a matrix, consisting of *n* number of observations and *m* chemical species. Mathematically,

$$\mathbf{X} = \mathbf{GF} + \mathbf{E} \quad (5.8)$$

Where, **G** is an *n* by *p* matrix of source contributions describing the temporal variation of the sources, **F** is a *p* by *m* matrix of source profiles and **E** represents the unexplained data variance by the model. PMF solves equation 5.8 using an explicitly weighted least square approach and minimizes the objective function $Q(\mathbf{X}, \sigma, \mathbf{G}, \mathbf{F})$ defined as:

$$Q = \frac{\|\mathbf{X} - \mathbf{GF}\|_F^2}{\sigma} = \sum_{i=1}^n \sum_{j=1}^m \left(\frac{x_{ij} - \sum_{h=1}^p g_{ih} f_{hj}}{\sigma_{ij}} \right)^2 \quad (5.9)$$

$\|\mathbf{X} - \mathbf{GF}\|_F^2$ denotes the Frobenius norm of **E** and σ is the known matrix of error estimates.

These error estimates (σ) of individual data points are used to determine the weights of the least square fit on the data matrix. The G (source contributions) and F (source profiles) are determined so that the Frobenius norm of E divided by σ at each time step is minimized.

The PMF output also produces a matrix called Explained Variation (EV) which summarizes the relative importance of each factor in explaining the variability of different species in the PMF input; i.e., a large EV value of a species in a factor indicates that this particular factor explains a major portion of that species variability. EV is represented as a matrix of dimensions $p+1$ by m (similar to F matrix dimension but with one extra row ($p+1$)) which is a measure of how much variation in a species remains unexplained by the PMF solution. The EV values range from 0 (no variance explained) to 1 (100% variance explanation). PMF modeling guidelines suggested that if any value on the $(p+1)^{\text{th}}$ row exceeds 0.25, it indicates that species corresponding to that row is practically not explained. The details of the EV calculation are found elsewhere (Junto *et al.*, 1994; Lee *et al.*, 1999; Paatero 2000). In this study, the input variables used in the PMF analysis are assimilated monthly mean AOD values of SO_4 , BC, OC, coarse mode sea salt (SSC), fine mode sea salt (SSF), coarse mode dust (dustC) and fine mode dust (dustF) obtained from the four year model simulation. The data error estimates were assumed to be 25% of the model predicted AOD. The sensitivity of the PMF solution to this error assumption was not evaluated and may be assessed in future studies. The PMF solution was obtained by trial and error until physically realistic sources were obtained, while simultaneously minimizing Q value as the principal criterion. The total AOD was regressed against the G matrix to obtain the source profiles (AOD ratio) and contributions (AOD) in terms of AOD units. The PMF results are described in section 5.3.

5.3 Results and Discussion

Figure 5.1 shows the observed data from AERONET and MODIS used in this study. The sparsely available AERONET AOD data (top right panel figure 5.1) was integrated with MODIS AOD as described above in the methodology section. It was challenging to utilize the SSA data, which was available only at very few locations in the model domain for the simulated period as seen in top left panel of figure 5.1.

The simulated SSA, calculated from assimilated model run, was compared with observed AERONET SSA, whenever available. Illustrative plots for Kanpur (80.4° E, 26.4° N), India (figure 5.2) shows a systematic positive bias (~ 0.05) in the simulated SSA. Similar positive bias was seen at other AERONET sites across the domain. Since the availability of observed SSA is limited in this modeling domain, SSA bias correction of 0.05 was applied across the domain. The SSA bias information was integrated into the assimilated model by adjusting the BC (absorbing) and dust (scattering) AODs in such a way the assimilated total AOD remained unchanged as described in the methodology section. Figure 5.3 shows the results of the SSA bias correction (0.05) on the regional distribution of SSA, BC and dust aerosols over the four years. The BC AOD distribution is significantly altered by the SSA bias correction as seen from the higher BC AOD values in South Asia, East Asia and Southeast Asia regions consistent with their high absorbing aerosol emissions pattern. The dust distribution before and after SSA bias correction does not show any noticeable differences. For the rest of the paper, the results discussion will focus on the output from this SSA bias corrected run.

5.3.1 Model Evaluation

The predicted aerosol distributions have been evaluated using surface observations at ABC and EANET sites throughout Asia. Illustrative results are presented in Figure 5.4, where the available observed and predicted monthly mean PM_{10} values at a sample of ABC and EANET sites are shown. The top two panels, which show

Kathmandu and Hanimadhoo, represent data from ABC sites and the rest of the data are from EANET sites. The impact of the assimilation on the predicted PM mass distributions is discussed in detail in *Adhikary et al.*, (2008). The predicted values capture many of the important aspects in the observed values in terms of regional differences in aerosols. For example in Jinyunshan, located downwind of Chinese desert regions, the predicted high PM₁₀ values ($\sim 160 \mu\text{g}/\text{m}^3$) and the seasonal variations are seen in observations. The model also does fairly well in predicting the lower PM₁₀ values ($\sim 60 \mu\text{g}/\text{m}^3$) farther away from dust source regions as evident from the time series of Gosan (Korea) and Petaling Jaya (Malaysia) where the simulated PM₁₀ matches the observations closely. The modeled values are also able to capture important aspects of the seasonal cycles across the region, as seen at Chiang Mai, Jinyunshan and Gosan. This seasonality is discussed in detail later in the section.

5.3.2 Regional Distribution

The calculated four year mean AOD distribution derived from the STEM model calculations after assimilation is shown in top right panel of figure 5.5, and can be compared with the satellite-derived distribution top left panel of figure 5.5. It is important to point out that the above discussion reflects the four-year mean aerosol distributions. The seasonal variability of the aerosol mass and composition in Asia is large and is discussed later in this section. The assimilated AOD distribution accurately captures the magnitude and spatial pattern of the observed AOD. The highest predicted AOD values occur over the desert regions of Gobi and Taklimakan in East Asia and desert regions of India-Pakistan border and the Middle East. These are also places where the assimilation process did not provide a significant constraint, as observed AOD data in these regions are limited in time coverage due to difficulties in retrieval over desert areas. Vast regions with AOD > 0.3 are seen throughout South and East Asia with significant contribution

(60 to 80%) from the anthropogenic aerosols. Below we discuss in more detail the aerosol components contributing to these elevated AOD values.

The calculated four year mean distribution of PM_{10} is shown in second left panel of Figure 5.5. The high PM regions include areas in and downwind of major desert areas (e.g., Central China, Middle East, Pakistan), locations around heavily populated and industrialized areas (e.g., Indo Gangetic Plain, Eastern China), and areas impacted by biomass burning (e.g., Southeast Asia). The $PM_{2.5}$ fraction represents an important sub-component of the PM_{10} mass, and plays important roles in human health and radiative effects. The $PM_{2.5}$ fraction accounts for 60-80% of the total mass throughout South, Southeast and East Asia. The regional distributions of sulfate and BC, important constituents of $PM_{2.5}$, are also shown in Figure 5.5. The sulfate distribution (bottom left panel) shows the highest concentration in the Indo Gangetic plain and East China. These are highly populated areas with substantial fossil fuel consumption (largely coal), which leads to high sulfate concentrations. In contrast, the BC distribution (bottom right panel) has high BC values extending into more rural regions, as shown in southern India and SE Asia. This reflects the fact that BC has additional emission sources including biofuels and open biomass burning.

5.3.3. $PM_{2.5}$ Composition of India, China and Southeast

Asia

India and China have vast regions with high aerosol loading. The East China (100-120 E, 20 – 40 N) region has high anthropogenic emissions when compared to the entire region of China, which is dominated by dust. This study has found that mean $PM_{2.5}$ concentration values of India and East China are approximately 30 and 25 $\mu\text{g}/\text{m}^3$, respectively with highly varying composition. In India the anthropogenic aerosol components comprising Sulfate, OC, BC and other $PM_{2.5}$, are the major contributors to $PM_{2.5}$, while sulfate and dust play a larger role in the $PM_{2.5}$ composition in East China as

seen in figure 5.6. The $PM_{2.5}$ composition in Southeast Asia was dominated by anthropogenic species unlike in India and China.

To further illustrate the regional variability in the aerosol composition, the mean predicted aerosol mass and composition at selected megacities and regional ABC observation sites are shown in figure 5.7. The major cities of Asia have high aerosol amounts. In fact the ten most polluted world cities in terms of PM_{10} are located in Asia (World Bank 2007). The levels of $PM_{2.5}$ in these cities exceed the WHO annual guideline for $PM_{2.5}$ of $10 \mu\text{g}/\text{m}^3$ by factors of 2 to 5. The contribution of anthropogenic aerosols to $PM_{2.5}$ mass increases from west to east across the domain (*cf.*, the Indian Megacities Mumbai, New Delhi and Kolkata). The fine mode aerosol composition varies between the cities. Sulfate is a significant anthropogenic component of $PM_{2.5}$ throughout Asia (*cf.*, New Delhi and Beijing). The exception is in the Southeast Asian megacities (e.g., Jakarta) where the carbonaceous aerosols dominate the $PM_{2.5}$ composition, consistent with high open burning emissions of the region. Virtually all the cities have BC levels exceeding a few $\mu\text{g}/\text{m}^3$ (e.g., BC at Jakarta is $\sim 6 \mu\text{g}/\text{m}^3$). Other $PM_{2.5}$ (e.g. construction dust) contributes in important ways to $PM_{2.5}$ in Asian megacities, in particular at New Delhi, Kolkata, Manila and Jakarta. Dust is a significant contributor to PM throughout most of Asia, with the exception being Southeast Asia. Megacities in the Middle East and West Asia (Tehran and Karachi) have the highest fine mode dust contribution to $PM_{2.5}$.

Calculated PM concentrations at regional and background monitoring sites operated by ABC and the World Meteorological Organization Global Atmospheric Watch (WMO GAW) program are also shown in figure 5.7. These sites, have high PM_{10} levels (20 to $70 \mu\text{g}/\text{m}^3$), reflecting the extent of the elevated levels of PM_{10} in Asia. The Waliguan and ABC KRSU Lidar sites are located in the arid regions of West Asia and have high dust contribution to PM, while Gosan and Hanimaadhoo, located downwind of the populated regions of China and India, have significant anthropogenic contribution. Gosan has the highest sulfate concentration among the regional observation sites,

reflecting the fact that it is in the major pathway of the East Asia outflow and thus measures sulfate-rich aerosols from China throughout most of the year. Its composition is very similar to the Chinese cities (e.g., Beijing) with an added importance of sea salt, reflecting its island location. Bukit Koto Tabang has the highest carbonaceous aerosol contribution among the regional sites, reflecting the large contribution from open biomass burning.

The mean aerosol species contribution to AOD of the megacities and regional observation sites is shown in figure 5.7. Primary contributors to AOD are different than the primary contributors to aerosol mass. The fine mode and anthropogenic components dominate the AOD because they have higher optical efficiencies than coarse-mode particles. Relative humidity also plays a role, with AOD increasing with RH due to hygroscopic growth of aerosol particles (Yoon *et al.*, 2006). Throughout most of Asia sulfate is a major contributor to the AOD. However, fine mode dust is also an important contributor to AOD. The contribution of BC to AOD is significant, and in most regions the BC contribution represents 5-10% of the total AOD. The significant contribution of absorbing aerosol in Asia has implications for atmospheric radiative forcing, photochemistry, heterogeneous chemistry, and global climate change.

5.3.4 Seasonality

The aerosol loading in Asia is greatly impacted by the prevalent seasonal cycles. In terms of precipitation, there are two broad seasons namely monsoon and dry seasons in the Asian region. However, the transition period between these two seasons and duration they last, varies across the region. For example, in India, the seasonal cycle is characterized by the monsoon (June – September), postmonsoon (October – November), the dry (December- April) and the post dry transition (late April – May) seasons (Adhikary 2008). The regional distribution of the BC seasonality in India is shown in figure 5.8. The BC concentration builds up during the post monsoon and dry winter

seasons. There is a decrease in concentration during the post dry transition period. This decrease is seen through the monsoon season.

In China, there is strong outflow of pollutants in spring and fall seasons with significant dust sources in spring and agricultural burning in late spring. The monsoonal flow in early fall brings in relatively marine air masses from the Pacific and Indian oceans over East Asia. The seasonality of the regional distribution of BC over East Asia is shown in figure 5.9. It is clearly evident that BC concentrations persist over the region for all seasons due to emissions from industrial activities. However, the buildup of concentration is enhanced during the post monsoon (top right panel) and winter (bottom left panel) seasons due to BC emissions from residential sector.

In Southeast Asia the seasonality is characterized by monsoon (May – October), the early dry (November-December) and peak dry (January-April) seasons (Pochanart *et al.*, 1998). Most of the open burning occurs during the dry season as can be seen in from the enhancement in BC (bottom left panel) of figure 5.10. In insular Southeast Asia (Indonesia) the peak biomass burning occurs in the months of June through November (top left panel) due to the different meteorology prevailing in the Southern Hemisphere.

There is great diversity in this region even in terms of seasonality of aerosols as seen in the discussion above. The annual mean monthly variation of PM_{2.5} aerosols at regional sites is shown in figure 5.11 to further characterize this seasonality. The mean seasonal values shown here were calculated as monthly averages of specific months for the years 2001-2004. Distinct seasonal cycles are shown in the various regions. At Hanimadhoo, high anthropogenic aerosol loading with significant amounts of sulfate, OC and other PM_{2.5}, can be seen building from September through March which represents the post-monsoonal and the dry periods in South Asia. There is a sharp decline in anthropogenic aerosols in the transition months of April –May and continuing through the monsoon season. The fine mode dust is a significant contributor to PM_{2.5} during the monsoon period with peak dust loading occurring in March.

The spring and early summer features East Asian outflow can be seen in the seasonal cycle of Gosan, where dust along with anthropogenic aerosols peaks around March – April signifying the impact of long range transport of dust mixed with pollution along its path. There is another peak of anthropogenic aerosols around June, which represents the impact of biomass burning in late spring/early summer. At Bukit Koto Tabang, the impact of widespread open burning in South East Asia is reflected in the carbonaceous aerosols, which are persistent throughout the year with a seasonal high in February. The monsoonal months have lower aerosol amounts when compared to the dry months.

The results presented above indicate that the aerosols and the contributions from various species vary significantly by region and season. To help synthesize and characterize the contributions to AOD in a particular region and to better see how the various species are correlated within the seasonal cycles, PMF was applied to the 4 – year monthly average sulfate AOD, BC AOD, OC AOD, Sea Salt (coarse and fine) and dust AOD (coarse and fine) data at selected sites. The application of PMF to model values provides a means to search for factors that can represent the source, transport and removal processes which link emissions, aerosol distributions and AOD. The general PMF guidelines including looking at Q and EV values and interpretability of the resolved sources were adhered to in obtaining the PMF solution. After careful examination of the various factor combinations, a three factor solution was considered best to explain the variation in AOD while yielding physically meaningful factors. For example, a megacity located far from oceans and sand desert should not have a high factor loading of dust and sea salt as the factors that primarily explain the variation in AOD. Since there are seven AOD constituents, a three – factor was found to best explain most of the variability (~ 80%). The three factors include a factor related to high dust conditions, a factor that reflects marine flows associated with the monsoons, and a mixed combustion factor.

We first discuss the results of PMF analysis at Gosan and Hanimaadhoo in detail as these locations are influenced by the continental outflow from the Indian subcontinent and East Asia; thereby providing an opportunity to study the influence of diverse emission sources. We show here the averaged four year contributions in order to better ascertain the influence of seasonality. To illustrate, the resulting AOD factor profiles and contributions are displayed in figures 5.12 and 5.13. The output is arranged in a multi-panel plot format. The top three left and right panels in figures 5.12 and 5.13 correspond to the AOD profiles and contributions, respectively. The fourth panel in both figures shows the aggregate of profiles and contributions. The bottom left panel shows the variation explained in each species by the three factors. The bottom right panel shows a comparison of the PMF modeled AOD (which is sum of the individual factor contributions) with the total AOD from the assimilated STEM model.

The three factor PMF solution for Hanimaadhoo is shown in Figure 12. The mixed combustion factor (denoted by blue color) shows strong association of SO_4 , BC and OC in the profile (top left panel) and accounts for majority (~80%) of the variation in BC and OC along with a substantial portion of variation in SO_4 (bottom left panel). This factor peaks during the months of January and February (top right panel) consistent with the results of earlier studies (Ramanathan *et al.*, 2007; Stone *et al.*, 2007). The monsoon is (denoted by green color) associated with OC, sea salt and dust (in second left panel) and explains most of the variation of sea salt species. This factor shows a seasonal cycle with maximum contribution in July and August (second right panel). This period represents long range transport from low latitudes, with long stretches over the sea, and generally from the areas influenced by outflow from Africa. This is in contrast to the seasonality of the first factor that reflects outflow from the Indian subcontinent. Likewise, the dust factor is associated with high dust loading (in third left panel) along with minor contributions of SO_4 and accounts for most of the variation in dust. This factor peaks occur through the months of May through August (third right panel), reflecting

transport conditions bringing dust from the Middle-east and the western regions of S. Asia. A detailed discussion of the transport patterns impacting aerosol composition at Hanimaadhoo is presented by Adhikary et al. (2007). The PMF three factor model explains more than 80% of the variation in the individual species as evident by the low values (<0.2) of unexplained variation of each species denoted by yellow color (bottom left panel). This PMF solution explains 90% of the assimilated STEM total AOD as seen in the bottom right panel.

Figure 5.13 shows the PMF results for Gosan. The aerosol distributions at Gosan are dominated by pollution sources from East Asia, and 80% of the variation in sulfate, BC and OC is explained by the mixed combustion factor (top left panel). This factor also shows a significant contribution throughout the year, with maximum values in the winter and spring (top right panel). The variations within this period reflect changes in transport patterns, as well as removal processes (e.g., the decrease in AOD in May due to a springtime precipitation feature that occurs in this region at this time). The monsoon associated with monsoonal flows comprised of sea salt, SO_4 and dust explains $\sim 90\%$ of the sea salt contribution to AOD, and its maximum contribution is in the summer months reflecting southerly transport conditions and aerosol distributions of lower latitude marine conditions. The sulfate contribution in this factor reflects the contribution from volcanic emissions to the south (including those from Kyushu, Japan). Most of the variation in the fine and coarse mode dust is explained by the dust factor (bottom left panel), which shows a distinct peak around the months of February through May (third right panel), reflecting the long range transport of dust occurring due to springtime dust events. The total AOD calculated by PMF matches closely with the assimilated STEM total AOD as shown in the bottom right panel. This PMF solution could explain approximately 90% of the variation in each species as shown by the low values (< 0.1) of the unexplained variation (yellow) in the bottom left panel.

Even though similar factors were identified at Gosan and Hanimaadhoo the composition of the factors varies significantly at the two locations. For instance, the dust factor at Hanimaadhoo includes traces of sulfate along with dust contributions. In contrast at Gosan, the dust factor is dominated by dust species. Differences can also be found in the composition of the mixed combustion and marine at the two locations. For example, the BC and OC contribution to the anthropogenic pollution factor profile is smaller at Gosan, while it has a more significant contribution at Hanimaadhoo. This is expected behavior since Hanimaadhoo is predominantly influenced by the continental outflow from the Indian subcontinent where the carbonaceous aerosol to SO₂ emissions are higher than in China (Adhikary *et al.*, 2008). Overall these differences in the factors reflect differences in regional emissions.

To obtain a regional perspective of seasonality, the PMF results at selected locations across the domain are summarized in figure 5.14 where the panels on the left show the variability of the individual species explained by the three factors while the right panels show the seasonal variation of the factor contributions on an annual basis. The dust factor is a combination of fine and coarse dust AOD, with smaller contributions from sulfate, BC and OC, which reflect pollution mixed with dust during the transport. The dust factor is shown to have a significant contribution to the seasonal cycle of AOD throughout Asia. For example the dust contribution is shown clearly in the springtime in Beijing and the summertime at Hanimaadhoo.

The monsoon factor is a combination of sea salt with BC, sulfate, OC, with a contribution from dust at certain sites (e.g. Karachi), The monsoon shows clearly the arrival of the monsoonal flows at the sites along with the BC, sulfate and OC components associated with these flows, as seen in the South Asia sites of Delhi, and Dhaka, and at the high altitude Himalaya ABC Pyramid site. The monsoonal flows and their contribution to AOD are also clearly seen in East Asia (e.g., Beijing and Waliguan). The mixed combustion factor is dominated by the BC, sulfate and OC components. The

seasonal contribution of this factor at some sites reflects the seasonal changes in the flows, and is high when the flow directions are such that pollution sources are upwind of the site. This is shown at the remote sites such as the ABC Pyramid site where the monsoonal flows bring with them aerosols from the polluted regions in the Indo Gangetic plain and the Kathmandu Valley. This is also the case at Hanimadhoo where the flow conditions in the pre- and post-monsoon bring with them pollution from the continents. At many sites, the pollution contribution is high throughout the year (e.g., Delhi). But the increase contribution in winter reflects the fact that winds are weak and local pollution levels are able to accumulate for longer periods. At other sites changes in the emissions drive the seasonality in the combustion factor. This is the case at Bukit Koto Tabang, where the seasonal cycle in open burning drives the seasonality in AOD.

There is a significant variation in relative contribution of the PMF factors to the total AOD across the region. To illustrate these differences, the PMF factor contributions to total AOD at various locations are shown for April (figure 5.16), July (figure 5.17) and October (figure 5.18). The dust factor is the major contributor to AOD during April representing the impact of the spring time dust activity in the region as seen in figure 5.17. The strong impact of the onset of the monsoon can be seen throughout the region by the enhanced contribution of monsoon factor to AOD. The mixed combustion factor is the major contributor to AOD (figure 5.18) during October except at Waliguan, indicating the build up of local pollution.

It is useful to further split this mixed combustion factor into factors that reflect various source categories (e.g., open burning, biofuels and industry). However, it was not possible to distinguish the contribution of these sources in this study due to lack of individual sector-specific species contributions to AOD. The inclusion of additional species (e.g., nitrates) and source contributions (e.g., biofuel and open burning AODs) are required to further resolve this factor. Such analysis is currently underway.

5.3.5 Implications to Human Health

High aerosol levels have a direct impact on human health. Throughout Asia humans are exposed to ABC particles both indoors and outdoors. The most serious health impacts of particles associated with ABCs include cardiovascular and pulmonary effects leading to chronic respiratory problems, hospital admissions and deaths. The PM_{10} values exceed the 2005 WHO Guideline (World Health Organization, 2006) for annual mean PM_{10} of $20 \mu\text{g}/\text{m}^3$ throughout ~80% of Asia; in some regions by factors of 2 to 4. Figure 18 shows the grid cell population exposure to $PM_{2.5}$ levels greater than the WHO annual guideline of $10 \mu\text{g}/\text{m}^3$ (for grid cells with concentrations $> 10 \mu\text{g}/\text{m}^3$ the $PM_{2.5}$ concentration is multiplied by the population in that grid using annual population from the Gridded Population of the World Version 3 (GPWv3) available at <http://sedac.ciesin.columbia.edu/gpw>). Over 3 billion people in Asia live in areas that exceed the WHO annual guideline for $PM_{2.5}$. This may represent a conservative estimate of exposure as seasonal exposure levels can be significantly higher than the annual mean values, and sub-grid concentration “hot spots” also exist that can not be represented by the grid spacing used in the present simulations. The result shows that the Ganges Valley in India, the Pearl River Delta and Eastern China regions are primary hotspots for PM exposure. Exposure hotspots also occur at megacities and urban centers within the model domain. Recently these data have been used by health specialists in Asia to estimate the health impacts due to exposure to these levels of aerosol (Ramanathan *et al.*, 2008b). Using concentration-response relationships from the existing literature, it is estimated that exposure to each increase in anthropogenic $PM_{2.5}$ of $10 \mu\text{g}/\text{m}^3$ results in ~165,000 excess deaths per year in India and China, with a 95 per cent confidence interval of 90,000 - 250,000. This outdoor exposure risk is in addition to a WHO estimate of 381,000 and 407,000 for China and India, respectively, from indoor air pollution caused by solid fuel use (Ramanathan *et al.*, 2008b).

5.4 Summary

Multi-year aerosol distributions in the region of Asia were generated using the STEM model assimilated with satellite derived AOD via OI method at a monthly scale. The available fine mode and total AOD data from MODIS along with ground-based AERONET AOD was used to produce improved AOD and aerosol distributions. The AERONET SSA was also used to provide additional constraints to adjust the scattering and absorbing aerosols separately. The comparison of EANET PM₁₀ measurements with the assimilated predictions showed that assimilation greatly improved the modeled aerosol distributions. The four year average PM and AOD distribution at selected megacities and regional observation sites showed the assimilated model was able to capture the regional differences in the emission distributions. The model was also able to capture the seasonal cycle of the aerosol distributions. The PMF receptor model technique was applied on the modeled AOD constituents to understand the seasonality. The PMF results showed that the seasonal cycle of Asian aerosols were driven by the seasonal variations in emissions associated with combustion processes such as residential heating and open biomass burning, monsoonal flows the bring in strong on-shore flows across large regions and strong flows across arid and semi-arid regions resulting in large quantities of wind blown dust. This study has found that the over 3 billion people in Asia live in areas that exceed the WHO annual PM_{2.5} guideline of 10 µg/m³, point toward the need for stringent emission controls to reduce the adverse health impacts of Asian aerosols.

The results from this study can be used to reduce the uncertainty associated with emissions by identifying the regions which had major changes in the aerosol distribution before and after assimilation. The results can serve as input to radiation models and provide the estimates of aerosol radiative forcing in Asia. This study has only used the size based satellite and ground based AERONET AOD observations along with SSA measurements for assimilation. Other AOD parameters from satellites and ground based

observation including angstrom exponent and asymmetry parameter, can be used as constraints in assimilation process to further improve the aerosol distributions. This study has showed that combining the assimilated model predictions with receptor models will lead to enhance understanding of aerosols. The feedback from receptor based methods such as PMF should greatly assist in constraining the fine mode aerosols further in assimilation studies, which will be the future direction of this study.

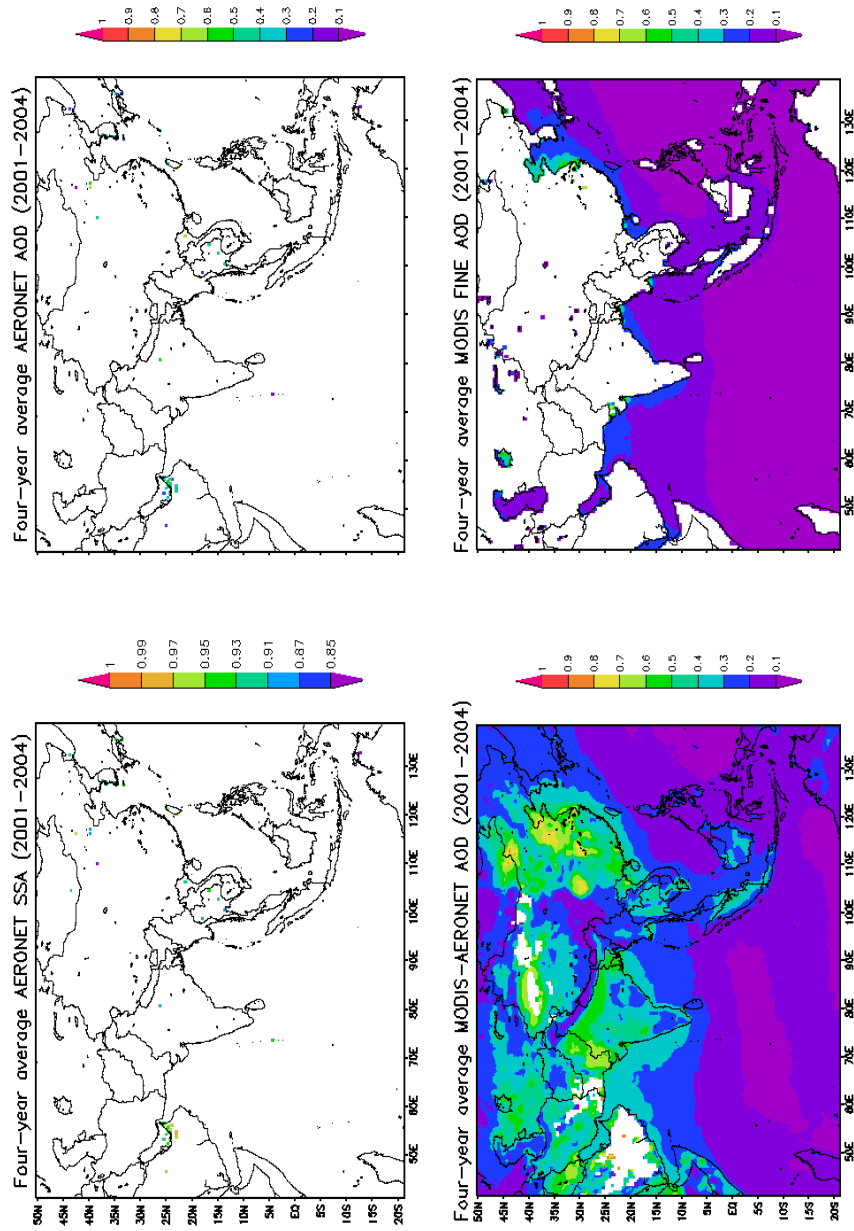


Figure 5.1 Four year average distributions of AERONET SSA, AERONET AOD, MODIS-AERONET AOD and MODIS fine mode AOD over land for 2001-2004.

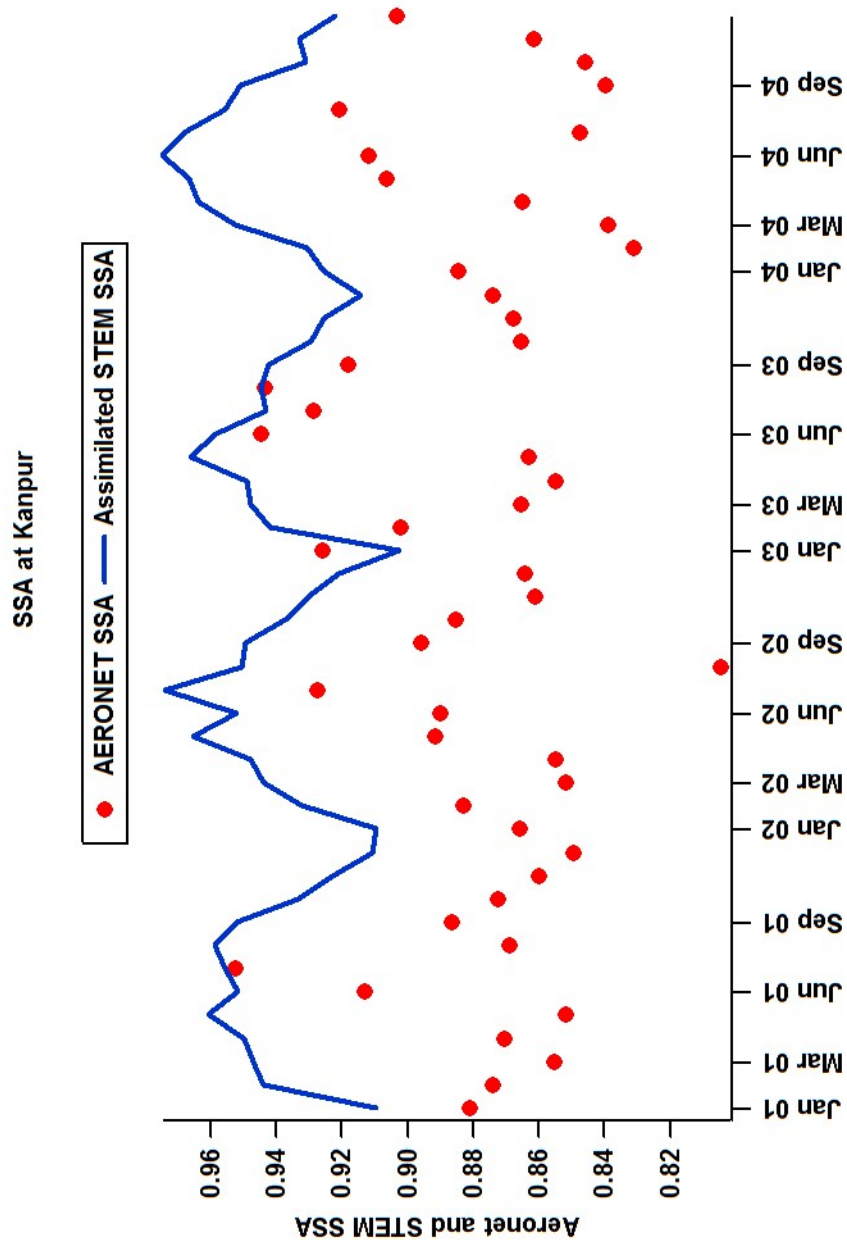


Figure 5.2 Comparison of modeled SSA with AERONET SSA observations at Kanpur

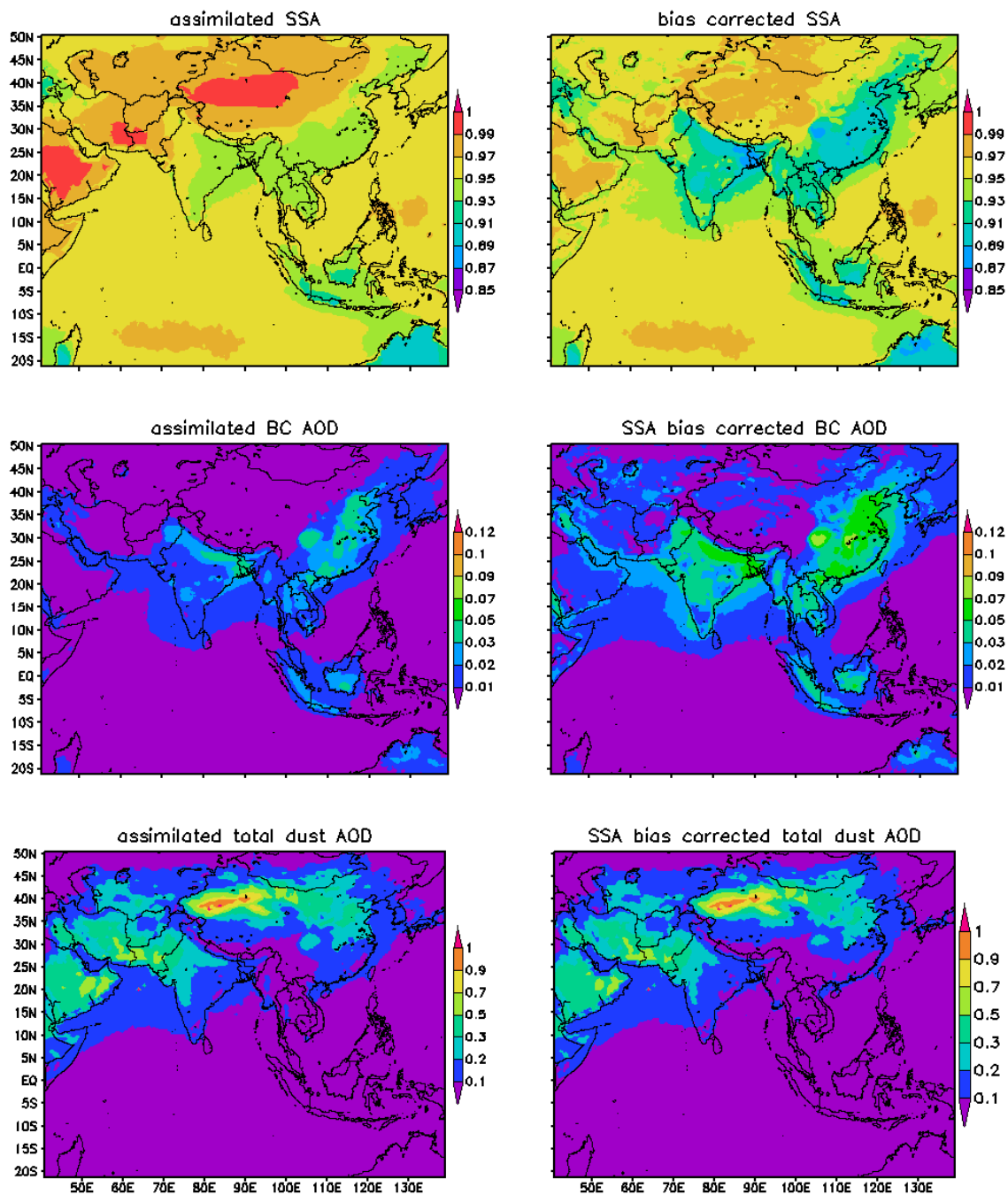


Figure 5.3 Regional distributions of SSA, BC AOD and dust AOD before and after SSA bias correction

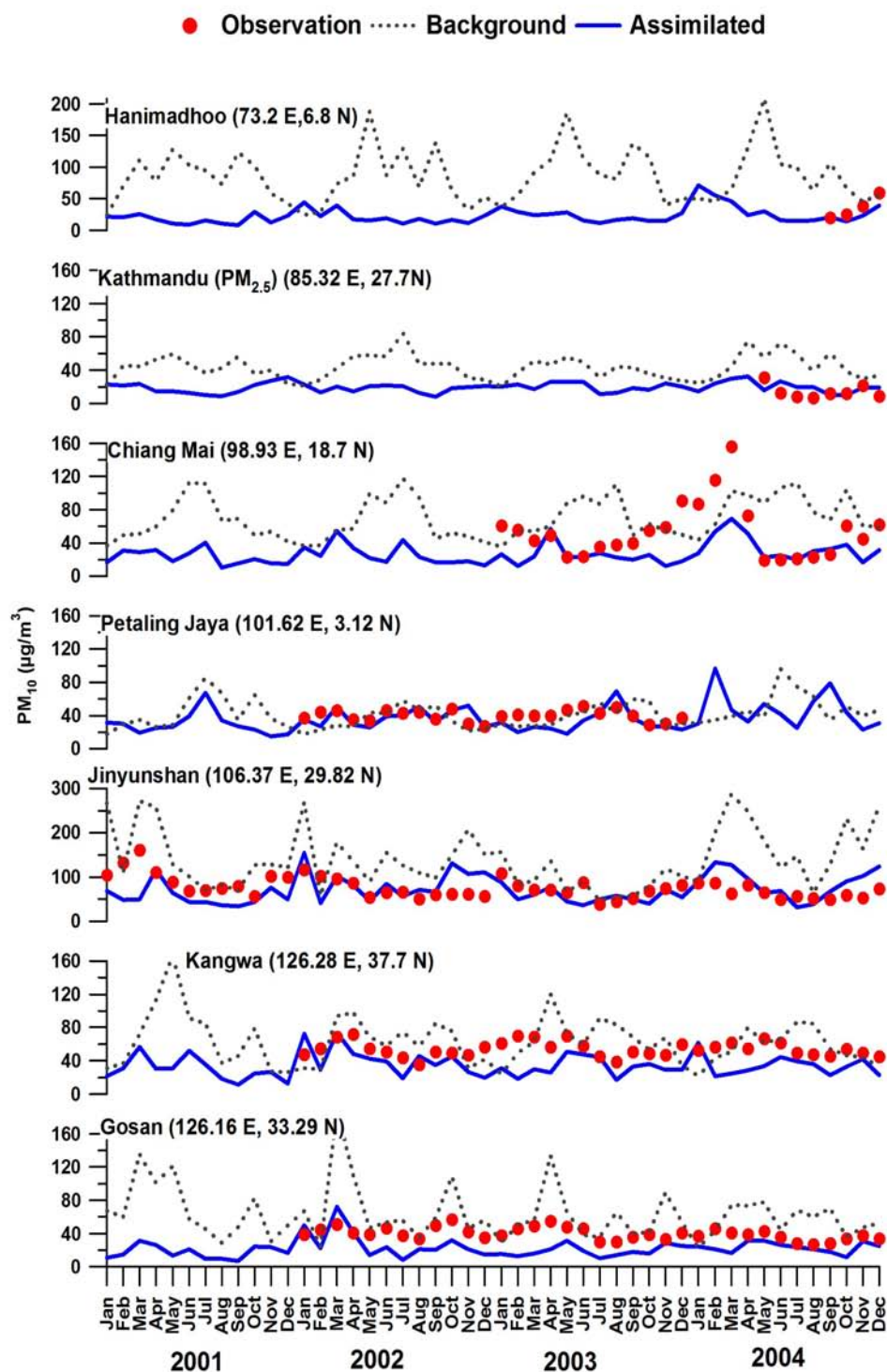


Figure 5.4 Comparison of observed and modeled PM₁₀ (μg/m³) at selected EANET locations

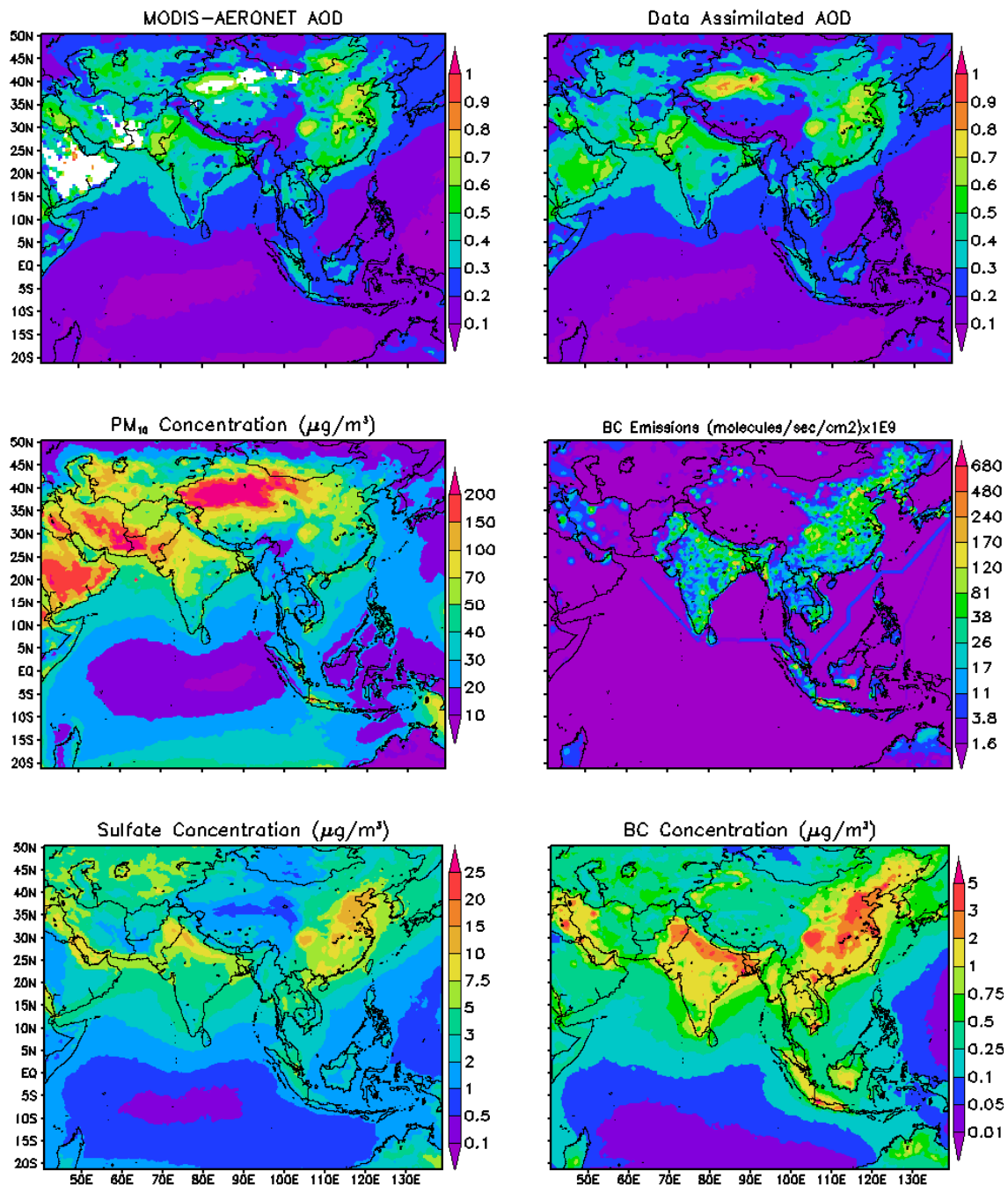


Figure 5.5 Four year averaged distributions of MODIS-AERONET AOD, Modeled AOD, PM₁₀ mass, BC emissions, Sulfate and BC mass.

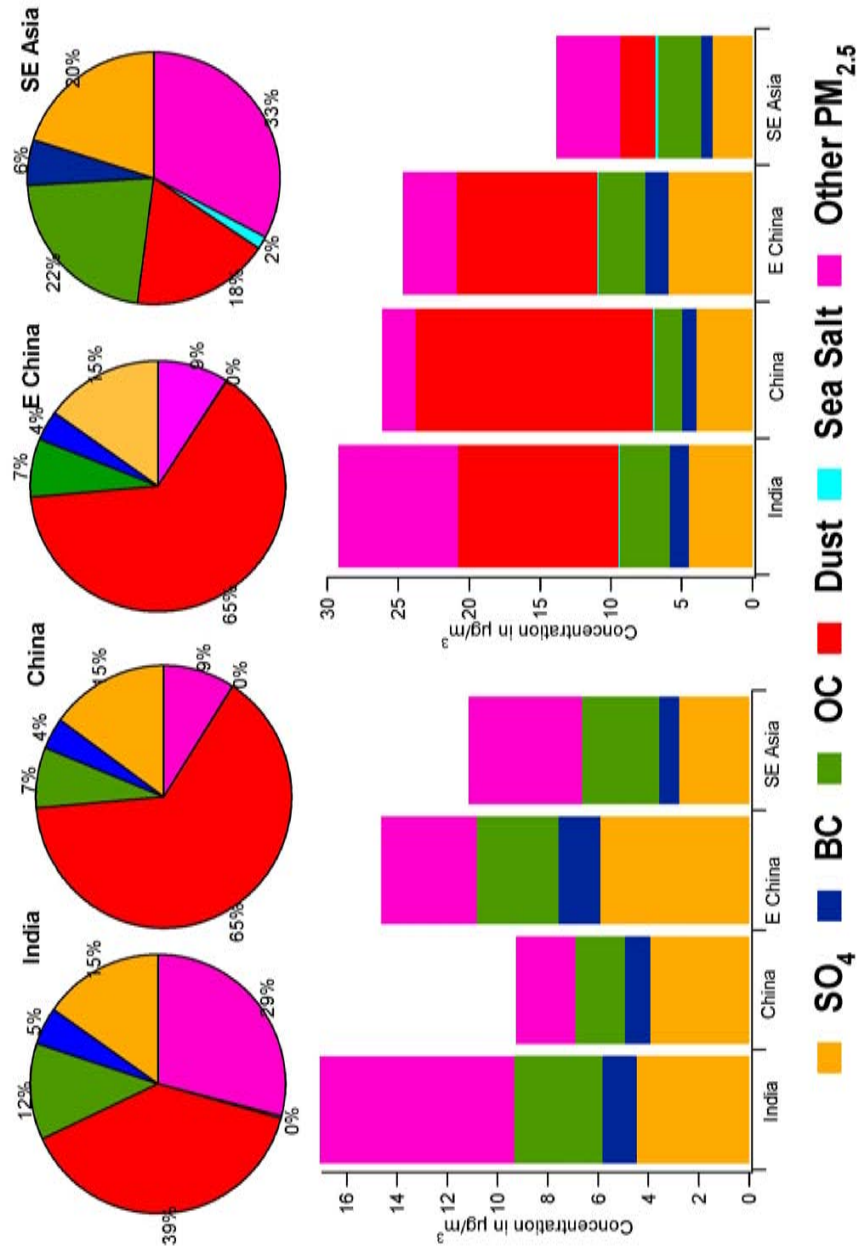


Figure 5.6 Composition of four year averaged PM_{2.5} aerosols for the regions India, China, East China and Southeast Asia

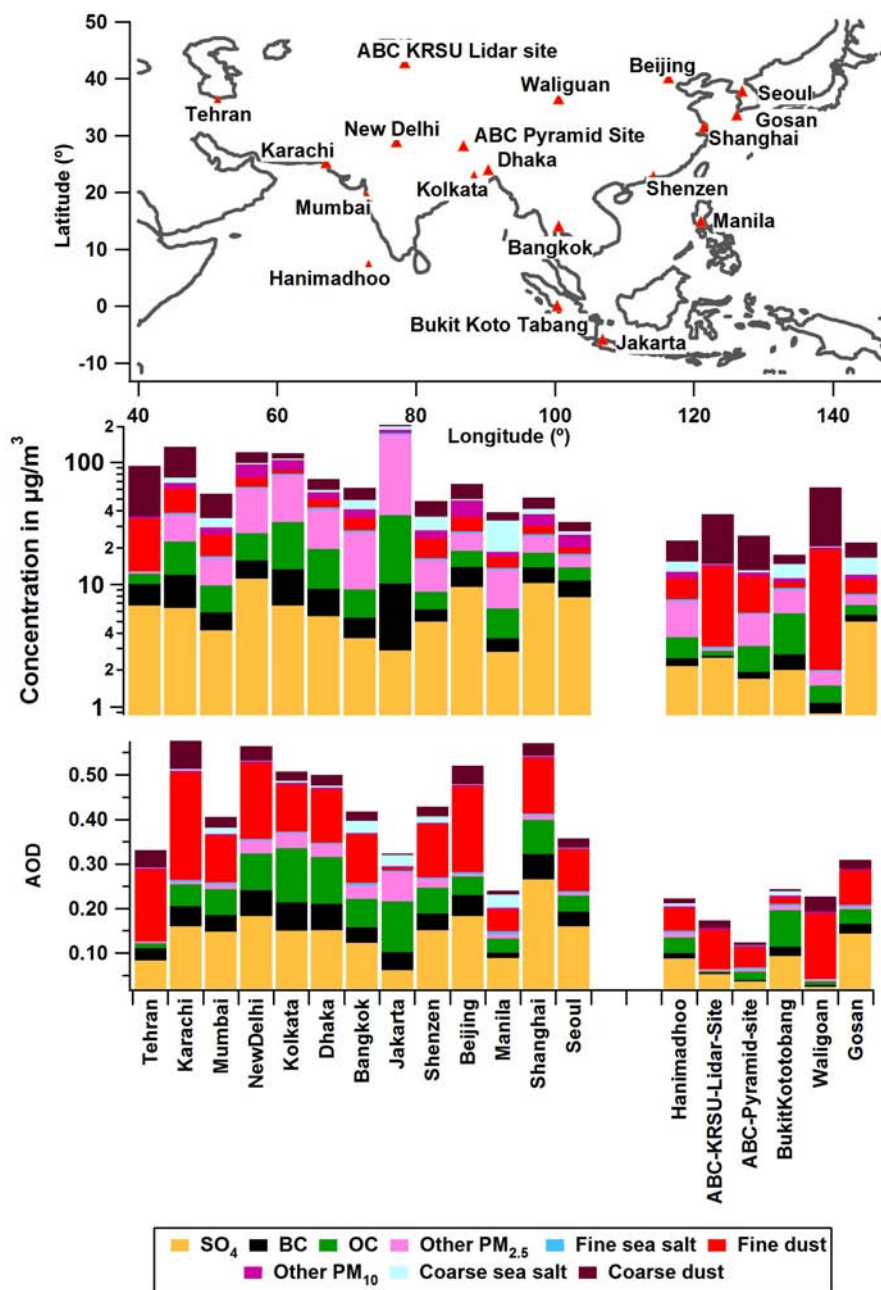


Figure 5.7 Composition of four year averaged AOD and PM₁₀ mass at selected megacities and regional observation sites. The PM₁₀ is plotted on log scale to highlight the pollution related aerosols

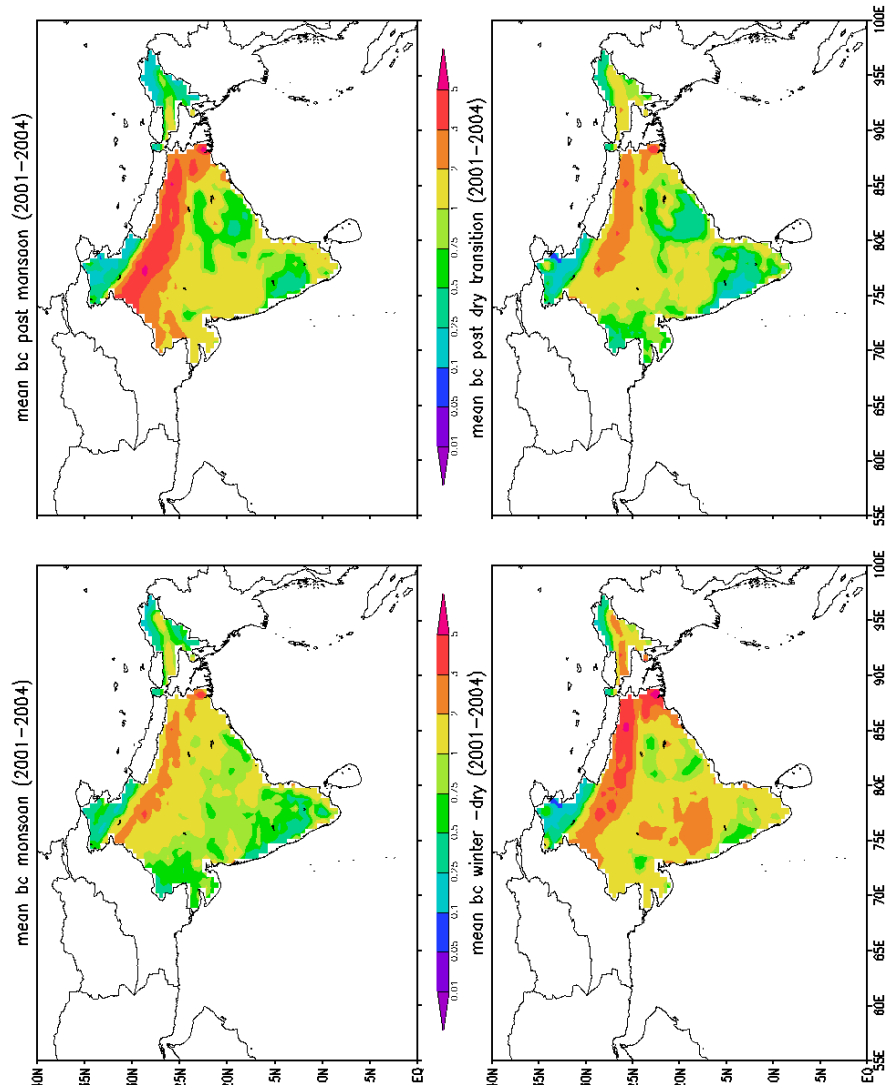


Figure 5.8 Average seasonal distribution of India BC concentration ($\mu\text{g}/\text{m}^3$) during 2001 - 2004

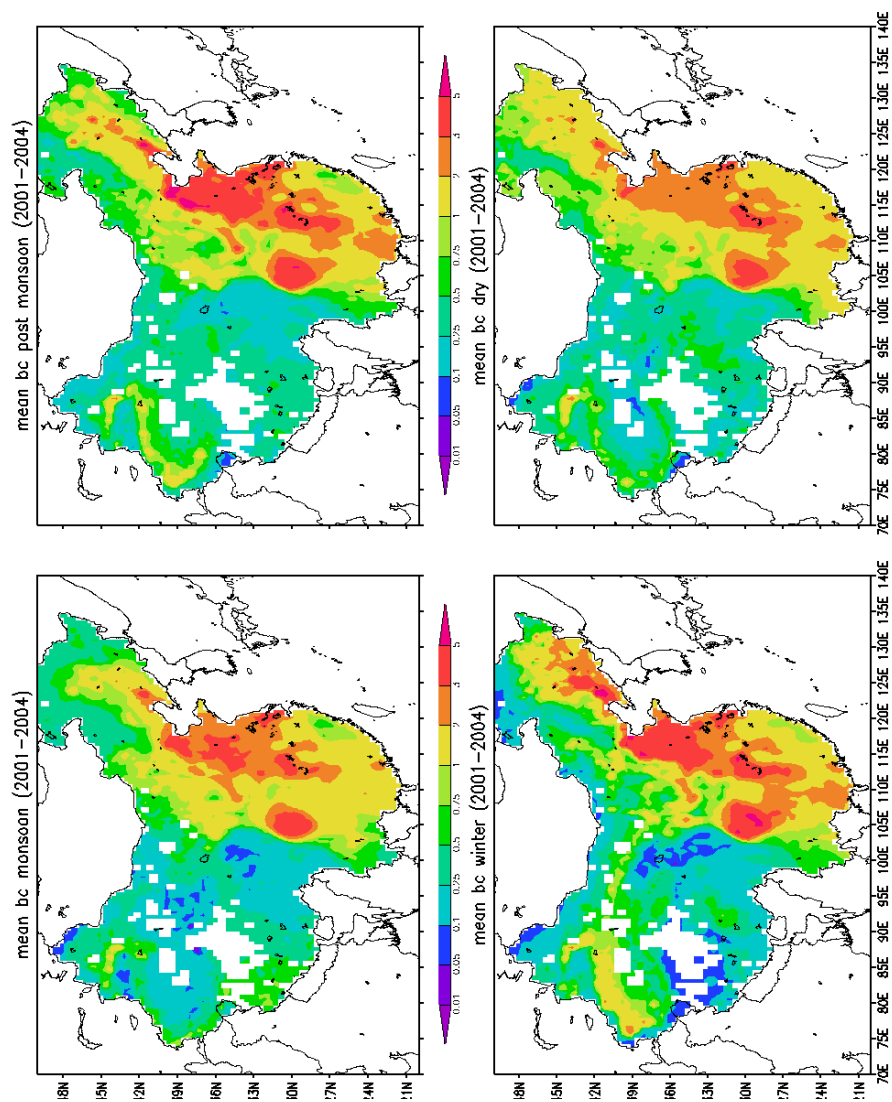


Figure 5.9 Average seasonal distribution of China BC concentration ($\mu\text{g}/\text{m}^3$) during 2001 -2004

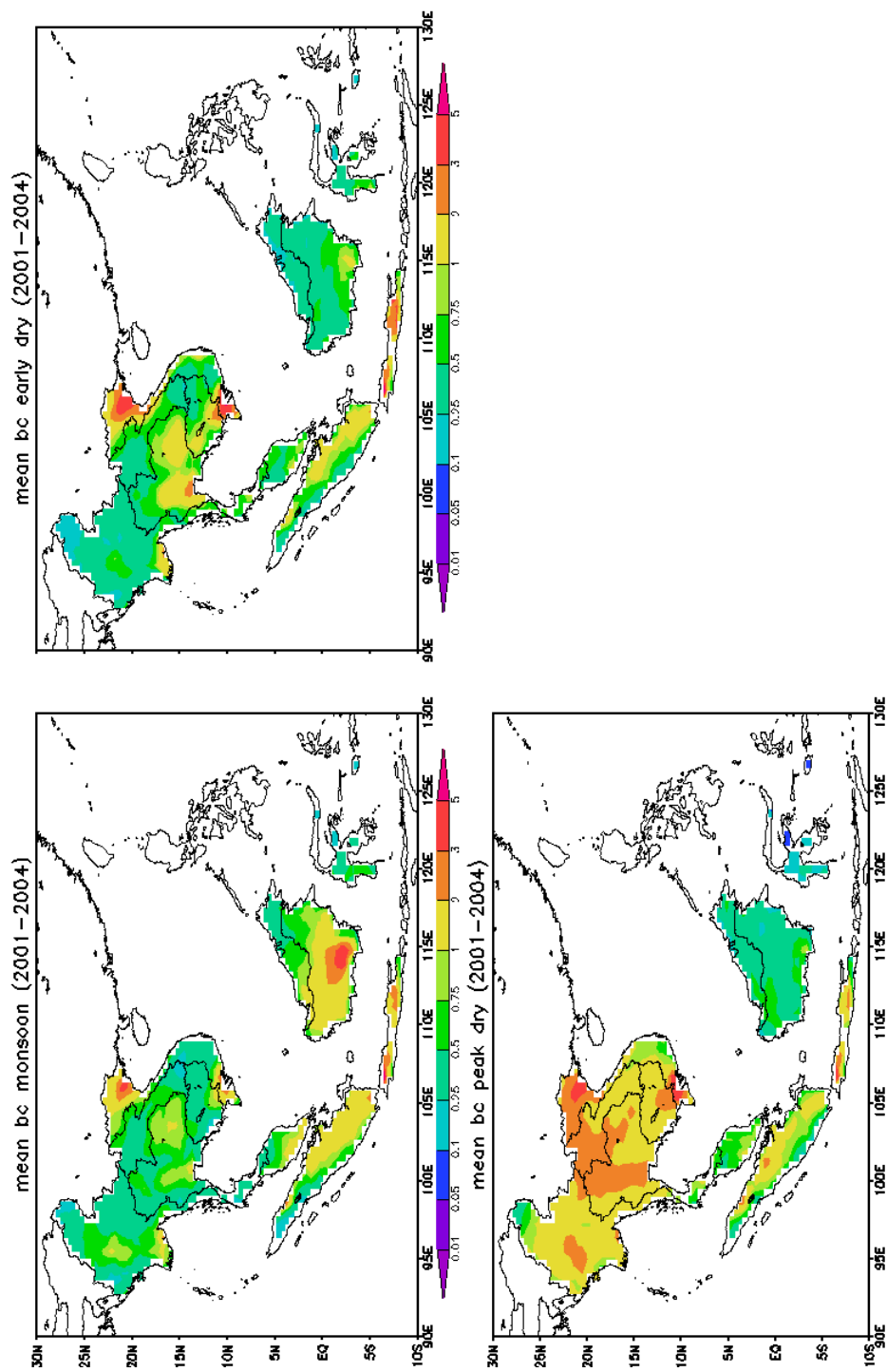


Figure 5.10 Average seasonal distribution of Southeast Asia BC concentration ($\mu\text{g}/\text{m}^3$) during 2001 – 2004

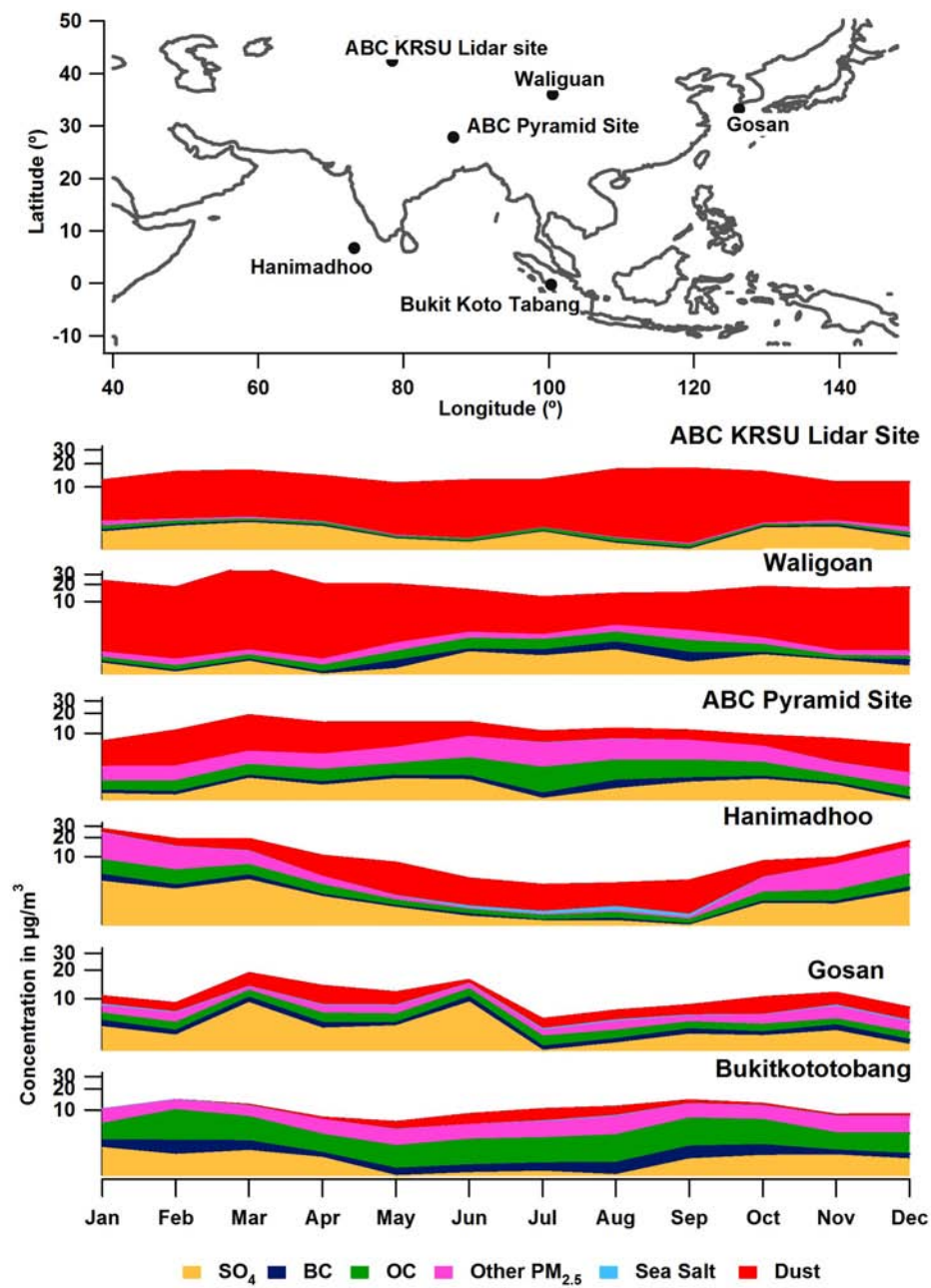


Figure 5.11 Seasonal cycle of PM_{2.5} aerosols at regional observation sites

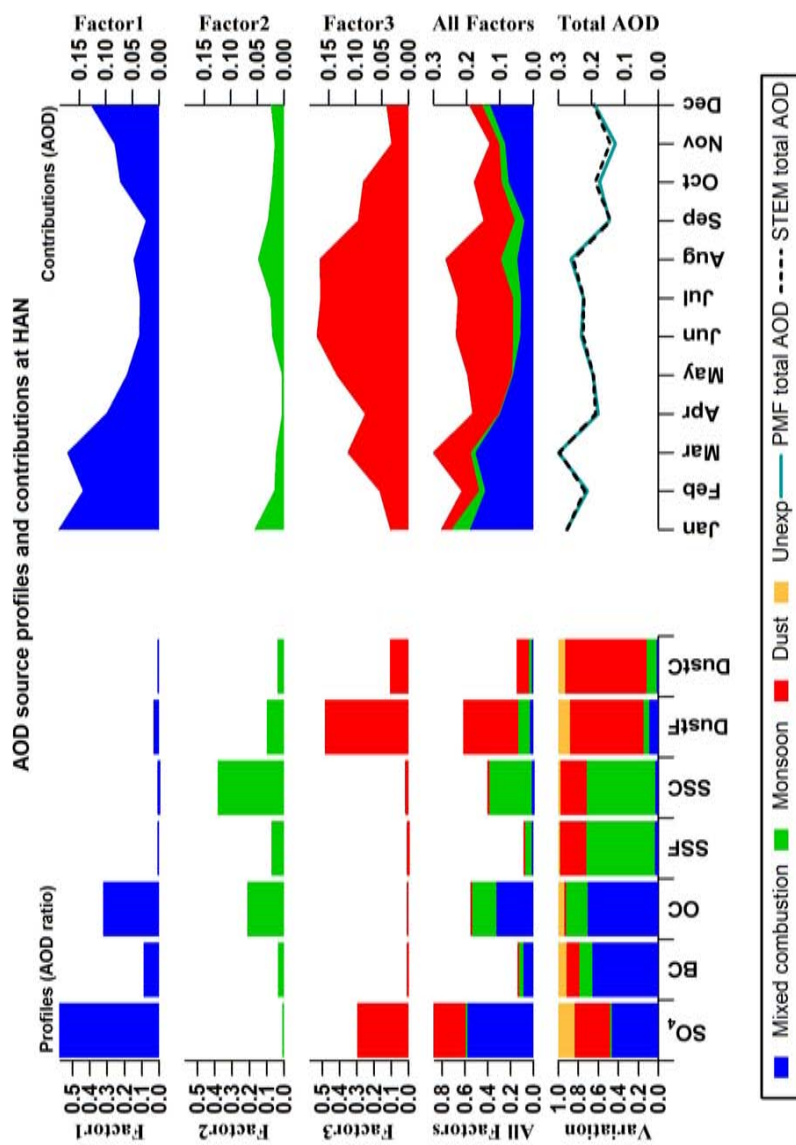


Figure 5.12 Source profiles and contributions of PMF modeled AOD at Hanimadhoo

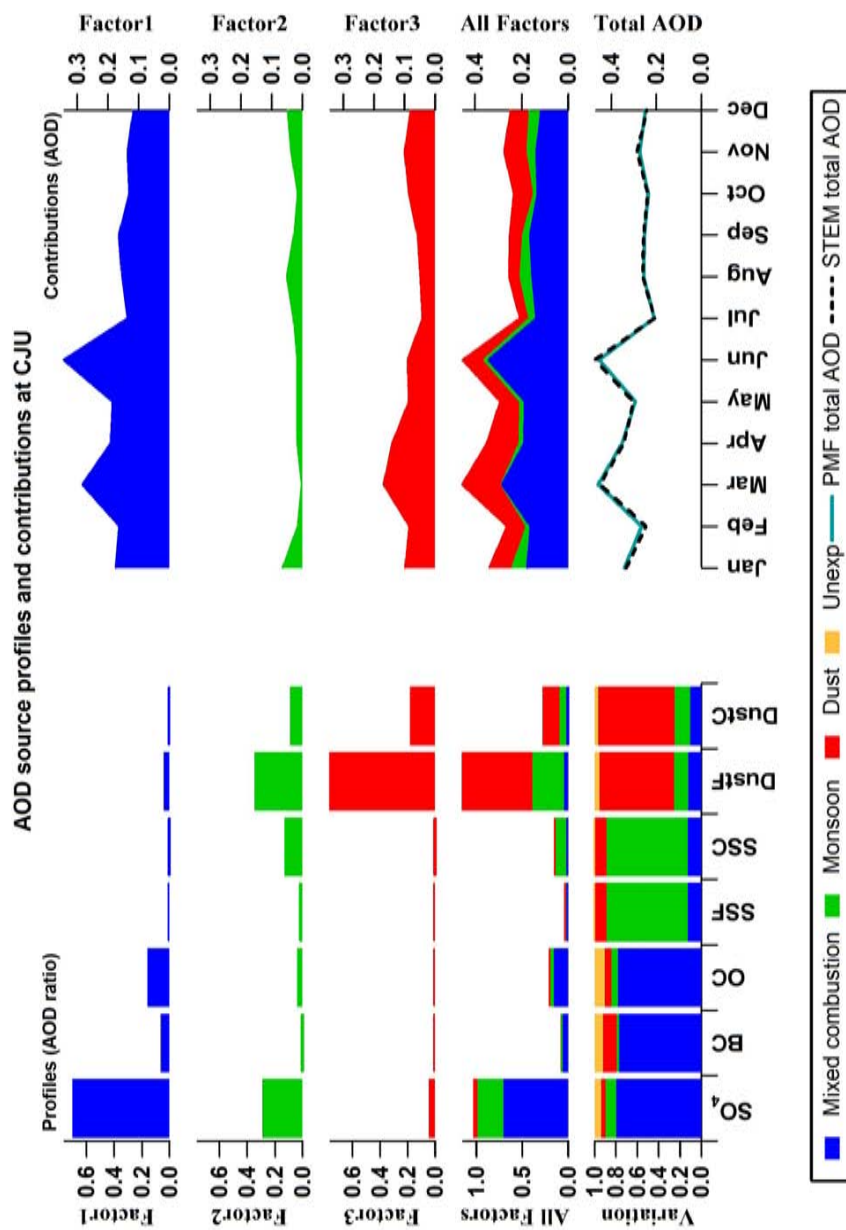


Figure 5.13 Source profiles and contributions of PMF modeled AOD at Gosan, Korea

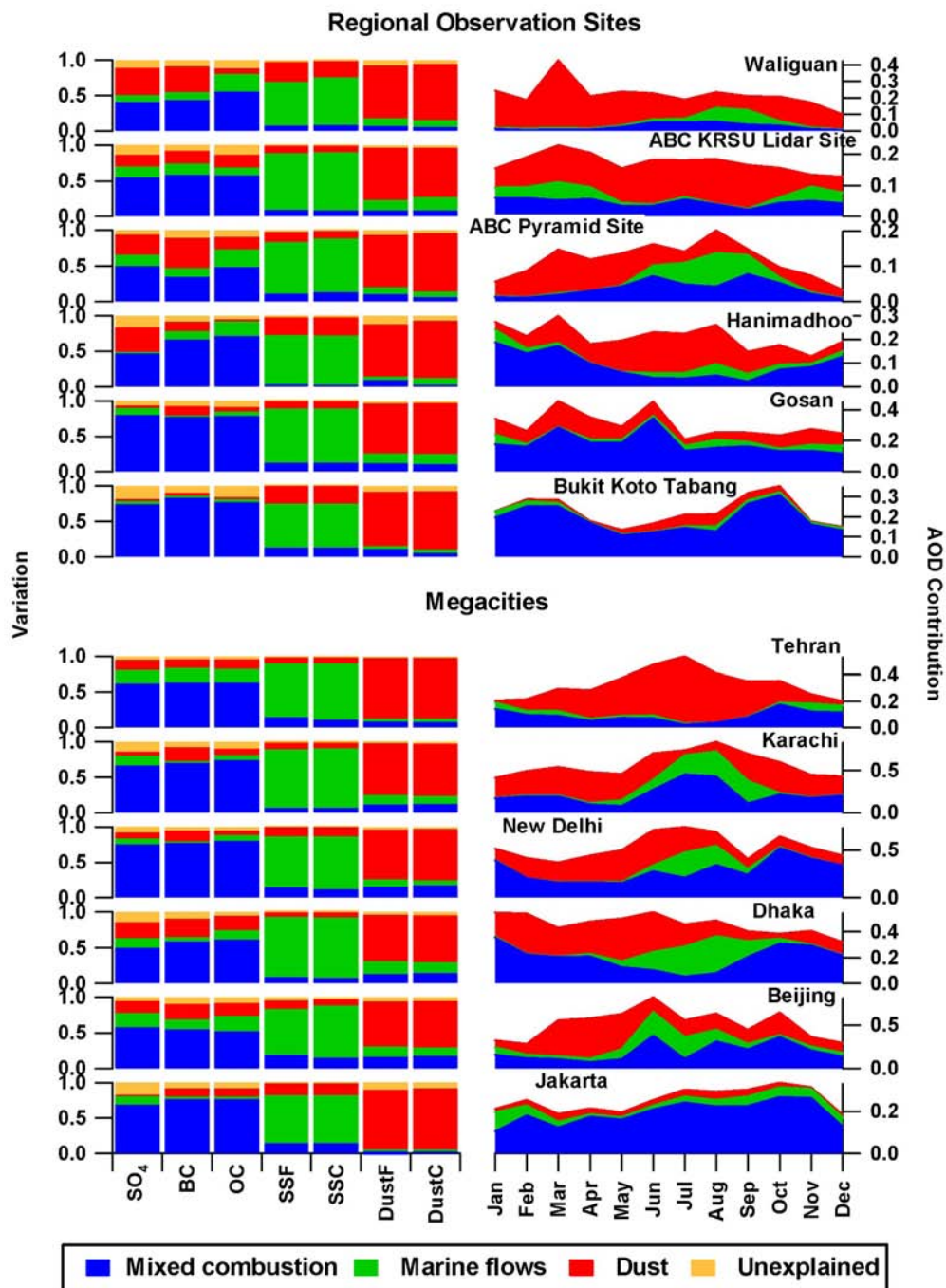


Figure 5.14 Source profiles and contributions of PMF modeled AOD at selected megacities and regional observation sites. See figure 4 for the location of the sites

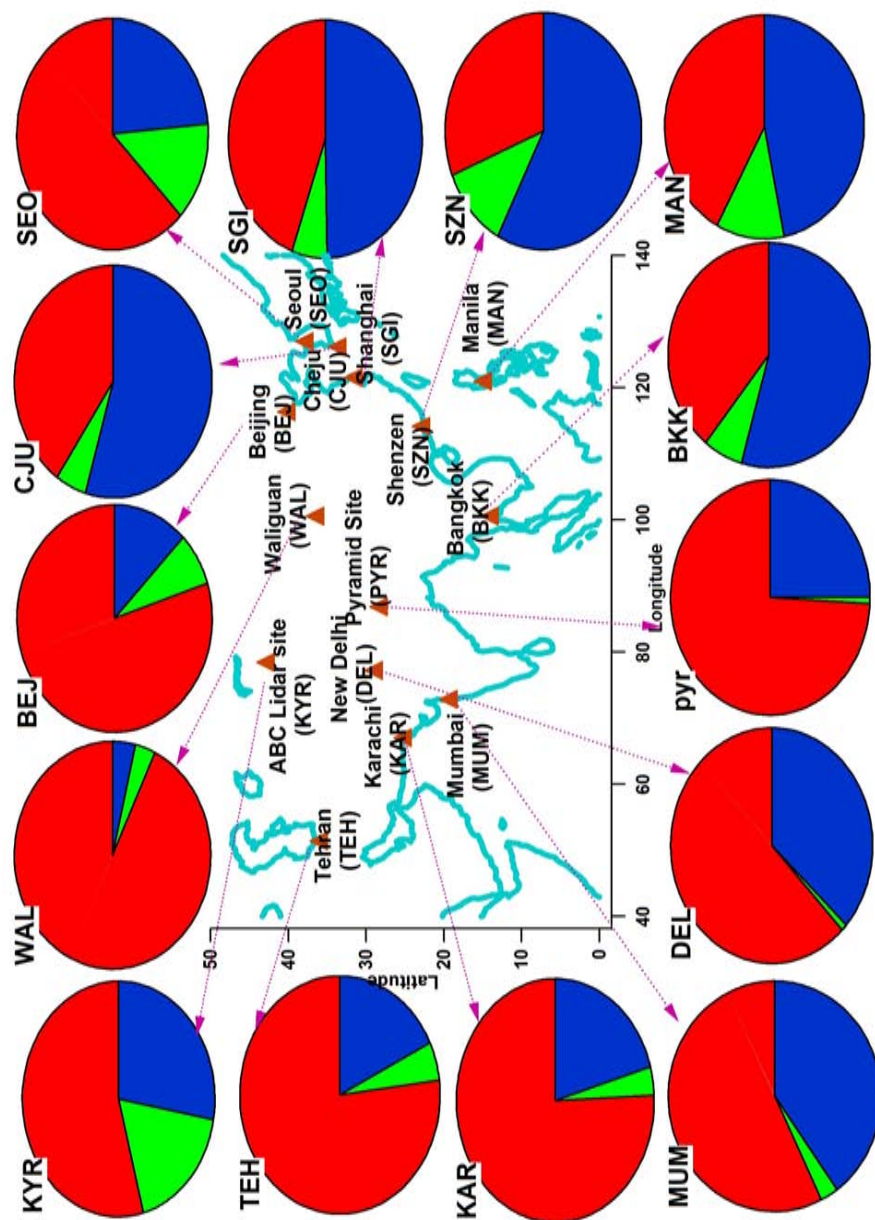


Figure 5.15 Contribution of PMF factors to total AOD at selected locations for the month of April representing the regional dust outflow

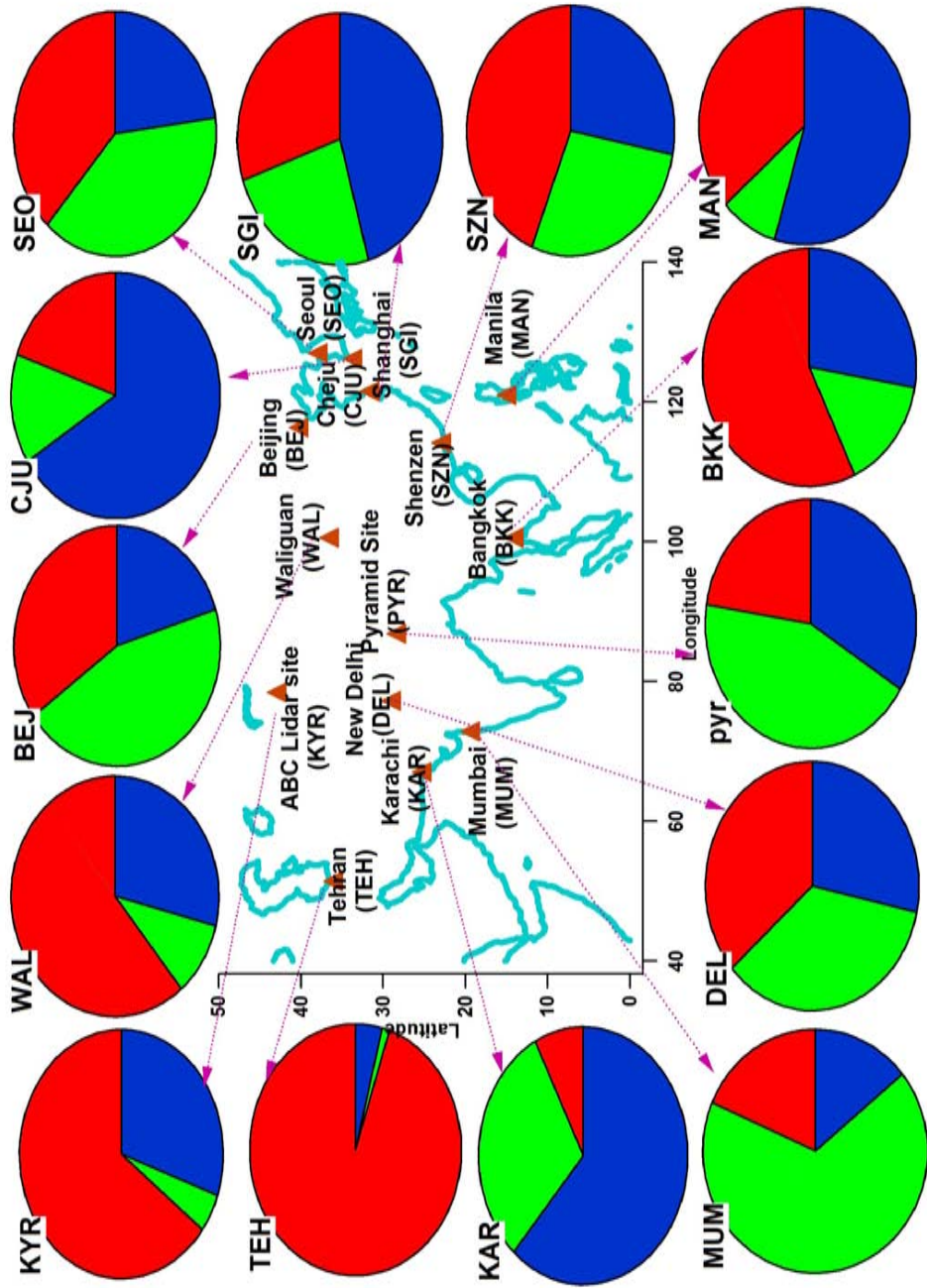


Figure 5.16 Contribution of PMF factors to total AOD at selected locations for the month of July representing the monsoon flow

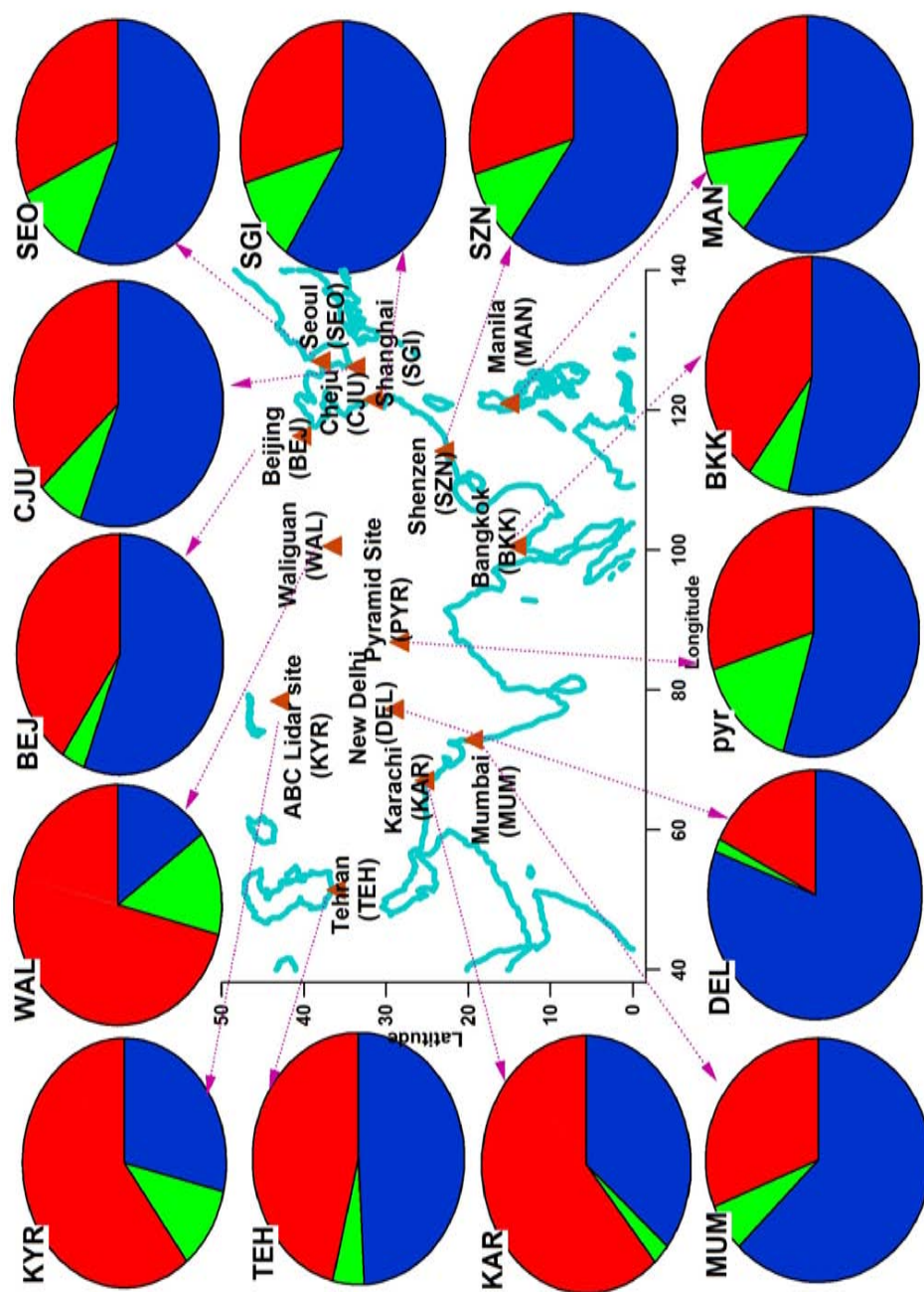


Figure 5.17 Contribution of PMF factors to total AOD at selected locations for the month of October representing the local pollution influence

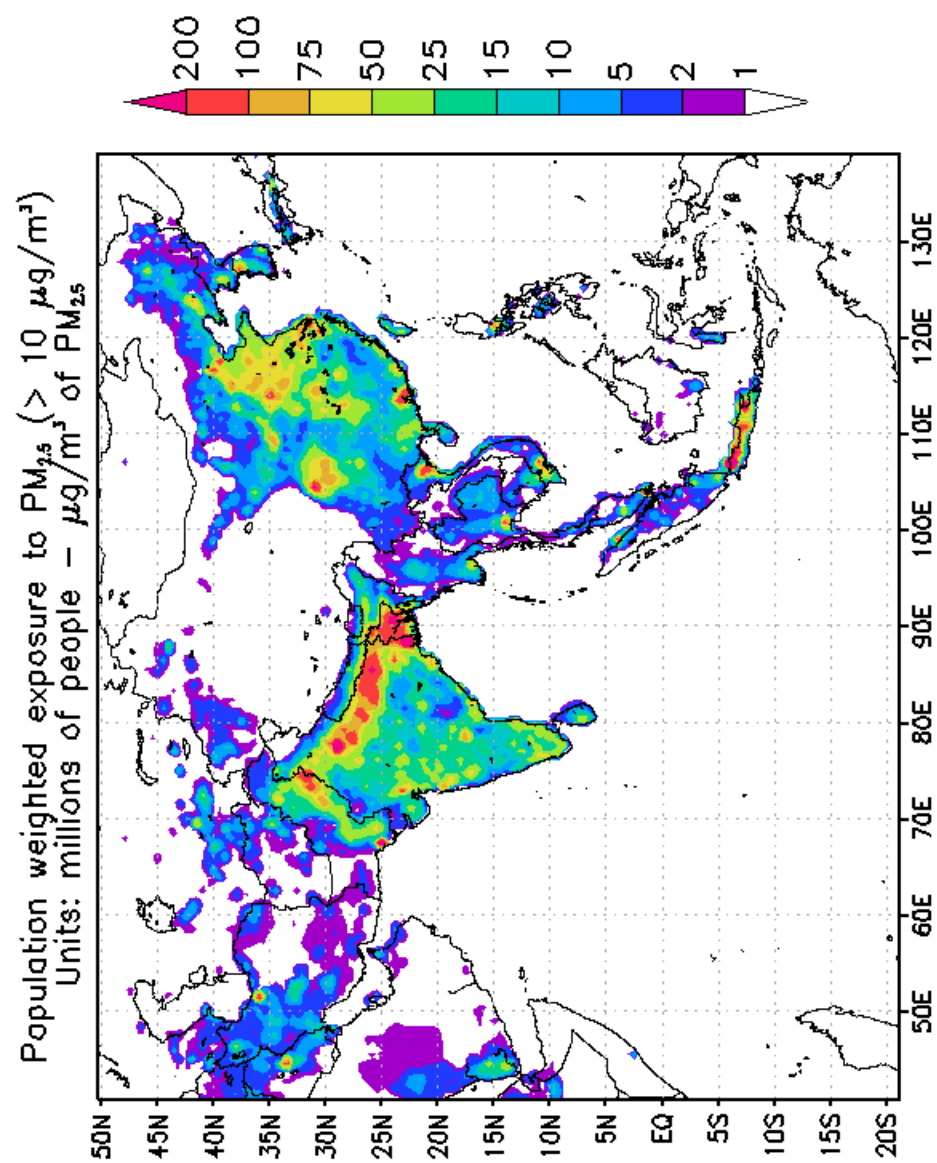


Figure 5.18 Population weighted exposure to $PM_{2.5}$ levels greater than WHO guideline of $10 \mu g/m^3$.

CHAPTER 6

SUMMARY AND FUTURE DIRECTION

Aerosols are ubiquitous components of the atmosphere and play a vital role as climate forcing agents by absorbing and scattering the sunlight, thereby altering the radiative balance of the atmosphere. The human exposure to aerosols is associated with various adverse impacts including respiratory problems and increased mortality rates. The rapidly growing emissions of aerosols from Asia is the leading contributor to global atmospheric aerosol loading which has potential implications to local, regional and global air quality. There is great necessity to devise emission reduction strategies for effective air quality management worldwide. The source receptor (S/R) relationships play a critical role in formulating policy making decisions. This research has focused on improving the understanding of the complex S/R relationships of aerosols on regional and intercontinental scales with particular emphasis on Asian aerosols.

This chapter presents an overall summary of this research that primarily focused on assessing the source-receptor relationships of aerosols through the application of various modeling methods. This dissertation work has contributed to enhanced understanding of the Asian aerosols and its impact on the downwind regions at regional and continental scales by designing an innovative analysis framework that combines the chemical transport models with receptor oriented models. The results from this work have great implications to health and policy-making decisions, which are summarized below.

6.1 Summary

The long range transport of dust aerosols gets mixed with local pollutants along the transit path and greatly enhances the aerosol loadings of the downwind receptors. The impact of large –scale episodic Asian dust events originating in the major desert regions of China, was studied through the application of receptor based methods including the

Positive Matrix Factorization (PMF) and Potential Source Contribution Function (PSCF). This study found that the dust episodes have pervasive impact on the remote background sites like Gosan (Chapter 2).

The inter-continental and hemispheric transport of aerosols has received great attention in recent times due to its capability to offset the domestic mitigation strategies aimed at reducing aerosol emissions. The intercontinental transport of aerosols is generally studied by global scale models. This research has studied the influence of intercontinental transport of aerosols through a series of emission perturbation simulations in the major source regions in the Northern Hemisphere including East Asia (EA), North America (NA), Europe (EU) and South Asia (SA) using a regional scale chemical transport model for April 2008. The results of the emission perturbation simulations described in chapter 3 have focused primarily on sulfate and BC due to their unique role as climate forcing agents. This modeling analysis shows that the contribution of aerosols from regions outside NA to the NA concentrations of sulfate and BC are ~ 30 and 20 % respectively, which has great significance for policy relevant decisions. This study also identified that long range transport of aerosols from NA, EU and EA regions is the major contributor to sulfate and BC concentrations in the Arctic region. This finding can greatly assist in formulating mitigation strategies aimed at reducing the continental transport of pollution into the Arctic region.

The transpacific transport of aerosols from Asia has significant impact on the aerosol loadings over the Pacific and has potential implications to North American air quality. This impact was studied through a regional scale modeling study evaluated with observations from the INTEX-B field campaign (chapter 4). The source region tagged tracers and air mass back trajectories were utilized to identify the potential source regions influencing the airborne and ground based observations. Iterative trajectory calculations were designed to identify possible instances of quasi-lagrangian sampling between the INTEX-B DC-8 and C-130 aircraft. The impact of emissions from specific sectors of

Asia including residential, transportation, power and industry, was analyzed through a series of sectoral emission simulations using the STEM tracer model. The sectoral simulation results showed that emissions from the residential and power sectors were the largest contributors to BC and sulfate concentrations over Asia and the outflow regions. This is greatly relevant from a policy perspective as these sectors can serve as potential targets when emission reduction strategies are formulated.

Chemical transport models are prone to great uncertainty that stems from the various modeling components. This uncertainty can be reduced by incorporating satellite-based observations that provide a higher spatial and temporal representation, into the chemical transport models by data assimilation methods. The regional distribution and seasonal cycle of Asian aerosols were described by multi year STEM model constrained by satellite-derived AOD using Optimal Interpolation technique (chapter 5). The ground based Single Scattering Albedo (SSA) was used as an additional constraint to improve the scattering and absorbing aerosol distributions. Furthermore, the PMF technique was combined with model output to characterize the seasonal cycle of Asian aerosols. This study has showed the vast majority of the Asian population was exposed to unhealthy PM levels that exceed $10 \mu\text{g}/\text{m}^3$, which is the WHO annual $\text{PM}_{2.5}$ standard. This finding is greatly relevant for policy decisions that are designed to reduce the human health effects of aerosols.

6.2 Future Direction

This research study has significantly contributed to methodical innovations by designing a modeling framework that combines the chemical transport models with receptor models to facilitate enhanced understanding of aerosol S/R relationships. The S/R relationships for various other source categories (e.g., industry, biofuels and open burning) can be obtained in a similar manner by implementing PMF on the individual sector-specific species contributions to AOD if they are available from CTM simulations.

This methodology can be further improved by utilizing the feedback from the PMF technique as additional constraints for data assimilation. This study has only applied PMF receptor technique due to the sparse availability of information of various pollution sources. There are several other receptor models available (for instance Chemical Mass Balance (CMB)) that can be utilized in a similar manner. The observations used as input to the OI algorithm implemented in this study are AOD and SSA. Other optical parameters including Angstrom Exponents, Asymmetry parameter can serve as additional constraints for assimilation.

The changes in the regional distribution of aerosols before and after implementing data assimilation methods can be used to identify sectors and regions where the emission values in the underlying emission inventory are uncertain. This information can be used further to produce improved estimates of emissions inventory, thereby reducing the uncertainty in the aerosol distributions simulated by CTMs. The output from the trajectory ensemble methods can be combined with gridded emissions inventory to obtain the improved pollution sources information that can be relevant from a policy standpoint.

One of the important steps in implementing the advanced data assimilation techniques like 4D – Var assimilation is the choice of control variables that would be adjusted to achieve better agreement between model predictions and actual observations. The PMF technique can be valuable tool in this regard as PMF can summarize a large number of variables into a few factors that account for most of the variability. This can greatly reduce the number of control variables while retaining the much of observed variability and possibly lead to design of an efficient assimilation process.

REFERENCES

- Adhikary, B. (2008). Characterization of the seasonal cycle, regional distribution and outflow of South Asian aerosols : a three dimensional chemical transport model analysis. Thesis (Ph.D.), Chemical and Biochemical Engineering. Iowa City, The University of Iowa: xiii, 219 leaves, bound.
- Adhikary, B., G. R. Carmichael, S. Kulkarni, C. Wei, Y. Tang, A. Dallura, M. Mena-Carrasco, D. G. Streets, Q. Zhang, R. B. Pierce, J. A. Al-Saadi, L. K. Emmons, G. G. Pfister, M. A. Avery, J. D. Barrick, D. R. Blake, W. H. Brune, R. C. Cohen, J. E. Dibb, A. Fried, B. G. Heikes, L. G. Huey, D. W. O'Sullivan, G. W. Sachse, R. E. Shetter, H. B. Singh, T. L. Campos, C. A. Cantrell, F. M. Flocke, E. J. Dunlea, J. L. Jimenez, A. J. Weinheimer, J. D. Crouse, P. O. Wennberg, J. J. Schauer, E. A. Stone, D. A. Jaffe and D. R. Reidmiller (2009). "Trans-Pacific transport and evolution of aerosols and trace gases from Asia during the INTEX-B field campaign." Atmos. Chem. Phys. Discuss. **9**(4): 16381-16439.
- Adhikary, B., G. R. Carmichael, Y. Tang, L. R. Leung, Y. Qian, J. J. Schauer, E. A. Stone, V. Ramanathan and M. V. Ramana (2007). "Characterization of the seasonal cycle of south Asian aerosols: A regional-scale modeling analysis." Journal of Geophysical Research, [Atmospheres] **112**(D22).
- Adhikary, B., S. Kulkarni, A. Dallura, Y. Tang, T. Chai, L. R. Leung, Y. Qian, C. E. Chung, V. Ramanathan and G. R. Carmichael (2008). "A regional scale chemical transport modeling of Asian aerosols with data assimilation of AOD observations using optimal interpolation technique." Atmospheric Environment **42**(37): 8600-8615.
- Al-Saadi, J., A. J. Soja, R. B. Pierce, J. Szykman, C. Wiedinmyer, L. Emmons, S. Kondragunta, X. Zhang, C. Kittaka, T. Schaack and K. Bowman (2008). "Intercomparison of near-real-time biomass burning emissions estimates constrained by satellite fire data." Journal of Applied Remote Sensing **2**(1): 021504-24.
- Anthes, R. A. and T. T. Warner (1978). "Development of Hydrodynamic Models Suitable for Air Pollution and Other Mesometeorological Studies." Monthly Weather Review **106**(8): 1045-1078.
- Ashbaugh, L. L., W. C. Malm and W. Z. Sadeh (1985). "A Residence Time Probability Analysis of Sulfur Concentrations at Grand-Canyon-National-Park." Atmos. Environ. **19**(8): 1263-1270.
- Bates, T. S., T. L. Anderson, T. Baynard, T. Bond, O. Boucher, G. Carmichael, A. Clarke, C. Erlick, H. Guo, L. Horowitz, S. Howell, S. Kulkarni, H. Maring, A. McComiskey, A. Middlebrook, K. Noone, C. D. O'Dowd, J. Ogren, J. Penner, P. K. Quinn, A. R. Ravishankara, D. L. Savoie, S. E. Schwartz, Y. Shinozuka, Y. Tang, R. J. Weber and Y. Wu (2006). "Aerosol direct radiative effects over the northwest Atlantic, northwest Pacific, and North Indian Oceans: estimates based on in-situ chemical and optical measurements and chemical transport modeling." Atmospheric Chemistry and Physics **6**: 1657-1732.

- Bench, G., P. G. Grant, D. Ueda, S. S. Cliff, K. D. Perry and T. A. Cahill (2002). "The use of STIM and PESA to measure profiles of aerosol mass and hydrogen content, respectively, across mylar rotating drums impactor samples." *Aerosol Sci. Technol.* **36**(5): 642-651.
- Bertschi, I. T., D. A. Jaffe, L. JaeglÃ©, H. U. Price and J. B. Dennison (2004). "PHOBEA/ITCT 2002 airborne observations of transpacific transport of ozone, CO, volatile organic compounds, and aerosols to the northeast Pacific: Impacts of Asian anthropogenic and Siberian boreal fire emissions." *J. Geophys. Res.* **109**: D23S12, doi:10.1029/2003JD004328.
- Bey, I., D. J. Jacob, J. A. Logan and R. M. Yantosca (2003). "Asian chemical outflow to the Pacific in spring: Origins, pathways, and budgets (vol 106, pg 23097, 2001)." *Journal of Geophysical Research-Atmospheres* **108**(D5).
- Bonasoni, P., P. Laj, F. Angelini, J. Arduini, U. Bonafè, F. Calzolari, P. Cristofanelli, S. Decesari, M. C. Facchini, S. Fuzzi, G. P. Gobbi, M. Maione, A. Marinoni, A. Petzold, F. Roccatò, J. C. Roger, K. Sellegri, M. Sprenger, H. Venzac, G. P. Verza, P. Villani and E. Vuillermoz (2008). "The ABC-Pyramid Atmospheric Research Observatory in Himalaya for aerosol, ozone and halocarbon measurements." *Science of The Total Environment* **391**(2-3): 252-261.
- Bond, T. C., D. G. Streets, K. F. Yarber, S. M. Nelson, J.-H. Woo and Z. Klimont (2004). "A technology-based global inventory of black and organic carbon emissions from combustion." *J. Geophys. Res.* **109**.
- Bouttier, F. and P. Courtier. (1999). "Data Assimilation concepts and Methods." from http://www.ecmwf.int/newsevents/training/rcourse_notes/DATA_ASSIMILATION/ASSIM_CONCEPTS/Assim_concepts2.html.
- Brook, J. R., E. Vega and J. G. Watson (2004). Chapter 7: Receptor Methods. *Particulate matter science for policy makers : a NARSTO assessment*. P. H. McMurry, M. F. Shepherd and J. S. Vickery. Cambridge ; New York, Cambridge University Press: xxxi, 510.
- Calori, G. and G. R. Carmichael (1999). "An urban trajectory model for sulfur in Asian megacities: model concepts and preliminary application." *Atmospheric Environment* **33**(19): 3109-3117.
- Carmichael, G. R., B. Adhikary, S. Kulkarni, A. D'Allura, Y. H. Tang, D. Streets, Q. Zhang, T. C. Bond, V. Ramanathan, A. Jamroensan and P. Marrapu (2009). "Asian Aerosols: Current and Year 2030 Distributions and Implications to Human Health and Regional Climate Change." *Environmental Science & Technology* **43**(15): 5811-5817.
- Carmichael, G. R., G. Calori, H. Hayami, I. Uno, S. Y. Cho, M. Engardt, S.-B. Kim, Y. Ichikawa, Y. Ikeda, J.-H. Woo, H. Ueda and M. Amann (2002). "The MICS-Asia study: model intercomparison of long-range transport and sulfur deposition in East Asia." *Atmospheric Environment* **36**(2): 175-199.
- Carmichael, G. R., M. S. Hong, H. Ueda, L. L. Chen, K. Murano, J. K. Park, H. G. Lee, Y. Kim, C. Kang and S. Shim (1997). "Aerosol composition at Cheju Island, Korea." *Journal of Geophysical Research-Atmospheres* **102**(D5): 6047-6061.

- Carmichael, G. R. and L. K. Peters (1984). "An Eulerian transport/transformation/removal model for SO₂ and sulfate--I. Model development." Atmospheric Environment **18**(5): 937-951.
- Carmichael, G. R. and L. K. Peters (1984). "An Eulerian transport/transformation/removal model for so₂ and sulfate--II. Model calculation of SO_x transport in the eastern United States." Atmospheric Environment (1967) **18**(5): 953-967.
- Carmichael, G. R. and L. K. Peters (1986). "A second generation model for regional-scale transport/chemistry/deposition." Atmospheric Environment (1967) **20**(1): 173-188.
- Carmichael, G. R., A. Sandu, T. Chai, D. N. Daescu, E. M. Constantinescu and Y. Tang (2008). "Predicting air quality: Improvements through advanced methods to integrate models and measurements." Journal of Computational Physics **227**(7): 3540-3571.
- Carmichael, G. R., Y. Tang, G. Kurata, I. Uno, D. Streets, J. H. Woo, H. Huang, J. Yienger, B. Lefer, R. Shetter, D. Blake, E. Atlas, A. Fried, E. Apel, F. Eisele, C. Cantrell, M. Avery, J. Barrick, G. Sachse, W. Brune, S. Sandholm, Y. Kondo, H. Singh, R. Talbot, A. Bandy, D. Thornton, A. Clarke and B. Heikes (2003). "Regional-scale chemical transport modeling in support of the analysis of observations obtained during the TRACE-P experiment." Journal of Geophysical Research-Atmospheres **108**(D21).
- Carter, W. P. L. (2000). Development and evaluation of the SAPRC-99 chemical mechanism, final report to California Air Resources Board. Riverside,CA,USA., Air Pollution Research Center and College of Engineering Center for Environmental Research and Technology, University of California.
- Carter, W. P. L. (2009). "Development of the SAPRC-07 Chemical Mechanism and Updated Ozone Reactivity Scales." from <http://www.cert.ucr.edu/~carter/SAPRC/saprc07.pdf>.
- Chai, T. F., G. R. Carmichael, A. Sandu, Y. H. Tang and D. N. Daescu (2006). "Chemical data assimilation of Transport and Chemical Evolution over the Pacific (TRACE-P) aircraft measurements." Journal of Geophysical Research-Atmospheres **111**(D2).
- Cheng, M. D., P. K. Hopke and Y. S. Zeng (1993). "A Receptor-Oriented Methodology for Determining Source Regions of Particulate Sulfate Observed at Dorset, Ontario." Journal of Geophysical Research-Atmospheres **98**(D9): 16839-16849.
- Chin, M., T. Diehl, P. Ginoux and W. Malm (2007). "Intercontinental transport of pollution and dust aerosols: implications for regional air quality." Atmos. Chem. Phys. **7**(21): 5501-5517.
- Chow, J. C. and J. G. Watson (2002). "Review of PM_{2.5} and PM₁₀ apportionment for fossil fuel combustion and other sources by the chemical mass balance receptor model." Energy & Fuels **16**(2): 222-260.

- Chow, J. C., J. G. Watson, J. L. Mauderly, D. L. Costa, R. E. Wyzga, S. Vedal, G. M. Hidy, S. L. Altshuler, D. Marrack, J. M. Heuss, G. T. Wolff, C. A. Pope and D. W. Dockery (2006). "Health effects of fine particulate air pollution: Lines that connect." J. Air Waste Manage. Assoc. **56**(10): 1368-1380.
- Chueinta, W., P. K. Hopke and P. Paatero (2000). "Investigation of sources of atmospheric aerosol at urban and suburban residential areas in Thailand by positive matrix factorization." Atmospheric Environment **34**(20): 3319-3329.
- Chung, C. E., V. Ramanathan, D. Kim and I. A. Podgorny (2005). "Global anthropogenic aerosol direct forcing derived from satellite and ground-based observations." Journal of Geophysical Research, [Atmospheres] **110**(D24).
- Collins, W. D., P. J. Rasch, B. E. Eaton, D. W. Fillmore, J. T. Kiehl, C. T. Beck and C. S. Zender (2002). "Simulation of aerosol distributions and radiative forcing for INDOEX: Regional climate impacts." J. Geophys. Res. **107**.
- Collins, W. D., P. J. Rasch, B. E. Eaton, B. V. Khatatov, J.-F. Lamarque and C. S. Zender (2001). "Simulating aerosols using a chemical transport model with assimilation of satellite aerosol retrievals: Methodology for INDOEX." J. Geophys. Res. **106**(D7): 7313-7336. .
- D'Allura, A. (2009). Meteorological and air quality forecasting products during the ARCTAS campaign. "7th International Conference on Air Quality " Istanbul (Turkey).
- Diaz, A. M., J. P. Diaz, F. J. Exposito, P. A. Hernandez-Leal, D. Savoie and X. Querol (2006). "Air masses and aerosols chemical components in the free troposphere at the subtropical Northeast Atlantic region." J. Atmos. Chem. **53**(1): 63-90.
- Dillner, A. M., J. J. Schauer, W. F. Christensen and G. R. Cass (2005). "A quantitative method for clustering size distributions of elements." Atmospheric Environment **39**(8): 1525-1537.
- Dunlea, E. J., P. F. DeCarlo, A. C. Aiken, J. R. Kimmel, R. E. Peltier, R. J. Weber, J. Tomlison, D. R. Collins, Y. Shinozuka, C. S. McNaughton, S. G. Howell, A. D. Clarke, L. K. Emmons, E. C. Apel, G. G. Pfister, A. van Donkelaar, R. V. Martin, D. B. Millet, C. L. Heald and J. L. Jimenez (2008). "Evolution of Asian aerosols during transpacific transport in INTEX-B." Atmos. Chem. Phys. Discuss. **8**(4): 15375-15461.
- EANET. (2001). "EANET Data on the Acid Deposition in the East Asian Region: 2001." from <http://www.eanet.cc/product.html>.
- EANET. (2002). "EANET Data on the Acid Deposition in the East Asian Region: 2002 ", from <http://www.eanet.cc/product.html>.
- EANET. (2003). "EANET Data on the Acid Deposition in the East Asian Region: 2003 ", from <http://www.eanet.cc/product.html>.
- EANET. (2004). "EANET Data on the Acid Deposition in the East Asian Region: 2004." from <http://www.eanet.cc/product.html>.

- Elbern, H. and H. Schmidt (1999). "A four-dimensional variational chemistry data assimilation scheme for Eulerian chemistry transport modeling." Journal of Geophysical Research-Atmospheres **104**(D15): 18583-18598.
- Elbern, H. and H. Schmidt (2001). "Ozone episode analysis by four-dimensional variational chemistry data assimilation." Journal of Geophysical Research-Atmospheres **106**(D4): 3569-3590.
- Elbern, H., H. Schmidt and A. Ebel (1997). "Variational data assimilation for tropospheric chemistry modeling." Journal of Geophysical Research-Atmospheres **102**(D13): 15967-15985.
- Elbern, H., H. Schmidt, O. Talagrand and A. Ebel (2000). "4D-variational data assimilation with an adjoint air quality model for emission analysis." Environ. Modell. Softw. **15**: 539-548.
- EPA, U. S. (2001). "Draft guidance for demonstrating attainment of air quality goals for PM_{2.5} and regional haze." from http://www.epa.gov/scram001/guidance_sip.htm.
- Generoso, S., I. Bey, J.-L. AttiÄ© and F. o.-M. BrÄ©on (2007a). "A satellite- and model-based assessment of the 2003 Russian fires: Impact on the Arctic region." J. Geophys. Res. **112**.
- Generoso, S., F. M. BrÄ©on, F. Chevallier, Y. Balkanski, M. Schulz and I. Bey (2007b). "Assimilation of POLDER aerosol optical thickness into the LMDz-INCA model: Implications for the Arctic aerosol burden." J. Geophys. Res. **112**.
- Gong, S. L. (2003). "A parameterization of sea-salt aerosol source function for sub- and super-micron particles." Global Biogeochemical Cycles **17**(4).
- Guttikunda, S. K. (2002). Impact assessment of Asian megacity emissions on global, regional, and urban air quality. Chemical and biochemical engineering, The University of Iowa. **Thesis** xviii, 217 leaves, bound.
- Hadley, O. L., V. Ramanathan, G. R. Carmichael, Y. Tang, C. E. Corrigan, G. C. Roberts and G. S. Mauger (2007). "Trans-Pacific transport of black carbon and fine aerosols ($D < 2.5 \mu m$) into North America." Journal of Geophysical Research-Atmospheres **112**(D5): D05309, doi:10.1029/2006JD007632.
- Hakami, A., D. K. Henze, J. H. Seinfeld, T. Chai, Y. Tang, G. R. Carmichael and A. Sandu (2005). "Adjoint inverse modeling of black carbon during the Asian Pacific Regional Aerosol Characterization Experiment." Journal of Geophysical Research-Atmospheres **110**(D14).
- Han, J. S., K. J. Moon, S. J. Lee, Y. J. Kim, S. Y. Ryu, S. S. Cliff and S. M. Yi (2006). "Size-resolved source apportionment of ambient particles by positive matrix factorization at Gosan background site in East Asia." Atmos. Chem. Phys. **6**(1): 211-223.
- Han, J. S., K. J. Moon, S. Y. Ryu, Y. J. Kim and K. D. Perry (2005). "Source estimation of anthropogenic aerosols collected by a DRUM sampler during spring of 2002 at Gosan, Korea." Atmospheric Environment **39**(17): 3113-3125.

- Hess, M., P. Koepke and I. Schult (1998). "Optical Properties of Aerosols and Clouds: The Software Package OPAC." Bulletin of the American Meteorological Society **79**(5): 831-844.
- Hines, K. M. and D. H. Bromwich (2008). "Development and Testing of Polar Weather Research and Forecasting (WRF) Model. Part I: Greenland Ice Sheet Meteorology." Monthly Weather Review **136**(6): 1971-1989.
- Holloway, T., A. Fiore and M. G. Hastings (2003). "Intercontinental Transport of air pollution: Will emerging science lead to a new hemispheric treaty?" Environmental Science & Technology **37**(20): 4535-4542.
- Hopke, P. K. (2003). "Recent developments in receptor modeling." Journal of Chemometrics **17**(5): 255-265.
- Hopke, P. K. (2006). The Use of the Back Trajectory Model HY-SPLIT-4 to Assess Source/Receptor Relationships.
- Hsu, Y.-K., T. M. Holsen and P. K. Hopke (2003). "Comparison of hybrid receptor models to locate PCB sources in Chicago." Atmospheric Environment **37**(4): 545-562.
- Huang, S. L., K. A. Rahn and R. Arimoto (1999). "Testing and optimizing two factor-analysis techniques on aerosol at Narragansett, Rhode Island." Atmospheric Environment **33**(14): 2169-2185.
- Huebert, B. J., T. Bates, P. B. Russell, G. Y. Shi, Y. J. Kim, K. Kawamura, G. Carmichael and T. Nakajima (2003). "An overview of ACE-Asia: Strategies for quantifying the relationships between Asian aerosols and their climatic impacts." Journal of Geophysical Research-Atmospheres **108**(D23).
- Husar, R. B., D. M. Tratt, B. A. Schichtel, S. R. Falke, F. Li, D. Jaffe, S. Gasso, T. Gill, N. S. Laulainen, F. Lu, M. C. Reheis, Y. Chun, D. Westphal, B. N. Holben, C. Gueymard, I. McKendry, N. Kuring, G. C. Feldman, C. McClain, R. J. Frouin, J. Merrill, D. DuBois, F. Vignola, T. Murayama, S. Nickovic, W. E. Wilson, K. Sassen, N. Sugimoto and W. C. Malm (2001). "Asian dust events of April 1998." Journal of Geophysical Research-Atmospheres **106**(D16): 18317-18330.
- Jacob, D. J. (1999). Introduction to atmospheric chemistry. Princeton, N.J., Princeton University Press
- Jacob, D. J., J. H. Crawford, M. M. Kleb, V. S. Connors, R. J. Bendura, J. L. Raper, G. W. Sachse, J. C. Gille, L. Emmons and C. L. Heald (2003). "Transport and Chemical Evolution over the Pacific (TRACE-P) aircraft mission: Design, execution, and first results." Journal of Geophysical Research-Atmospheres **108**(D20): 1-19.
- Jacob, D. J., J. H. Crawford, H. Maring, A. D. Clarke, J. E. Dibb, R. A. Ferrare, C. A. Hostetler, P. B. Russell, H. B. Singh, A. M. Thompson, G. E. Shaw, E. McCauley, J. R. Pederson and J. A. Fisher (2009). "The ARCTAS aircraft mission: design and execution." Atmos. Chem. Phys. Discuss. **9**(4): 17073-17123.

- Jaffe, D., T. Anderson, D. Covert, R. Kotchenruther, B. Trost, J. Danielson, W. Simpson, T. Berntsen, S. Karlsdottir, D. Blake, J. Harris, G. Carmichael and I. Uno (1999). "Transport of Asian air pollution to North America." Geophys. Res. Lett. **26**(6): 711-714.
- Juntto, S. and P. Paatero (1994). "Analysis of Daily Precipitation Data by Positive Matrix Factorization." Environmetrics **5**(2): 127-144.
- Khattatov, B. V., J.-F. Lamarque, L. V. Lyjak, R. Menard, P. Levelt, X. Tie, G. P. Brasseur and J. C. Gille (2000). "Assimilation of satellite observations of long-lived chemical species in global chemistry transport models." J. Geophys. Res. **105**.
- Kim, E. and P. K. Hopke (2005). "Identification of fine particle sources in mid-Atlantic US area." Water Air and Soil Pollution **168**(1-4): 391-421.
- Kim, E., P. K. Hopke, D. M. Kenski and M. Koerber (2005). "Sources of fine particles in a rural Midwestern US area." Environmental Science & Technology **39**(13): 4953-4960.
- Kim, S.-W., A. Jefferson, S.-C. Yoon, E. G. Dutton, J. A. Ogren, F. P. J. Valero, J. Kim and B. N. Holben (2005). "Comparisons of aerosol optical depth and surface shortwave irradiance and their effect on the aerosol surface radiative forcing estimation." J. Geophys. Res. **110**.
- Kim, Y. P. and J. H. Seinfeld (1995). "Atmospheric Gas-Aerosol Equilibrium .3. Thermodynamics of Crustal Elements Ca²⁺, K⁺, and Mg²⁺." Aerosol Sci. Technol. **22**(1): 93-110.
- Koch, D., T. C. Bond, D. Streets, N. Unger and G. R. van der Werf (2007). "Global impacts of aerosols from particular source regions and sectors." J. Geophys. Res. **112**.
- Koch, D. and J. Hansen (2005). "Distant origins of Arctic black carbon: A Goddard Institute for Space Studies ModelE experiment." J. Geophys. Res. **110**.
- Kulkarni, S. (2004). Surface elemental composition of aerosols at Beijing (China), Gosan (Korea), and Tango (Japan) during ACE-Asia. M.S. Thesis, Chemical and Biochemical Engineering. Iowa City, The University of Iowa: xiv, 183 leaves, bound.
- Kurata, G., G. R. Carmichael, D. G. Streets, T. Kitada, Y. Tang, J. H. Woo and N. Thongboonchoo (2004). "Relationships between emission sources and air mass characteristics in East Asia during the TRACE-P period." Atmospheric Environment **38**(40): 6977-6987.
- Lapina, K. and K. G. Paterson (2004). "Assessing source characteristics of PM_{2.5} in the eastern United States using positive matrix factorization." J. Air Waste Manage. Assoc. **54**(9): 1170-1174.
- Lathiere, J., D. A. Hauglustaine, A. D. Friend, N. De Noblet-Ducoudre, N. Viovy and G. A. Folberth (2006). "Impact of climate variability and land use changes on global biogenic volatile organic compound emissions." Atmospheric Chemistry and Physics **6**: 2129-2146.

- Latto, A. (2009). Quasi-lagrangian sampling of air pollution by aircraft during the Intercontinental Chemical Transport Experiment Phase B. Department of Meteorology, Florida State University. **M.S. Thesis**.
- Laupsa, H., B. Denby, S. Larssen and J. Schaug (2009). "Source apportionment of particulate matter (PM_{2.5}) in an urban area using dispersion, receptor and inverse modelling." Atmospheric Environment **43**(31): 4733-4744.
- Lee, E., C. K. Chan and P. Paatero (1999). "Application of positive matrix factorization in source apportionment of particulate pollutants in Hong Kong." Atmospheric Environment **33**(19): 3201-3212.
- Lee, J. H., Y. Yoshida, B. J. Turpin, P. K. Hopke, R. L. Poirot, P. J. Lioy and J. C. Oxley (2002). "Identification of sources contributing to Mid-Atlantic regional aerosol." J. Air Waste Manage. Assoc. **52**(10): 1186-1205.
- Levy, H., M. D. Schwarzkopf, L. Horowitz, V. Ramaswamy and K. L. Findell (2008). "Strong sensitivity of late 21st century climate to projected changes in short-lived air pollutants." Journal of Geophysical Research-Atmospheres **113**(D6): D06102, doi:10.1029/2007JD009176.
- Liang, Q., L. Jaegle, D. A. Jaffe, P. Weiss-Penzias, A. Heckman and J. A. Snow (2004). "Long-range transport of Asian pollution to the northeast Pacific: Seasonal variations and transport pathways of carbon monoxide." Journal of Geophysical Research-Atmospheres **109**(D23): D23S07, doi:10.1029/2003JD004402.
- Liu, J., D. L. Mauzerall and L. W. Horowitz (2005). "Analysis of seasonal and interannual variability in transpacific transport." J. Geophys. Res. **110**.
- Liu, J., D. L. Mauzerall and L. W. Horowitz (2008). "Source-receptor relationships between East Asian sulfur dioxide emissions and Northern Hemisphere sulfate concentrations." Atmos. Chem. Phys. **8**(13): 3721-3733.
- Liu, J., D. L. Mauzerall, L. W. Horowitz, P. Ginoux and A. M. Fiore (2009). "Evaluating inter-continental transport of fine aerosols: (1) Methodology, global aerosol distribution and optical depth." Atmospheric Environment **43**(28): 4327-4338.
- Ma, C.-J., S. Tohno, M. Kasahara and S. Hayakawa (2004). "Properties of individual Asian dust storm particles collected at Kosan, Korea during ACE-Asia." Atmospheric Environment **38**(8): 1133-1143.
- Madronich, S. (2002). "The Tropospheric Visible Ultra-violet (TUV) model web page." from <http://www.acd.ucar.edu/TUV>.
- McNaughton, C. S., A. D. Clarke, V. Kapustin, Y. Shinozuka, S. G. Howell, B. E. Anderson, E. Winstead, J. Dibb, E. Scheuer, R. C. Cohen, P. Wooldridge, A. Perring, L. G. Huey, S. Kim, J. L. Jimenez, E. J. Dunlea, P. F. DeCarlo, P. O. Wennberg, J. D. Crouse, A. J. Weinheimer and F. Flocke (2009). "Observations of heterogeneous reactions between Asian pollution and mineral dust over the Eastern North Pacific during INTEX-B." Atmos. Chem. Phys. Discuss. **9**(2): 8469-8539.

- Mena-Carrasco, M., Y. Tang, G. R. Carmichael, T. Chai, N. Thongbongchoo, J. E. Campbell, S. Kulkarni, L. Horowitz, J. Vukovich, M. Avery, W. Brune, J. E. Dibb, L. Emmons, F. Flocke, G. W. Sachse, D. Tan, R. Shetter, R. W. Talbot, D. G. Streets, G. Frost and D. Blake (2007). "Improving regional ozone modeling through systematic evaluation of errors using the aircraft observations during the International Consortium for Atmospheric Research on Transport and Transformation." Journal of Geophysical Research, [Atmospheres] **112**(D12).
- Millet, D. B., A. H. Goldstein, R. Holzinger, B. J. Williams, J. D. Allan, J. L. Jimenez, D. R. Worsnop, J. M. Roberts, A. B. White, R. C. Hudman, I. T. Bertschi and A. Stohl (2006). "Chemical characteristics of North American surface layer outflow: Insights from Chebogue Point, Nova Scotia." Journal of Geophysical Research-Atmospheres **111**(D23).
- Penner, J. E., M. Andreae, v. Annegarn, L. Barrie, J. Feichter, D. Hegg, A. Jayaraman, R. Leaitch, D. Murphy, J. Nganga and G. Pitari (2001). Climate change 2001: The scientific basis :contribution of working group I to the third assessment report of the Intergovernmental Panel on Climate Change., Cambridge University Press: 289 - 348.
- NRC (2009). Global Sources of Local Pollution: An Assessment of Long-Range Transport of Key Air Pollutants to and from the United States. The National Academic Press. Washington DC, USA.
- Olivier, J. G. J., A. F. Bouwman, J. J. M. Berdowski, C. Veldt, J. P. J. Bloos, A. J. H. Visschedijk, C. W. M. van der Maas and P. Y. J. Zandveld (1999). "Sectoral emission inventories of greenhouse gases for 1990 on a per country basis as well as on 1°×1°." Environmental Science & Policy **2**(3): 241-263.
- Paatero, P. (2000). User's guide for Positive Matrix Factorization programs PMF2 and PMF3. University of Helsinki, Finland.
- Paatero, P., P. K. Hopke, X. H. Song and Z. Ramadan (2002). "Understanding and controlling rotations in factor analytic models." Chemometrics and Intelligent Laboratory Systems **60**(1-2): 253-264.
- Paatero, P. and U. Tapper (1993). "Analysis of Different Modes of Factor-Analysis as Least-Squares Fit Problems." Chemometrics and Intelligent Laboratory Systems **18**(2): 183-194.
- Paatero, P. and U. Tapper (1994). "Positive Matrix Factorization - a Nonnegative Factor Model with Optimal Utilization of Error-Estimates of Data Values." Environmetrics **5**(2): 111-126.
- Pan, L., T. Chai, G. R. Carmichael, Y. Tang, D. Streets, J.-H. Woo, H. R. Friedli and L. F. Radke (2007). "Top-down estimate of mercury emissions in China using four-dimensional variational data assimilation." Atmospheric Environment **41**(13): 2804-2819.
- Park, R. J., D. J. Jacob, B. D. Field, R. M. Yantosca and M. Chin (2004). "Natural and transboundary pollution influences on sulfate-nitrate-ammonium aerosols in the United States: Implications for policy." J. Geophys. Res. **109**.

- Paterson, K. G. (1999). "Analysis of air quality data using positive matrix factorization (vol 33, pg 635, 1999)." Environmental Science & Technology **33**(18): 3283-3283.
- Paterson, K. G., J. L. Sagady and D. L. Hooper (1999). "Analysis of air quality data using positive matrix factorization." Environmental Science & Technology **33**(4): 635-641.
- Peltier, R. E., A. H. Hecobian, R. J. Weber, A. Stohl, E. L. Atlas, D. D. Riemer, D. R. Blake, E. Apel, T. Campos and T. Karl (2008). "Investigating the sources and atmospheric processing of fine particles from Asia and the Northwestern United States measured during INTEX B." Atmos. Chem. Phys. **8**(6): 1835-1853.
- Penner, J. E., M. Andreae, v. Annegarn , L. Barrie, J. Feichter, D. Hegg, A. Jayaraman, R. Leaitch, D. Murphy, J. Nganga and G. Pitari (2001). Climate change 2001: The scientific basis :contribution of working group I to the third assessment report of the Intergovernmental Panel on Climate Change., Cambridge University Press: 289 - 348.
- Pfister, G. G., L. K. Emmons, P. G. Hess, J. F. Lamarque, J. J. Orlando, S. Walters, A. Guenther, P. I. Palmer and P. J. Lawrence (2008). "Contribution of isoprene to chemical budgets: A model tracer study with the NCAR CTM MOZART-4." Journal of Geophysical Research-Atmospheres **113**(D5): D02204, doi:10.1029/2007JD008797.
- Pielke, R. A., W. R. Cotton, R. L. Walko, C. J. Tremback, W. A. Lyons, L. D. Grasso, M. E. Nicholls, M. D. Moran, D. A. Wesley, T. J. Lee and J. H. Copeland (1992). "A comprehensive meteorological modeling system—RAMS." Meteorology and Atmospheric Physics **49**(1): 69-91.
- Pochanart, P., J. Hirokawa, Y. Kajii, H. Akimoto and M. Nakao (1998). "Influence of regional-scale anthropogenic activity in northeast Asia on seasonal variations of surface ozone and carbon monoxide observed at Oki, Japan." J. Geophys. Res. **104**.
- Pochanart, P., O. Wild and H. Akimoto (2004). Air Pollution Import to and Export from East Asia. Air Pollution: 99-130.
- Polissar, A. V., P. K. Hopke and P. Paatero (1998). "Atmospheric aerosol over Alaska - 2. Elemental composition and sources." Journal of Geophysical Research-Atmospheres **103**(D15): 19045-19057.
- Polissar, A. V., P. K. Hopke, P. Paatero, Y. J. Kaufmann, D. K. Hall, B. A. Bodhaine, E. G. Dutton and J. M. Harris (1999). "The aerosol at Barrow, Alaska: long-term trends and source locations." Atmospheric Environment **33**(16): 2441-2458.
- Polissar, A. V., P. K. Hopke and R. L. Poirot (2001). "Atmospheric aerosol over Vermont: Chemical composition and sources." Environmental Science & Technology **35**(23): 4604-4621.
- Quinn, P. K., T. S. Bates, E. Baum, N. Doubleday, A. M. Fiore, M. Flanner, A. Fridlind, T. J. Garrett, D. Koch, S. Menon, D. Shindell, A. Stohl and S. G. Warren (2008). "Short-lived pollutants in the Arctic: their climate impact and possible mitigation strategies." Atmos. Chem. Phys. **8**(6): 1723-1735.

- Ramanathan, V., M. Agrawal, H. Akimoto, M. Aufhammer, S. Devotta, L. Emberson, S. I. Hasnain, M. Iyengararasan, A. Jayaraman, M. Lawrance, T. Nakajima, T. Oki, H. Rodhe, M. Ruchirawat, S. K. Tan, J. Vincent, J. Y. Wang, D. Yang, Y. H. Zhang, H. Autrup, L. Barregard, P. Bonasoni, M. Brauer, B. Brunekreef, G. Carmichael, C. E. Chung, J. Dahe, Y. Feng, S. Fuzzi, T. Gordon, A. K. Gosain, N. Htun, J. Kim, S. Mourato, L. Naeher, P. Navasumrit, B. Ostro, T. Panwar, M. R. Rahman, M. V. Ramana, M. Rupakheti, D. Settachan, A. K. Singh, G. S. Helen, P. V. Tan, P. H. Viet, J. Yinlong, S. C. Yoon, W.-C. Chang, X. Wang, J. Zelikoff and A. and Zhu (2008b). "Atmospheric Brown Clouds: Regional Assessment Report with Focus on Asia".
- Ramanathan, V. and G. Carmichael (2008a). "Global and regional climate changes due to black carbon." Nat. Geosci. **1**(4): 221-227.
- Ramanathan, V., P. J. Crutzen, J. T. Kiehl and D. Rosenfeld (2001). "Atmosphere - Aerosols, climate, and the hydrological cycle." Science **294**(5549): 2119-2124.
- Ramanathan, V., P. J. Crutzen, J. Lelieveld, A. P. Mitra, D. Althausen, J. Anderson, M. O. Andreae, W. Cantrell, G. R. Cass, C. E. Chung, A. D. Clarke, J. A. Coakley, W. D. Collins, W. C. Conant, F. Dulac, J. Heintzenberg, A. J. Heymsfield, B. Holben, S. Howell, J. Hudson, A. Jayaraman, J. T. Kiehl, T. N. Krishnamurti, D. Lubin, G. McFarquhar, T. Novakov, J. A. Ogren, I. A. Podgorny, K. Prather, K. Priestley, J. M. Prospero, P. K. Quinn, K. Rajeev, P. Rasch, S. Rupert, R. Sadourny, S. K. Satheesh, G. E. Shaw, P. Sheridan and F. P. J. Valero (2001). "Indian Ocean Experiment: An integrated analysis of the climate forcing and effects of the great Indo-Asian haze." Journal of Geophysical Research, [Atmospheres] **106**(D22): 28371-28398.
- Ramanathan, V., F. Li, M. V. Ramana, P. S. Praveen, D. Kim, C. E. Corrigan, H. Nguyen, E. A. Stone, J. J. Schauer, G. R. Carmichael, B. Adhikary and S. C. Yoon (2007). "Atmospheric brown clouds: Hemispherical and regional variations in long-range transport, absorption, and radiative forcing." Journal of Geophysical Research **112**(D22).
- Rasch, P. J., W. D. Collins and B. E. Eaton (2001). "Understanding the Indian Ocean Experiment (INDOEX) aerosol distributions with an aerosol assimilation." J. Geophys. Res. **106**.
- Reidmiller, D. R., D. A. Jaffe, D. Chand, S. Strode, P. Swartzendruber, G. M. Wolfe and J. A. Thornton (2009). "Interannual variability of long-range transport as seen at the Mt. Bachelor observatory." Atmospheric Chemistry and Physics **9**(2): 557-572. Schichtel, B. A., M. G. Barna, K. A. Gebhart and W. C. Malm (2005). "Evaluation of a Eulerian and Lagrangian air quality model using perfluorocarbon tracers released in Texas for the BRAVO haze study." Atmospheric Environment **39**(37): 7044-7062.
- Schichtel, B. A., W. C. Malm, K. A. Gebhart, M. G. Barna and E. M. Knipping (2006). "A hybrid source apportionment model integrating measured data and air quality model results." Journal of Geophysical Research-Atmospheres **111**(D7).

- Seinfeld, J. H., G. R. Carmichael, R. Arimoto, W. C. Conant, F. J. Brechtel, T. S. Bates, T. A. Cahill, A. D. Clarke, S. J. Doherty, P. J. Flatau, B. J. Huebert, J. Kim, K. M. Markowicz, P. K. Quinn, L. M. Russell, P. B. Russell, A. Shimizu, Y. Shinozuka, C. H. Song, Y. H. Tang, I. Uno, A. M. Vogelmann, R. J. Weber, J. H. Woo and X. Y. Zhang (2004). "ACE-ASIA - Regional climatic and atmospheric chemical effects of Asian dust and pollution." Bulletin of the American Meteorological Society **85**(3): 367-+.
- Seinfeld, J. H. and S. N. Pandis (1998). Atmospheric chemistry and physics : from air pollution to climate change. New York, John Wiley
- Senaratne, I. and D. Shooter (2004). "Elemental composition in source identification of brown haze in Auckland, New Zealand." Atmospheric Environment **38**(19): 3049-3059.
- Shim, C., Y. Wang, H. B. Singh, D. R. Blake and A. B. Guenther (2007). "Source characteristics of oxygenated volatile organic compounds and hydrogen cyanide." J. Geophys. Res. **112**.
- Shutthanandan, V., S. Thevuthasan, R. Disselkamp, A. Stroud, A. Cavanagh, E. M. Adams, D. R. Baer, L. A. Barrie, S. S. Cliff, M. Jimenez-Cruz and T. A. Cahill (2002). "Development of PIXE, PESA and transmission ion microscopy capability to measure aerosols by size and time." Nucl. Instrum. Methods Phys. Res. Sect. B-Beam Interact. Mater. Atoms **189**: 284-288.
- Singh, H. B., W. H. Brune, J. H. Crawford, F. Flocke and D. J. Jacob (2009). "Chemistry and transport of pollution over the Gulf of Mexico and the Pacific: spring 2006 INTEX-B campaign overview and first results." Atmospheric Chemistry and Physics **9**(7): 2301-2318.
- Sirois, A. and J. W. Bottenheim (1995). "Use of Backward Trajectories to Interpret the 5-Year Record of Pan and O-3 Ambient Air Concentrations at Kejimikujik National-Park, Nova-Scotia." Journal of Geophysical Research-Atmospheres **100**(D2): 2867-2881.
- Skamarock, W. C., J. B. Klemp, J. Dudhia, D. O. Gill, D. M. Barker, W. Wang and J. G. Powers (2005). A description of the Advanced Research WRF Version 2, NCAR Tech Notes-468+STR.
- Stith, J. L., V. Ramanathan, W. A. Cooper, G. C. Roberts, P. J. DeMott, G. Carmichael, C. D. Hatch, B. Adhikary, C. H. Twohy, D. C. Rogers, D. Baumgardner, A. J. Prenni, T. Campos, R. Gao, J. Anderson and Y. Feng (2009). "An overview of aircraft observations from the Pacific Dust Experiment campaign." Journal of Geophysical Research-Atmospheres **114**.
- Stohl, A. (1996). "Trajectory statistics-A new method to establish source-receptor relationships of air pollutants and its application to the transport of particulate sulfate in Europe." Atmospheric Environment **30**(4): 579-587.
- Stohl, A. (1998). "Computation, accuracy and applications of trajectories - A review and bibliography." Atmospheric Environment **32**(6): 947-966.

- Stohl, A., S. Eckhardt, C. Forster, P. James, N. Spichtinger and P. Seibert (2002). "A replacement for simple back trajectory calculations in the interpretation of atmospheric trace substance measurements." Atmospheric Environment **36**(29): 4635-4648.
- Stone, E. A., G. C. Lough, J. J. Schauer, P. S. Praveen, C. E. Corrigan and V. Ramanathan (2007). "Understanding the origin of black carbon in the atmospheric brown cloud over the Indian Ocean." Journal of Geophysical Research **112**(D22).
- Streets, D. G., T. C. Bond, G. R. Carmichael, S. D. Fernandes, Q. Fu, D. He, Z. Klimont, S. M. Nelson, N. Y. Tsai, M. Q. Wang, J. H. Woo and K. F. Yarber (2003). "An inventory of gaseous and primary aerosol emissions in Asia in the year 2000." J. Geophys. Res., [Atmos.] **108**(D21).
- Streets, D. G., K. F. Yarber, J. H. Woo and G. R. Carmichael (2003). "Biomass burning in Asia: Annual and seasonal estimates and atmospheric emissions." Global Biogeochem. Cycles **17**(4).
- Tang, Y., G. R. Carmichael, L. W. Horowitz, I. Uno, J.-H. Woo, D. G. Streets, D. Dabdub, G. Kurata, A. Sandu, J. Allan, E. Atlas, F. Flocke, L. G. Huey, R. O. Jakoubek, D. B. Millet, P. K. Quinn, J. M. Roberts, D. R. Worsnop, A. Goldstein, S. Donnelly, S. Schauffler, V. Stroud, K. Johnson, M. A. Avery, H. B. Singh and E. C. Apel (2004a). "Multiscale simulations of tropospheric chemistry in the eastern Pacific and on the U.S. West Coast during spring 2002." J. Geophys. Res. **109**: D23S11, doi:10.1029/2004JD004513.
- Tang, Y. H., G. R. Carmichael, G. Kurata, I. Uno, R. J. Weber, C. H. Song, S. K. Guttikunda, J. H. Woo, D. G. Streets, C. Wei, A. D. Clarke, B. Huebert and T. L. Anderson (2004b). "Impacts of dust on regional tropospheric chemistry during the ACE-Asia experiment: A model study with observations." Journal of Geophysical Research-Atmospheres **109**(D19).
- Tang, Y. H., G. R. Carmichael, J. H. Seinfeld, D. Dabdub, R. J. Weber, B. Huebert, A. D. Clarke, S. A. Guazzotti, D. A. Sodeman, K. A. Prather, I. Uno, J. H. Woo, J. J. Yienger, D. G. Streets, P. K. Quinn, J. E. Johnson, C. H. Song, V. H. Grassian, A. Sandu, R. W. Talbot and J. E. Dibb (2004). "Three-dimensional simulations of inorganic aerosol distributions in east Asia during spring 2001." Journal of Geophysical Research-Atmospheres **109**(D19).
- Tang, Y. H., G. R. Carmichael, N. Thongboonchoo, T. F. Chai, L. W. Horowitz, R. B. Pierce, J. A. Al-Saadi, G. Pfister, J. M. Vukovich, M. A. Avery, G. W. Sachse, T. B. Ryerson, J. S. Holloway, E. L. Atlas, F. M. Flocke, R. J. Weber, L. G. Huey, J. E. Dibb, D. G. Streets and W. H. Brune (2007). "Influence of lateral and top boundary conditions on regional air quality prediction: A multiscale study coupling regional and global chemical transport models." Journal of Geophysical Research-Atmospheres **112**(D10): D10S18, doi:10.1029/2006JD007515.
- Tang, Y. H., G. R. Carmichael, I. Uno, J. H. Woo, G. Kurata, B. Lefer, R. E. Shetter, H. Huang, B. E. Anderson, M. A. Avery, A. D. Clarke and D. R. Blake (2003). "Impacts of aerosols and clouds on photolysis frequencies and photochemistry during TRACE-P: 2. Three-dimensional study using a regional chemical transport model." Journal of Geophysical Research-Atmospheres **108**(D21).

- TF-HTAP. (2007). "Hemispheric Transport of Air Pollution 2007, United Nations Economic Commission for Europe, New York and Geneva." *Air Pollution Studies* 16. from <http://www.htap.org/>.
- Tombette, M., V. Mallet and B. Sportisse (2009). "PM10 data assimilation over Europe with the optimal interpolation method." *Atmos. Chem. Phys.* **9**(1): 57-70.
- Uno, I., G. R. Carmichael, D. G. Streets, Y. Tang, J. J. Yienger, S. Satake, Z. Wang, J. H. Woo, S. Guttikunda, M. Uematsu, K. Matsumoto, H. Tanimoto, K. Yoshioka and T. Iida (2003). "Regional chemical weather forecasting system CFORS: Model descriptions and analysis of surface observations at Japanese island stations during the ACE-Asia experiment." *Journal of Geophysical Research-Atmospheres* **108**(D23).
- Uno, I., S. Satake, G. R. Carmichael, Y. H. Tang, Z. F. Wang, T. Takemura, N. Sugimoto, A. Shimizu, T. Murayama, T. A. Cahill, S. Cliff, M. Uematsu, S. Ohta, P. K. Quinn and T. S. Bates (2004). "Numerical study of Asian dust transport during the springtime of 2001 simulated with the Chemical Weather Forecasting System (CFORS) model." *Journal of Geophysical Research-Atmospheres* **109**(D19).
- van Aardenne, J. A., G. R. Carmichael, H. LevyII, D. Streets and L. Hordijk (1999). "Anthropogenic NOx emissions in Asia in the period 1990-2020." *Atmospheric Environment* **33**(4): 633-646.
- van der Werf, G. R., J. T. Randerson, L. Giglio, G. J. Collatz, P. S. Kasibhatla and A. F. Arellano (2006). "Interannual variability in global biomass burning emissions from 1997 to 2004." *Atmospheric Chemistry and Physics* **6**: 3423-3441.
- VanCuren, R. A. (2003). "Asian aerosols in North America: Extracting the chemical composition and mass concentration of the Asian continental aerosol plume from long-term aerosol records in the western United States." *Journal of Geophysical Research-Atmospheres* **108**(D20): 4623, doi:10.1029/2003JD003459.
- Volkamer, R., J. L. Jimenez, F. San Martini, K. Dzepina, Q. Zhang, D. Salcedo, L. T. Molina, D. R. Worsnop and M. J. Molina (2006). "Secondary organic aerosol formation from anthropogenic air pollution: Rapid and higher than expected." *Geophys. Res. Lett.* **33**: L17811, doi:10.1029/2006GL026899.
- Vukovich, J. and T. Pierce. (2002). "The Implementation of BEIS3 within the SMOKE modeling framework." from <http://www.epa.gov/ttn/chief/conference/ei11/modeling/vukovich.pdf>.
- Wang, Y., C. Shim, N. Blake, D. Blake, Y. Choi, B. Ridley, J. Dibb, A. Wimmers, J. Moody, F. Flocke, A. Weinheimer, R. Talbot and E. Atlas (2003). "Intercontinental transport of pollution manifested in the variability and seasonal trend of springtime O3 at northern middle and high latitudes." *J. Geophys. Res.* **108**.
- Wang, Y. Q., X. Y. Zhang, R. Arimoto, J. J. Cao and Z. X. Shen (2004). "The transport pathways and sources of PM10 pollution in Beijing during spring 2001, 2002 and 2003." *Geophys. Res. Lett.* **31**(14).

- Warneke, C., R. Bahreini, J. Brioude, C. A. Brock, J. A. de Gouw, D. W. Fahey, K. D. Froyd, J. S. Holloway, A. Middlebrook, L. Miller, S. Montzka, D. M. Murphy, J. Peischl, T. B. Ryerson, J. P. Schwarz, J. R. Spackman and P. Veres (2009). "Biomass burning in Siberia and Kazakhstan as an important source for haze over the Alaskan Arctic in April 2008." Geophys. Res. Lett. **36**.
- Watson, J. G., T. Zhu, J. C. Chow, J. Engelbrecht, E. M. Fujita and W. E. Wilson (2002). "Receptor modeling application framework for particle source apportionment." Chemosphere **49**(9): 1093-1136.
- Wesely, M. L. and B. B. Hicks (2000). "A review of the current status of knowledge on dry deposition." Atmospheric Environment **34**(12-14): 2261-2282.
- Willeke, K. and P. A. Baron (1993). Aerosol measurement : principles, techniques, and applications. New York, Van Nostrand Reinhold
- Wolfe, G. M., J. A. Thornton, V. F. McNeill, D. A. Jaffe, D. Reidmiller, D. Chand, J. Smith, P. Swartzendruber, F. Flocke and W. Zheng (2007). "Influence of trans-Pacific pollution transport on acyl peroxy nitrate abundances and speciation at Mount Bachelor Observatory during INTEX-B." Atmospheric Chemistry and Physics **7**(20): 5309-5325.
- Woo, J. H., D. G. Streets, G. R. Carmichael, Y. H. Tang, B. Yoo, W. C. Lee, N. Thongboonchoo, S. Pinnock, G. Kurata, I. Uno, Q. Y. Fu, S. Vay, G. W. Sachse, D. R. Blake, A. Fried and D. C. Thornton (2003). "Contribution of biomass and biofuel emissions to trace gas distributions in Asia during the TRACE-P experiment." Journal of Geophysical Research-Atmospheres **108**(D21).
- World Health Organization. (2006). WHO Air quality guidelines for particulate matter, ozone, nitrogen dioxide and sulfur dioxide - Global update 2005 - Summary of risk assessment.
- World Bank. (2007). "World Development Indicators." from http://siteresources.worldbank.org/DATASTATISTICS/Resources/table3_13.pdf.
- Xie, Y. and C. M. Berkowitz (2006). "The use of positive matrix factorization with conditional probability functions in air quality studies: An application to hydrocarbon emissions in Houston, Texas." Atmospheric Environment **40**(17): 3070-3091.
- Yienger, J. J., M. Galanter, T. A. Holloway, M. J. Phadnis, S. K. Guttikunda, G. R. Carmichael, W. J. Moxim and H. Levy (2000). "The episodic nature of air pollution transport from Asia to North America." Journal of Geophysical Research-Atmospheres **105**(D22): 26931-26945.
- Yoon, S. C. and J. Kim (2006). "Influences of relative humidity on aerosol optical properties and aerosol radiative forcing during ACE-Asia." Atmospheric Environment **40**(23): 4328-4338.

- Zhang, L., D. J. Jacob, K. F. Boersma, D. A. Jaffe, J. R. Olson, K. W. Bowman, J. R. Worden, A. M. Thompson, M. A. Avery, R. C. Cohen, J. E. Dibb, F. M. Flock, H. E. Fuelberg, L. G. Huey, W. W. McMillan, H. B. Singh and A. J. Weinheimer (2008). "Transpacific transport of ozone pollution and the effect of recent Asian emission increases on air quality in North America: an integrated analysis using satellite, aircraft, ozonesonde, and surface observations." Atmospheric Chemistry and Physics **8**(20): 6117-6136.
- Zhang, Q., J. L. Jimenez, M. R. Canagaratna, J. D. Allan, H. Coe, I. Ulbrich, M. R. Alfarra, A. Takami, A. M. Middlebrook, Y. L. Sun, K. Dzepina, E. Dunlea, K. Docherty, P. F. DeCarlo, D. Salcedo, T. Onasch, J. T. Jayne, T. Miyoshi, A. Shimono, S. Hatakeyama, N. Takegawa, Y. Kondo, J. Schneider, F. Drewnick, S. Borrmann, S. Weimer, K. Demerjian, P. Williams, K. Bower, R. Bahreini, L. Cottrell, R. J. Griffin, J. Rautiainen, J. Y. Sun, Y. M. Zhang and D. R. Worsnop (2007). "Ubiquity and dominance of oxygenated species in organic aerosols in anthropogenically-influenced Northern Hemisphere midlatitudes." Geophys. Res. Lett. **34**: L13801, doi:10.1029/2007GL029979.
- Zhang, Q., D. G. Streets, G. R. Carmichael, K. He, H. Huo, A. Kannari, Z. Klimont, I. Park, S. Reddy, J. S. Fu, D. Chen, L. Duan, Y. Lei, L. Wang and Z. Yao (2009). "Asian emissions in 2006 for the NASA INTEX-B mission." Atmos. Chem. Phys. Discuss. **9**(1): 4081-4139.
- Zhang, X. Y., S. L. Gong, Z. X. Shen, F. M. Mei, X. X. Xi, L. C. Liu, Z. J. Zhou, D. Wang, Y. Q. Wang and Y. Cheng (2003). "Characterization of soil dust aerosol in China and its transport and distribution during 2001 ACE-Asia: 1. Network observations." Journal of Geophysical Research-Atmospheres **108**(D9).
- Zhou, L., P. K. Hopke and W. Liu (2004). "Comparison of two trajectory based models for locating particle sources for two rural New York sites." Atmospheric Environment **38**(13): 1955-1963.
- Zhou, L. M., P. K. Hopke, C. O. Stanier, S. N. Pandis, J. M. Ondov and J. P. Pancras (2005). "Investigation of the relationship between chemical composition and size distribution of airborne particles by partial least squares and positive matrix factorization." Journal of Geophysical Research-Atmospheres **110**(D7).